STRUCTURAL PERFORMANCE OF LONGITUDINALLY POST-TENSIONED PRECAST DECK PANEL BRIDGES

Andrew James Woerheide

Thesis submitted to the faculty of the Virginia Polytechnic Institute and State University in partial fulfillment of the requirements for the degree of

Master of Science

in

Civil Engineering

Carin L. Roberts-Wollmann, Committee Chair

Thomas E. Cousins

Matthew R. Eatherton

July 20, 2012

Blacksburg, Virginia

Keywords: Bridge Deck, Deck Panels, Post-tensioning, Shear Studs, Prestress Losses

STRUCTURAL PERFORMANCE OF LONGITUDINALLY POST-TENSIONED PRECAST DECK PANEL BRIDGES

Andrew James Woerheide

As the aging bridges and infrastructure within the US continue to deteriorate, traffic delays due to construction will become more and more common. One method that can reduce delays due to bridge construction is to use precast deck panels. Precast deck panels can significantly reduce the overall length of the construction project. The panels can be manufactured ahead of time, and with higher quality control than is possible in the field. One of the reasons precast deck panels are not widely accepted is because of a lack of research concerning the required post-tensioning force, shear stud pocket placement, and proper joint design.

In a recent dissertation (Swenty 2009) numerous recommendations were made for joint design, shear stud pocket design, and post-tensioning force for full-depth precast deck panel bridges. Design drawings were included for the replacement of a bridge located in Scott County, Virginia. The research in this report focuses on the short-term and long-term testing of this bridge. The short-term testing involved performing a live load test in which two trucks of known weight and dimensions were positioned on the bridge in order to maximize the negative moment at the joints over the piers and document strains and deflections at a number of other critical locations. The long-term testing involved monitoring the strains within the deck and on one of the six girders for a number of months in order to document the changes in strain due to creep and shrinkage. The results of these tests were compared to 2D beam-line models and to the parametric study results of Bowers' research on prestress loss within full-depth precast deck panel bridges. It was determined that the bridge was acting compositely and that the post-tensioning force was sufficient in keeping the joints in compression during testing.

Acknowledgments

I first want to thank Dr. Roberts-Wollmann, Dr. Cousins, and Dr. Eatherton for all of their support and guidance throughout not only this project, but all of my time at Virginia Tech. It was a pleasure working with all of you on this project. Your patience and help throughout these years have been invaluable for my education and my thesis.

I want to thank all of my friends and classmates who have helped me on this project and in my classes. In particular I want to thank Marc, Kedar, and Nathan for helping with the live load test and for always being there to answer my questions. Without all of you I would not have been able to get through graduate school. I also want to thank Brett, Dennis, and Dave for all of their help and patience as well. I really appreciate all of the work you all do within the lab, and how much time you spend helping students.

I also have to thank my family. They have always been there for me and have supported me throughout my entire collegiate career. Without all of them none of this would have been possible.

Table of Contents

List of Figures

List of Tables

Chapter 1: Introduction

In 2007, Americans collectively spent nearly 4.2 billion hours stuck in traffic. That amounts to $87.2 billion spent on wasted fuel and lost productivity (James 2009). Although there are many different reasons for why this traffic congestion occurs, a significant contributor to this problem is construction. In a recent report produced by ASCE in 2009, the bridges across the US were given an overall grade of C. It was reported that more than 26% of the nation's bridges are structurally deficient or functionally obsolete. It was determined that a $17 billion annual investment would be needed in order to substantially improve current bridge conditions. As the infrastructure continues to deteriorate, construction will be necessary in order to repair or replace many of these bridges across the country.

One solution for minimizing traffic delays is to reduce the amount of time spent on bridge construction and repair. Precast deck panels are an effective way to achieve this. Traditional cast-in-place decks require workers to install extensive formwork, place the reinforcement throughout the length of the bridge, place the concrete, and then wait for the concrete to harden before traffic can drive over it. For precast deck panel bridges, the deck panels can be cast off-site before the construction even begins in the field. When they are constructed in this way, there is a greater amount of quality control and the panels can be built very rapidly. The panels can then be placed directly on the supporting girders without the need for any formwork. The panels will, however, need to be longitudinally post-tensioned and the shear pockets will need to be grouted, which adds to the total construction time. The panels are typically prestressed transversely during the panel casting process.

One of the issues restraining widespread implementation of precast deck panels is that there are relatively few design standards available. There has been limited research on the topic and

recommendations about longitudinal post-tensioning and joint design vary greatly. Further research must be performed in order to create guidelines and design aids for precast deck panel bridges.

1.1 General Project Information

This thesis is a continuation of the work performed by Matthew Swenty (2009). In this dissertation he studied many of the aspects of precast deck panels, including the design of transverse and longitudinal joints and shear stud pocket blockouts. Using his conclusions regarding these topics, along with the research performed by Susan Bowers (2007), Swenty developed the design for the replacement of a three-span steel girder bridge in Scott County, Virginia. The original bridge was built using a conventional cast-in-place deck and steel girders. The new bridge still has steel girders, but has a precast panel deck instead of a cast-in-place deck. This report focuses on the construction process of the bridge as well as short-term and long-term testing. The ultimate goal is to determine whether or not the recommendations by Swenty and Bowers are accurate and applicable for precast deck panels on steel girders.

The bridge being replaced is located in Scott County, Virginia on VA-65/VA 72 S and runs over Staunton Creek. Figure 1-1 presents a photograph of the bridge prior to construction. It was a two lane bridge with three spans, which were discontinuous over the interior piers. This discontinuity between spans allowed for water to leak through the joints, which ultimately resulted in serious rust and corrosion problems.

Figure 1-2 presents a photograph showing some of the rust resulting from these leaking joints.

Figure 1-1. Photograph of the Original Bridge

Figure 1-2. Photograph of the Corrosion at the Joints between Spans

The new bridge is also two lanes, but is continuous over the interior supports. The girders are galvanized W18x71 beams, and have one moment resisting splice along their lengths. There are three beams supporting each traffic lane, which means that there are six beam lines in total. The bridge was built in two separate phases of construction. It was built in this way in order to leave at least one lane of the bridge open to traffic throughout the entire construction process. There were two traffic lights installed at either end of the bridge which controlled the direction of traffic. The first phase, which will be referred to as Phase I, involved the demolition and reconstruction of the northern lane. The second phase, which will be referred to as Phase II, replaced the northern lane. Figure 1-3 presents a plan view of the new bridge's dimensions and orientation, and Figure 1-4 presents a diagram showing the construction staging process.

Due to the time constraints of this project, most of the short-term and long-term testing was performed on only the Phase I side of the bridge. The construction on the Phase I side of the bridge began in October of 2011. The deck panels, however, were cast throughout the month of September in 2011. The panels were cast at Newcrete Stone and Lime Co. in Roaring Springs, Pennsylvania. The concrete panel release strengths of the panels are given in Appendix A. Each phase of the bridge consists of ten panels along the length of the bridge. The interior panels measured 9 ft 10 in. long, and the exterior panels measured 9 ft 11 in. long, which results in an overall bridge length of 100 ft. The panels were fabricated with 6000 psi design compressive strength, self-consolidating concrete (SCC). The panels were prestressed transversely, and fitted with ducts for the longitudinal post-tensioning. Figure 1-5 presents a photograph showing one of the panels being constructed at the Newcrete plant. During the construction of the panels, Geokon vibrating-wire gauges were installed in three separate panels. They were installed near the edge of the panels in order to measure the compressive strain at the joint between the panels. A photograph of one of the gauges is presented in Figure 1-6.

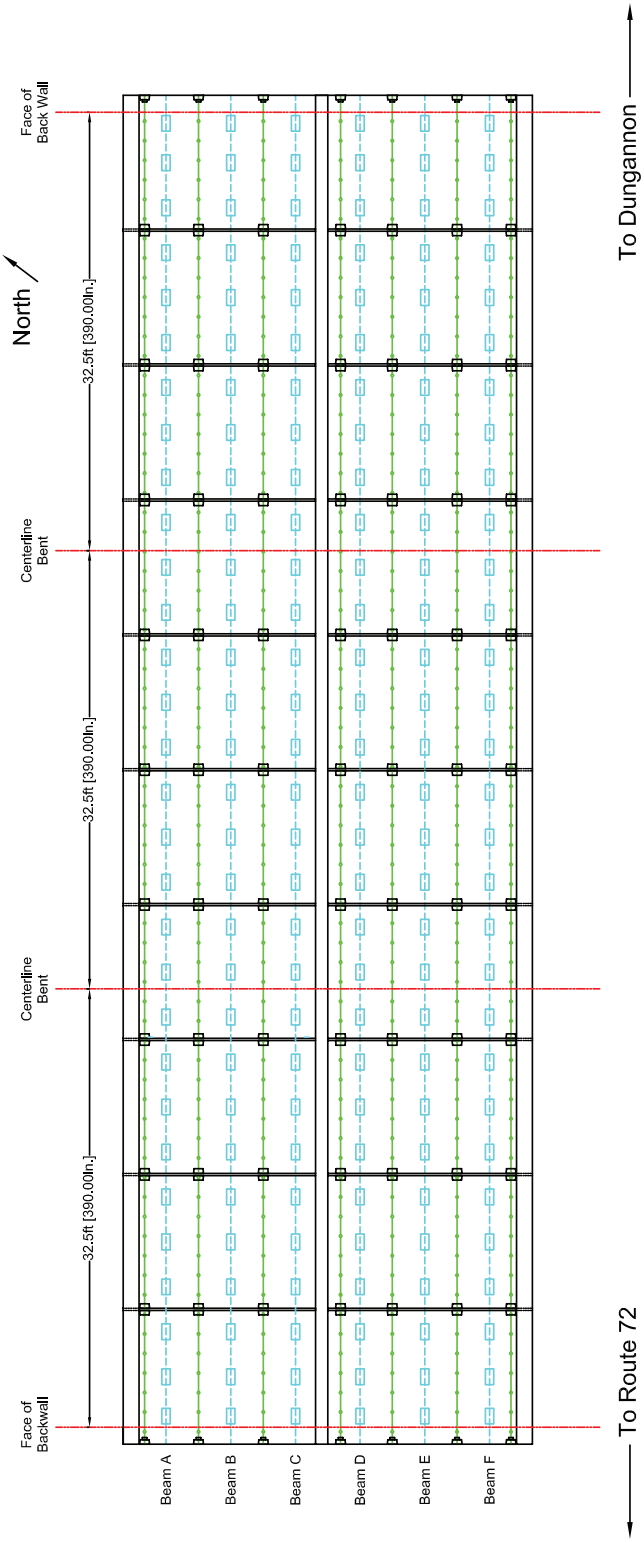

Figure 1-3. Plan View of the New Bridge Design

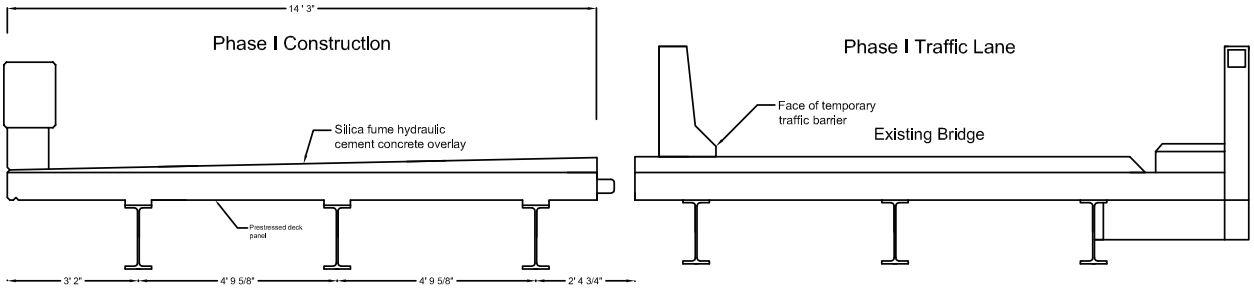

Phase I Sequence of Construction

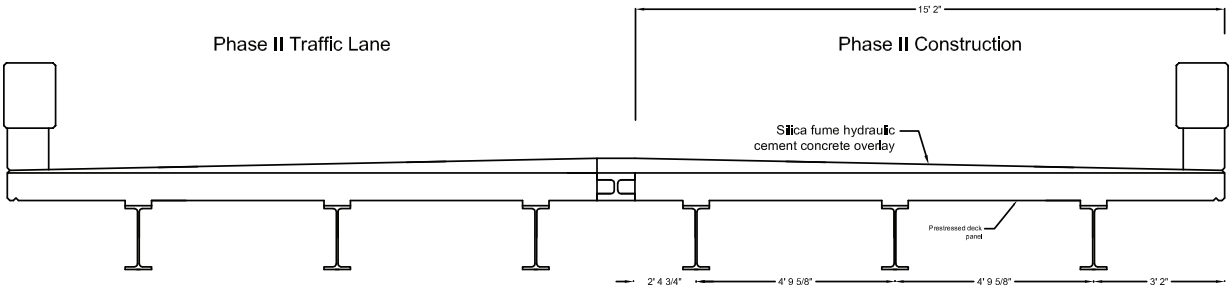

Phase II Sequence of Construction

Figure 1-4. Phase I and II Construction Staging Process

Figure 1-5. Photograph of a Deck Panel Being Constructed at Newcrete

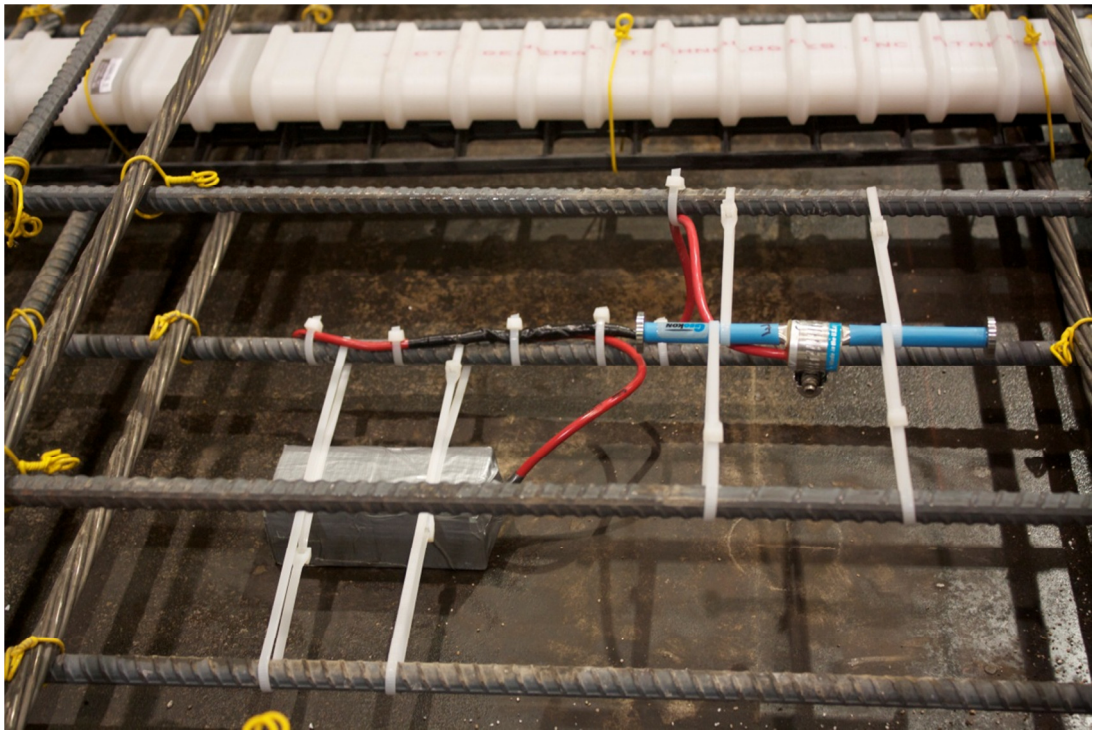

Figure 1-6. Photograph of a Geokon Vibrating-Wire Gauge

The galvanized beams were set into the Phase I side of the bridge in October, 2011. On November 2, four vibrating wire gauges were installed on the interior beam on the Phase I side of the bridge. Figure 1-7 presents a photograph showing the installation of two of the vibrating-wire gauges on the interior beam. The panels were set onto the beams on November 4. Shortly after the panels were set and the joints between the panels were grouted, the gauges set inside two of the panels within the Phase I side of the bridge were connected to the data logger and began recording strain data. The panels were post-tensioned with a jacking force of 41 kips per strand for twelve strands, which resulted in a midspan stress of 172.5 ksi in each strand. The post-tensioning calculations and the actual post-tensioning of the panels were performed by Dywidag-Systems International (DSI).

After the panels were post-tensioned, the shear studs were placed within the shear pockets and then the haunch and the shear pockets were filled with grout on November 28. Note that the shear stud pockets are spaced 3 ft 4 in. from center-to-center, which means that the studs are spaced farther apart than the AASHTO maximum spacing limit of 24 in. The bridge was assumed to be acting fully-compositely by early December. A live load test was conducted on February 2, 2012. This live load test consisted of driving two VDOT dump trucks of known dimensions and loadings across the bridge while measuring the strains and deflections using a data logger. The exact sequence of the test is discussed in further detail in chapter 3 of this report. Along with the short-term data, long-term strain recordings were measured from November 2 to June 6. A timeline of important dates is presented in Table 1-1. This data was used to compare to Bowers' model for prestress losses over time. The whole bridge was completed and opened to traffic in May 2012. Figure 1-8 presents a photograph showing the finished bridge on the day the long-term data collection was ended.

Table 1-1. Timeline of Important Events

Date	Day #	Event
9/12/2011	0	Poured panels
11/4/2011	53	Panels set on bridge
11/7/2011	56	Leveling bolts set
11/16/2011	65	Post-tensioning
11/28/2011	76	Haunch poured
12/2/2011	80	Deck and beams assumed composite
2/2/2012	143	Live load test
5/1/2012	232	Bridge construction was completed

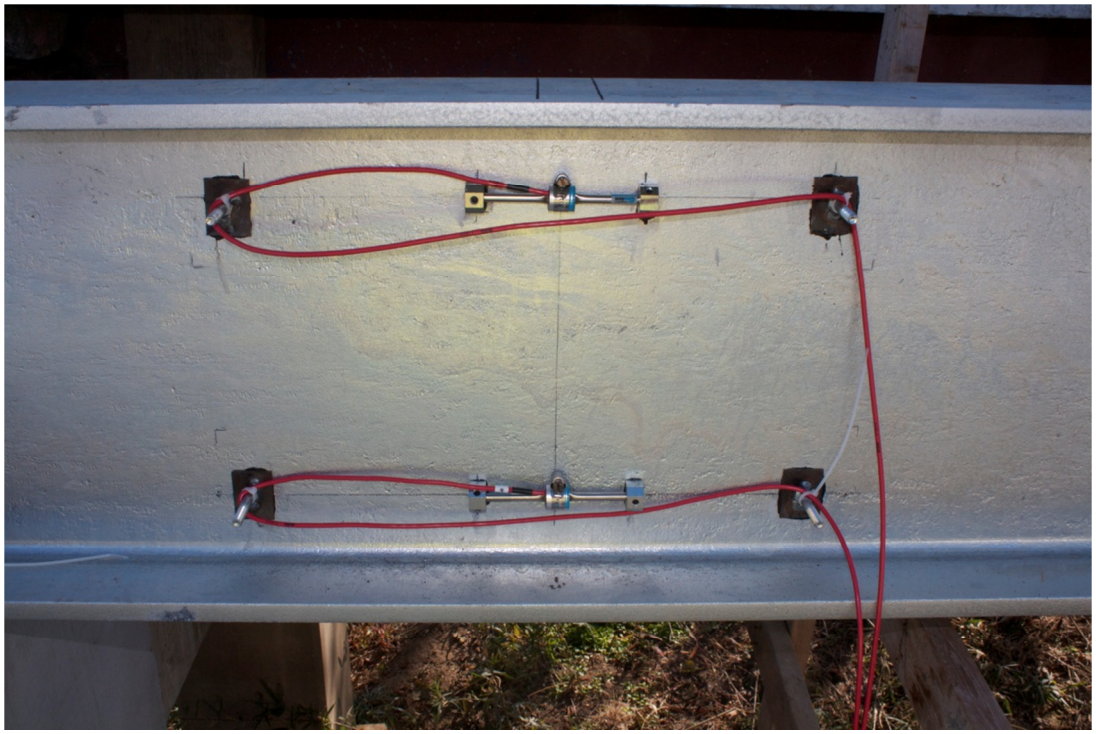

Figure 1-7. Photograph of Vibrating-Wire Gauges on the Side of the Interior Beam on the Phase I Side of the Bridge

Figure 1-8. Photograph of the Completed Bridge from June 2012

1.2 Objectives and Scope of Work

In Swenty's dissertation he attempted to answer the following questions: Which transverse deck panel connection techniques will crack the least and be the most durable under the worst case service loading conditions? Do current recommendations for longitudinal post-tensioning in deck panels (based on Bowers' research) keep the deck and joints in compression? The purpose of this project is to test Swenty's recommendations regarding joint and shear blockout design by measuring the strains across the joints during long-term and short-term testing and by looking at the strain distribution within the beams and concrete. Another goal of this research is to compare strains within the bridge to a model for prestress loss created by Bowers, in order to determine if the model is accurate and keeps the deck in compression throughout the monitoring process. It is also important to determine whether or not the 3 ft 4 in. shear stud pocket spacing affects the composite action between the girders and deck panels, due to the fact that this spacing means the shear studs are further apart than the AASHTO recommended maximum spacing of 2 ft.

In order to complete these goals, the bridge was studied by way of short-term testing and long-term testing. The construction was monitored and documented both qualitatively and quantitatively. After the first phase of the bridge was completed, a live load test was conducted in order to compare predicted strains and deflections to strains and deflections measured while trucks of known dimensions and weights were driven across the surface of the deck. This test aids in determining whether or not the post-tensioning force was sufficient to keep the joints in compression under maximum loading conditions. Gauges were placed in numerous locations throughout the depth of the bridge and on all three girders. These gauges allowed for determining whether or not the strains were linear throughout the entire cross-section, which would indicate that the shear pocket spacings are sufficient to make the deck and girders act compositely. The bridge was also monitored by recording strains on one girder and

within two panels for the entire duration of this project. This data was used to compare to Bowers' model to determine whether or not it can successfully predict the strain distribution over a significant period of time.

Chapter 2: Literature Review

Due to the fact that this report is a continuation of a number of other dissertations and theses researched at Virginia Tech, this section focuses on summarizing these previous projects and explaining why this research project is necessary and how it will contribute to the field of structural engineering.

2.1 Matthew Swenty's Dissertation

The research performed by Swenty (2009) investigated transverse joints and blockouts on full-depth concrete deck panels. Swenty studied two cast-in-place and four post-tensioned joints which were tested using a cyclical loading pattern. The joints were designed and tested within the laboratory at Virginia Tech, where it was possible to simulate negative bending effects caused by a HL-93 vehicle load. Of the four post-tensioned joints, two were post-tensioned to 167 psi of initial stress and two were post-tensioned to 340 psi of initial stress across the joint. The two joints with the highest level of initial prestress performed the best. These joints did not exhibit any full-depth cracking, did not allow any water to leak through, and managed to sustain a linear strain distribution throughout the design service life. Swenty concluded that full depth deck panels may be effectively used on continuous bridges if a sufficient level of prestressing force is used during the post-tensioning.

Swenty's research also attempted to determine whether the current design standards and recommendations for required longitudinal post-tensioning force for full-depth deck panels would keep the deck and joints in compression throughout their service life. In his literature review, Swenty concluded that there is a lack of design standards and that most of the current methods are either not widely accepted or contradictory. The recommended procedures for designing the panels, attaching the panels to the girders, grouting the shear connector pockets, and connecting the panels together transversely and longitudinally vary greatly between states. The American Association of State Highway

and Transportation Officials (AASHTO 2008) Load and Resistance Factored Design (LRFD) only specify that deck panels are permitted in bridge construction, but do not give any guidelines for designing the joints and shear connectors, or what type of grout to use. The Precast Concrete Institute (PCI 2003) Bridge Design Manual mentions some of the benefits and common problems associated with different transverse joint designs and different types of non-shrink grout, but does not present any standard guidelines for design.

According to Swenty, the current lack of accepted design standards indicates that research on this topic is necessary for the advancement and national acceptance of this type of bridge design. A better understanding of panel joints, post-tensioning levels, construction techniques, and grouting materials will provide structural engineers with tools to create cost-effective and efficient designs.

Swenty also discussed the current design standards regarding the design and usage of shear studs within precast deck panel bridges. In typical cast-in-place bridge designs, the shear studs are spaced evenly along each girder. In full-depth deck panels, the shear connectors are concentrated in shear pockets along the length of the girder. These shear pockets are eventually filled with grout to create composite behavior between the deck panels and the girders. In the AASHTO LRFD bridge design specifications, the shear studs are allowed to be spaced a maximum of 24 in. apart. Using a shear stud pocket spacing of 24 in. would result in a large number of shear pockets along the length of the bridge. Having so many grouted pockets may adversely affect the durability of the deck and its ability to resist water leakage. Tests performed by Menkulaski and Roberts-Wollmann (2005) showed that the current design specifications regarding the required shear connectors may need to be revised. Sullivan (2006) performed a number of tests on different shear stud reinforcement designs within deck panels. While his results are discussed more in depth in section 2.2 of this report, he determined that the LFRD design

specification was accurate in determining shear stud capacity with up to 4 ft spacing between stud pockets, which is 2 ft greater than the current requirements. The topic of shear stud spacing is also discussed in more depth in section 2.3 of this report which summarizes the PCI Committee on Bridges report. The report focuses on extending the shear stud spacing limit for full-depth concrete deck panels.

Swenty further determined that there are relatively few guidelines for calculating the post-tensioning force required for full-depth precast deck panel design. The AASHTO bridge design specification does not currently provide any recommendations at all. Longitudinal post-tensioning has, however, been proven to be critical in improving the performance and durability of precast deck panel bridges. There has also not been much guidance offered in the design of the transverse joints. Keeping the joints in compression is extremely important in order to resist spalling and cracking. The most in-depth study on this topic of post-tensioning levels was performed by Bowers (2007). She performed a number of parametric studies on post-tensioning levels in a variety of different bridge types, which included steel and concrete girder bridges with both simple and continuous spans. Her research involved determining the effects of the long-term stress loss and redistribution caused by creep and shrinkage. Her methods and results are discussed in greater detail in section 2.4 of this report.

From his research, Swenty concluded that the post-tensioned joint with the highest level of initial stress of 0.340 ksi performed the best. He also determined that the model developed by Bowers et al. was effective in determining the appropriate level of post-tensioning force needed. Due to stress losses from creep and shrinkage, approximately 5% of the post-tensioning force was lost during the first two months. He also determined that it was important to keep the maximum amount of tensile stress in the deck near $1.5\sqrt{f'_c}$ in order to reduce surface cracking due to service loads. The best performing shear pockets were wire brushed or had exposed aggregate and used Five Star Highway Patch grout.

Swenty took all of these conclusions regarding transverse joint design, shear pocket design, and post-tensioning force, and incorporated them into an actual design for a full-depth precast deck panel bridge. He submitted the design documents to VDOT in 2009. His designs formed the basis for the final design of the Route 65 Bridge over Staunton Creek. In his conclusion, Swenty recommended studying the implementation of his designs in the real world, both during construction and in the long-term. This recommendation formed the basis of this report and acted as a guide for most of this project's research goals.

2.2 Sean Sullivan's Dissertation

The research performed by Sullivan (2007) investigated constructability, creep and shrinkage behavior, strength and fatigue performance of transverse joints, different types of shear connectors, and the effect of different shear pocket spacings within full-depth precast deck panels. Of particular importance to this report are his conclusions regarding the AASHTO maximum shear stud spacing of 24 in. Through his research, Sullivan determined that the AASHTO LRFD shear friction equations were applicable to full-depth deck panel systems when the shear stud pockets were spaced at 48 in. His test samples were not only able to reach the required flexural strength and the required vertical shear strength, but he determined that they could use up to 25% fewer shear connectors than required by AASHTO and still meet the strength requirements.

In order to make these conclusions, Sullivan conducted a series of load tests in which both hooked reinforcing bars and shear studs were spaced in pockets 2 and 4 ft apart. These tests were performed on a 40 ft simply supported bridge, which consisted of two AASHTO Type II concrete girders spaced 8 ft

center-to-center and an 8 in. thick deck panels. In order to use shear studs, five ¼ in. thick steel plates were embedded in the top of the concrete girders. Overall, both the 2 and 4 ft spacings performed exceptionally well.

During these tests, the deck panels were post-tensioned to 269 psi after all instantaneous losses. The change in strain in the deck due to creep and shrinkage was measured to be -40 με. At 10,000 days, the average compressive stress in the deck was analytically determined to be 201 psi. Sullivan reported no serious issues with the transverse panel joints, and determined that the post-tensioning force was, therefore, sufficient to keep the joints in compression and make the deck perform like a cast-in-place deck. This level of post-tensioning was not calculated using any type of advanced time-dependent model such as developed by Bowers.

Overall, Sullivan's research provides further support for the argument that the AASHTO 24 in. maximum stud spacing limit can be extended to at least 48 in., especially when used in conjunction with AASHTO Type II concrete girders. Whether or not this shear stud pocket spacing recommendation extends to steel girder bridges is not covered in his report.

2.3 PCI Committee on Bridges Task Force on Extending the Stud Spacing Limit for Full-Depth Precast Concrete Deck Panels from 24 in. to 48 in.

This report is a work in progress written by Sameh Badie (2012). The report details some of the research work already performed on the topic of shear stud spacing, discusses some of the current arguments against extending the stud spacing limits, and proposes some solutions for some of the most common issues associated with extended stud spacings. According to Badie (2012), there have been four

different groups of researchers to study this issue. These groups include researchers at University of Illinois at Chicago, University of Wisconsin, George Washington University/University of Nebraska, and Virginia Tech.

The major concerns engineers have about increasing the spacing limit are longitudinal splitting cracks forming in the deck over girder lines, separation of the deck and the girders, bearing failure of the slab in front of the shear stud pockets, and crushing failure of the grout near the base of the studs. Regarding longitudinal splitting cracks, Badie (2012) suggests simply installing more transverse reinforcement within the slab. Greater reinforcement in this direction would significantly limit the effects of the splitting force caused by the shearing reaction between the deck and the studs. Concerning the separation of the deck from the girders, Badie concludes that, while this may be an issue in small-scale laboratory tests, it has never affected full-scale bridge designs. The reason for this is the fact that the decks on bridges actually built in the field are significantly heavier than the decks manufactured for laboratory tests. This extra weight helps to keep the deck and girders in contact throughout their service life. Regarding the bearing failure issue, Badie determines that, while critical for deck performance, there are equations that have already been developed in order to check this limit state. On the issue of grout crushing failure at the base of the shear studs, Badie determines that the best solution is to provide lateral confinement around the stud clusters. Lateral confinement of this type has been proven successful in a number of other applications where large stress concentrations tend to lead to premature failure, such as in columns and in the end zones of post-tensioned members.

It is clear from this report that studying the behavior of the shear stud pockets is an important issue and, while Badie successfully offers solutions for some of the main concerns regarding increasing the spacing

limit, there is still a need for further research. Only two of the other research groups listed in the first section of this report have done any testing on full-scale bridges in the field.

2.4 Susan Bowers' Thesis

The research performed by Bowers (2007) focuses on the effects of creep, shrinkage, and relaxation on the longitudinal post-tensioning force within precast deck panel bridges. Her main goal was to develop a Mathcad model which would accurately predict the amount of post-tensioning force required to keep the transverse joints in compression throughout the bridge's service life. Her parametric studies included bridges with both steel and prestressed concrete girders, as well as bridges with single spans or continuous spans over one or two interior piers.

In Bowers' literature review, she determined that the recommended levels of post-tensioning in full-depth precast deck panel bridges varied significantly across the country. It also became clear that in order to have an efficient and long-lasting precast deck panel bridge, it was important to have an efficient construction sequence, select the appropriate grout, have transverse prestressing and longitudinal post-tensioning, and choose particular types of shear connectors and transverse joints. The most common problems associated with the precast deck panel joints were construction procedures, material quality, and maintenance issues. Many of the different departments of transportation across the country witnessed issues regarding leaking and cracking at the joint interfaces. Most of these issues could be solved by using better joint designs and by applying the correct level of post-tensioning force.

Bowers' Mathcad model used the age-adjusted effective modulus method along with a series of strain compatibility relationships to determine the long-term effects of shrinkage and creep on the bridge

systems. Through her research, she determined that continuously spanning steel girder bridges experienced the greatest amount of prestress loss. She also determined that larger span lengths lost more precompression at the joints than shorter span lengths. In her conclusion, Bowers presented a table of minimum recommended initial prestress levels. For precast deck panel bridges with steel girders, Bowers recommended 200 psi of required post-tensioning for bridges with one span, 650 psi for two spans, and 500 psi for three spans. Alternatively, Bowers suggests that designers could use her Mathcad models to predict the exact level of post-tensioning required no matter what type of bridge was being designed. Swenty used this Mathcad sheet in his initial designs, and this sheet was also the basis for the comparison between the long-term strains and the predicted strains within the results section of this report.

2.5 Summary

As presented in the reports by Swenty, Sullivan, Bowers, and Badie, there is a definite lack of full-scale bridge research in the areas of shear stud spacing limits and post-tensioning force recommendations. One of the goals of this project was to determine whether Bowers' model for calculating the required level of post-tensioning force is accurate for real-world applications. Her model was tested in the short-term during the post-tensioning operations and in the long-term over the months that the strains in the bridge were monitored. If accurate, Bowers' model could be an efficient and effective way in which many full-depth precast panel bridges can be designed in the future. Another goal of this project was to determine whether Swenty's recommendations for transverse joint design, grouting technique, and overall design were correct and are applicable to real-world structures. Sullivan's research regarding extended shear stud spacing limits was also tested during the live load test was performed once the bridge was constructed. Overall, there is a clear need for this type of research and this project acts as a

continuation and conclusion to the recommendations presented in the research and reports by Swenty, Bowers, and Sullivan.

Chapter 3: Experimental Procedure

The Route 65 bridge is a segmental precast deck panel bridge and was constructed in two phases. In the first phase the installation of traffic lights allowed vehicles to drive over the southern lane as the northern lane was demolished and reconstructed. Once the northern lane was completed, traffic was redirected so that vehicles traveled in the northern lane (Phase I lane) and the southern lane was demolished and reconstructed. After both lanes had been rebuilt, the two sides of the bridge were connected and full two-lane traffic flow was restored. Figure 3-1 shows a side view of the bridge looking north. Figure 3-2 shows a plan view of the bridge with the Phase I construction occurring in the upper lane, and Phase II construction occurring in the lower lane.

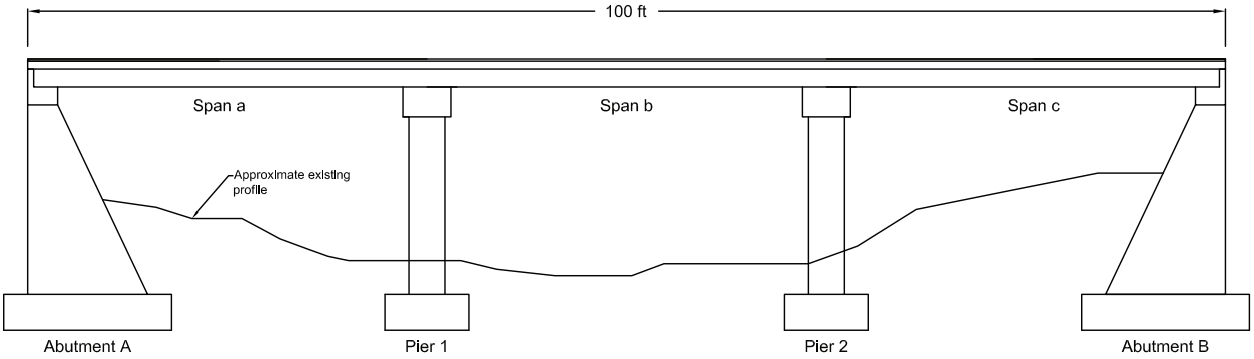

Figure 3-1. Side View of Route 65 Bridge

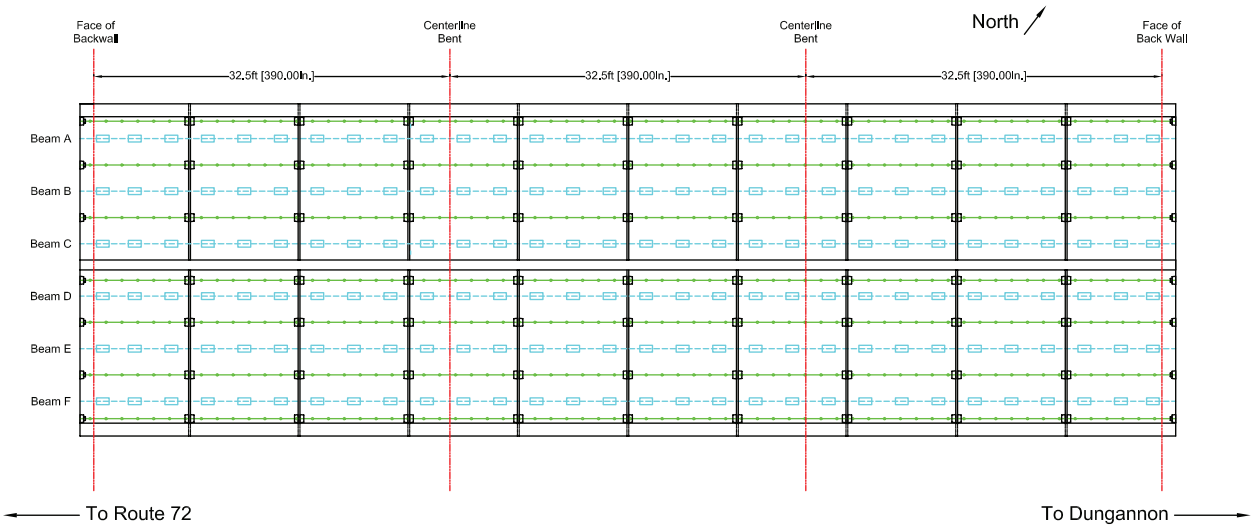

Figure 3-2. Plan View of Route 65 Bridge

The construction during each phase of the project began by removing the old deck and girders. The existing piers, however, were restored and expanded instead of being removed. The girders and cross-bracing members were then installed. The precast panels were set onto the girders and the transverse joints between the panels were grouted. The post-tensioning strands were fed through the ducts and tensioned. The shear studs were welded into the shear stud pockets and grout was poured into the shear stud pockets and into the haunch. Once the grout attained 75% of its ultimate strength the deck and girders were considered to be fully composite. The overlay was then placed on the deck panel surface and the barrier rail was cast. The lane was then opened to traffic.

In an effort to record and understand the long-term structural behavior of the bridge, vibrating-wire strain gauges were installed on the Phase I side of the bridge. The gauges recorded data for eight months, from November 2011 to June 2012. Four of these gauges were installed on the steel girders and four gauges were installed into the deck panels. These gauges were placed at two critical locations along the length of the bridge. They were placed at the panel joint nearest Pier 1 and at the panel joint nearest 0.4*L of the first span (where L is the length of the span between the supports at the backwall

and the interior pier) between Abutment A and Pier 1. The gauge location nearest Pier 1 is 3 ft 9 in. from the center of the pier, and the gauge location near 0.4*L is 8 ft 1 in. from the center of Abutment A. These positions were of importance because one of the main goals of this research is to determine the performance of the deck panel system under maximum moment. The location near Pier 1 will have the maximum negative moment and the location near 0.4*L will have the maximum positive moment.

A short-term live load test was also performed on the bridge in order to study the effects of large and controlled loads in specified positions. This live load test was only conducted on the Phase I side of the bridge. The trucks used during the live load test were at the legal limit of 25 tons. The Phase II side was still under construction and was not yet connected to the Phase I side. A number of temporary gauges were attached to the bridge for this test. These gauges were added to girders and deck in order to give a more complete view of the strain profile throughout the composite deck and girders. The gauges were placed along all three girders in order to compare the strains and deflections of all the members on the Phase I side and determine load distribution among the three girders.

3.1 Desired Data

From the long-term analysis, the collected data is used to characterize the response of the bridge due to events such as the setting and post-tensioning of the panels, but is also used to determine the overall strain re-distribution over time and record any losses due to creep and shrinkage. The four gauges present in panels 2B and 4B are for monitoring post-tensioning force, and the four gauges on beam C are for monitoring effects of strain re-distribution and documenting the forces transferred through the shear stud connectors.

For the short-term live load test, there were a number of goals for the data collected. The first of which was to characterize the behavior of the deck panel joints when subjected to large negative moments. The second goal was to look at the performance of the bridge with respect to composite-action and comparing measured strains and deflections to a predictive model. In order to verify that the post-tensioning and shear stud connections were effective in making the deck and girders act as a single unit, the model was designed with a cast-in-place deck rather than a segmental deck.

3.2 Long-term Gauge Installation

In order to record data over the duration of construction and the life-span of this project, Geokon vibrating wire gauges were selected to be installed both within the concrete deck panels and on one girder within the bridge. This type of strain gauge was selected due to its durability, long-term accuracy and precision, and because each gauge also contains a thermistor for recording temperature.

According to the long-term testing plan, two Geokon 4200 model vibrating wire gauges were installed into the test panel on 9/8/11, and four of the same type of vibrating wire gauges were placed in the into panels 2B and 4B on 9/12/11. As soon as the beams were set in the bridge, four Geokon 4000 model vibrating wire gauges were installed on the interior beam on the Phase I side of the bridge (beam C) on 11/2/11. Data collection began on that date in order to capture the strains induced by placement of the panels. After the panels were set onto the bridge, data collection of all eight installed vibrating wire gauges began on 11/12/11.

3.2.1 Geokon Vibrating Wire Gauges

Geokon model 4200 vibrating wire gauges were placed into the panels and model 4000 vibrating wire gauges were placed onto beam C. Both gauges have a resolution of 1.0 με and an accuracy of ±0.5%. They records strains based on the theory that as the concrete or steel beams deform, the two end blocks move relative to one another. This causes a steel wire contained within the gauge to display an increase or decrease in tension. The wire is then plucked by an electromagnet and the resulting resonant frequency is recorded and converted into a strain measurement. Both of the gauges are waterproof and supply a frequency output which is able to be transmitted over long lengths of wire without any signal degradation. Figure 3-3 and Figure 3-4 present photographs of these two vibrating wire gauges. Note that the only real difference between the 4200 and 4000 models is the way in which the gauges attach to the material they are monitoring.

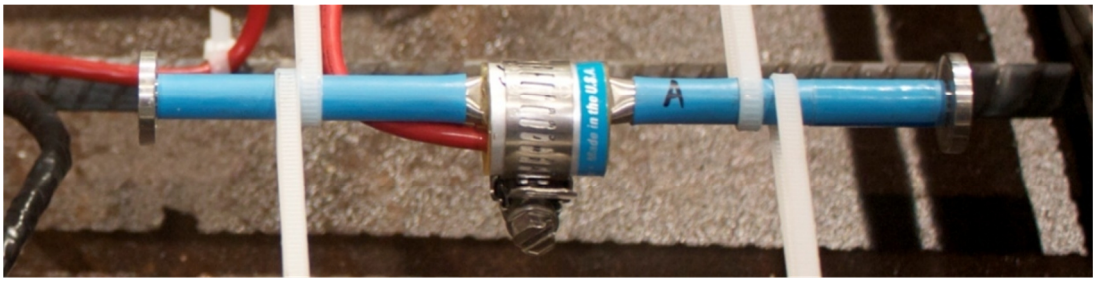

Figure 3-3. Geokon Model 4200 Vibrating Wire Strain Gauge

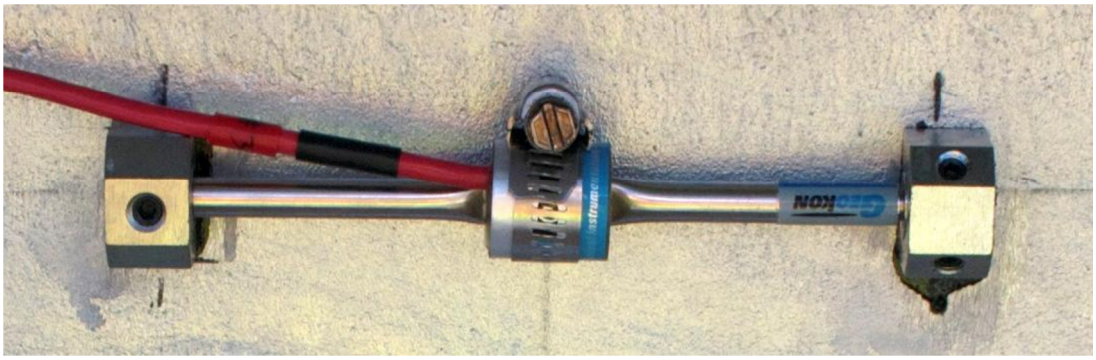

Figure 3-4. Geokon Model 4000 Vibrating Wire Strain Gauge

The 4200 model gauge has fixed end blocks which move with the surrounding concrete, while the 4000 model has detachable end blocks which are either glued or welded to steel. Both models can be read with the GK-403 Readout Box or by a Campbell Scientific data logger. Loctite 410 Instant Adhesive glue was used for both the long-term installation of the 4000 model gauges and for the short-term installation of the BDI strain transducers for the live load test. This glue was chosen due to its strength, weather resistance, and short set time. The placement of 4200 model gauges was performed according to the following diagram. Figure 3-5 clearly defines which panels are to receive vibrating wire gauges and their approximate locations within the panels.

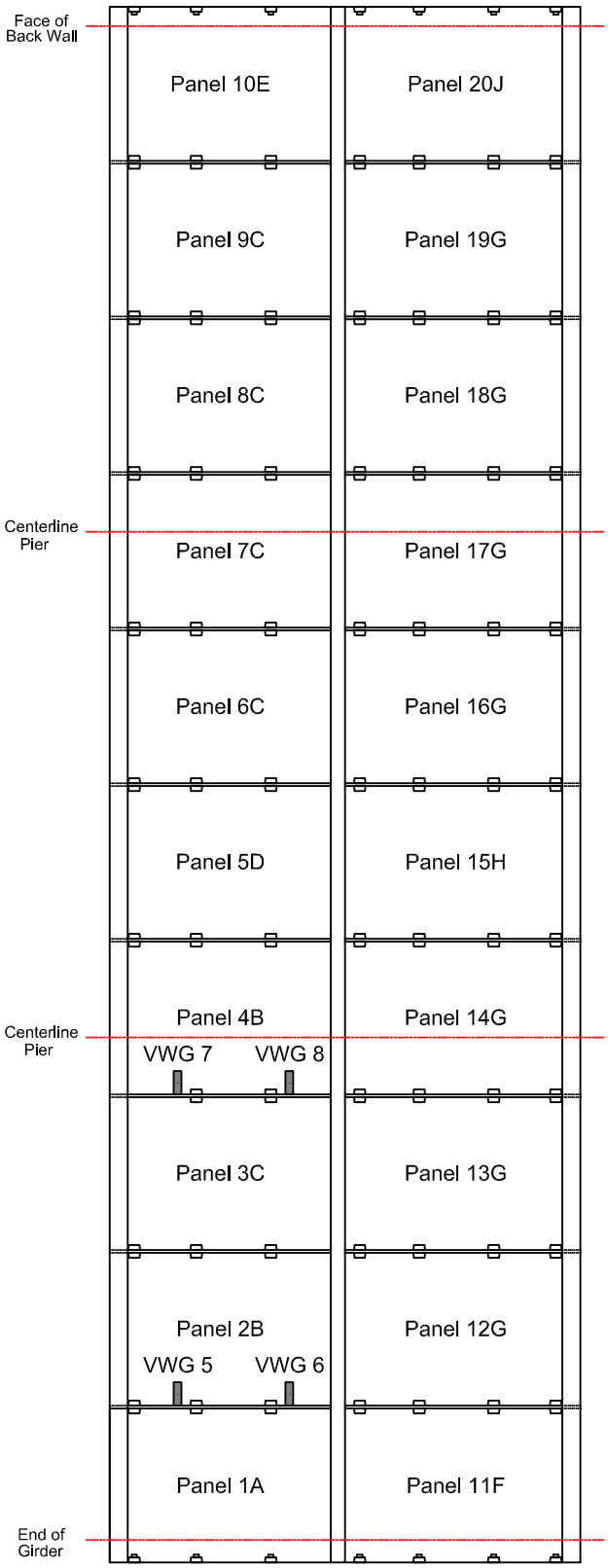

Figure 3-5. Panel Numbering and VWG Location

Figure 3-6 presents a more detailed view of the location of the vibrating wire gauges within panels 2B and 4B, and Figure 3-7 shows the location of the VWGs on beam C. Note that the yellow lines represent prestressing strands, the gray lines represent rebar, the red lines show the shear stud pockets and beam lines, and the green lines show the longitudinal post-tensioning ducts.

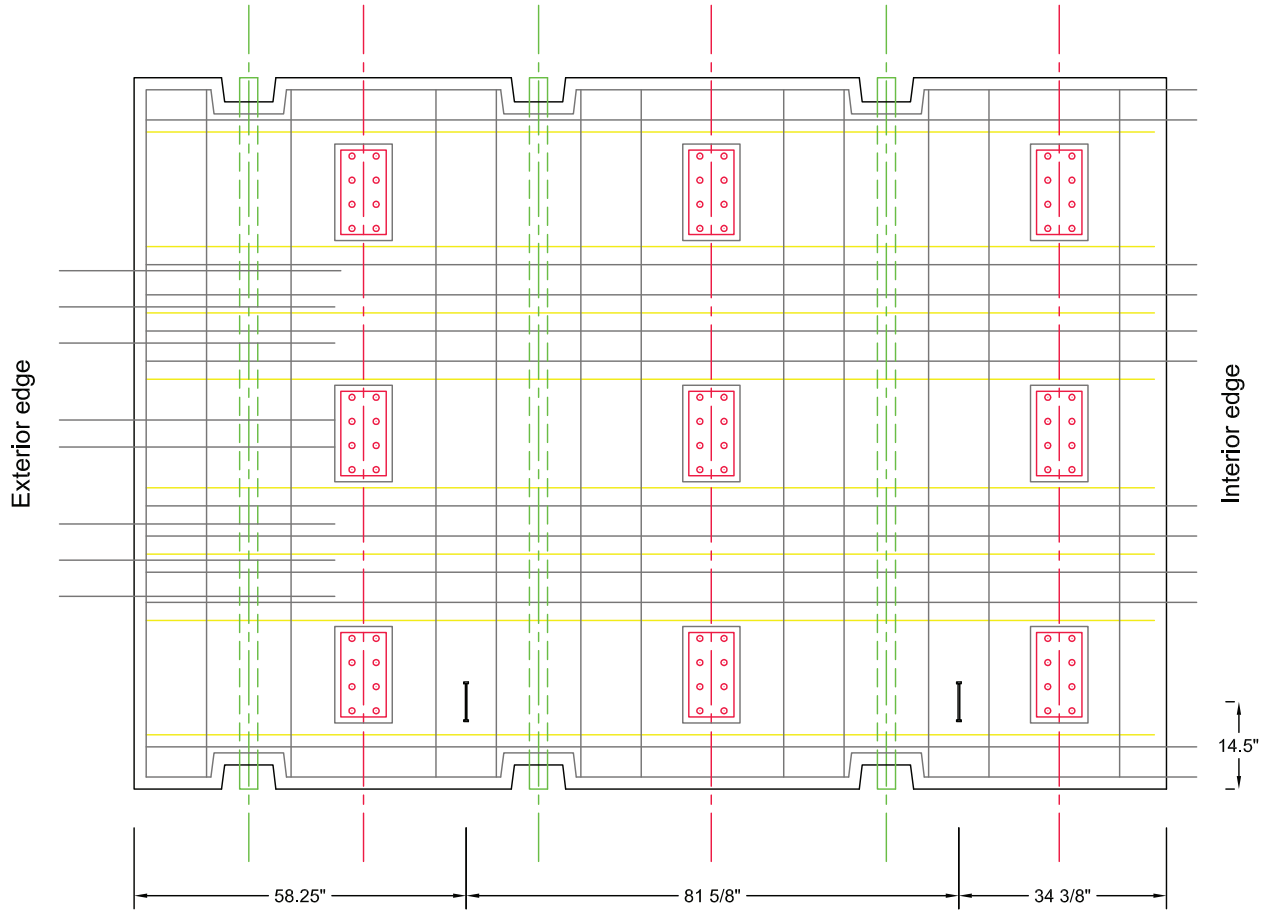

Figure 3-6. Detailed Panel Drawing with Vibrating Wire Gauge Location

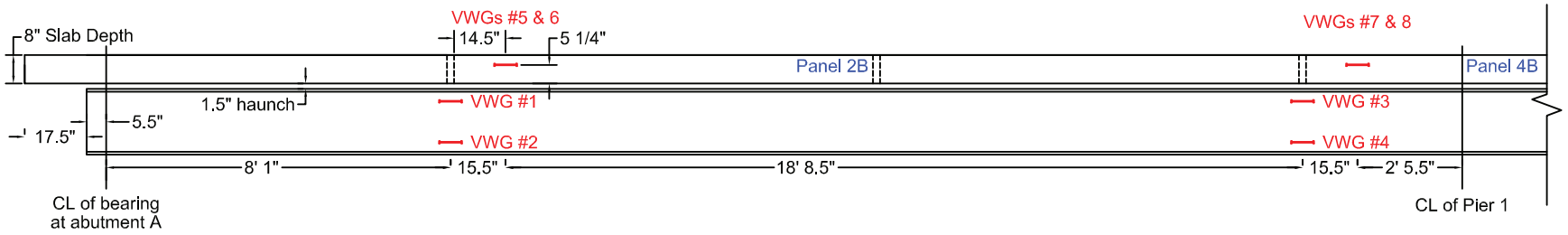

Figure 3-7. Longitudinal Positioning of 4000 Model Vibrating Wire Gauges on Beam C

The 4200 model gauges were held within the top mat of rebar by zip-ties and are approximately 5.5 in. from the bottom of the panel. The wires for these gauges were then run along the rebar and bundled into a foam enclosure that was glued to the bottom of the formwork. This enclosure was placed in such a way that when the panels were put into place in the actual bridge, the wires could be easily accessed from underneath the bridge. Figure 3-8 presents a picture showing the wire enclosure and the short length of wire running from the vibrating wire gauge. Note that within this foam enclosure, the wire ends in a military connector. The military connector was added so that it would be very simple to connect the embedded vibrating wire gauges to the data logger.

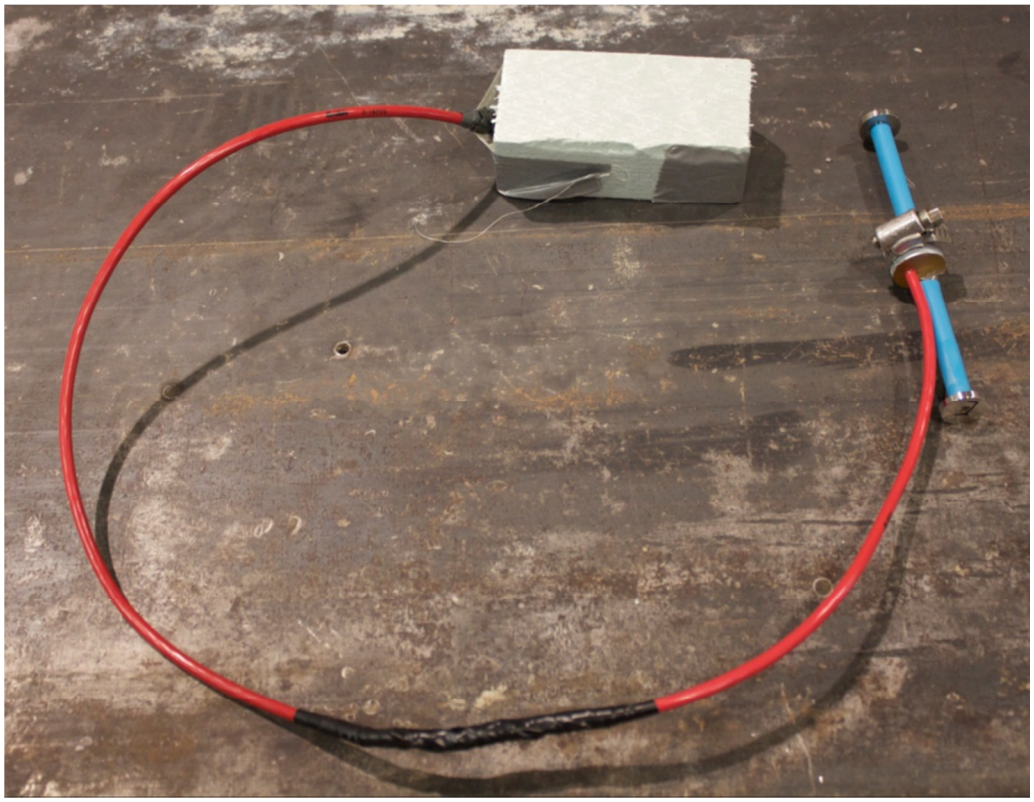

Figure 3-8. 4200 Model Vibrating Wire Gauge and Foam Wire Enclosure

Figure 3-9 shows how the foam enclosure and vibrating wire gauges were placed within the concrete panel formwork.

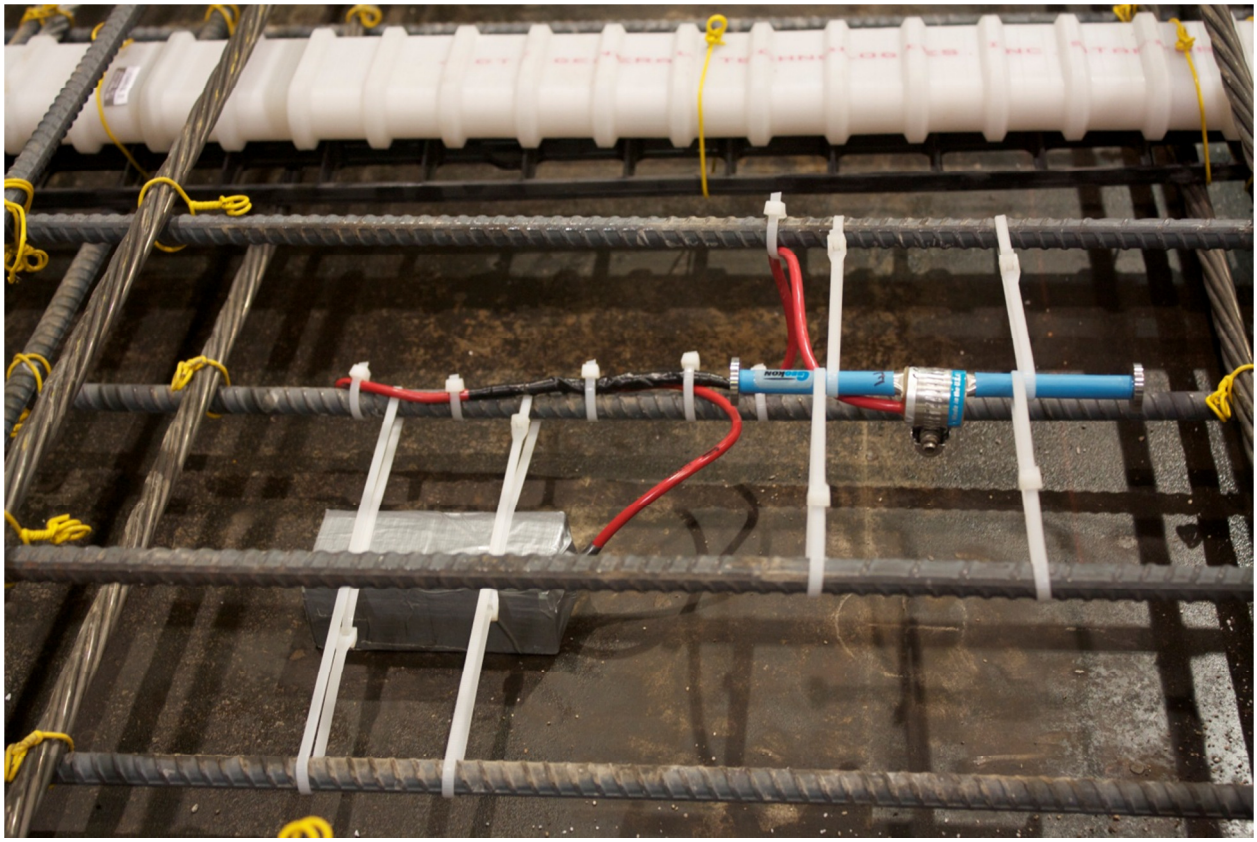

Figure 3-9. Placement of 4200 Model Vibrating Wire Gauge

The foam wire enclosure was wrapped in duct tape to keep out moisture and cement paste, and was attached to the bottom of the steel form by silicone glue.

After the beams had been set on the phase I side of the bridge, the 4000 model vibrating wire gauges were attached to the bridge in the locations shown in Figure 3-7 with a vertical orientation as shown in Figure 3-10.

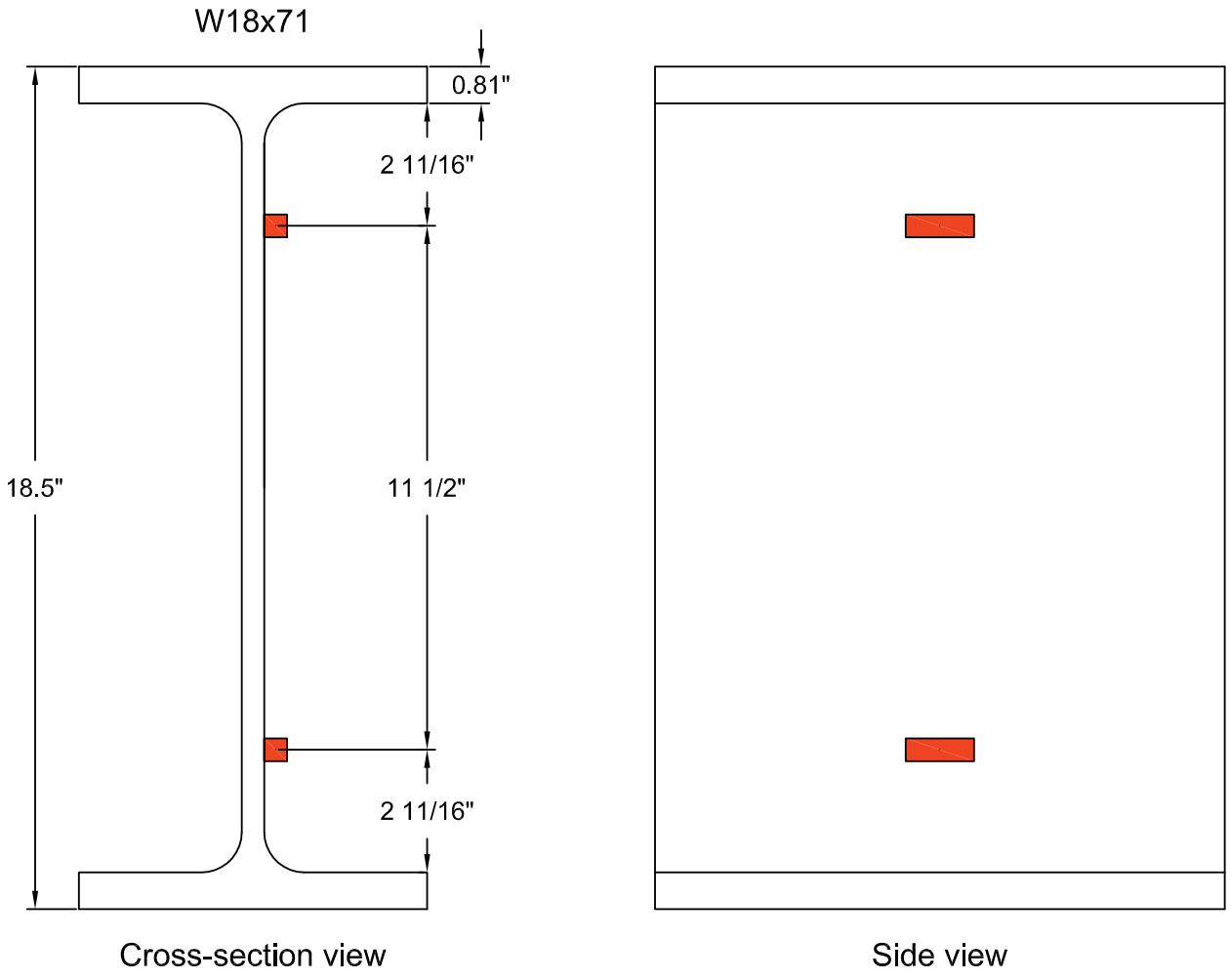

Figure 3-10. Vertical Positioning of 4000 Model Vibrating Wire Gauges on Beam C

Originally, the 4000 model vibrating wire gauges were to be placed on the top and bottom flanges of the beam. This plan was modified due to the larger than expected size of the gauge cover plates. The gauge cover plates help to protect the gauge from physical impacts, tampering, and moderate the temperature differential between the beam and the gauge. A photo of the installed 4000 model gauges is shown in Figure 3-11. A photo of the gauges with the cover plates installed is shown in Figure 3-12.

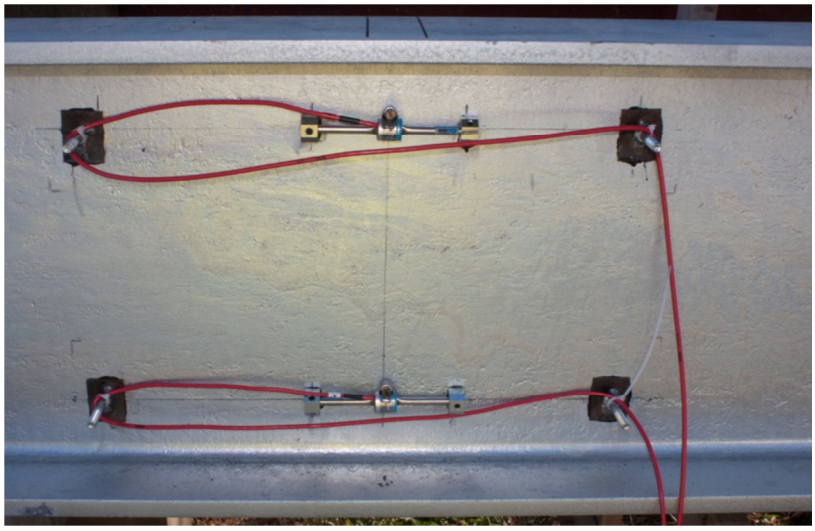

Figure 3-11. Photograph of Installed 4000 Model Vibrating Wire Gauges on Beam C

Figure 3-12. Photograph of Gauge Cover Plates on Beam C

3.2.2 CR23X Data Logger

Once the 4000 model gauges were mounted onto beam C, the wires were run along the top of the bottom flange and over to the western end of the bridge. The wires were then connected to a Campbell Scientific CR23X data logger which was attached to the back wall of the pier as shown in Figure 3-13.

Figure 3-13. Photograph of CR23X data logger on the western back wall

The CR23X has an internal battery which lasts approximately one day when fully charged. The battery is recharged daily by a solar panel attached to a tree approximately 15 yards to the right of the data logger box in the picture in Figure 3-13. The wire for the solar panel was buried a couple of inches below the surface of the ground and runs along the back wall to the data logger. The CR23X has a memory capacity of 2,688 Kb. When collecting data at one reading per hour the device has enough memory to store about one year's worth of data. When data is collected at a rate of one reading per minute, the

data logger can only store approximately one month of data. Data was, however, collected from the CR23X system approximately once per month in order to check that all of the gauges were still reading data and to make sure that nothing had damaged the solar panel.

Overall, the CR23X data logger and Geokon model 4200 and 4000 gauges worked well to monitor the strain changes over time. The data logger's battery which is powered by a solar panel was, however, vulnerable to dropping below the required voltage for taking measurements due to prolonged periods of heavy cloud cover. Throughout the entire time using the device, the recording of measurements only stopped six times. The shortest amount of time the recordings stopped was 5 minutes, while the longest time the recordings stopped was 12 hours. The average amount of time that the recordings stopped when the battery dropped below the required voltage was approximately 5 hours. The Campbell Scientific user manual mentions that measurements would not be taken if the battery dropped below 12 volts, but from field testing, measurements continued to be recorded until the battery dropped below 10.5 volts. See Figure 3-14 for a graph showing the measured battery voltages in blue, and the field proven bottom limit for usability of 10.5 volts in red.

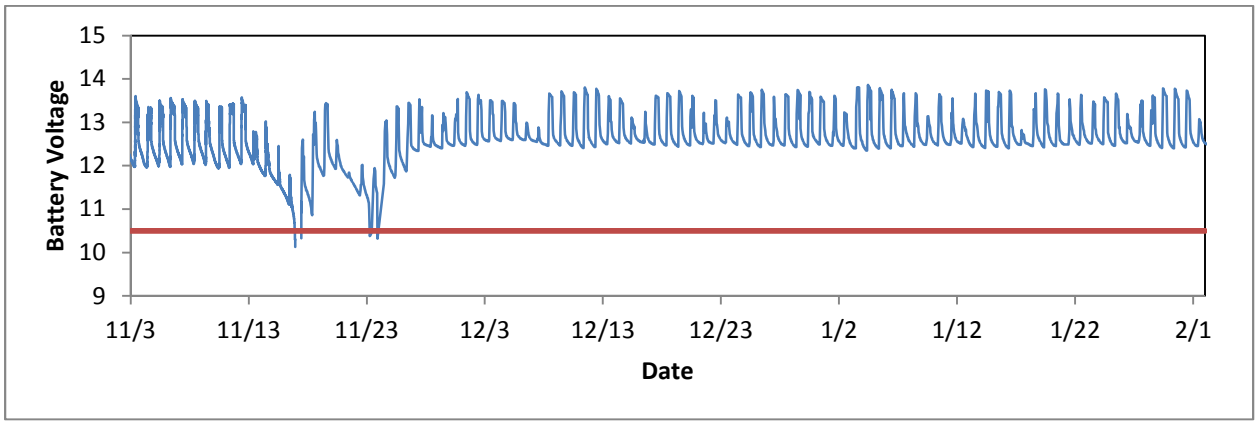

Figure 3-14. Voltage measurements over time

The reason for why the data logger is so slow to record measurements is because the vibrating wire gauges have to be connected to a multiplexer before being connected to the CR23X. The multiplexer physically switches between channels so that each gauge's strain measurement is recorded. The model of multiplexer used is a Campbell Scientific AM16/32a. This physical process of switching between channels takes up time, but also the process in which the wire is plucked and read takes up time as well. The multiplexer is plugged into a vibrating wire gauge interface. The interfacing device is a Campbell Scientific AVW1. It allows the data logger to send the correct signal to read the vibrating wire gauges. Due to this process, it was not possible to read all of the gauges faster than one minute. This means that it takes approximately 7.5 seconds to read each gauge. A wiring diagram for the CR23X and multiplexer is shown below in Figure 3-15.

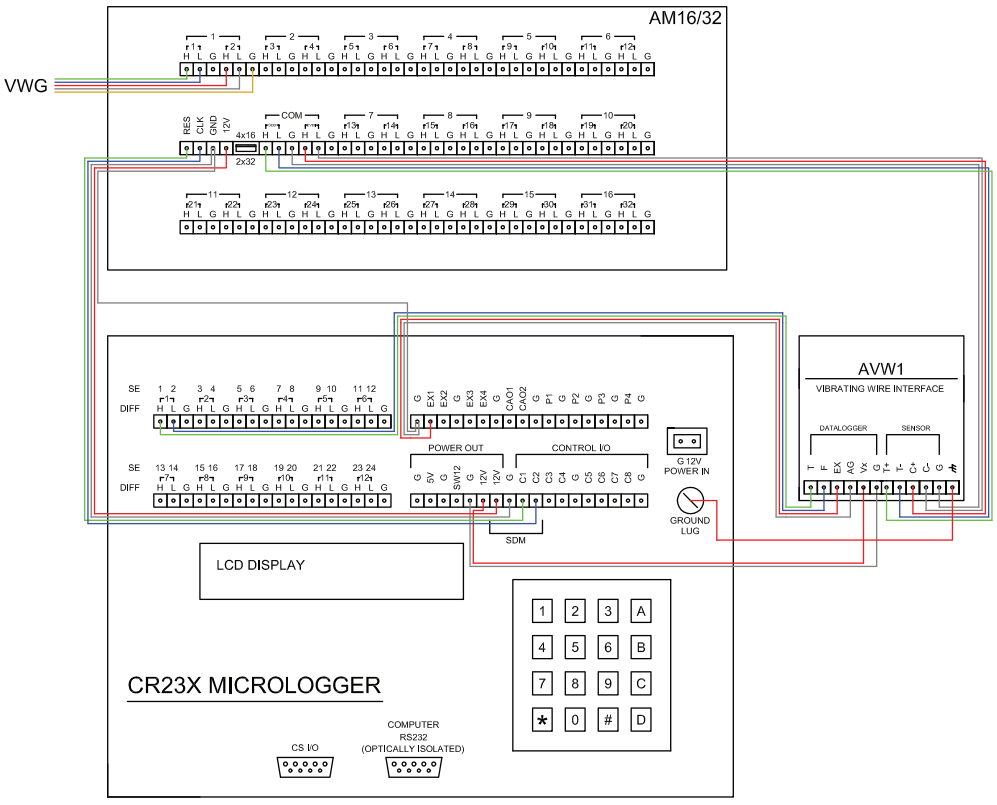

Figure 3-15. Wiring Diagram for CR23X Data Logger (Note that the blue wires are actually white)

In order to collect the data from the CR23X a computer must be physically connected to the data logger via a serial cable. The software used to collect the data is Campbell Scientific's PC200W data logger interfacing program. Collection time ranged from a few seconds to fifteen minutes depending on the amount of data stored on the device. Each time that data was collected, the memory on the device was cleared in order to make room for new measurements and keep the overall size of the data file stored on the device small. The program was written using Notepad, but could be written or edited using any simple text editor. The actual code used with the CR23X data logger is presented in Appendix B.

Data was collected every minute from 11/2/11 to 11/26/11, and collected every hour from 11/26/11 to 2/2/12. Data was collected more rapidly during the first month in order to fully document the strains induced by the post-tensioning and panel setting operations, which were expected to occur over the course of a few hours.

3.3 Short-term Gauge Installation

In order to characterize the structural response of the precast-deck panel bridge system with respect to live loads, a live load test was performed on 2/2/12. There were five different types of gauges used during the live load test. The vibrating wire gauges already installed were used during the live load test along with deflectometers (twangers), BDI strain transducers, linear variable differential transformers (LVDTs), all of which were installed onto the bridge the morning of the test. One 350Ω strain gauge was also used during the test as a way to synchronize data between data collection devices and provide markers in the data showing where the truck was positioned. The locations of all the gauges used during the live load test are shown in Figure 3-16 on the next page.

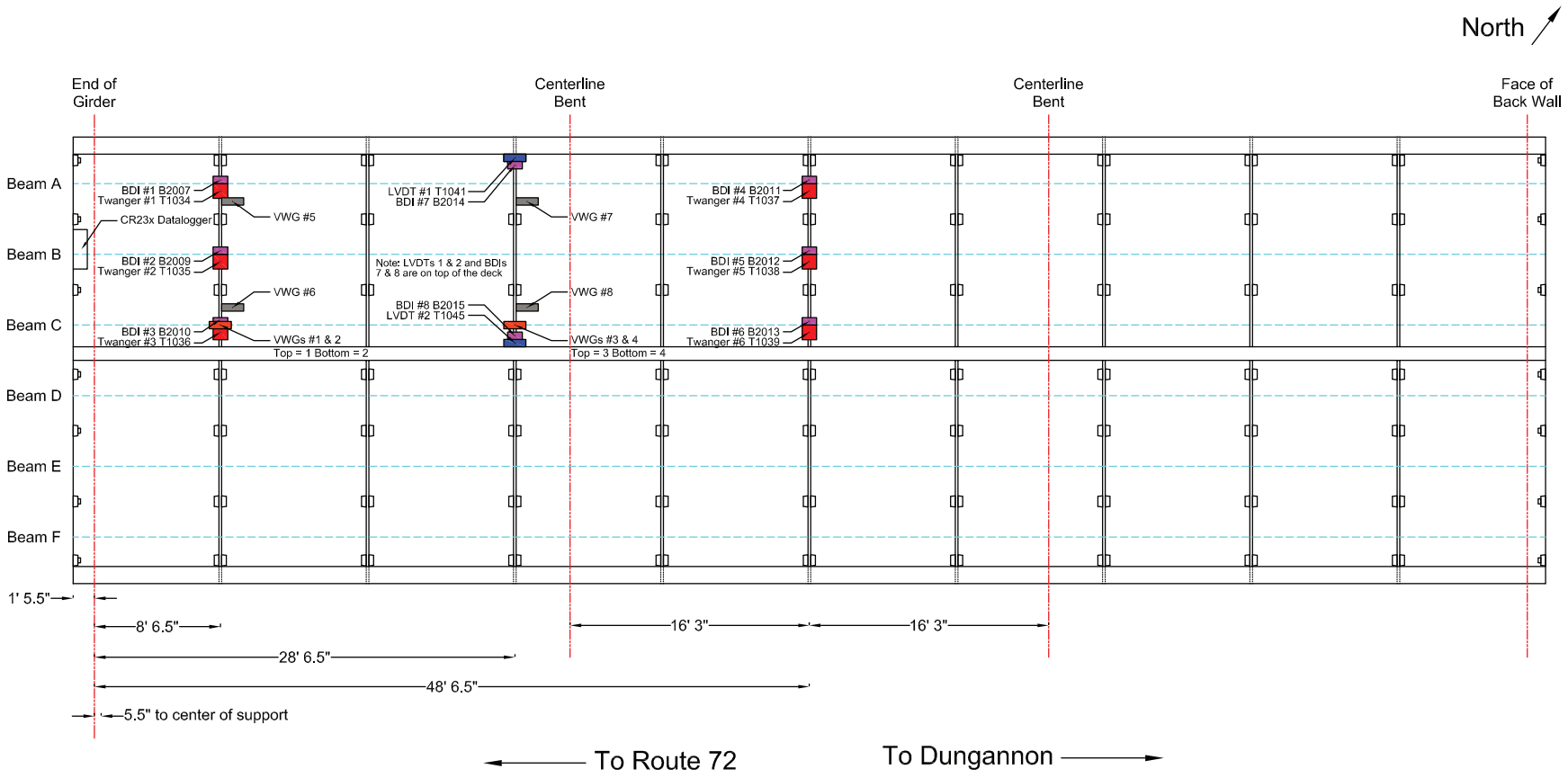

Figure 3-16. Gauge Layout for Live Load Test

3.3.1 BDI Strain Transducers

Eight BDI (Bridge Diagnostics Inc.) strain transducers were used during the live load testing of the Phase I side of the bridge. Six were placed on the bottom of the three girders to record strains in the longitudinal direction of the bridge. The BDI strain transducers are designed for short-term applications because they are easy to attach and remove, are very durable, and are simple to collect data from using BDI Wifi Data Collector System. Figure 3-17 is a photograph of a BDI strain transducer on the bottom of a beam.

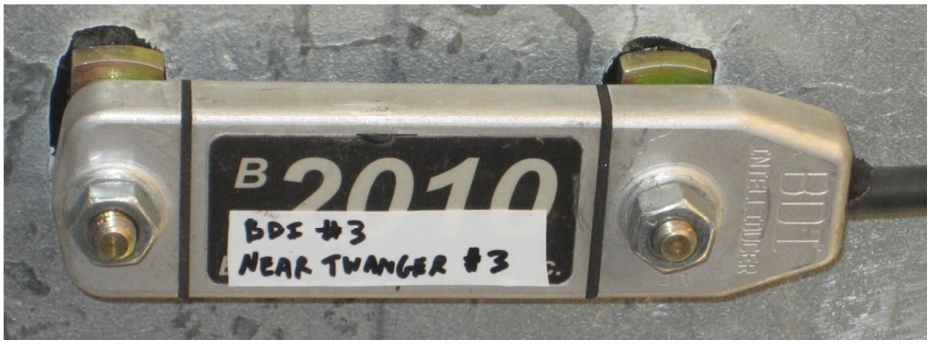

Figure 3-17. Photograph of BDI Strain Transducer

The BDI strain transducers can be attached to both concrete and steel surfaces and are typically applied using some type of instant adhesive. The glue is applied to the bottom of small metal tabs which are connected to a threaded rod which is secured to the BDI gauge by a pair of nuts. These nuts can be unscrewed at the end of testing so that the gauge is not damaged during removal of the tabs. The glue that was used to attach the BDI gauges was the same glue that was used for the long-term installation of the gauges (Loctite 410 glue and Loctite 7452 accelerator).

Within the strain transducer case there is a full-wheatstone bridge with four active foil strain gauges. The circuit is completed within the gauge itself, which means that the cable length does not affect the strain reading recorded by the data logger. The transducers come calibrated from the factory and are accurate within ±2%.

The gauges were placed longitudinally at the bottom of each girder along the joint between panels 1A and 2B, and panels 5D and 6C, as depicted in Figure 3-16. Also, BDI gauges were placed on top of the deck above the joint between panels 3C and 4B. The gauges were placed in these locations in order to verify predictions about elastic neutral axis location and load induced strain distributions. The panel joint between 1A and 2B is the closest joint to 0.4L of the first span, which is the theoretical location of maximum positive moment in the bridge. The panel joint between 5D and 6C is at the center of the middle span, which also has very large positive moments. The panel joint between panels 3C and 4B is the closest joint to a pier, which means that it has the highest negative moment. The BDI gauges on top of the deck also served to monitor the strain at the joint.

3.3.2 Deflectometers (Twangers)

Deflectometers (commonly referred to as twangers) are devices specially fabricated at Virginia Tech which measure vertical deflection of the girders. They consist of a triangular sheet of metal sandwiched between two thick rectangular plates. A full-bridge strain gauge is attached to the triangle piece of metal just outside of the sandwiched section. The two rectangular plates are attached to the bottom of the girder by two 4 in. C-clamps. The tip of the triangular section is then pulled down using a heavy gage wire attached to a 6 in. x 12 in. concrete cylinder weight. As the bridge deflects, the rectangular plates move with the bottom of the girder while the tip of the rectangular section is held stationary by the

weight. The measurements recorded by the strain gauges can then be converted into inches of deflection. The twangers were calibrated in the lab to 0.001 in. and have an effective range of 1 in. Figure 3-18 presents a photograph showing a twanger attached to one of the beams in the bridge.

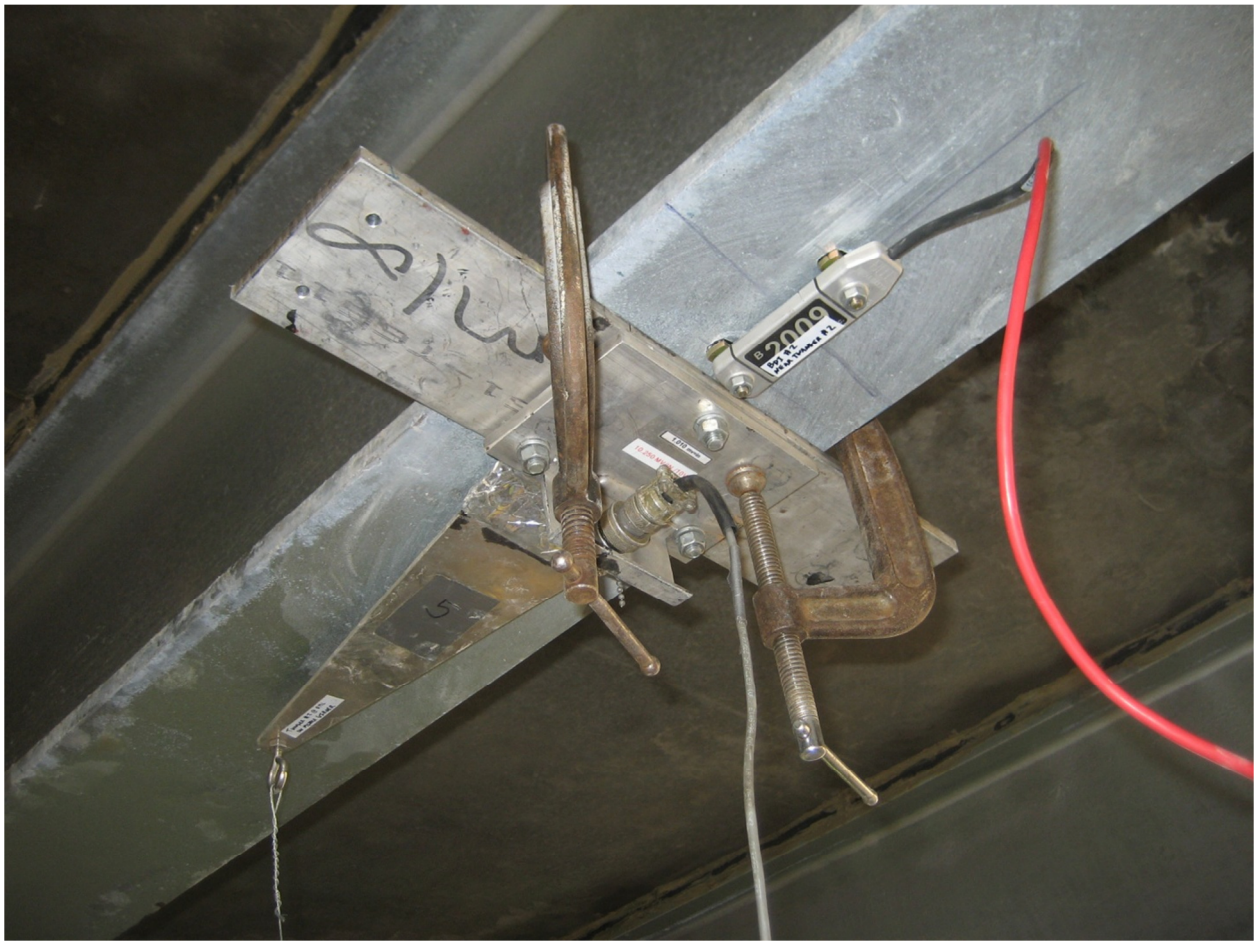

Figure 3-18. Photograph of Twanger Attached to Bottom of Girder

Note that the twangers were placed approximately 2 in. from the exact location of the panel joint. The twangers were slightly off-center because it was not possible place the twangers and the BDI gauges at exactly the same point, and since the BDI gauges are more sensitive than the twangers, it was determined that the twangers would be offset a couple of inches.

3.3.3 Linear Variable Differential Transformer (LVDT)

There were two LVDT's used during the live load test. The LVDTs are Trans-Tek series 350 DC-DC Gaging Transformers. They were placed above the joint between panels 3C and 4B. This location is of particular interest because it is the panel joint with the largest negative moment. If there was a point in the bridge where a crack would form between panels under extreme truck loads, this is where it would occur.

The LVDT is a gauge with a plunger-type rod which can be pushed inwards or pulled outwards. It is this relative displacement that is measured in mV and converted into inches. The LVDT provided a very accurate way in which to measure small displacements with an effective range of only 0.1 in., but it was calibrated to 0.001 in. in the lab. The LVDT was held in place above the crack by two L-shaped brackets. One bracket held the LVDT by securing it with a nut on either side of the bent up plate. The other acted as the back stop for the plunger rod. Before the live load test began, the plunger rod was placed halfway through its range so as to collect data for expansions and contractions of the deck surface. Figure 3-19 presents a photograph showing the placement of an LVDT on the interior side of the bridge deck. Note that only two gauges were used on top of the deck because there were only two locations to put gauges where cars would not hit them: on the interior side of the temporary guard rail and under the permanent Kansas corral style permanent guard rail.

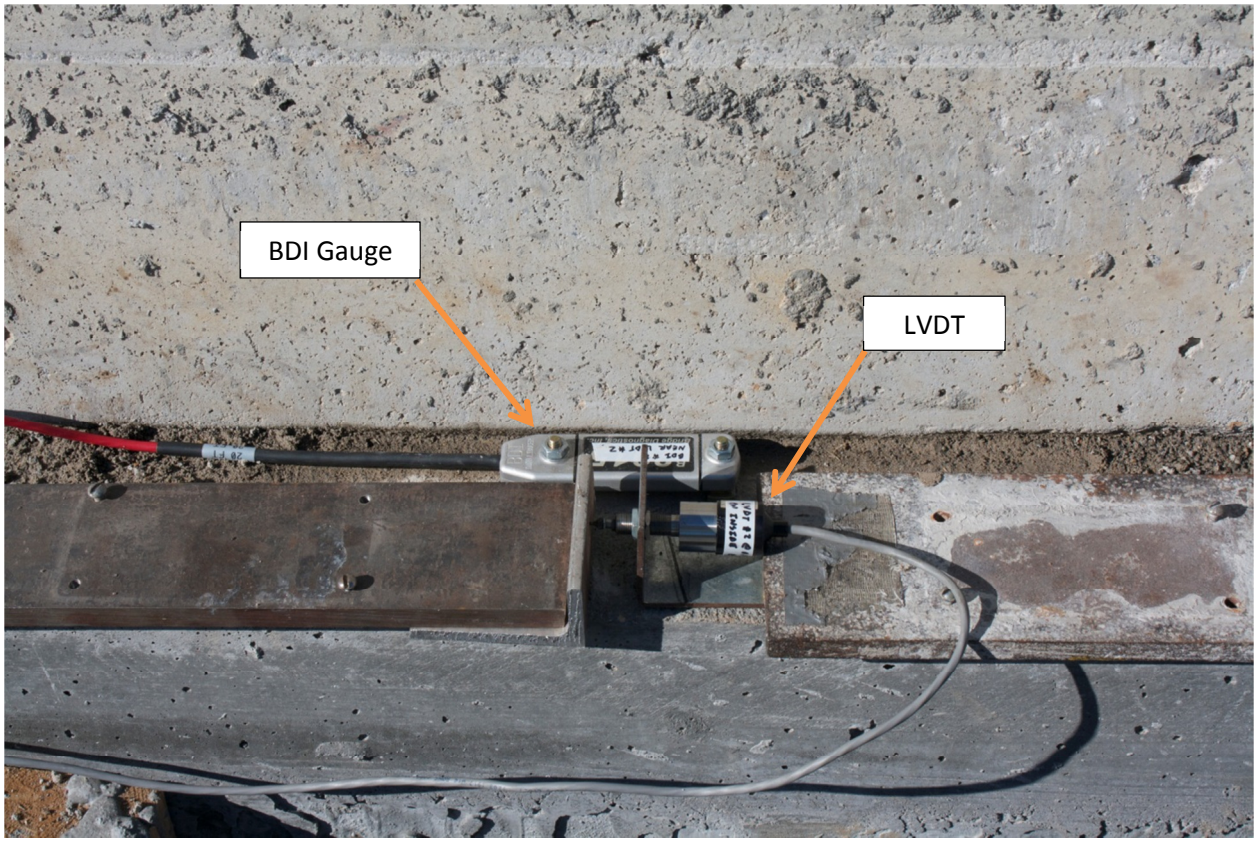

Figure 3-19. Photograph of LVDT Setup on Interior Edge of Panel

3.3.4 BDI STS-Wifi

The BDI STS-Wifi (Strutural Testing System) is a data collection system designed for use during live load tests and other short-term testing applications. The system consists of six nodes, one router, and one laptop computer. The gauges are plugged into the nodes. Each node has four plug adapters, all of which must be filled for the node to be operational. The nodes make a wireless connection to the router which then sends the collected data to a laptop, also through a wireless connection. The data can then be monitored and saved as a text file using the WinSTS3408 software program. Overall, the system is very simple to use. Each intelliducer plug can connect to any node and will still show up in the software with the correct calibration factor and label. The batteries in the nodes and router will last for

over six hours of continuous testing. The nodes and router can also be powered by an AC adapter if the batteries do run out. Figure 3-20 and Figure 3-21 present photographs showing the router and a node, into which two BDI strain transducers and two twangers are plugged in using the intelliducer adapter.

Figure 3-20. Photograph of STS-Wifi Router

One of the greatest advantages of using the Wifi system is that cable lengths for each of the gauges are significantly shortened. With the systems used for live load tests prior to the Wifi system, cables had to run from the gauge all the way to the data logger. This resulted in hundreds of feet of tangled wires draped over the bridge. With the Wifi system, the cable lengths are kept to about 15 ft, as they only need to run from the gauges to the node. The wireless signal can travel 300 ft without any obstructions. The Wifi signal distance is, however, cut considerably if it passes through concrete or any other type of solid material. The Wifi signal will not, however, pass through steel beams or solid steel plates.

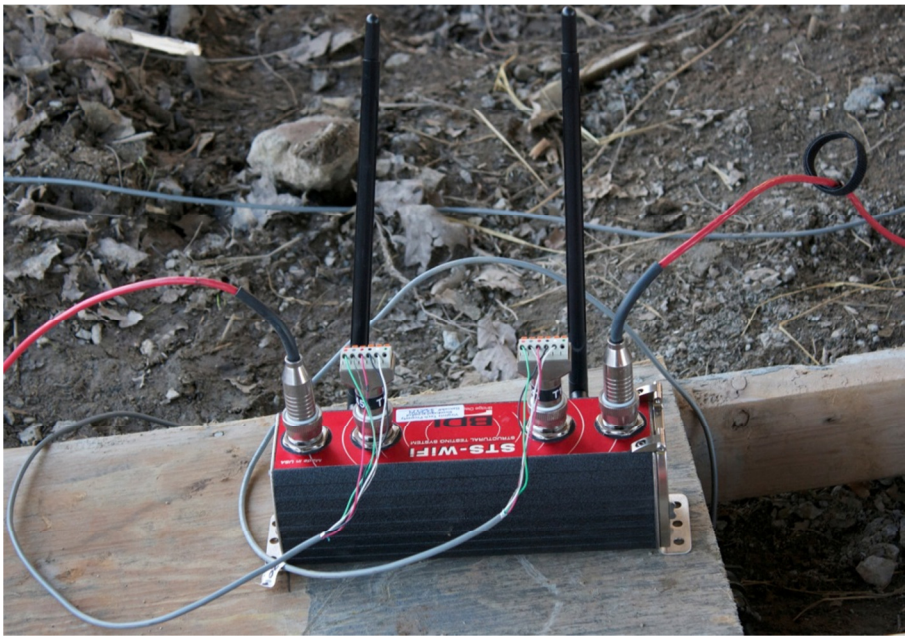

Figure 3-21. Photograph of a STS-Wifi Node

The Wifi system works seamlessly with all of the BDI strain transducers, the other gauges required an intelliducer adapter in order to connect to the nodes. It was through the use of this adapter that the twangers, LVDTs, and clicker were connected to the nodes. While the BDI strain transducer calibration data was already programmed into the software, each gauge which used the intelliducer adapter needed to be calibrated through a process of plotting the mV output with the actual deflection measured by a calibration device. The slope of that line was then recorded in the software as the calibration factor. The calibration data for all of the gauges is located in Appendix C. Figure 3-22 is a screen shot of the WinSTS3408 software used during the live load tests.

One of the limitations of the Wifi system is that it has a limited capability to read types of gauges not manufactured by BDI. Standard quarter-bridge and full-bridge strain gauges, and LVDTs work with the system, but it is not able to read vibrating wire gauges. This required that during the live load test runs,

there needed to be two data logger systems running simultaneously. In order to synchronize the data, the clicker was plugged into both the system reading the vibrating wire gauges and the Wifi system. It was also important to use the same data collection rate of 50 Hz for each device.

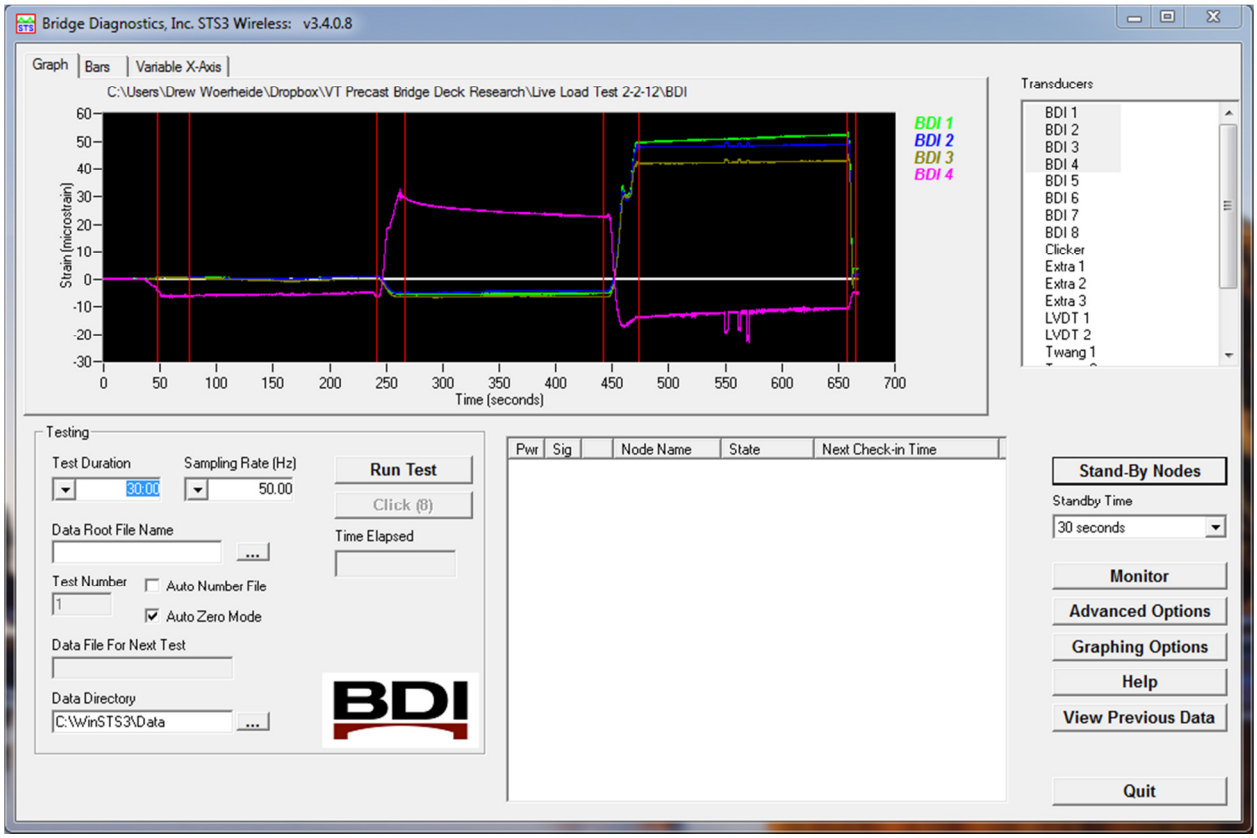

Figure 3-22. WinSTS3408 Software Program Interface

3.3.5 CR3000 Data Logger and CR23X

Strain data was collected from the eight vibrating wire gauges during the live load tests with the Campbell Scientific CR23X and the CR3000 data logger systems. Both systems were necessary during testing because both systems had limitations. The CR23X system's limitation was that it could not read all eight vibrating wire gauges faster than once per minute. This meant that it could be used for static load tests but not for dynamic load tests. The limitation of the CR3000 system was that, while it could read the vibrating wire strain gauges much faster at 50Hz, it had not previously been used during a live load test in the field. This meant that it was necessary to repeat a number of static tests already completed using the CR23X so that the data could be compared to make sure that the CR3000 system was functioning properly and accurately. A photograph of the CR3000 data logger is shown in Figure 3-23.

Figure 3-23. Photograph of CR3000 Data Logger

3.3.6 Truck Location Strain Gauge Marker (Clicker)

In order to synchronize the data recorded by the two different data loggers used during each live load test run and to document the location of the middle tire of each truck, a strain gauge clicker device was built in the lab. The "clicker" consists of a small section of steel packing strap and two 350 Ω quarter-bridge strain gauges. The strain gauge wires could be plugged into two different data logger systems so that when the steel strap was temporarily bent, there was a spike in the strain measurements recorded at the same time on each data logger. This allowed for each data set to be shifted in time such that the data could be matched up to one time-scale. The strain spikes also showed the position of each truck, which was especially important for the crawling and at-speed moving tests. Each of the two strain gauges had approximately 50 ft of wire so that it was possible for the person "clicking" to move with the truck as it drove across the bridge. A photograph of the "clicker" used for the live load test is shown in Figure 3-24.

Figure 3-24. Photograph of the Clicker Device

3.4 Short-Term Test Loading Procedure

The live load test occurred on Thursday February 2, 2012. The test runs consisted of running trucks of known weight over the bridge at a set speed for the dynamic tests, or parking the trucks at different locations along the bridge for the static tests. The dynamic tests were all performed with a single truck on the Phase I side of the bridge. The static tests consisted of two runs in which a single truck stopped in three different locations across the bridge, and six runs in which two trucks stopped particular locations to maximize the negative moment across the joint between panels 3C and 4B. Figure 3-25 presents the different truck locations which will be referred to in this section. Note that the red and green lines are the locations for the middle axle of the three axle dump trucks used during the live load test.

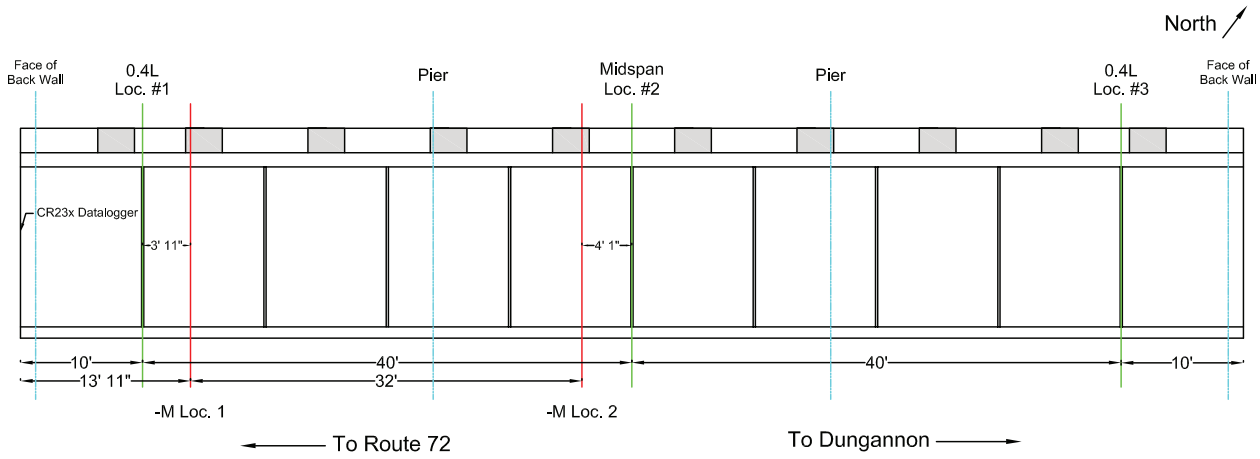

Figure 3-25. Live Load Test Truck Positions

A crew of four VT graduate students arrived at the bridge construction site on the day of the test at 8 AM. The students attached all of the deflection and strain measuring instruments, and the actual live load runs were performed from 1 PM until 4 PM. After the live load test, the temporary instruments were removed from the bridge.

3.4.1 Truck Description

The two trucks used for the live load test were dump trucks provided by VDOT. Each truck was loaded with stone and weighed approximately 27 tons. The weight of the trucks was distributed with 30% of the weight on the front axle and 70% on the back two axles. A diagram showing the wheel spacing and the measured weights of each axle is shown in Figure 3-26. Note that, while not visible in Figure 3-26, the width between the left and right side lines of tires is 6 ft.

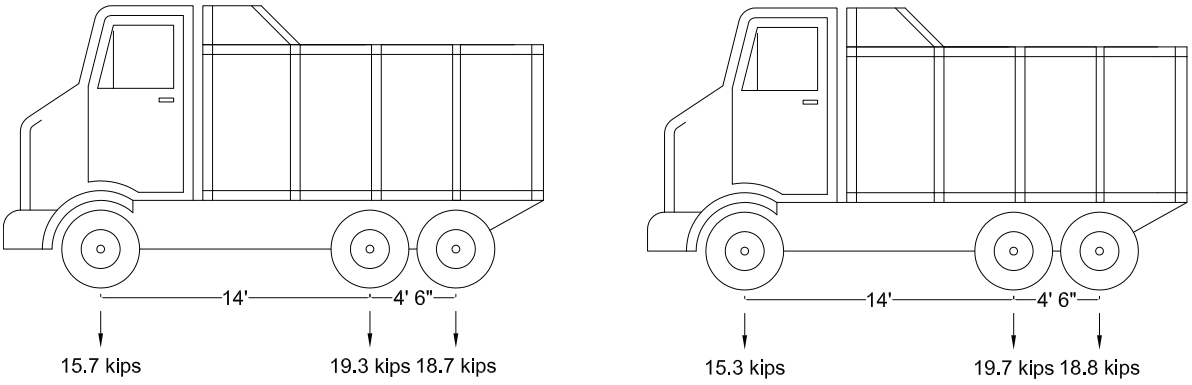

Truck #R08880 Truck #R05328

Figure 3-26. Truck Dimensions and Weights

The truck weights and dimensions of each truck were so similar that for the calculations average values were used for the front axle, middle axle, and rear axle were taken as 15.5 kips, 19.5 kips, 18.75 kips respectively.

3.4.2 Live Load Truck Runs

There were three different types of test runs performed on the Route 65 Phase I side of the bridge. There were eight static loadings, and eight dynamic loadings. Many of the runs were repeated a number of times in order to verify results. The first type of test run was performed during run #1 and run #5. In these runs the truck began on the East end of the bridge and stopped with the middle axle at the joint nearest to 0.4L of the third span (Loc. #3), midspan of the middle span (Loc. #2), and the joint nearest 0.4L of the first span (Loc. #1). The same truck was used for both runs (Truck #R05328). The difference between these two runs was that in run #1 the data was collected by the CR23X and STS-Wifi data loggers, and in run #5 the data was collected by the CR3000 and STS-Wifi data loggers. This meant that in run #1 the truck stopped at each location for two minutes, while the truck only stopped for 10

seconds at each of the three locations during run #5. The purpose for these two runs was to compare the measurements made by the CR23X and the CR3000, and to measure static load related strains in order to compare to the dynamic tests. If the two systems were measuring drastically different strains, the CR23X would be assumed to be more accurate because it has been used many times before, and the planned dynamic load runs would have been replaced with some other combination of static loads in which strains could be measured by the CR23X. Figure 3-27 shows the three locations the truck stopped.

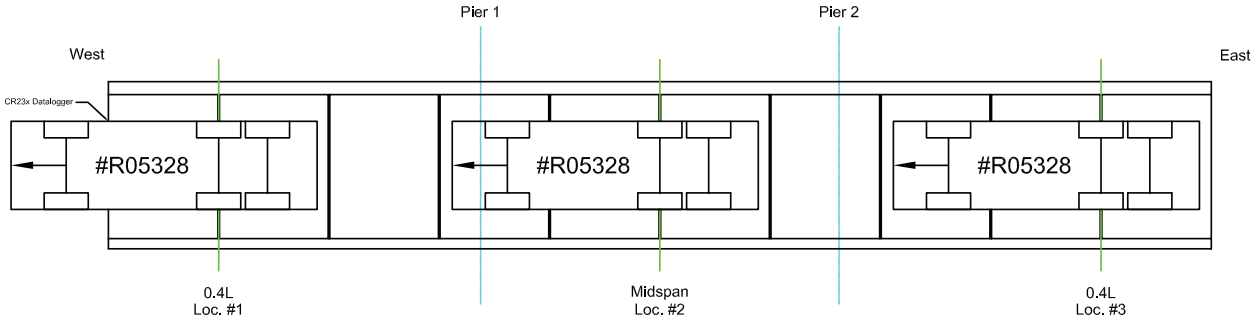

Figure 3-27. Stopping Locations for Runs 1 and 5

The second type of test run was performed during runs 2-4 and 6-8. In these tests, both trucks were moved onto the bridge and parked with the middle axle at the two locations calculated to create the maximum negative moment over the joint between panels 3C and 4B over the western pier. The trucks were placed facing away from each other with the rear two axles nearest to the joint. Runs 2-4 were recorded using the CR23X and STS-Wifi data loggers, and runs 6-8 were recorded using the CR3000 and STS-Wifi data loggers. The two trucks were in the same locations for each run and the only difference was that the trucks were parked for a much shorter time during runs 6-8 than during runs 2-4. Figure 3-28 shows the positions of the two trucks during runs 2-4 and 6-8.

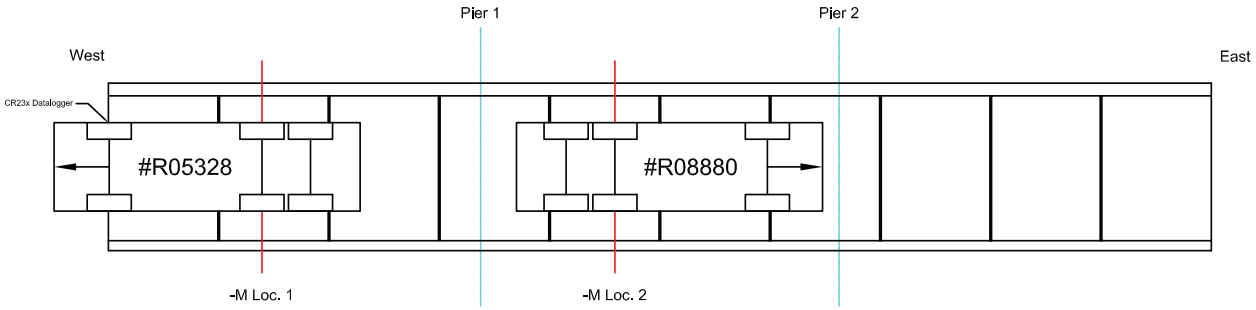

Figure 3-28. Stopping Locations for Runs 2-4 and 6-8

The third type of test run was performed during runs 9-12. Runs 9-12 are similar to runs 1 and 5 except that the trucks were moving throughout the entire test, rather than stopping at different locations. Each run is split between an A and a B run. Truck #R05328 was run over the bridge during the A runs and truck #08880 was run over the bridge during the B runs. Runs 9a, 9b, 10a and 10b were at crawling speeds, which typically means the trucks are driving between 1 and 2 miles per hour across the bridge. Runs 11a, 11b, 12a, and 12b were at the speed limit, or as fast the truck driver felt comfortable driving. The other difference between runs 9 and 11 when compared to runs 10 and 12 is that in runs 9 and 11 the trucks were driving from East to West, and in runs 10 and 12 the trucks were driving form West to East.

During the static load tests the “clicker” was strained when the trucks came on the bridge, when the trucks stopped in position, before the trucks left the position, and when the trucks were off of the bridge. During the crawling speed dynamic load tests the “clicker” was strained when the trucks came on the bridge, when the middle tire passed through 0.4L location #1, midspan location #2, 0.4L location #3, and when the trucks left the bridge. During the at-speed dynamic tests the “clicker” was strained when the trucks came on the bridge, when the trucks passed through the center of the bridge, and when the trucks left the bridge. The clicker data was especially important for the dynamic tests because it allowed for calculating the position of the truck throughout the run, while also calibrating the two

data loggers. Figure 3-29, Figure 3-30, Figure 3-31, Figure 3-32 and show the directions in which the trucks moved across the bridge during each dynamic test. Table 3-1 presents a quick reference guide for each of the 12 truck runs.

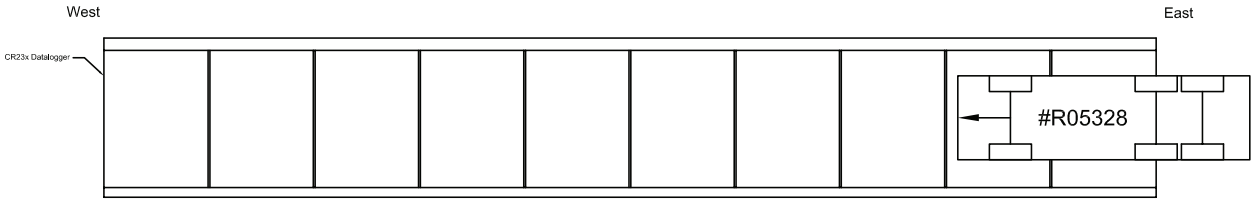

Figure 3-29. Truck Direction for Runs 9a and 11a

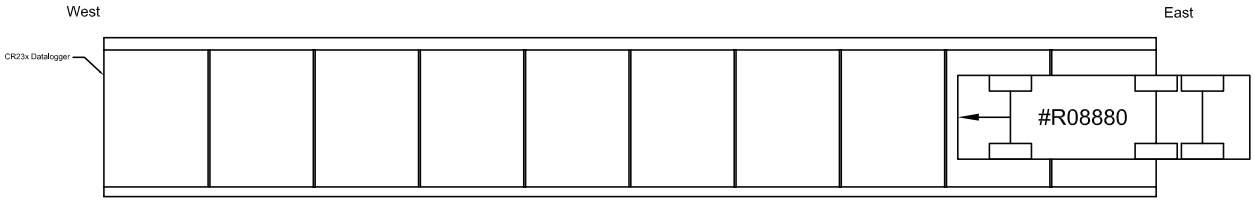

Figure 3-30. Truck Direction for Runs 9b and 11b

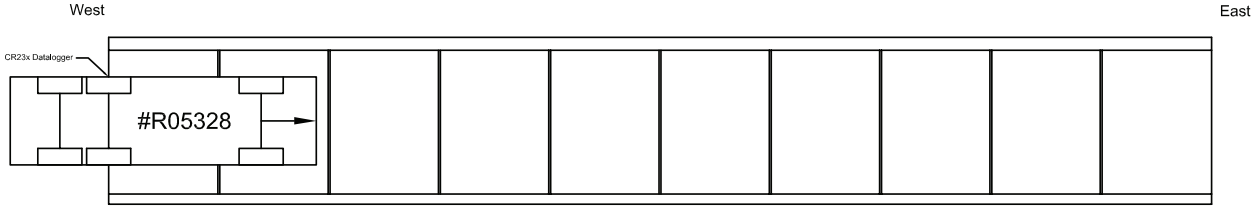

Figure 3-31. Truck Direction for Runs 10a and 12a

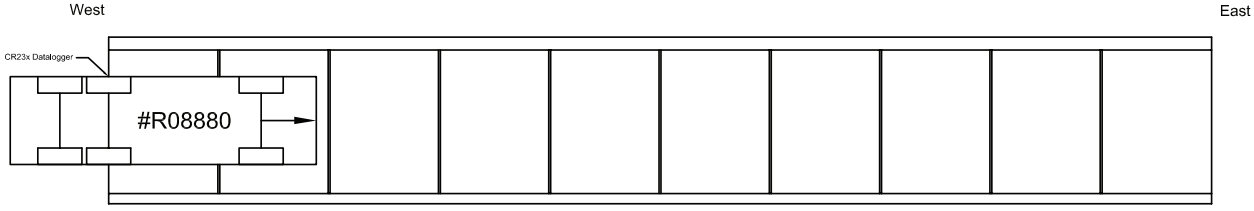

Figure 3-32. Truck Direction for Runs 10b and 12b

Table 3-1. Truck Run Quick Reference Guide

Run #	Run Type	Record Freq.	Truck #	Direction	Data Loggers
1	Stop at Loc. 1, 2, 3	1/min	R05328	E to W	BDI Wifi & CR23X
2	Static -M Test	1/min	R05328 & R08880	N/A	BDI Wifi & CR23X
3	Static -M Test	1/min	R05328 & R08880	N/A	BDI Wifi & CR23X
4	Static -M Test	1/min	R05328 & R08880	N/A	BDI Wifi & CR23X
5	Stop at Loc. 1, 2, 3	50 Hz	R05328	E to W	BDI Wifi & CR3000
6	Static -M Test	50 Hz	R05328 & R08880	N/A	BDI Wifi & CR3000
7	Static -M Test	50 Hz	R05328 & R08880	N/A	BDI Wifi & CR3000
8	Static -M Test	50 Hz	R05328 & R08880	N/A	BDI Wifi & CR3000
9a	Crawling	50 Hz	R05328	E to W	BDI Wifi & CR3000
9b	Crawling	50 Hz	R08880	E to W	BDI Wifi & CR3000
10a	Crawling	50 Hz	R05328	W to E	BDI Wifi & CR3000
10b	Crawling	50 Hz	R08880	W to E	BDI Wifi & CR3000
11a	At Speed Limit	50 Hz	R05328	E to W	BDI Wifi & CR3000
11b	At Speed Limit	50 Hz	R08880	E to W	BDI Wifi & CR3000
12a	At Speed Limit	50 Hz	R05328	W to E	BDI Wifi & CR3000
12b	At Speed Limit	50 Hz	R08880	W to E	BDI Wifi & CR3000

Chapter 4: Modeling Assumptions and Procedure

In order to validate and understand the results of the long-term and short-term testing procedures, it was necessary to create preliminary models to approximate the behavior and response of the bridge beam and deck panel system. Calculations were performed for the setting of the precast deck panels on the beams, post-tensioning of the deck, long-term strain distribution, and the live load test. The modeling results will be compared to measured values in Chapter 5.

4.1 Material Properties

In order to properly model the bridge and accurately predict the change in strains and stresses over time, material tests were performed in the months following the casting of the panels. Concrete cylinder strength, shrinkage bars, modulus of elasticity, and expansion coefficients were all recorded.

The concrete used in the precast deck panels was required to have at least 4000 psi strength before releasing the prestressing strands, and 6000 psi strength by 28 days. The concrete that was used in the panels was self-consolidating concrete, which greatly helped in evenly distributing the concrete throughout the panels and around the complicated rebar mats. All panels met the required strength of 4000 psi before releasing the strands, and based on tests of concrete samples at the Virginia Tech Structures Lab, the concrete had reached strengths above 6000 psi by 28 days. Table 4-1 presents the average values of two concrete cylinder strength measurements from the concrete used in panels 2B and 4B. It is apparent from Table 4-1 that the concrete strength at the time of the live load test was approximately 7000 psi.

Table 4-1. Concrete Cylinder Strength

Day	Date	Strength I (psi)	Strength II (psi)	Avg. Strength (psi)
14	9/26/2011	6760	6570	6670
28	10/10/2011	6760	6490	6630
60	11/11/2011	7320	6880	7100
180	3/10/2012	7040	6960	7000

The splitting tensile strength was also measured on two cylinders on the 28th day. There was no specified tensile strength requirement, but the results from the lab tests are shown in Table 4-2.

Table 4-2. Splitting Tensile Strength

Day	Date	Avg. Tensile Strength (psi)
28	10/10/2011	600

A modulus test was also performed on the concrete samples. The test occurred 98 days after casting. The estimated value of E (modulus of elasticity) of the concrete using equation 4-1 below was calculated to be 4415 ksi.

$$E = 57\sqrt{f'c} \tag{4-1}$$

The results from the modulus test showed the concrete having a much higher modulus of elasticity of 6287 ksi. The strain and loading data collected during the modulus are shown below in Figure 4-1. The results of this test were confirmed by tests performed on multiple concrete cylinders.

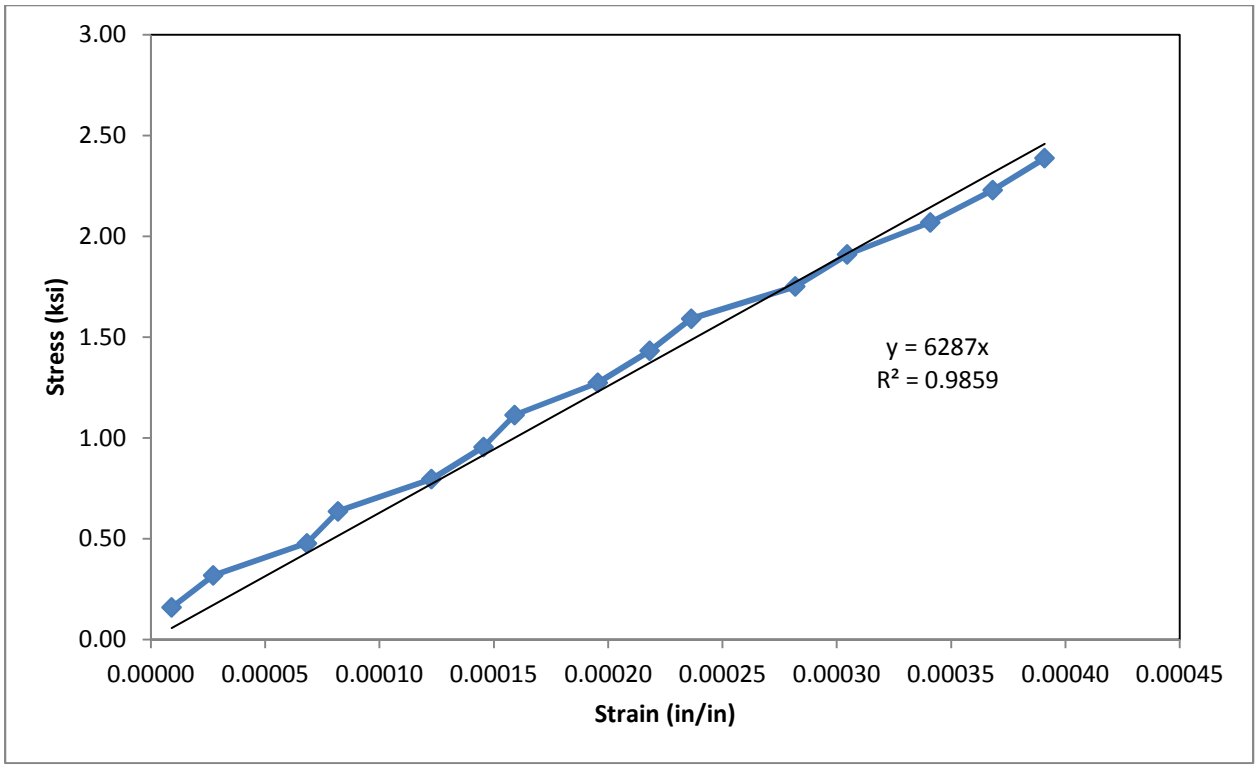

Figure 4-1. Results from Modulus Test on Concrete Cylinder Sample

Shrinkage bars were also monitored for 180 days after casting, with measurements taken every day for the first week and then less frequently after that. The measured shrinkage was compared with the ACI 209 shrinkage modeling equations. The results of the ACI 209 shrinkage model and the measured shrinkage strain are shown in Figure 4-2. The shrinkage strain calculations are located in Appendix G.

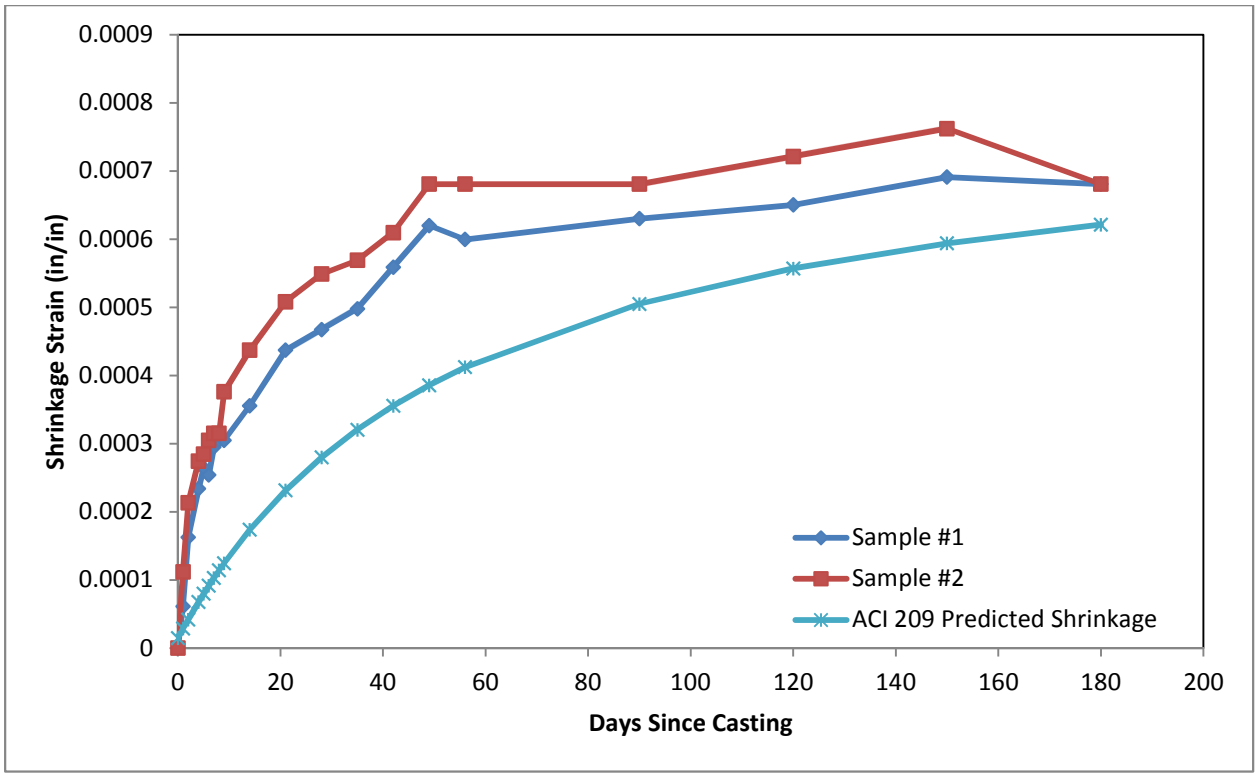

Figure 4-2. Shrinkage Bar Measurements and ACI 209 Shrinkage Prediction

The ACI 209 model predicts reasonably well the final magnitude of the shrinkage strain, but tends to underestimate the rate at which the shrinkage occurs. Measurements show that the shrinkage strain remains constant after about 50 days. In the ACI 209 model, the shrinkage strain is only about 66% of the ultimate strain at 50 days.

The coefficient of thermal expansion (CTE) for the concrete was also examined. The lengths of two shrinkage bars were measured at room temperature (22°C), -19.5°C, and 63.1°C. The changes in strain were then plotted versus temperature, with the slope of the lines equal to the CTE (με/°C). The value given for the CTE of concrete by the Geokon VWG user's manual is 10 με/°C, and the CTE given for steel is 12.2 με/°C. As shown in Figure 4-3, the measured value for the CTE for concrete was determined to be approximately 11.6 με/°C. This means that the concrete and the steel have a much closer expansion

rate, and will, therefore, have less of a strain differential than predicted by Geokon at varying temperatures.

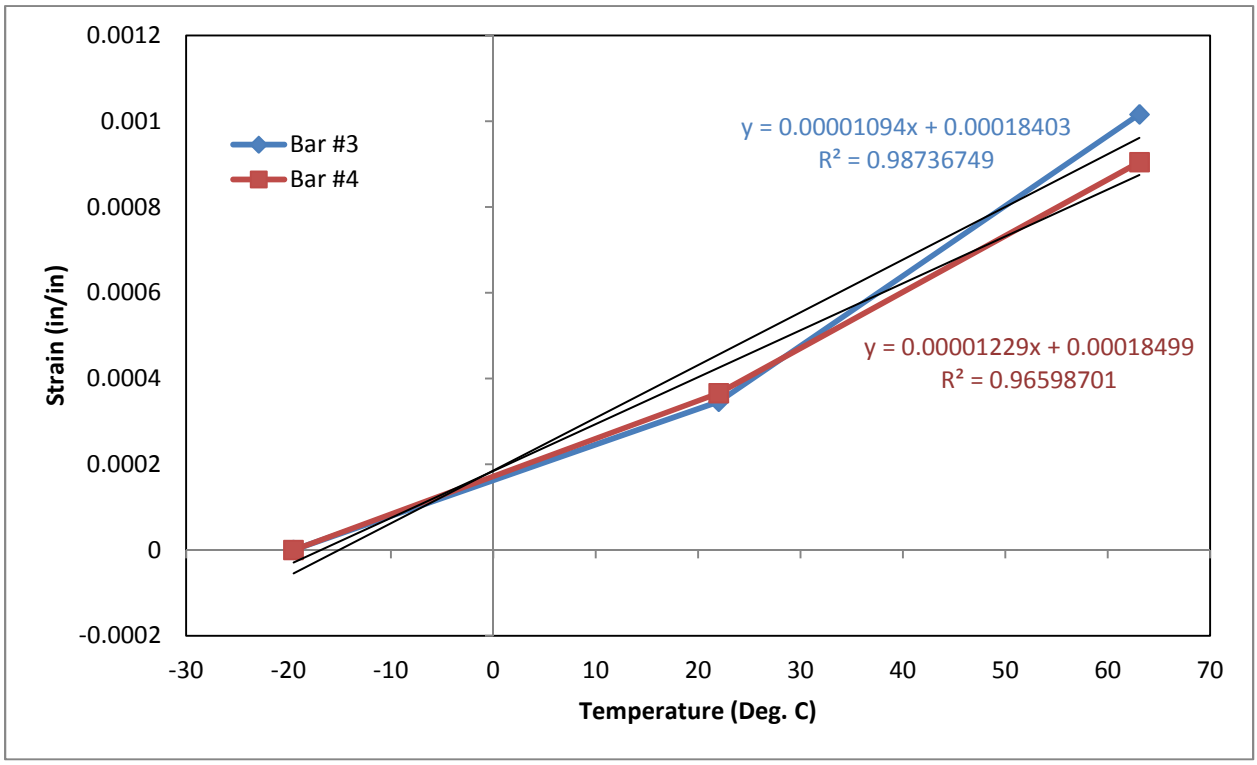

Figure 4-3. Measured Strain vs. Temperature

4.2 Predicting Strains due to Deck Panel Loads

In order to verify that the strain gauges were installed correctly and that the bridge was responding in a predictable manor, a simple model was created which consisted of a bridge beam with a distributed load modeling the precast deck panels. The deck panels, which were 14 ft 3 in. in the transverse direction and approximately 10 ft in the longitudinal direction of the bridge, were calculated to have a weight of approximately 15,000 lbs per panel. This weight was transformed into a distributed load to be applied along the length of the beam. This distributed load was divided among the three beams in two different ways. In the first model, the weight was divided evenly into the three beams. The second model divided the load proportionally based upon the tributary width for each beam. The tributary width was determined by dividing the spacing between the beams in half. Due to the overhang on beam A, and the lack of any overhang on Beam C, the loads were not the same on each beam. The distributed load on Beam C, when the weight was divided evenly, was 0.042 kip/in, and when the load was divided proportionally the distributed load was 0.0336 kip/in. The difference between these loadings is due to the fact that, based on tributary width, Beam C only receives 26.8% of the panel weight, but when divided evenly Beam C received 33.3% of the panel weight.

Once the loading on beam C was determined, the moment was calculated at the two locations along the length of the beam where the vibrating wire gauges were installed. The moments were calculated using SAP2000. The input loads and resultant moment diagrams from SAP2000 for both loading assumptions are shown in Figure 4-4 and Figure 4-5.

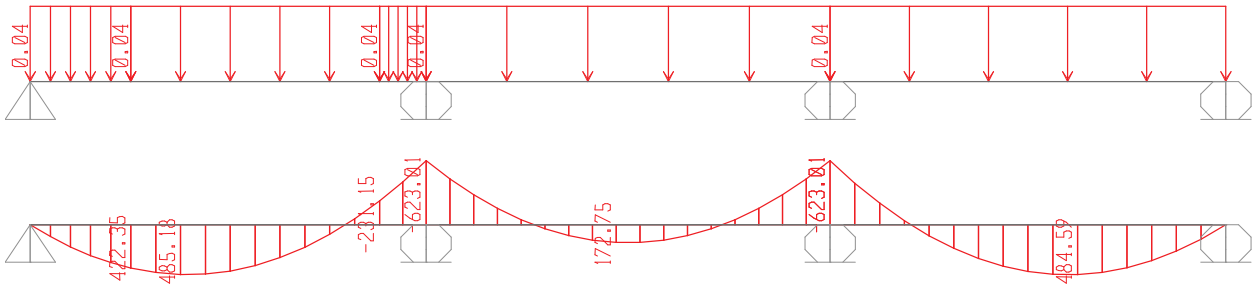

Figure 4-4. Input Loads and Moment Diagram for Evenly Divided Loading Scenario

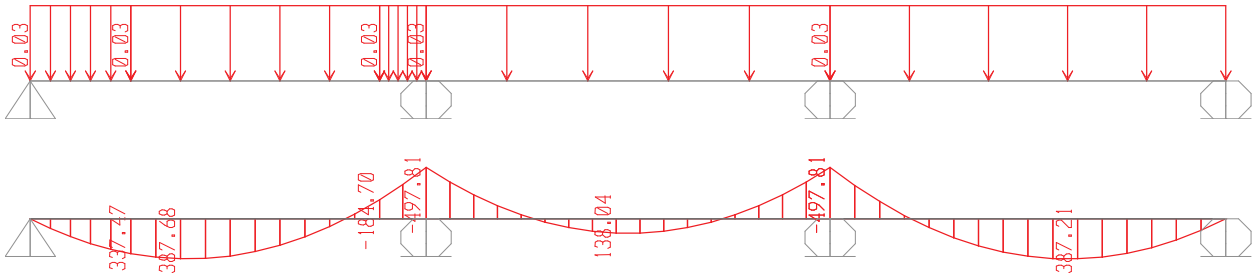

Figure 4-5. Input Loads and Moment Diagram for Proportionally Divided Loading Scenario

After calculating the moments along the length of beam C, the strains at the four different vibrating wire gauges were calculated using the Equation 4-2:

$$\varepsilon = \frac{My}{EI} \tag{4-2}$$

The y distance for gauges 1 and 3 (the gauges near the top of the beam) is -5.75 in, and the y distance for gauges 2 and 4 (the gauges near the bottom of the beam) is 5.75 in. This sign convention ensures that there are positive values for tensile strains and negative values for compressive strains. The modulus of elasticity (E) for the steel beam is 29,000 ksi, and the moment of inertia about the strong axis for the W18x71 beam is 1,170 in^4. The strains calculated by this procedure are presented in Table 4-3 and Table 4-4. Note that these gauges are located on beam C and are shown in detail in Figure 3-7.

Table 4-3. Predicted Strains due to Evenly Split Deck Panel Loads

	VWG 1 (με)	VWG 2 (με)	VWG 3 (με)	VWG 4 (με)
Predicted Strain	-72	72	39	-39

Table 4-4. Predicted Strains due to Proportionally Split Deck Panel Loads

	VWG 1 (με)	VWG 2 (με)	VWG 3 (με)	VWG 4 (με)
Predicted Strain	-57	57	31	-31

These calculated values were compared to measured strains in order to evaluate the portion of the load carried by Beam C. The load distribution is further affected by the use of the leveling bolts, which were designed to distribute the panel loads evenly to the girders before the haunch is cast. The calculations and results for the strains due to deck panels loads are contained in Appendix D.

4.3 Predicting Strains due to Post-tensioning

The amount of strain imposed through post-tensioning was predicted analytically and compared to measured strains to verify that the panels received sufficient post-tensioning force and to confirm that the vibrating wire gauges were functioning properly. Due to non-symmetric duct positioning as shown in Figure 4-6, the strains at the two gauges were assumed to be different and that there was a significant horizontal stress gradient across the panel. In the vertical direction, however, there was assumed to be no stress gradient within the 8 in. height of the panel due to the concentric post-tensioning.

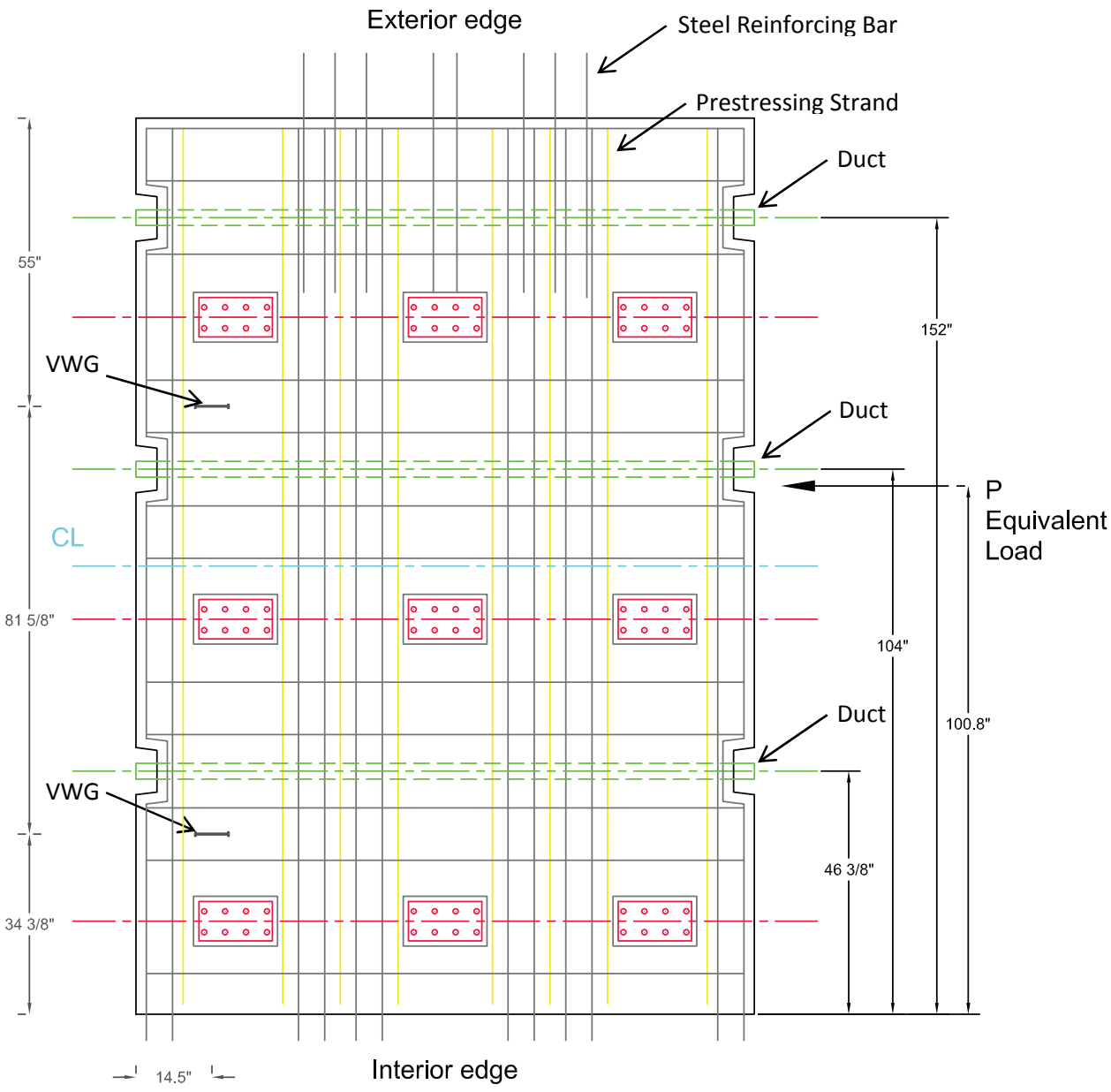

Figure 4-6. Post-tensioning Ducts and VWGs Locations

One of the first steps in calculating the strain gradient was determining the location for an equivalent post-tensioning force point load. The point load was determined to be 100.8 in. from the interior edge of the panel, which is 15.3 in. from the longitudinal centerline, closer to the exterior edge of the panel as shown in Figure 4-6. The VWG nearest the exterior edge of the panel has an eccentricity of 30.5 in. from the middle of the panel, and the VWG nearest the interior edge of the panel has an eccentricity of -51.1 in. The equation used to calculate the stress at the gauge locations is shown below in Equation 4-3:

$$\sigma = \frac{P}{A} + \frac{Pey}{I} \tag{4-3}$$

The cross-sectional area of the panel (A) was approximately 1368 in^2, the moment of inertia of the panel was 3,333,474 in^4, and the modulus of the panel was 4415 ksi determined by lab tests. The stress in each strand along the length of the bridge was interpolated from the post-tensioning graph submitted by Dywidag-Systems International (DSI). This graph was based upon an initial stress of 189 ksi, a wobble coefficient of 0.001 rad/ft, and an assumed seating loss of 0.38 in. The stresses at 1/20th points along the span are shown below in Figure 4-7, with the live end at 0 and the dead end at 1. The strands were stressed to 70% of the gross ultimate tensile strength (270 ksi) according to Swenty's design calculations. For reference, the total length of the bridge is 100 ft.

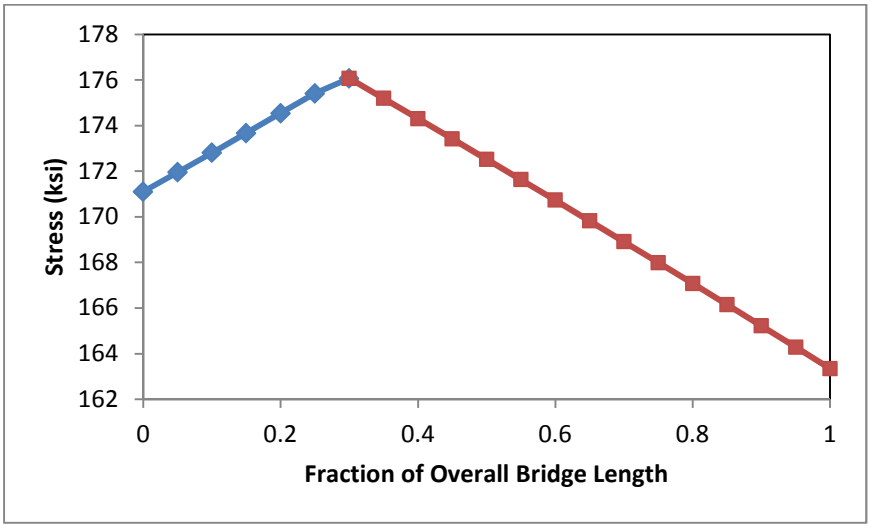

Figure 4-7. DSI Calculated Values for Strand Stresses

The interpolated stress was then multiplied by the area of a single 0.6 in. diameter strand (0.217 in^2) and the total number of strands in each panel (12) to calculate the total force provided by the post-tensioning at the gauge locations. It was determined that the force at VWGs 7 and 8 in panel 4B, which are located 824.5 in. from the live end, was 440 kips, and the force at VWGs 5 and 6 in panel 2B, which are located 1064.5 in. from the live end, was 430 kips. Using Equation 4-4, the stress at each VWG was converted into strain using the following stress-strain relationship:

$$\varepsilon = \frac{\sigma}{E} \tag{4-4}$$

The predicted strains for the four embedded vibrating wire gauges are shown below in Table 4-5. The calculations and the resulting predictions for strains due to post-tensioning are located in Appendix D. The strand elongation reports from the post-tensioning are located in Appendix E.

Table 4-5. Predicted Strains Due to Post-tensioning Force

	VWG 5 (με)	VWG 6 (με)	VWG 7 (με)	VWG 8 (με)
Predicted Strain	-85	-48	-87	-50

4.4 Predicting Live Load Test Strains

Through the length of the bridge there were three locations where gauges were installed and, therefore, it was these three locations which were modeled. The predictions also focused primarily on the extreme loading cases, such as when the truck or trucks were in a position to induce the maximum amount of moment and strain in the cross-section. This meant that predictions were made for gauges at 0.4L (joint between panels 1A and 2B) when the truck's middle tire was over the joint at 0.4L, and the predictions were made for the gauges at the center of the middle span (joint between panels 5D and 6C) when the truck's middle tire was over the joint at midspan. The loading scenario was different for the

gauges near Pier 1 at the joint between panels 3C and 4B. While the gauges at 0.4L and midspan were focused on capturing maximum positive moment effects, the most important data for the gauges at the pier was the negative moment effects. In order to cause the maximum amount of negative moment, two trucks were placed on either side of the joint with their rear tires facing. This position was determined, as were the other two truck positions, by creating influence lines for each point along the length of the bridge and moving the truck into the optimal position for creating the most positive or negative moment. The influence lines and the resulting truck positions are shown in Figure 4-8, Figure 4-9, and Figure 4-10.

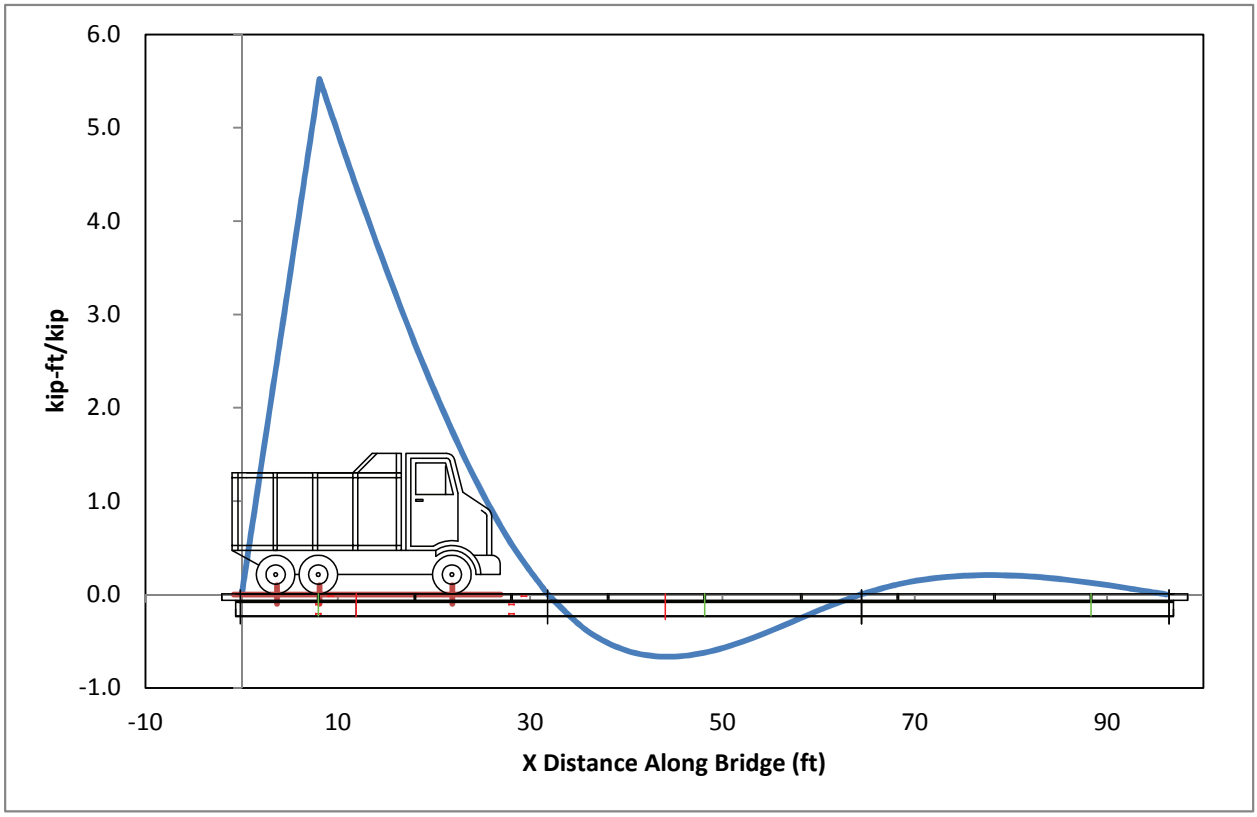

Figure 4-8. Influence Line for Maximizing Moment at Gauges at 0.4L

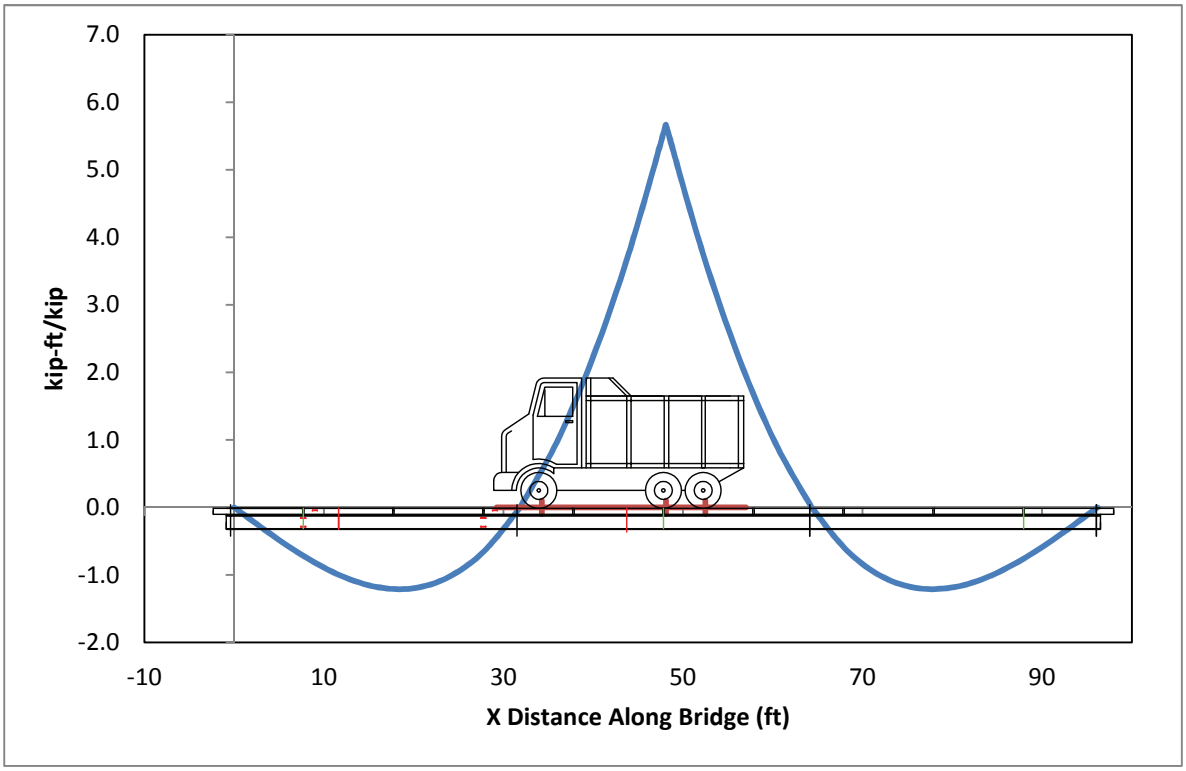

Figure 4-9. Influence Line for Maximizing Moment at Gauges at Midspan

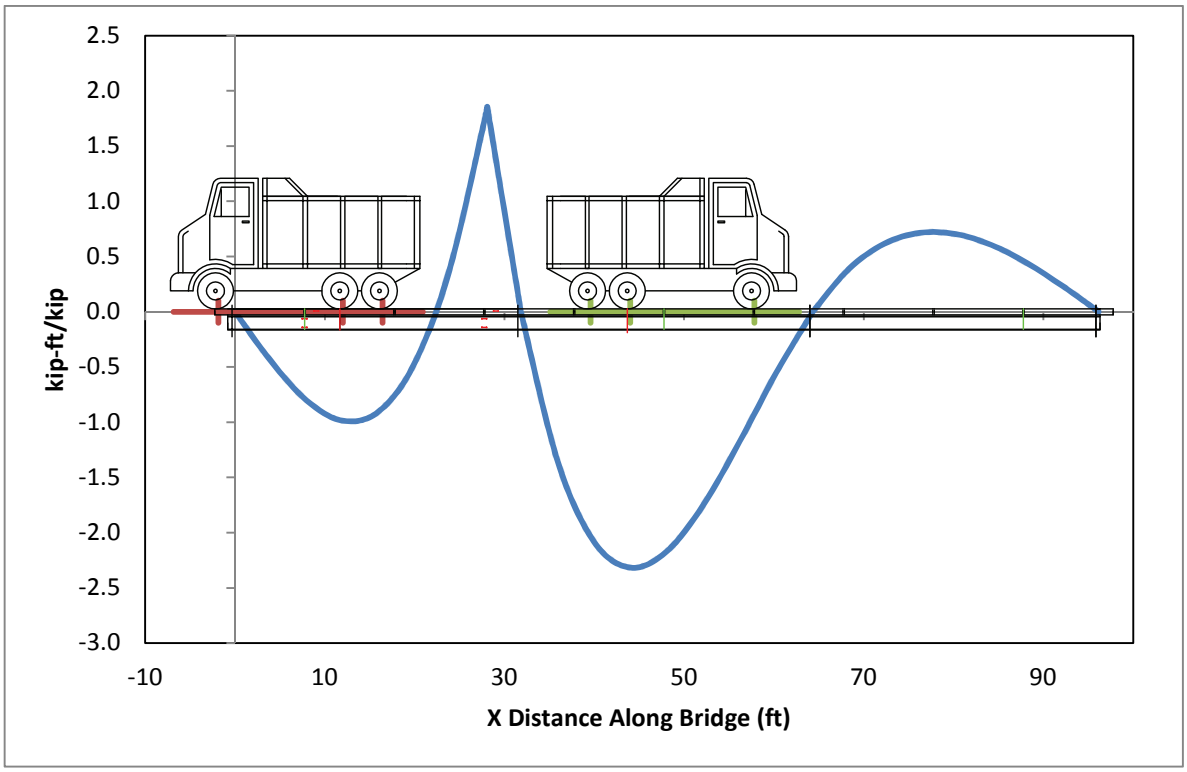

Figure 4-10. Influence Lines for Maximizing Negative Moment over Pier 1

Once the truck positions were determined it was necessary to calculate the composite moment of inertia for each beam and predict how much of the load from the trucks would be proportioned to each beam. The Phase I cross-section at the time of the live load test is shown in Figure 4-11.

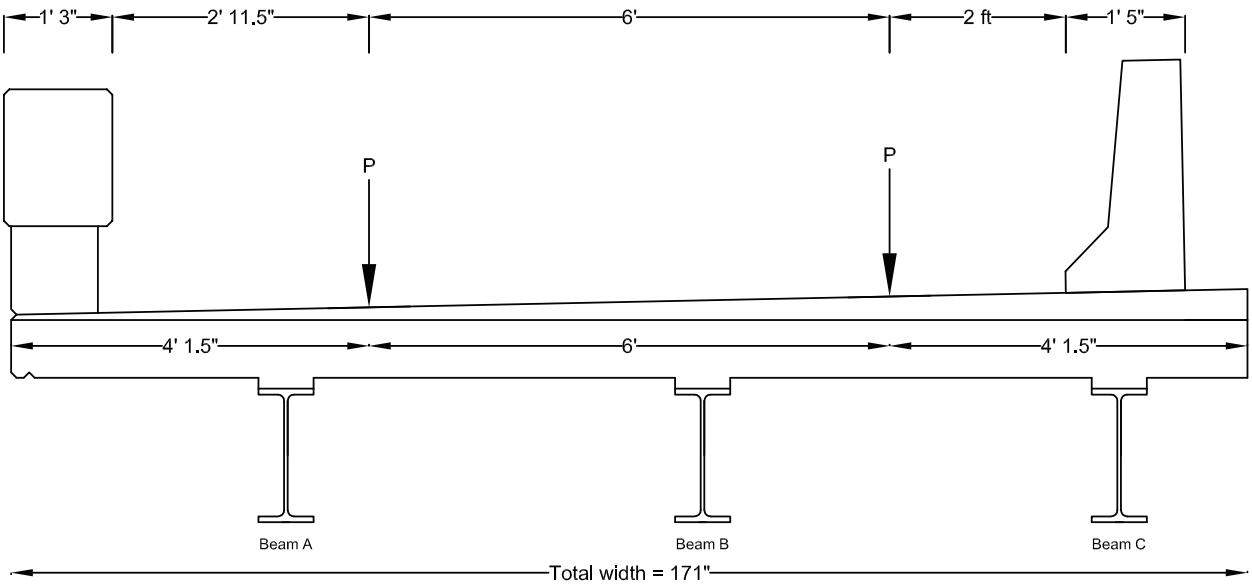

Figure 4-11. Phase I Cross-section at Time of Live Load Test Looking East

One of the major difficulties in predicting the strains is determining how to deal with the effect of the guard rails. The permanent Kansas corral-style guard rail on the left side in Figure 4-8 is continuous along the length of the bridge in the upper rectangular section, and is connected to the deck by solid posts located every 10 ft along the length of the bridge. The temporary New Jersey-style guard rail on the right side of Figure 4-11 consists of 12 ft long sections bolted to the deck approximately every 2 ft. If both barriers were fully composite with the bridge, they would add a significant amount of strength and greatly increase the moment of inertia. The composite moment of inertia for the whole bridge, not including the barriers, was calculated as 21,000 in^4, but when the full area of the barriers is considered, the moment of inertia increases more than ten times to 270,000 in^4. It is, therefore, quite difficult to quantify the effect of these semi-composite barriers on the tributary widths of the beams and the

impact it has on the total strength of the bridge. Neither barrier is completely composite, but both barriers will affect the total strength of bridge and, therefore, also affect the strains measured in the beams.

There were two different models developed to take into account the effects of the barriers and bracket the measured results. The two methods provide one set of predictions which are typically higher than the measured strains, and one set of predictions which are typically lower. In the first model the barriers were completely ignored. This model should predict strains higher than what were actually measured, because it underestimates the stiffness of the bridge. The second model took into account the fact that the barriers were present at the time of the live load test and that the barriers were, therefore, contributing to the stiffness of the bridge. Instead of modifying the stiffnesses of the individual composite beam sections, however, it assumed that the barriers would act as independent beams and would each support 1/5 of the load. The reasoning behind this assumption is based on the fact that determining the percent composite behavior for the barriers would be nearly impossible and that the transformed moment of inertias of the barriers are actually very similar to or greater than the moment of inertia of the steel beams. The W18x71 beams have a moment of inertia of 1170 in^4. The permanent barrier, only considering the continuous concrete area, has a transformed moment of inertia of 1860 in^4. The temporary barrier has a moment of inertia of 7288 in^4. Although neither barrier is truly continuous across the entire length of the bridge nor acts fully composite, it seems plausible to assume that they could carry the same loads as the steel beams. This model will form the lower boundary for the measured strains. The cross-sectional areas and dimensions for each of the three beams are pictured in Figure 4-12, Figure 4-13, and Figure 4-14. Note that the barriers are shown in the following diagrams for reference, but are not used when calculating the composite moment of inertia for the composite girders.

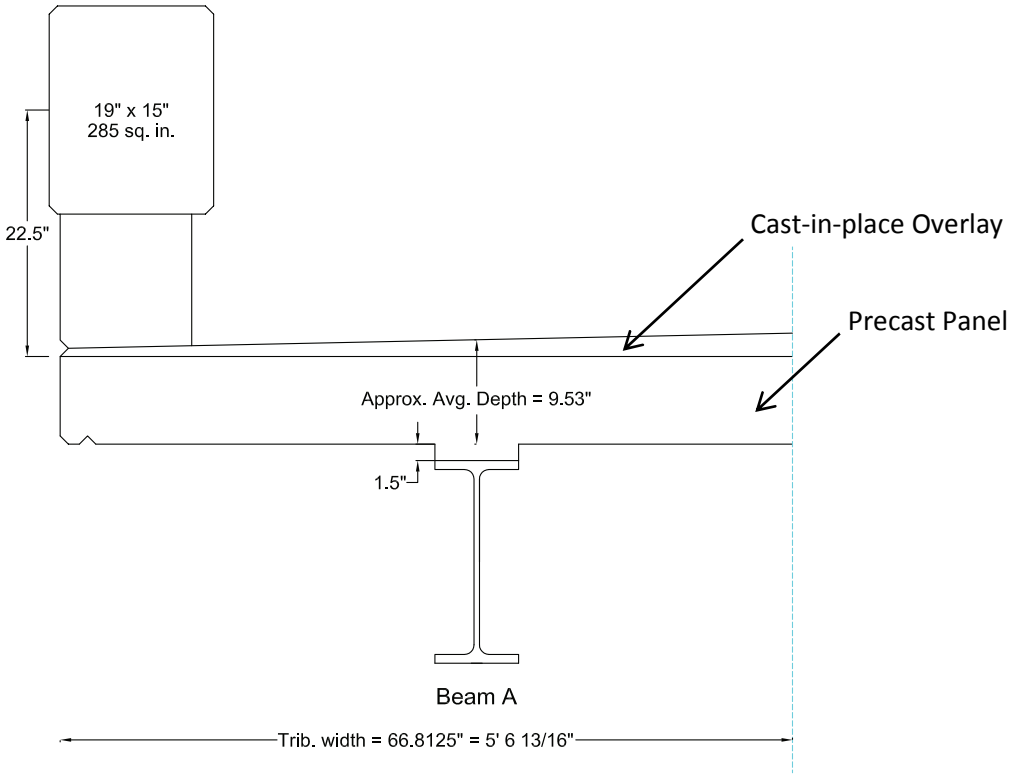

Figure 4-12. Beam A Composite Section Dimensions

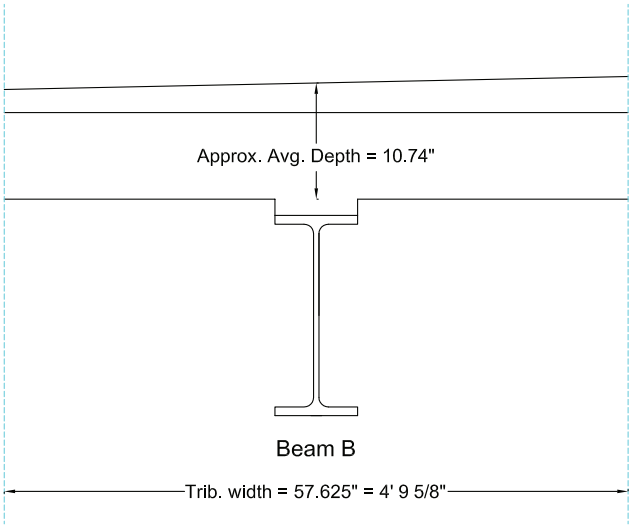

Figure 4-13. Beam B Composite Section Dimensions

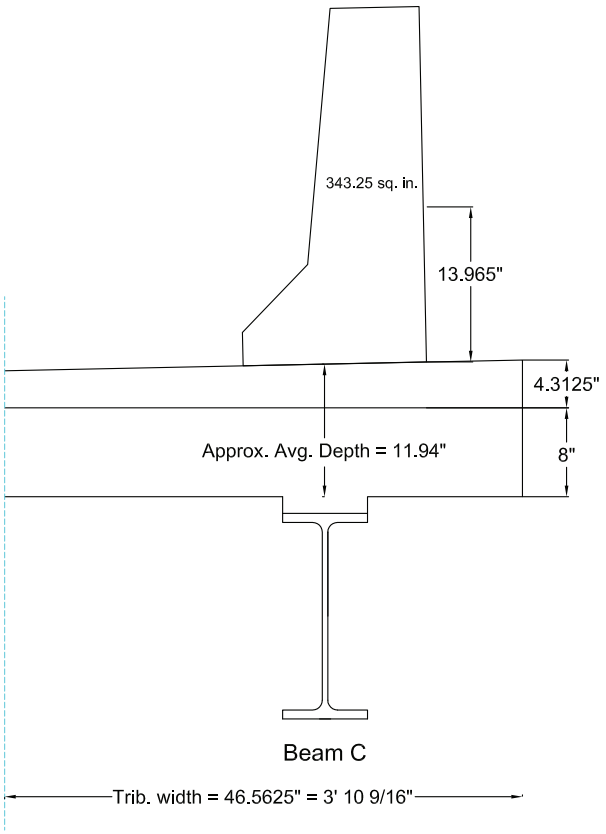

Figure 4-14. Beam C Composite Section Dimensions

It was calculated that the composite moment of inertia of beam A was 6567 in^4, beam B was 7140 in^4, and beam C was 7562 in^4. The elastic neutral axis was located 4.23 in. above the top of the steel beam in beam A, 4.71 in. in beam B, and 5.01 in. in beam C. Note that the barrier rail was approximated by a series of rectangles in order to simplify the analysis calculations. The simplified barrier is shown in Figure 4-15. The more stiffness contributed by the tributary width of the concrete deck, the higher the elastic neutral axis is located. All three moment of inertias are, however, very similar. It was this information, coupled with the fact that the beams are so closely spaced, that was the basis for the assumption that the beams would act together as a single composite member and, therefore, the truck axle weights should be split evenly among the beams.

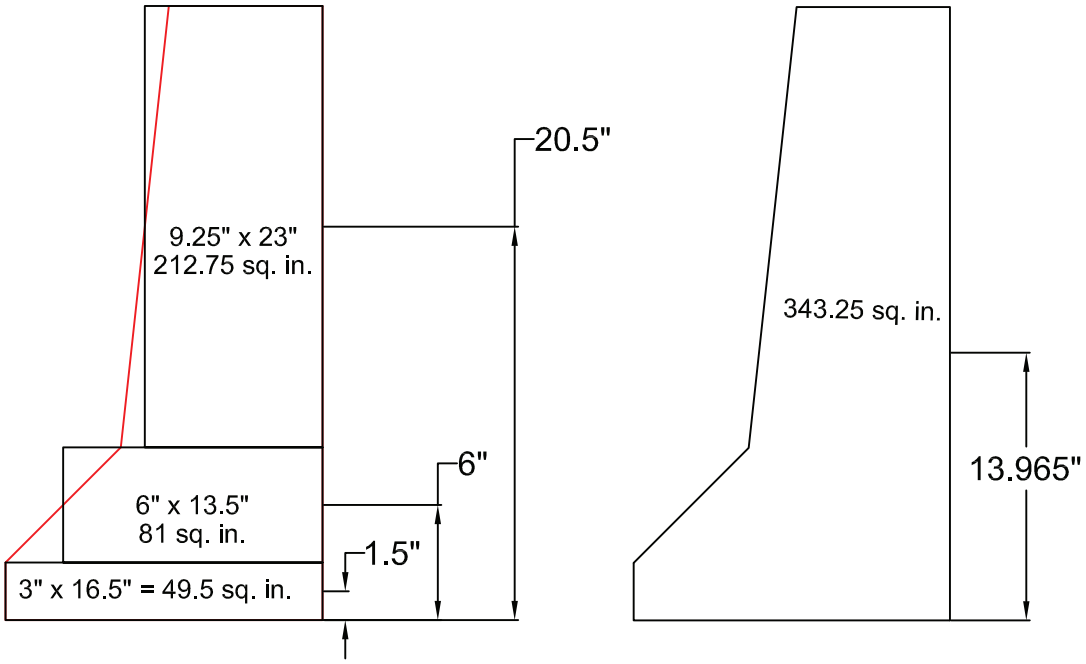

Figure 4-15. Barrier Rail Simplification

Once the proportion of the axle weight and the composite of moment of inertias were determined for each beam, the moment at each gauge location was calculated using the influence lines created previously. The strains were then calculated using equation 4-4, making sure to divide the equations for strain within concrete by the modular ratio $n = E_s/E_c$. The y distances used to calculate the strain at the different positions vertically through the beam are shown below in Figure 4-16.

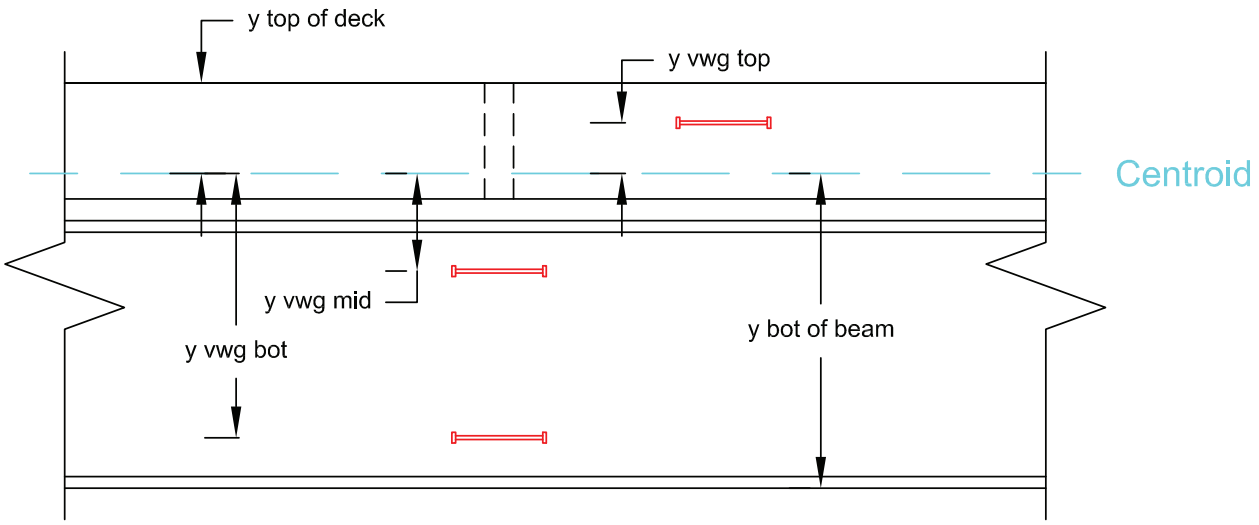

Figure 4-16. Y Distances in Composite Beam Section

The results from the calculations are shown in Table 4-6, Table 4-7, and Table 4-8. Note that the deflection predictions for the twangers are generated using Mastan2 by inputting the beam's composite moment of inertia and the assumed loading. The displacement for the LVDTs was assumed to be 0.000 in. because the actual displacement obtained from the strain prediction was significantly lower than the calibrated resolution of the LVDT gauge. The calculations for the predicted live load strains are located in Appendix F.

Table 4-6. Strain Predictions for Negative Moment Test

	VWG 3 (με)	VWG 4 (με)	VWG 7 (με)	VWG 8 (με)	BDI 7 (με)	BDI 8 (με)
3-Beam Predict.	-21	-48	7	4	15	11
5-Beam Predict.	-12	-29	4	3	9	7
	LVDT 1 (in)	LVDT 2 (in)				
3-Beam Predict.	0.000	0.000				
5-Beam Predict.	0.000	0.000				

Table 4-7. Strain Predictions for Gauges at 0.4L When Truck is at 0.4L

	BDI 1 (με)	BDI 2 (με)	BDI 3 (με)	Twanger 1 (in)	Twanger 2 (in)	Twanger 3 (in)
3-Beam Predict.	87	81	78	-0.038	-0.035	-0.033
5-Beam Predict.	52	49	47	-0.023	-0.021	-0.020
	VWG 1 (με)	VWG 2 (με)	VWG 5 (με)	VWG 6 (με)		
3-Beam Predict.	28	66	-10	-6		
5-Beam Predict.	17	40	-6	-3		

Table 4-8. Strain Predictions for Gauges at Midspan when Truck is at Midspan

	BDI 4 (με)	BDI 5 (με)	BDI 6 (με)	Twanger 4 (in)	Twanger 5 (in)	Twanger 6 (in)
3-Beam Predict.	90	84	81	-0.046	-0.042	-0.040
5-Beam Predict.	54	51	48	-0.027	-0.025	-0.024

4.5 Bowers' Model for Predicting Prestress Losses in Deck Panels

Prestress losses occur for a number of reasons, but the primary sources are creep and shrinkage. Shrinkage occurs as the concrete matures and water escapes and evaporates. Creep is caused by the constant and long-term application of post-tensioning loads. Both creep and shrinkage induce stresses and strains within the cross-section of the bridge.

In a simple-span composite steel girder bridge, the creep and shrinkage occurring in the deck is restrained by the girders. This process develops a net compressive axial force in the girders and ultimately results in a positive curvature throughout the cross-section which causes the bridge to deflect downwards. For a continuous three-span bridge, such as the Route 65 bridge being studied in this thesis, the two interior piers apply upward forces that keep the bridge from deflecting at those points. This results in large negative secondary moments which cause tension stress to form within the deck over the piers. Monitoring the stresses and strains produced over the piers is important because undesirable cracking may occur at joints when the tensile stresses are greater than $1.5\sqrt{f'_c}$, as determined by Swenty (2009) in his dissertation.

Bowers (2009) created a series of Mathcad models which required input information about the bridge and output the total change in stresses. The foundation for these calculations is a series of equilibrium equations, compatibility equations which relate strains throughout the cross-section, and constitutive relationships which relate the changes in strain to the changes in stress through the application of the modulus of elasticity, age adjusted modulus of elasticity, and creep and shrinkage coefficients. The calculations sheet used for this analysis is located in Appendix H.

Bowers' model requires input of steel girder properties such as its dimensions and modulus; deck section properties such as thickness, f'_c, and aging coefficient; strand properties such as the number of strands, area of strands, and the modulus. Other important inputs into the sheet are the number of days since casting that the deck was post-tensioned, the steel girders and the deck were made composite, and the end of service life. The calculations take into account the fact that, from the time when the post-tensioning occurs to when the deck and girders are made composite by pouring the haunch and filling the shear stud pockets with grout, the girder does not restrain any of the creep or shrinkage strains. After the bridge is composite, all of the equilibrium, compatibility, and constitutive equations change in order to incorporate the effects the girder has on the system.

In the construction process of the Route 65 bridge, the post-tensioning of the panels was performed 65 days after casting, the bridge was made composite at 80 days, and the end of service life was assumed to be 10,000 days. The end of service life variable could, however, be changed in order to reflect the change in strains on a particular date. The change in strain within Beam C at 10,000 days after casting, assuming the bridge is simply supported, was calculated and is represented by the graph in Figure 4-17.

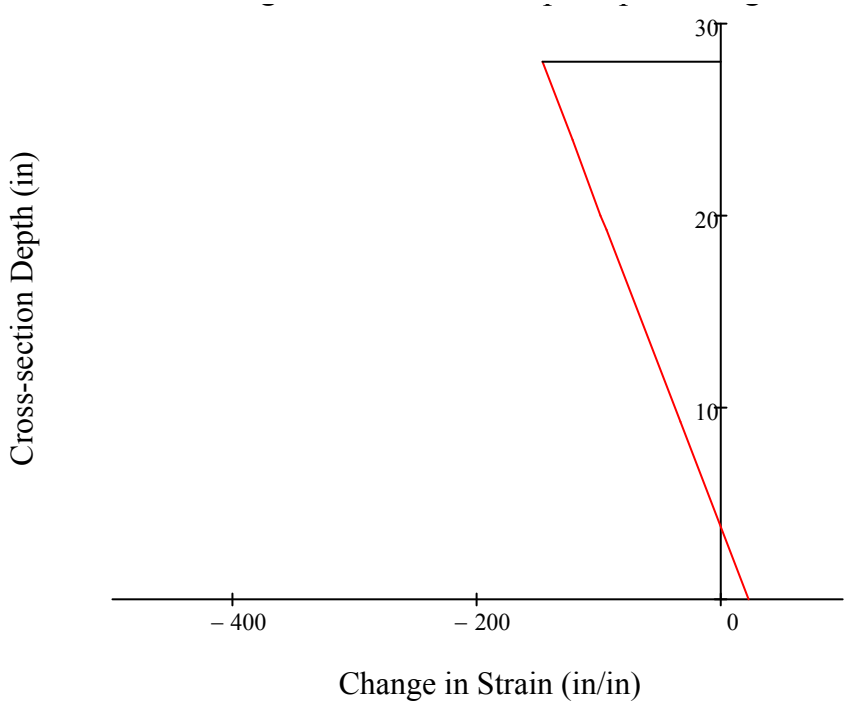

Figure 4-17. Change in Strains of a Simply-Supported Beam Cross-section

The strains calculated for a simply-supported beam were added to the effects of the secondary moments caused by the upward force from the two interior piers. The secondary moment diagram is shown in Figure 4-18.

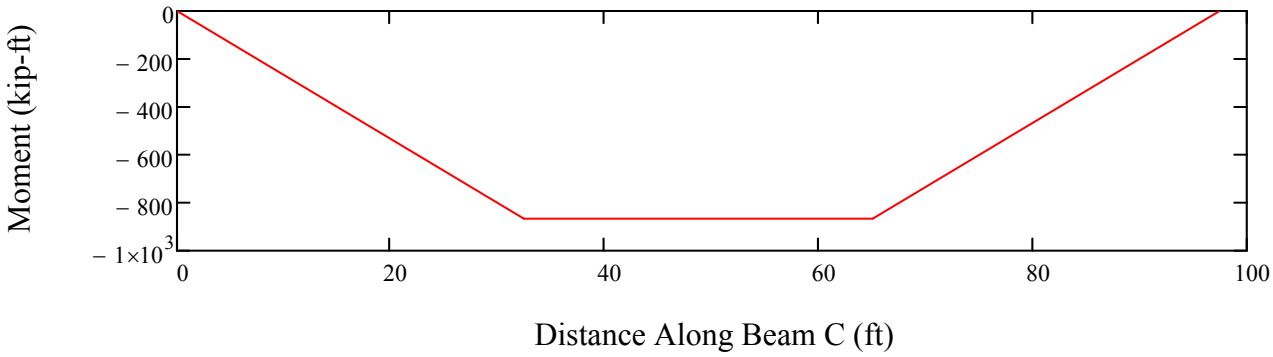

Figure 4-18. Secondary Moments Induced by Interior Piers

By adding the tensile strains produced by the pier forces to the strains in Figure 4-17, the final strains at the two gauge locations along beam C could be determined. Note that the gauge location closest to Pier 1, which is also the closest joint to the pier, is 3.75 ft to the left of the maximum secondary moment. The other gauge location between panels 1A and 2B is 23.75 ft to the left of the maximum secondary moment. The final strain distributions at 10,000 days after casting are shown in Figure 4-19 and Figure 4-20.

The final stress in the top of the deck over the piers was also calculated. With the effects of live load, the ultimate stress was determined to be 0.119 ksi in tension. This stress is just below the limit of $1.5\sqrt{f'_c}$, which equals 0.125 ksi. This means that, according to Bowers' model the post-tensioning force is sufficient to prevent cracks from forming over the piers

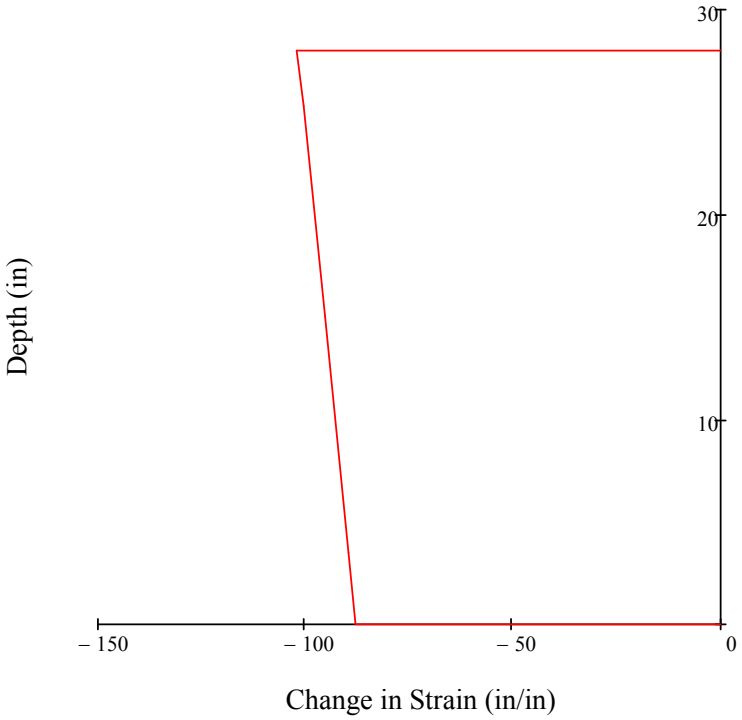

Figure 4-19. Change in Strain at Gauges Near Pier 1

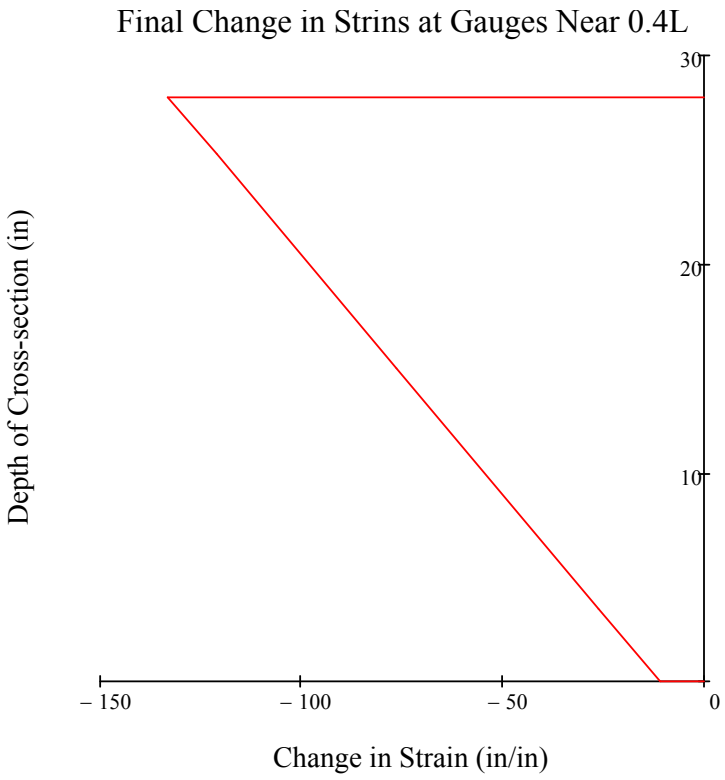

Figure 4-20. Change in Strain at Gauges Near 0.4L

Chapter 5: Experimental Results

The results of the long-term data analysis and the live load testing are presented in this section of the report. The results of these studies are compared to the predicted values discussed in Chapter 4.

5.1 Long-term Monitoring of the Bridge

Long-term monitoring of the eight vibrating wire strain gauges occurred from 11/2/2011 until 6/6/2012. On November 2, 2011 four vibrating wire gauges were installed at two locations along the length of Beam C. These gauges were labeled VWGs 1-4. The data logger and solar panel were also installed, which meant that the data logger was fully functioning and recorded data from this point forward. These gauges were installed before the panels were set on the beams in order measure the strain induced by the weight of the precast panels.

On 11/4/2012 the deck panels were set on the Phase I side of the bridge. On 11/12/2011 the wires from the four vibrating wire gauges within panels 2B and 4B were connected to the data logger. These gauges were labeled VWGs 5-8. Data collection began on 11/12/2011, which was four days before the deck panels were post-tensioned, which occurred on 11/16/2012. The haunch and shear pockets were poured on 11/28/2012, and it was assumed that the deck and beams were fully composite two days later.

Strain measurements from VWGs 1-4 were recorded once per minute from 11/2 until 11/12. The strain measurements from all eight VWGs were recorded once per minute from 11/12 until 11/17, and from 11/17 until 6/6 the strains were recorded once every hour. The gauges were initially reading once a minute, which is the fastest that they could be read by the CR23X data logger, in order to capture the

changes in strain from setting the panels and post-tensioning. The duration of these events was only a couple of hours, so it was necessary to collect the data from the gauges as fast as possible in order to document the changes in strain throughout the entire event. Having the data logger record every minute puts heavy demand on the data logger battery and it generates a large amount of data. The demand on the battery was so great that the data stopped recording at various times when the battery power became too low. The data logger began recording again when the solar panel had sufficiently recharged the battery. For these reasons, the data logger was set to record the strains only every hour after these initial events of setting the panels and post-tensioning the panels.

On 1/12/2012 VWG #4 detached from the bridge due to unknown reasons. It is possible that the glue became too brittle over time, and under the temperature induced stresses and vibrations from traffic it was not able to hold the gauge to the side of the girder. The gauge was reattached on 1/20/2012 and was set to the strain that was last recorded before the gauge fell off. Despite this attempt, the gauge's data did not seem to follow the same trends as before it detached and, therefore, these measurements were disregarded.

5.1.1 Deck Panel Loading Strains

On 11/4 the deck panels were placed upon the three beams on the Phase I side of the bridge. The strains were recorded throughout the process by VWGs 1-4. On 11/7 the leveling bolts, which were meant to evenly distribute the panel load between the three beams, were installed. Therefore, the final load distribution was represented by the data recorded after the leveling bolts were set. The strains measured by VWGs 1-4 are presented in the plot in Figure 5-1. Note that "Event 1" refers to the

placement of the panels, and “Event 2” refers to the setting of the leveling bolts. Also, positive values represent tensile strains and negative values represent compressive strains.

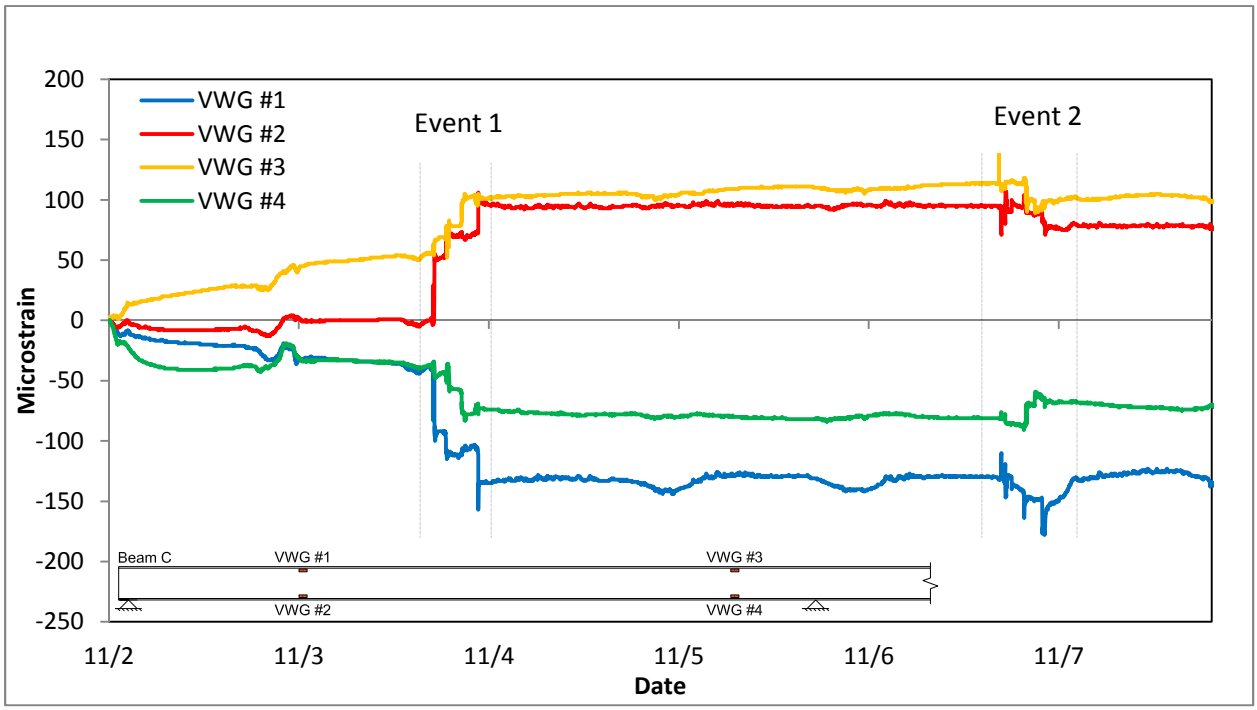

Figure 5-1. Measured Strains on Beam C from 11/2 to 11/8

From Figure 5-1, it can be determined that VWGs 2 and 3 measured tensile strains and VWGs 1 and 4 measured compressive strains. This is consistent with the predicted values of strain calculated using SAP2000. Table 5-1 presents a summary of the changes in strain at the four gauges and compares these changes to the predicted values. Note that summation of the strains induced by Event 1 and Event 2 will not always equal the total change because of the variation in strain between the end of Event 1 and the beginning of Event 2. Also note that the predicted strain values were taken from the model which assumed that the panel weight was divided evenly among the beams. This model turned out to be much more accurate than the other model which based the panel loads on each beam depending on its tributary width.

Table 5-1. Summary of Strains Induced by the Placement of the Deck Panels

	VWG #1 (με)	VWG #2 (με)	VWG #3 (με)	VWG #4 (με)
Event 1: Placement of deck panels	-91	101	51	-34
Event 2: Tightening leveling bolts	-3	-16	-12	13
Total Change	-88	84	51	-28
Predicted strains	-82	82	40	-40
% Difference	6.5%	2.1%	21.4%	-43.2%

Overall, the predicted strains were very accurate at 0.4L where VWGs 1 and 2 are located. The average percent difference was only 4.3% for both gauges. The predicted values were less accurate near the first pier where VWGs 3 and 4 are located, with an average percent difference of 32.3%. This difference may be due to a variety of reasons. It is possible that the bearing at the pier is different from what is modeled. If the bearing is acting more as a fixed support, rather than a roller support as it was modeled, it is possible that there is a very different strain gradient than what was assumed due to additional axial force. It is also possible that the strains measurements were affected by the gauges' proximity to the interior pier.

It should also be noted that, while the changes in strain in VWGs 1 and 2 are nearly equal but opposite signs, the changes in strain in VWGs 3 and 4 are not at all equal with a difference between the two gauges of 23 με. The gauges were placed exactly the same distance in from the edge of the steel, and because the centroid of the steel is at its middle during this non-composite portion of construction, the strain at the top VWG and the bottom VWG should be equal but with opposite signs. These differences between VWGs 3 and 4 could be attributed to the reasons stated previously.

5.1.2 Post-Tensioning Strains

On 11/16/2011 the post-tensioning strands were tensioned. A plot of the strains measured within the deck panels 2B and 4B is presented in Figure 5-2. Note that the strain values from VWGs 5-8 which were embedded into the concrete have been temperature corrected to reflect the actual strain in the concrete rather than the strain in the steel during temperature fluctuations. Also of importance is that during the tensioning process, four strands within the duct closest to the interior edge of the panel ruptured. This caused the compressive force within the panel to rapidly decrease. VWGs 6 and 8, which were on the side closest to the ruptured strands, showed a large decrease in strain when this rupture occurred. In Figure 5-2 "Event 3" refers to the initial post-tensioning in which the strands ruptured and "Event 4" refers to the point in time during the next day that the broken strands were replaced and tensioned again. Also note that most of the data from Event 4 is missing due to a drop in battery power.

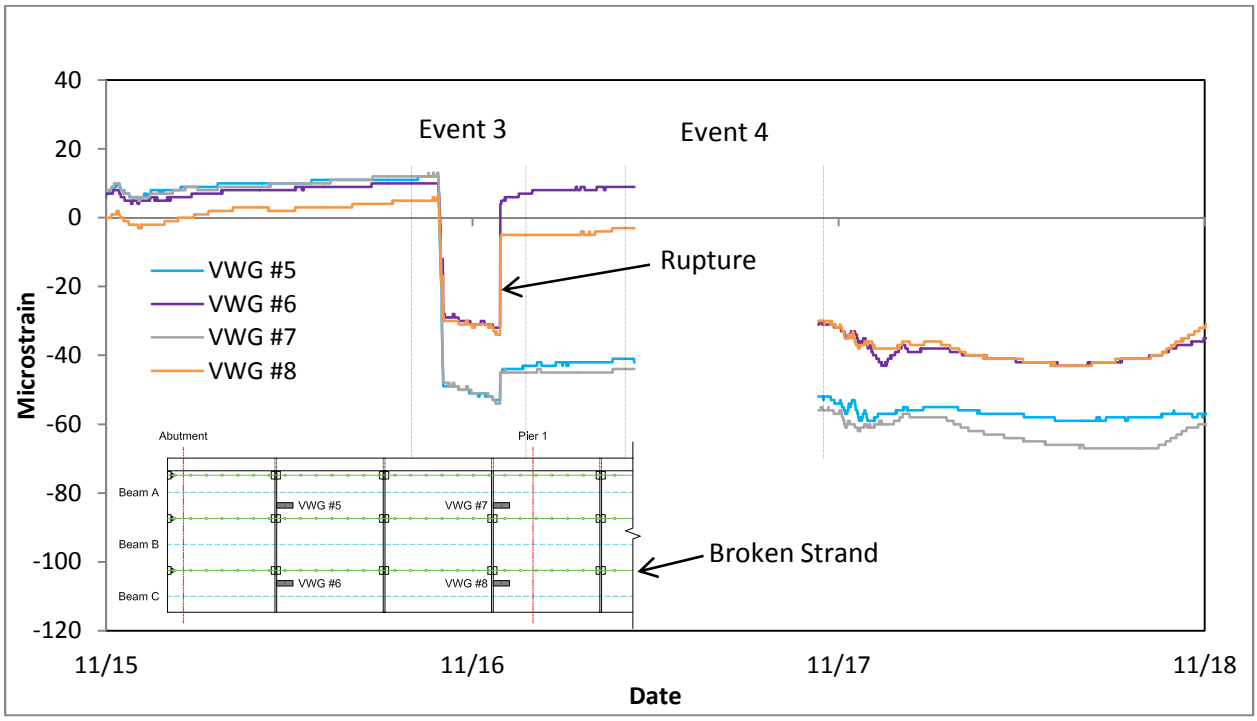

Figure 5-2. Measured Strains within Panels 2B and 4B from 11/15 to 11/18

Due to the drop in battery power, it was necessary to rely on the knowledge that the strands were re-tensioned in the morning of the 17th in order to determine the final strains within the panels. Fortunately, the data logger began recording strains at around 11 AM, which was about the time that the re-tensioning process was completed.

Table 5-2 presents a summary of the measured changes in strain and compares these measured changes to the predicted values. Note that the total change is not always equal to the addition of the changes in strain from events 3 and 4 due to the variations in strain between events 3 and 4. The predictions were based on theoretical strand stress with a modulus of elasticity of 28,500 ksi, and a loss of 0.013 kips/in of jacking force due to friction losses.

Table 5-2. Summary of Strains Induced by the Post-tensioning of the Deck Panels

	VWG #5 (με)	VWG #6 (με)	VWG #7 (με)	VWG #8 (με)
Event 3: Post-tensioning strand rupture	-49	2	-52	-5
Event 4: Re-tensioning strands	-32	-61	-30	-48
Total Change	-91	-69	-92	-63
Predicted strains	-85	-48	-87	-50
% Difference	7.1%	30.1%	5.5%	21.9%

The overall changes in strain within the panel due to the post-tensioning were close to the predicted values, especially for gauges 5 and 6. The average percent difference for these two gauges is 6.3%. The predicted values for gauges 6 and 8 were not as accurate, but had an average percent difference of 26%.

Presented in Figure 5-3 is a plot of the strains measured by VWGs 1-4. Since the deck panels and the beams had not been made composite, it was predicted that the change in strain would be minimal during the post-tensioning process. Overall the measured data followed that prediction.

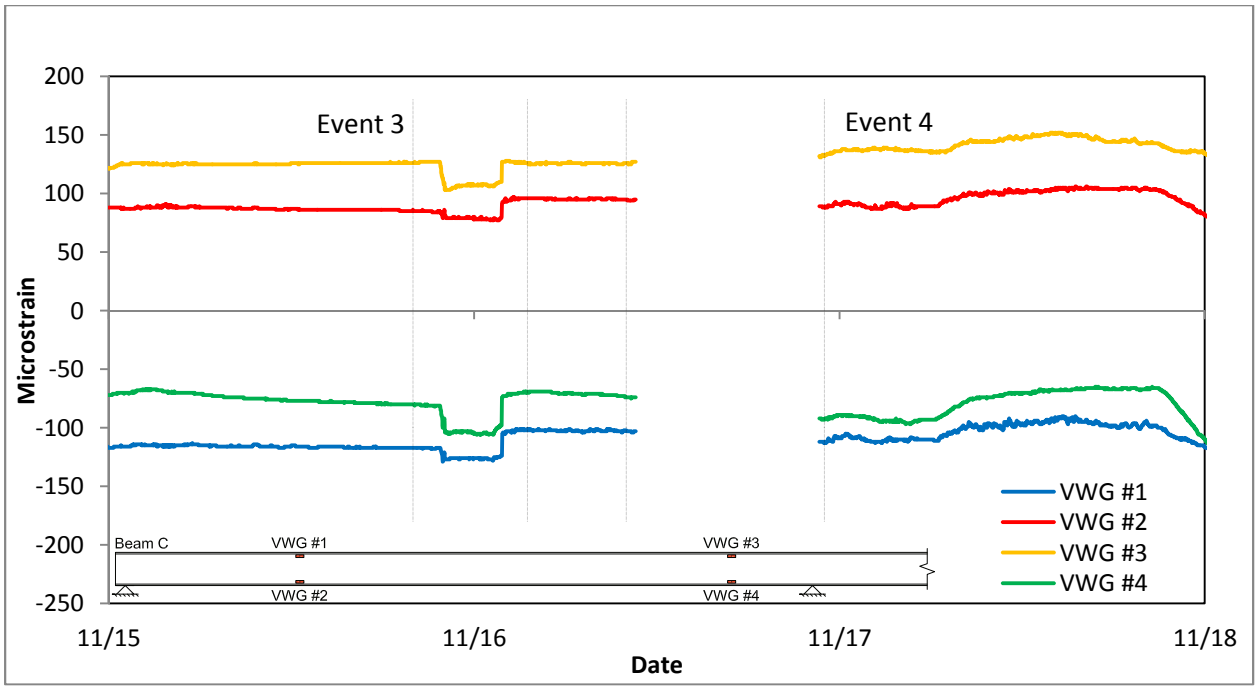

Figure 5-3. Measured Strains on Beam C from 11/15 to 11/8

Presented in Table 5-3 is a summary of the changes in strain during the initial tensioning and the re-tensioning. Overall the strains did not change very much. Figure 5-3 shows that during Event 3 all of the measured strains became more compressive, as some of the compression force was being transferred into the steel through friction. At the end of the events, however, there seems to be minimal change in measured strains. The average change was 6.25 με, which may have just been caused by temperature variation or by residual effects of the friction loss.

Table 5-3. Summary of the Changes in Strain on Beam C during the Post-tensioning

	VWG #1 (με)	VWG #2 (με)	VWG #3 (με)	VWG #4 (με)
Event 3: Post-tensioning strand rupture	16	10	0	10
Event 4: Re-tensioning strands	-11	-7	6	-19
Total Change	4	2	6	-13
Predicted strains	0	0	0	0

The temperature varied considerably in the days surrounding the four events previously discussed. Figure 5-4 presents a plot of the temperatures measured by VWGs 1-4 and Figure 5-5 presents a plot of the temperatures measured by VWGs 5-8.

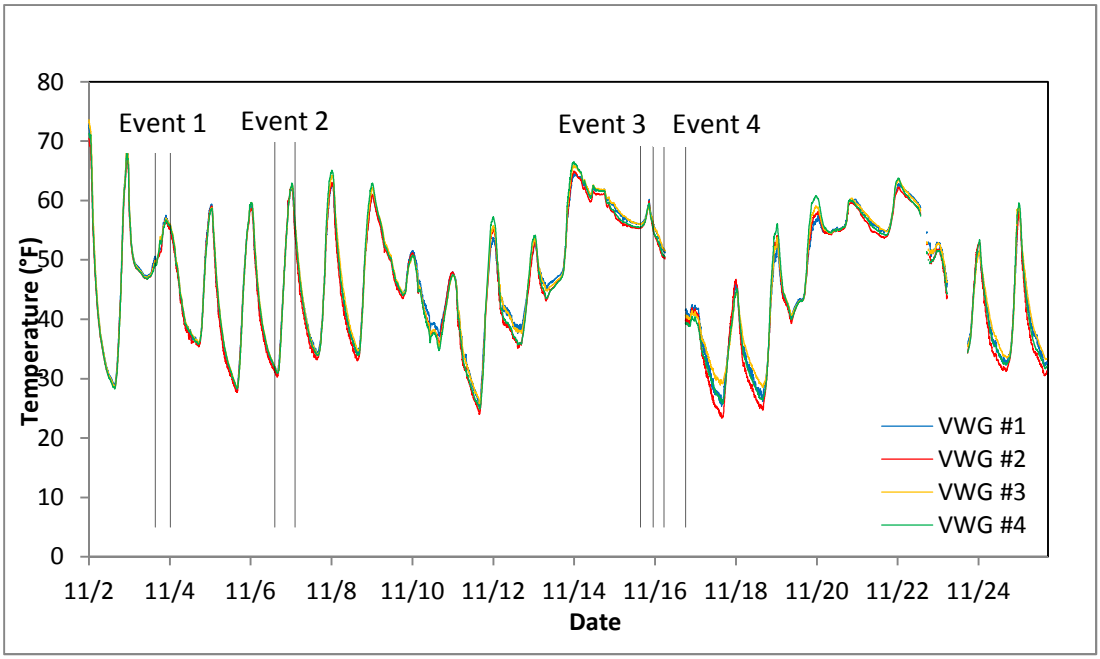

Figure 5-4. Recorded Temperatures on Beam C from 11/2 to 11/25

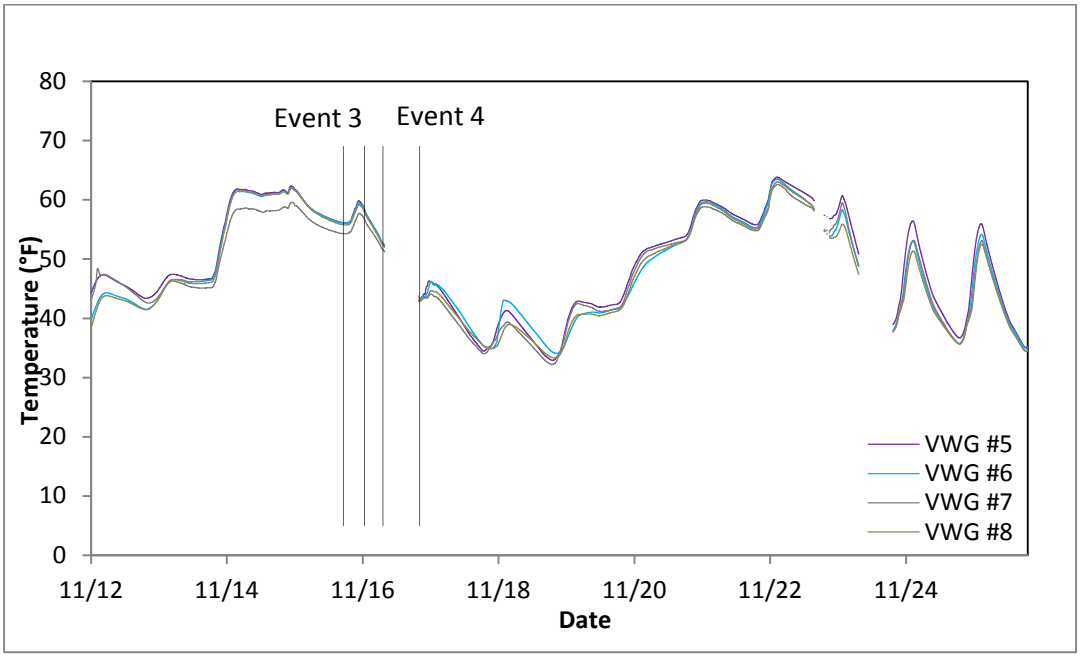

Figure 5-5. Recorded Temperatures within Beam C from 11/2 to 11/25

It is likely, therefore, that the difference between the predicted values and the measured strain values was in part due to the fluctuations in temperature. It was assumed for simplicity, that because these events occurred over such short time intervals the effects were negligible. Note that the Geokon temperature correction procedure, as explained by Laman (2012) was performed on the data from the embedded gauges in order to reflect the actual strain within the concrete, not the strain due to the difference in coefficients of thermal expansion between the steel and the concrete. This procedure does not, however, take into account the true stresses and strains developed from thermal gradients throughout the bridge.

5.1.3 Long-term Changes in Strain

The following graphs present the measured strain data from all eight vibrating wire gauges from installation until removal on 6/6/12. Note that again the strain values from VWGs 5-8 have been temperature adjusted to reflect the actual strain in the concrete. Figure 5-6 presents the measurements recorded by VWGs 1-4 which are located on the side of Beam C. Figure 5-7 presents the measurements recorded by VWGs 5-8 which are embedded within panels 2B and 4B.

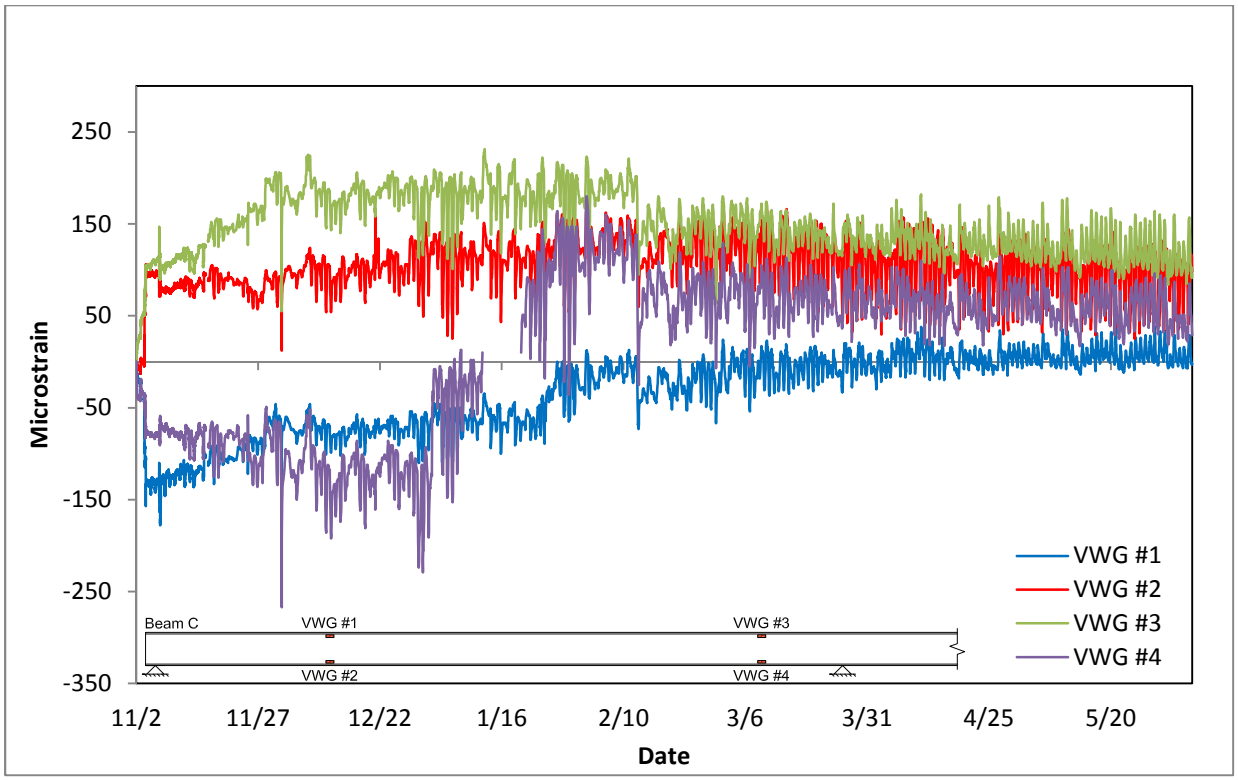

Figure 5-6. Measured Strains on Beam C from 11/2 to 6/6

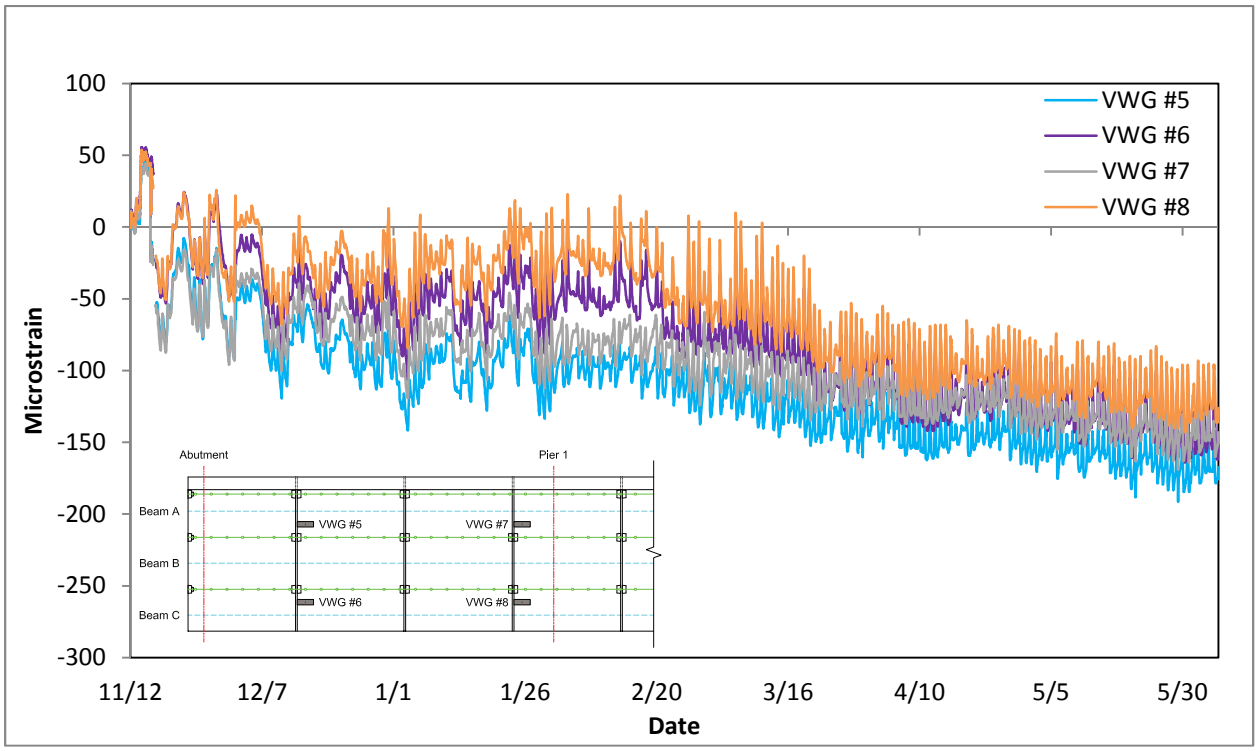

Figure 5-7. Measured Strains within Panels 2B and 4B from 11/2 to 6/6

While the strains within the panel have been adjusted to reflect the actual strain within the concrete, there are still large fluctuations in strain in all of the gauges as the temperature changes throughout the days.

In order to compare the long-term strain measurements to the models for post-tensioning loss produced by Bowers, it was necessary to eliminate these fluctuations in order to study the overall trends in the data. Although various sophisticated methods of modifying the data to remove the effects of the temperature gradient were attempted, none were successful. In order to understand the effects of the temperature variations throughout the deck and steel it would be necessary to have many more thermocouples throughout the depth of the bridge and in many more locations along the length. From the two gauges on the steel and the one gauge within the panel at each cross-section, there was not enough data to make any conclusions regarding temperature fluctuations.

A simplistic method was developed to determine the overall trends in the data. This method involved averaging the strains over a week so that the large variations in strain during each day would be smoothed out. The results of this averaging process are presented in Figure 5-8 and Figure 5-9. Note that points are typically only plotted every 15 days. Also, the timeline is now presented in days since casting.

Table 5-4 presents a reference between the two numbering systems. Also important is the fact that VWG 4 is assumed to be inaccurate after day 100, which is near the time in which the gauge detached from the bridge. It is unknown why a spike in the data occurred from day 120 to day 160, but it is most likely due to unaccounted temperature fluctuations.

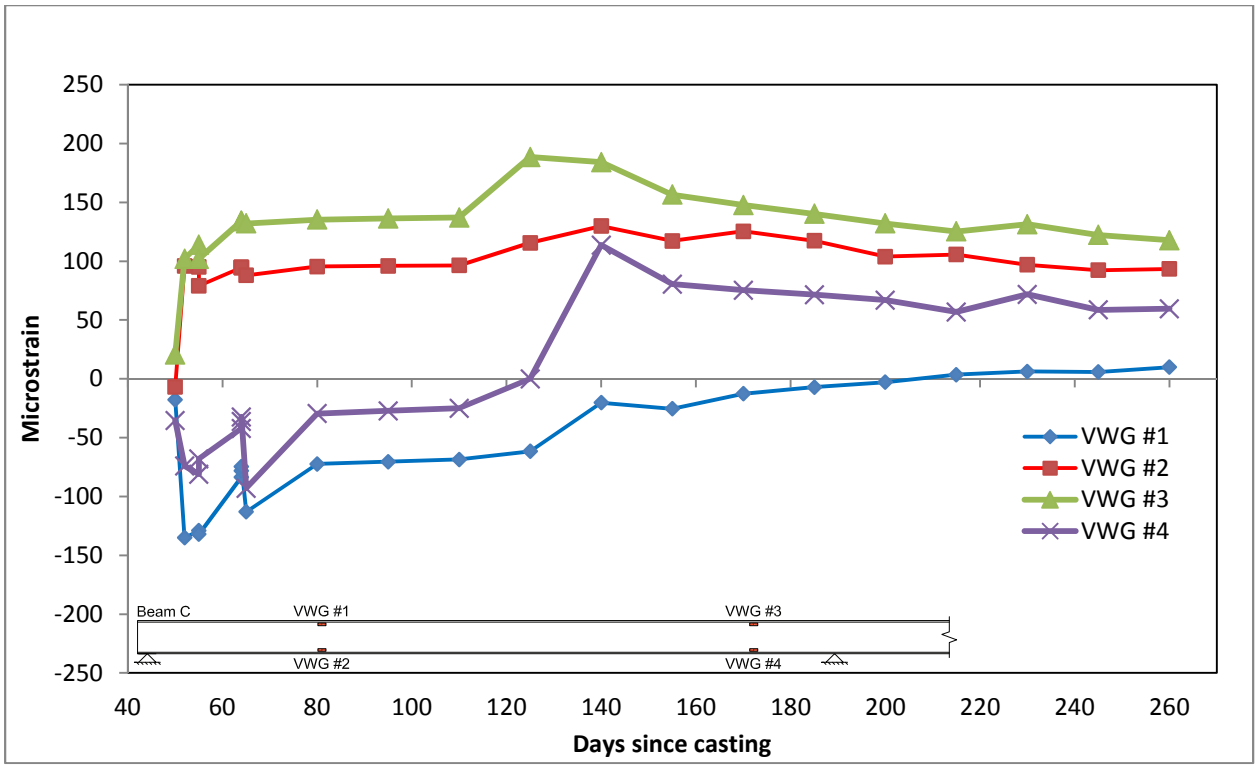

Figure 5-8. Average Strains Measured on Beam C from 11/2 to 6/6

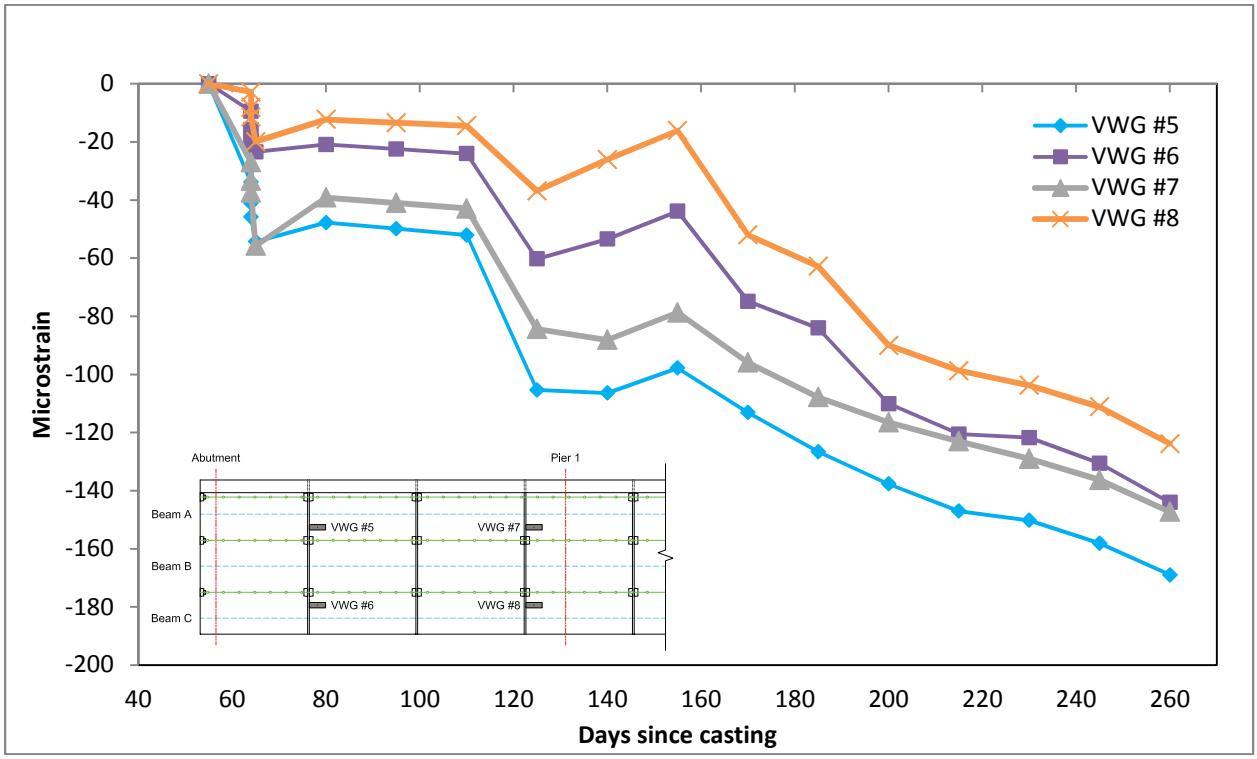

Figure 5-9. Average Strains Measured within Panels 2B and 4B from 11/2 to 6/6

Table 5-4. Summary of Dates and Days-since-pouring for Various Events

Timeline of important dates		
Date	**Day #**	**Event**
9/12/2011	0	Poured panels
11/4/2011	53	Panels set on bridge
11/7/2011	56	Leveling bolts set
11/16/2011	65	Post-tensioning
11/28/2011	76	Haunch poured
12/2/2011	80	Deck and beams assumed composite
2/2/2012	143	Live load test

Figure 5-9 shows that within the concrete, all of the gauges are experiencing a definite increase in compressive strain over time. Of the gauges attached to beam C, VWGs 2 and 3 are experiencing an increase in compressive strain, while VWGs 1 and 4 are experiencing an increase in tensile strain. In order to compare to Bowers model, a number of data points were selected and plotted against the results of the strain gradient calculated by Bowers model. The following plots present the averaged measured strains and the predicted strains for days 110, 140, and 215. Day 110 was selected due to its proximity to the point in time to when the deck and beams had just become composite, day 140 was selected due to its proximity in time to when the live load test occurred, and day 215 was selected because of its proximity to the end of the data recordings. Figure 5-10 and Figure 5-11 present the measured and predicted strains for day 110, Figure 5-12 and Figure 5-13 present the measured and predicted strains for day 140, and Figure 5-14 and Figure 5-15 present the measured and predicted for day 215.

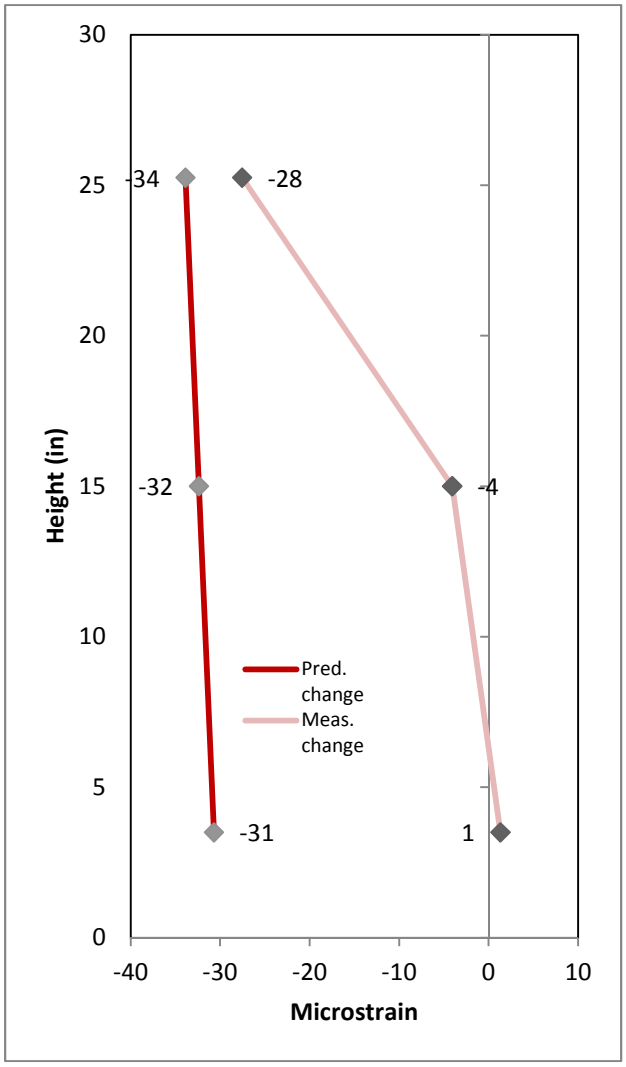

Figure 5-10. Day 110 Strains at Support

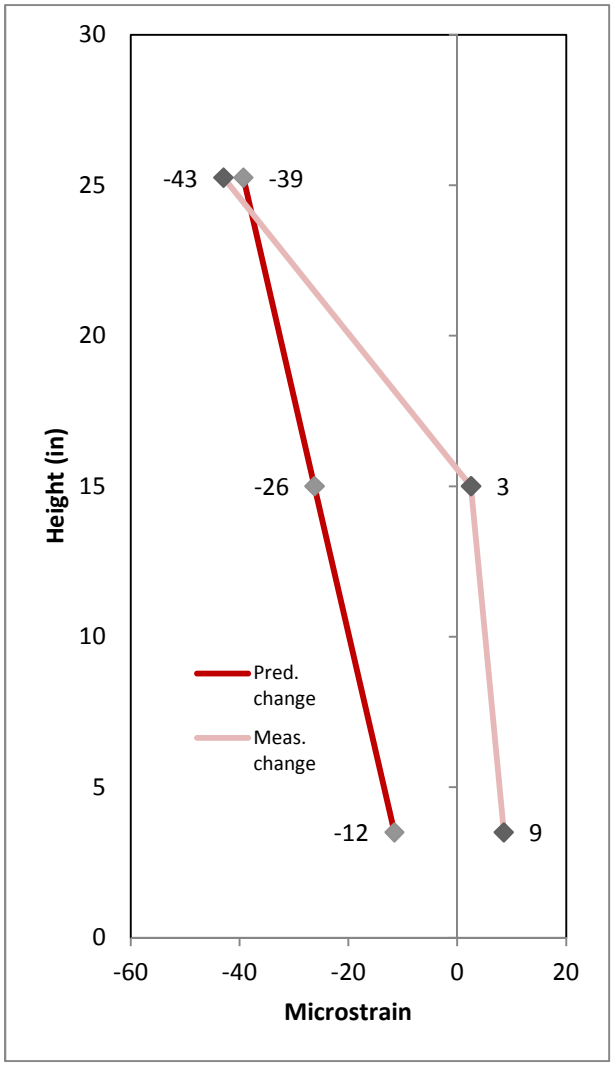

Figure 5-11. Day 110 Strains at 0.4L

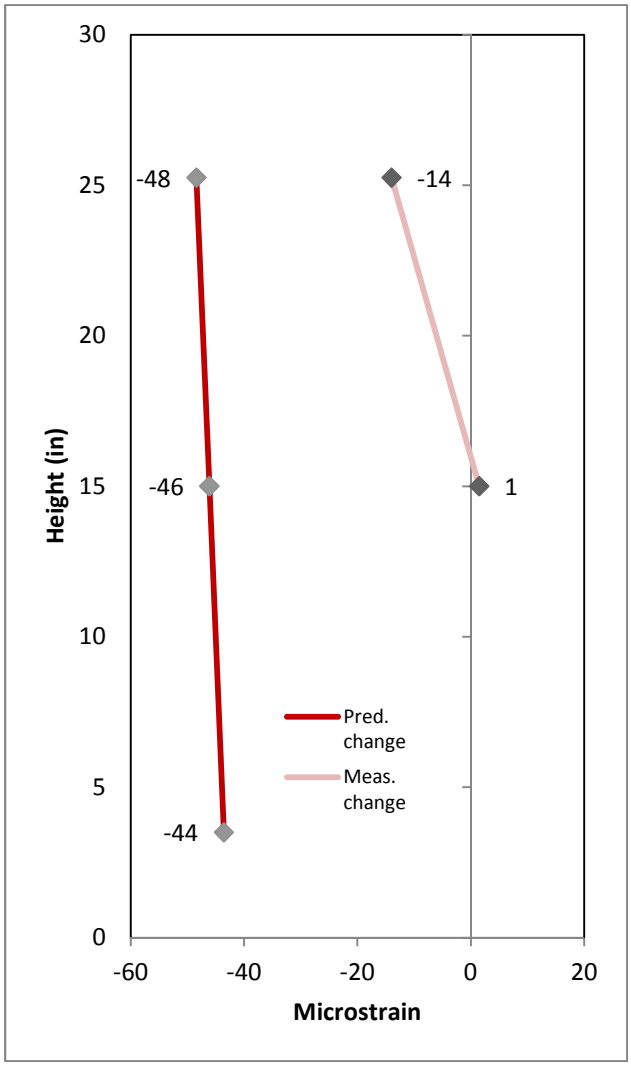

Figure 5-12. Day 140 Strains at Support

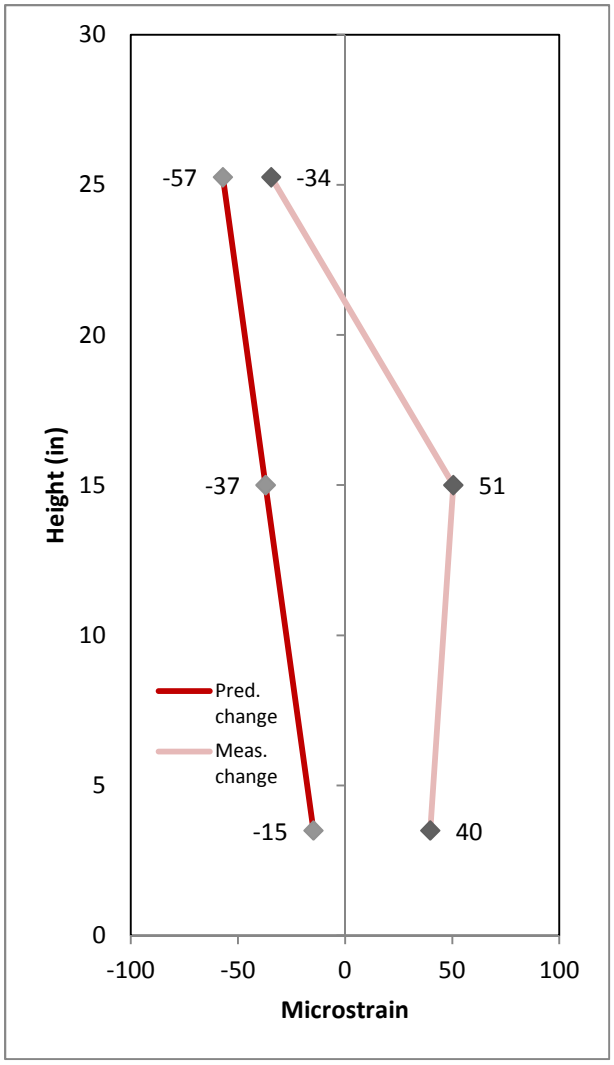

Figure 5-13. Day 140 Strains at 0.4L

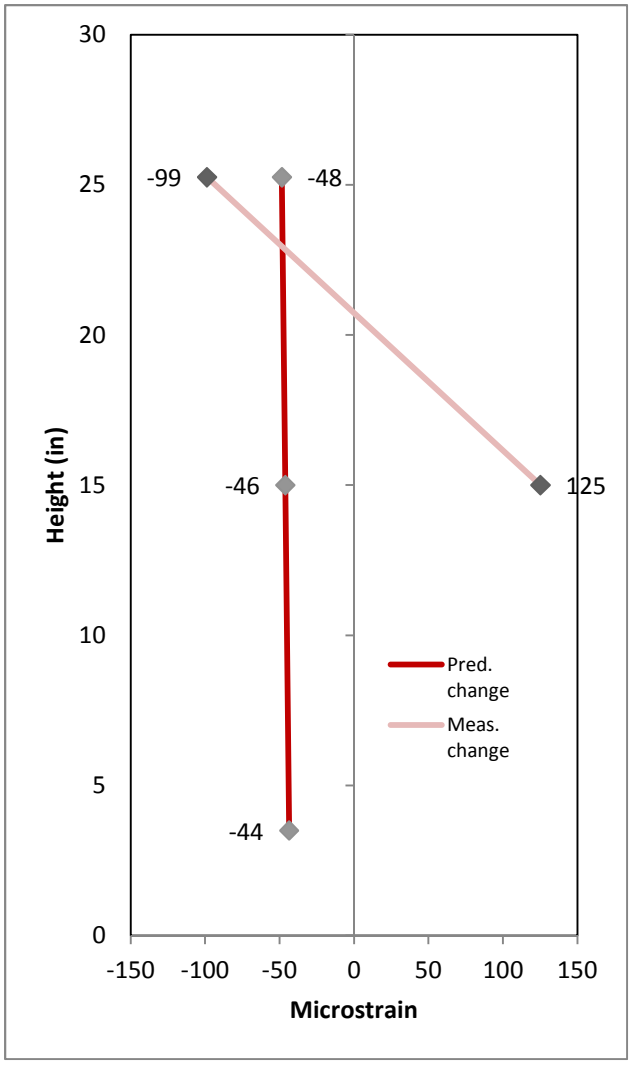

Figure 5-14. Day 215 Strains at Support

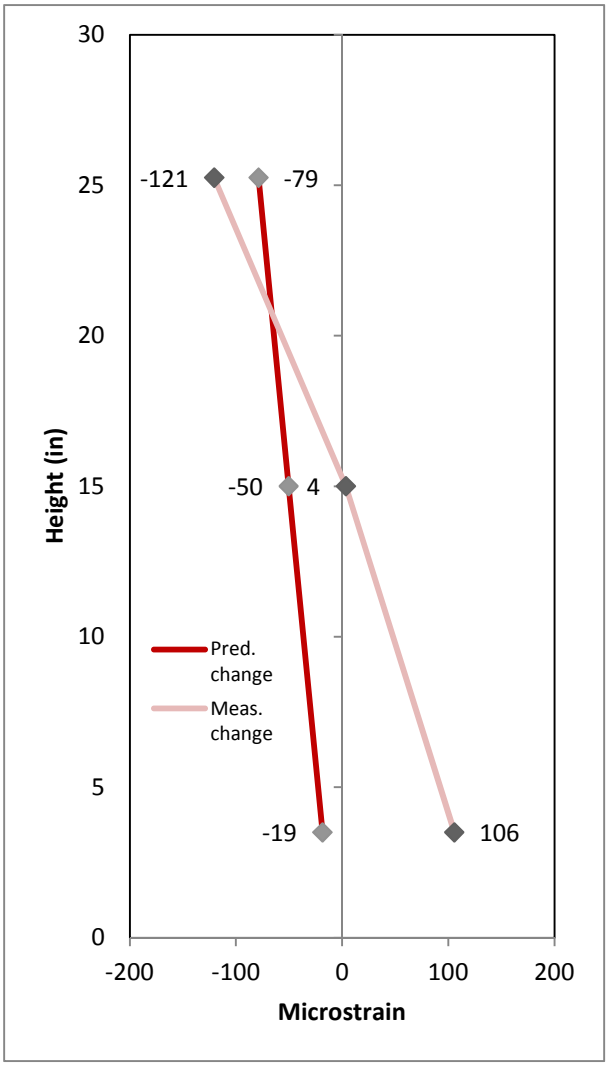

Figure 5-15. Day 215 Strains at 0.4L

From these graphs it is clear that Bowers' model and the measured data do not fit together perfectly. There is a significant amount of difference, with some measured values being more than three times as large as the predicted values. Unlike the live load test and the other events such as the setting of the panels and the post-tensioning process, these values are taken from much more extended time periods. The graphs do, however, show some of the same trends. All of the graphs show the top gauge within the deck increasing in compressive strain and the strain at the bottom of the beam becoming relatively more tensile. All of the plots except for Figure 5-14 have measured and predicted values with very similar slopes. All of the graphs also show a fairly linear strain distribution throughout the cross-section. This is critical in proving that the deck and beams are acting compositely and straining together.

While not all of the plots have values similar to the predicted strains, they all present gradients with the same direction of slope as the predicted strain gradients. This means that while Bowers' current model is unable to accurately predict the measured strains over time, it did predict the overall trends in the data. Also, up until about day 140, the model seemed to predict the general magnitude of the measured strains fairly well. The reasons for her model not following the data perfectly may in large part be due to temperature effects. It is also possible that the boundary conditions were not acting exactly as they were modeled. Bowers' model also calculates creep and shrinkage based on the AASHTO model, which may not follow the true behavior of the concrete. In addition to studying the boundary conditions and inputting the actual creep and shrinkage behavior, it is necessary for future researchers to further study the effects of temperature on the strains and stresses in a continuous three-span precast deck panel bridge in order to determine whether Bowers' model is truly accurate.

5.2 Live Load Test Results

The live load test of the Route 65 bridge took place on February 2, 2012. As described previously in section 3.4, there were sixteen different truck runs performed during this test in order to study several different aspects of the bridge and its structural system. On the morning of the 2nd the gauges were attached as described in section 3.3, and the bridge and the data loggers were prepared for the live load test. Setup commenced at 8 am and continued until the tests began at 1 pm. Live load testing concluded at 4 pm.

Data was collected during the live load test using three different data loggers. The BDI Wifi data acquisition system was used during all of the live load test runs, and recorded data from all of the temporary gauges at 50 Hz. The CR23X data logger, which was used to record strains from the eight previously installed vibrating wire gauges, was used in combination with the BDI Wifi system for runs 1-4. The CR3000 data logger, which can also be used to record strains from the eight previously installed vibrating wire gauges, was used in combination with the BDI Wifi system for runs 5-12. The fastest rate at which the CR23X data logger can record data is 1 measurement per minute. This means that the CR23X is really only capable of recording data from static loads. During runs 1-4, the trucks stopped in each of the predetermined positions for three minutes in order for the CR23X to record at least 2 data points for that location. The CR3000 data logger (which is a prototype device and is still being tested) takes measurements at 50 Hz. During runs 5-8 the trucks stopped in each position for approximately 30 seconds. Due to the much faster data collection rate, the CR3000 data logger is more suited to dynamic loading tests and other high-speed testing applications than the CR23X. This live load test was the first time that the CR3000 prototype data logger was used during a field test by Virginia Tech.

5.2.1 Results Comparison between the CR23X and CR3000 Data Loggers (Runs 1 and 5)

The data produced from runs 1 and 5 had two main purposes. The first of which was to verify that the CR23X and CR3000 data loggers were recording similar strains when subjected to the same loading pattern. If the data proved to be similar, it would verify that the CR3000 was working properly and recording accurate data despite the fact that it has never before been used. The second purpose was to provide a reference point for comparisons to the dynamic load tests. The dynamic tests were run in much the same pattern as test runs 1 and 5 except that the trucks did not stop at the three locations along the length of the bridge, and were, therefore, much shorter duration tests. Figure 5-16 presents a diagram showing the orientation of the truck and its location along the length of the bridge where it stopped.

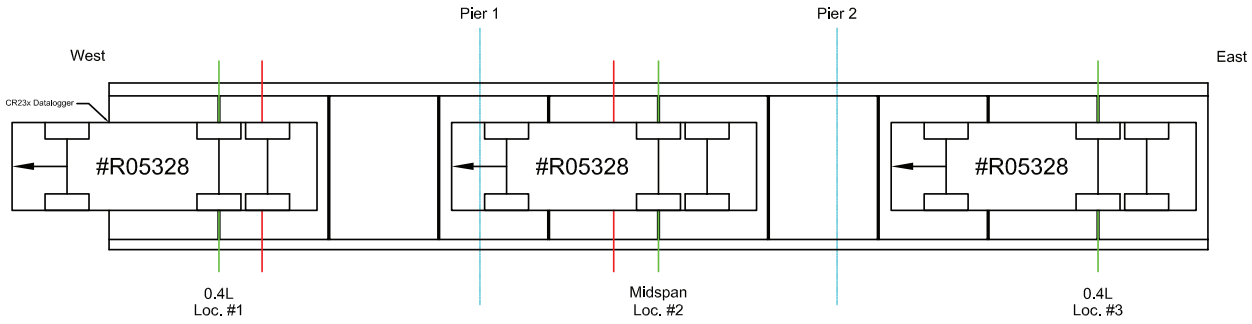

Figure 5-16. Stopping Positions for Runs 1 and 5

The data from runs 1 and 5 were compared at the end of run 8, which was the last of the static tests. If the recorded data sets were similar, the dynamic tests would have been run as planned. If the recorded data sets were not similar, it would be assumed that the CR3000 data logger was not working properly and the dynamic tests would be replaced by more static tests to be recorded by the CR23X. When the data from runs 1 and 5 was compared, however, the two data loggers produced nearly identical results. The measurements taken during runs 1 and 5 are presented in Table 5-5. Note that run 5 was the first

time that the CR3000 data logger was used during that day, and during this run it happened to exhibit a malfunction where the data file did not have a record of any of the strains measured during run 5 until the truck had already moved away from position #3 at 0.4L of the last span. Therefore, there is no data to compare from the CR3000 data logger at truck position #3. The data recordings only began after the truck was already stopped at position #2. The data, therefore, had to be zeroed using the equilibrium conditions after the truck had completely left the bridge as a reference point. It is unknown why this error occurred, but it did not occur on any of the other tests throughout the day.

Table 5-5. Comparison of Results from Runs 1 and 5

	Truck Location 3			Truck Location 2			Truck Location 1		
Gauge	Run 1 (CR23X)	Run 5 (CR3000)	Diff.	Run 1 (CR23X)	Run 5 (CR3000)	Diff.	Run 1 (CR23X)	Run 5 (CR3000)	Diff.
VWG 1 (με)	0	n/a	**n/a**	-2	-2	**0**	15	15	**0**
VWG 2 (με)	1	n/a	**n/a**	-5	-5	**0**	40	39	**1**
VWG 3 (με)	3	n/a	**n/a**	-9	-11	**2**	-3	-5	**2**
VWG 4 (με)	4	n/a	**n/a**	-24	-23	**-1**	-10	-10	**0**
VWG 5 (με)	-3	n/a	**n/a**	-3	1	**-4**	-6	-2	**-4**
VWG 6 (με)	2	n/a	**n/a**	3	1	**2**	-3	-4	**1**
VWG 7 (με)	-2	n/a	**n/a**	1	2	**-1**	1	2	**-1**
VWG 8 (με)	2	n/a	**n/a**	3	2	**1**	3	1	**2**
BDI 1 (με)	0	1	**0**	-5	-5	**0**	51	50	**1**
BDI 2 (με)	0	1	**-1**	-4	-5	**0**	49	48	**1**
BDI 3 (με)	0	1	**-2**	-6	-5	**-2**	43	44	**-1**
BDI 4 (με)	-6	-6	**0**	25	24	**0**	-12	-8	**-3**
BDI 5 (με)	-9	-9	**1**	47	51	**-4**	-12	-10	**-2**
BDI 6 (με)	-7	-8	**1**	45	46	**0**	-6	-7	**1**
Twanger 1 (in)	-0.001	-0.001	**0.000**	0.004	0.003	**0.001**	-0.030	-0.030	**0.000**
Twanger 2 (in)	-0.001	-0.001	**0.000**	0.005	0.005	**0.000**	-0.032	-0.031	**-0.001**
Twanger 3 (in)	-0.001	-0.001	**0.000**	0.006	0.006	**0.000**	-0.027	-0.026	**-0.001**
Twanger 4 (in)	0.006	0.005	**0.001**	-0.049	-0.049	**0.001**	0.005	0.005	**0.000**
Twanger 5 (in)	0.007	0.007	**0.001**	-0.044	-0.045	**0.000**	0.006	0.006	**0.000**
Twanger 6 (in)	0.009	0.008	**0.000**	-0.035	-0.035	**0.000**	0.008	0.008	**0.001**
LVDT 1 (in)	0.000	0.000	**0.000**	0.000	0.000	**0.000**	0.000	0.000	**0.000**
LVDT 2 (in)	0.000	0.000	**0.000**	0.000	0.000	**0.000**	0.000	0.000	**0.000**
BDI 7 (με)	4	-1	**4**	10	8	**2**	15	5	**11**
BDI 8 (με)	1	-1	**2**	10	6	**4**	8	2	**5**

During runs 1 and 5, the vibrating wire gauges were recorded by the CR23X and the CR3000 data loggers and the rest of the gauges were recorded by the BDI Wifi system. This means that the data collected by the BDI Wifi system acted as a control in order to verify that the bridge was subjected to the same loads during each run. If the results recorded by the BDI Wifi system did not match between the two tests, it

would not be possible to determine if the CR3000 system was working properly. Fortunately, the data collected by the BDI Wifi system was nearly identical, which meant that the bridge was subjected to the same loads during tests 1 and 5. The only gauges that showed some difference in values between the tests were BDI gauges 7 and 8, which were on top of the deck. These gauges, however, displayed a significant amount of drift during the tests. The drift was caused by sunlight warming and expanding the gauges during the length of the test. This error would be especially prevalent during the long test durations when using the CR23X data logger. Therefore, it could then be concluded that, because the measured strains of the eight vibrating wire gauges were also very similar between the two runs, the CR3000 data logger was working properly. It was, therefore, assumed that the data logger would function properly and record accurate measurements during the dynamic tests.

Figure 5-17 and Figure 5-18 present VWG data from VWGs 1-4 during runs 1 and 5. These two graphs illustrate the differences between the CR23X data logger and the CR3000 data logger. Notice the large variation in overall testing time, which was 1550 seconds during run 1 and only 110 seconds during run 5. Also notice that the plot from run 5 is missing a significant portion of data due to the malfunction described previously. The dotted vertical lines represent truck locations. The first and last lines (from left to right) represent the points in time when the truck travelled onto the bridge and when the truck travelled off of the bridge. The other lines represent the periods of time when the truck was stopped at the three locations described by Figure 5-15, with the first line showing when the truck stopped and the second line showing when the truck began moving again.

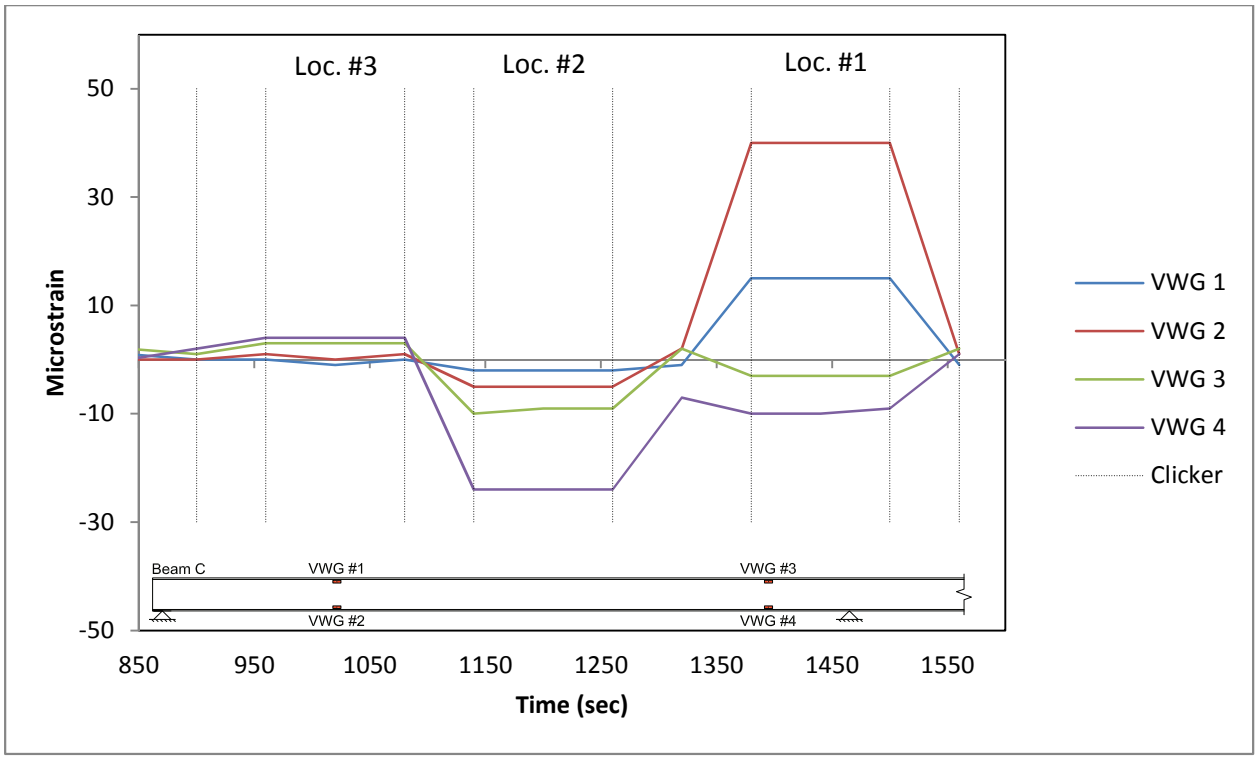

Figure 5-17. Test Run #1 Strain Plot for VWGS 1-4

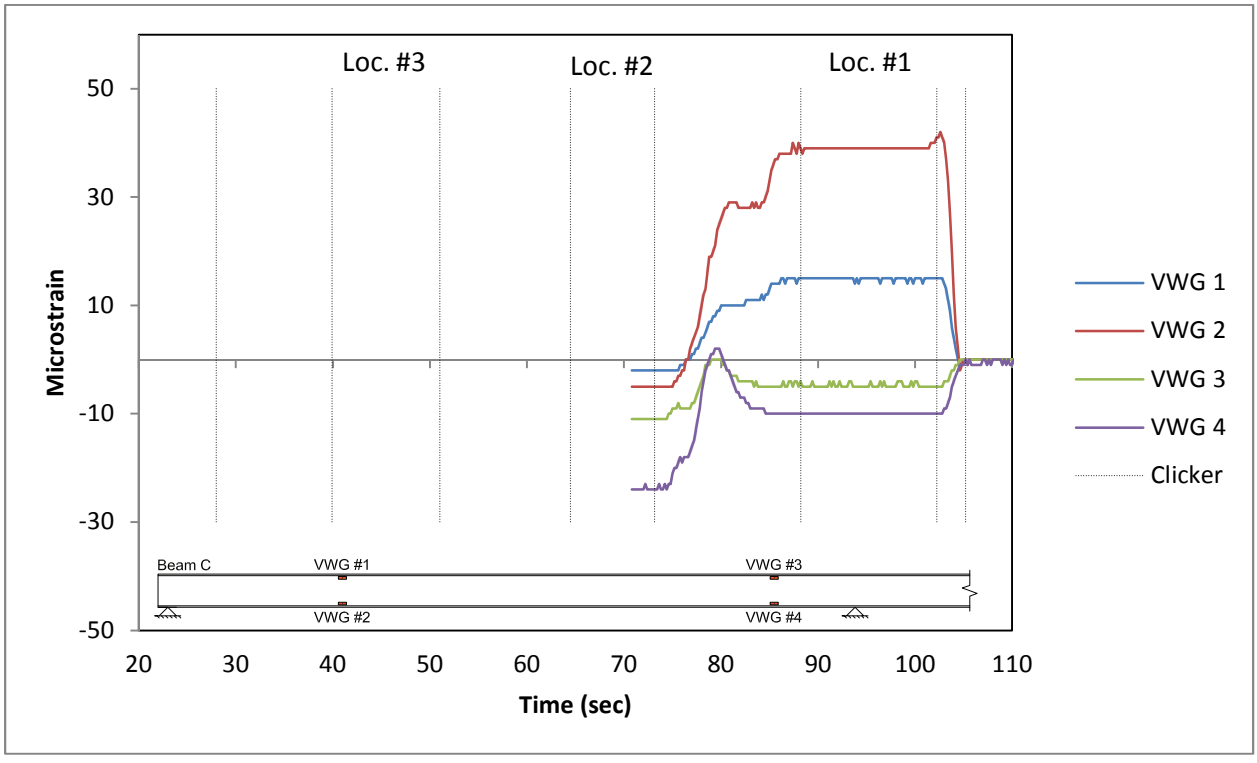

Figure 5-18. Test Run #5 Strain Plot for VWGS 1-4

Figure 5-19 and Figure 5-20 present the strain plots from BDI gauges 1-6 from runs 1 and 5, respectively. Note that the grey dotted lines represent the same points in time as described previously for Figure 5-17 and Figure 5-18.

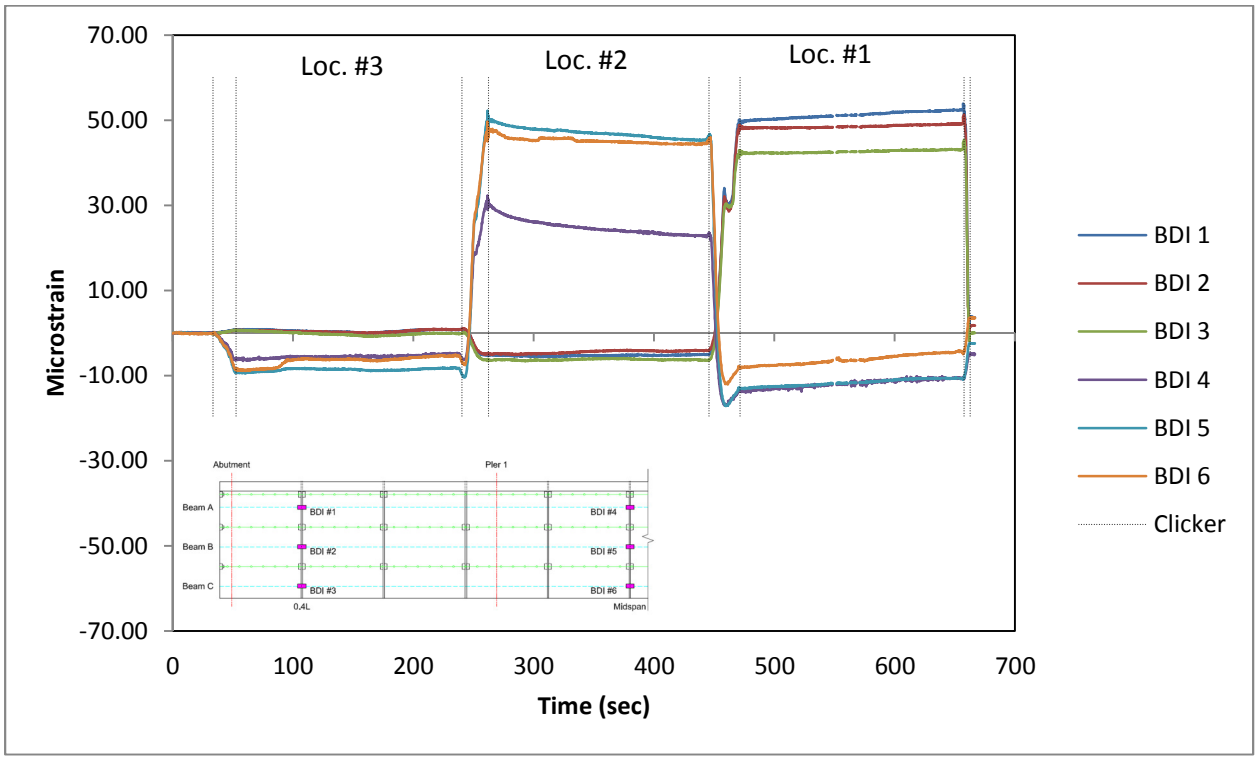

Figure 5-19. Test Run #1 Strain Plot for BDI gauges 1-6

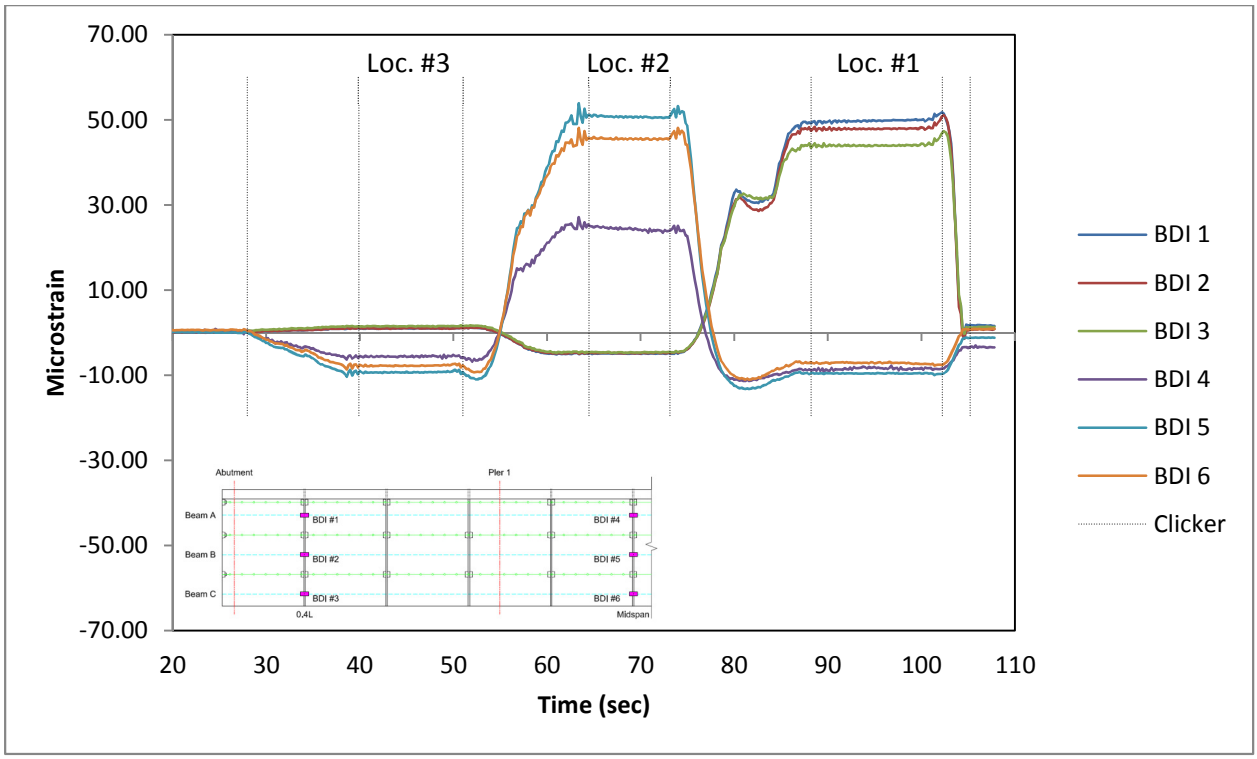

Figure 5-20. Test Run #5 Strain Plot for BDI gauges 1-6

The maximum difference between the VWG measurements recorded by the CR23X and the CR3000 data loggers is 4 με, which was measured by VWG 5 when the truck was at location 1 and 2. The average difference in VWG measurements was 1 με. The BDI Wifi system exhibited a similar outcome. The maximum difference between the BDI gauges located beneath the bridge was 4 με. The maximum difference between BDI gauges located on top of the bridge was 11 με which was measured by BDI gauge 7. This disparity, however, was caused by sunlight hitting the gauge which made it expand and record false increases in strain. The maximum difference between the twanger and LVDT readings was 0.001 in. The average difference in strain measurements between the two tests was 2 με among the BDI gauges and 0 in. among the twangers and LVDTs. Due to such similar data, it was concluded that the CR3000 data logger was working properly. All of the graphs created from tests 1 and 5 are located in Appendix I.

5.2.2 Negative Moment Test

Runs 2-4 and 6-8 were different from runs 1 and 5 because runs 2-4 and 6-8 utilized two trucks which only stopped once on the bridge. As described previously in section 3.4, the purpose of these runs was to maximize the negative moment over pier 1 in order to study the effects this negative moment has on the joint nearest the pier. For reference, Figure 3-28 is presented again as Figure 5-21 and shows the exact stopping positions of the two trucks.

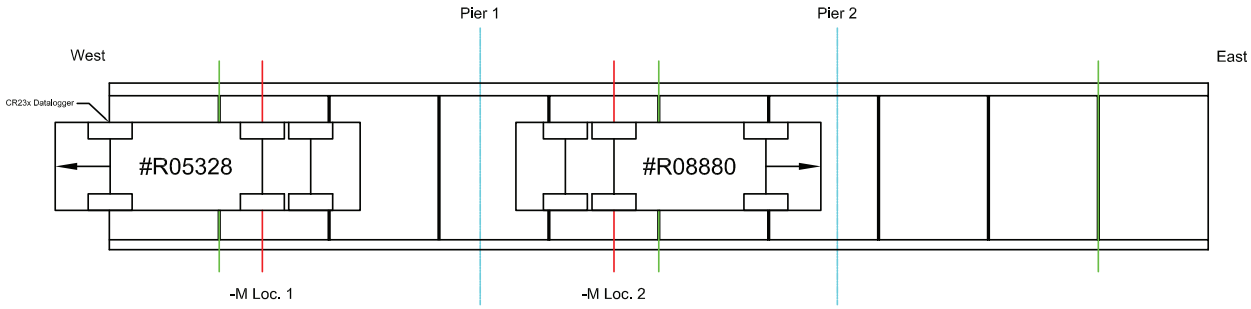

Figure 5-21. Stopping Positions for Runs 2-4 and 6-8

During these negative moment tests, the gauges of interest were the ones located at the panel joint between panels 4B and 3C. These gauges include LVDT 1 and 2, BDI gauges 7 and 8, and VWGs 3, 4, 7, and 8. LVDT 1 and BDI gauge 7 were located on top of the deck near the exterior edge of the traffic lane. LVDT 2 and BDI gauge 8 were also located on top of the deck, but were near the interior edge of the traffic lane. VWGs 7 and 8 were embedded within panel 4B 2.75 in. from the top of the panel. VWGs 3 and 4 were positioned on Beam C with VWG 3 near the top of the beam's cross-section and VWG 4 near the bottom. Figure 5-21 presents a simplified view of the bridge and the gauges used during the live load test.

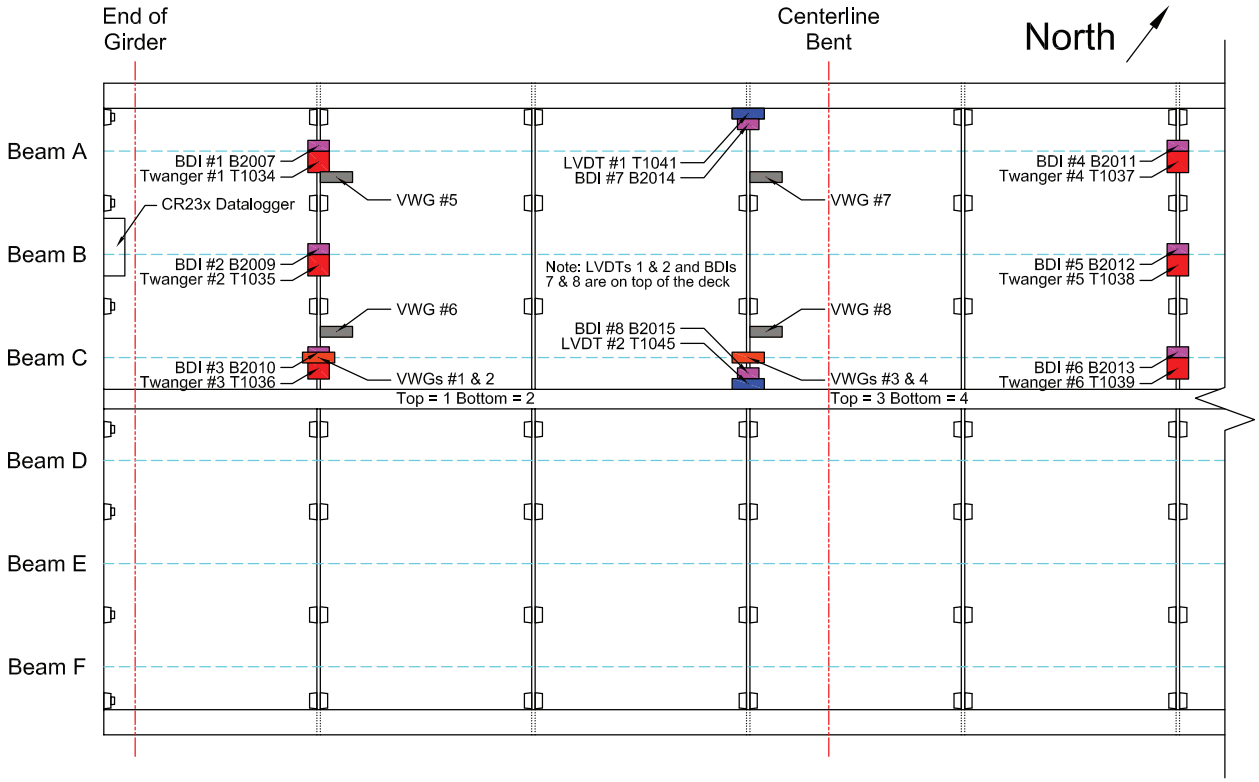

Figure 5-22. Simplified View of Live Load Test Gauges

Graphs showing the recorded data from all the test runs are located in Appendix I, but for discussion, the plots created from Run 2 are presented in Figure 5-23, Figure 5-24, Figure 5-27, Figure 5-28, Figure 5-29, and Figure 5-30. Figure 5-23 presents the recorded data from VWGs 1-4 during Test Run 2, and Figure 5-24 presents the data from VWGs 5-8. In Figure 5-23 and Figure 5-24 the area between the vertical dotted lines represents the period of time that the trucks were in position and stopped. In the rest of the figures, there are four lines with the additional two lines representing the time at which the truck entered and left the bridge. The middle two lines represent the same thing as the two lines in Figure 5-23 and Figure 5-24, which is that the trucks are stopped and in position. On the graphs, positive strain values indicate tension and negative strain values indicate compression.

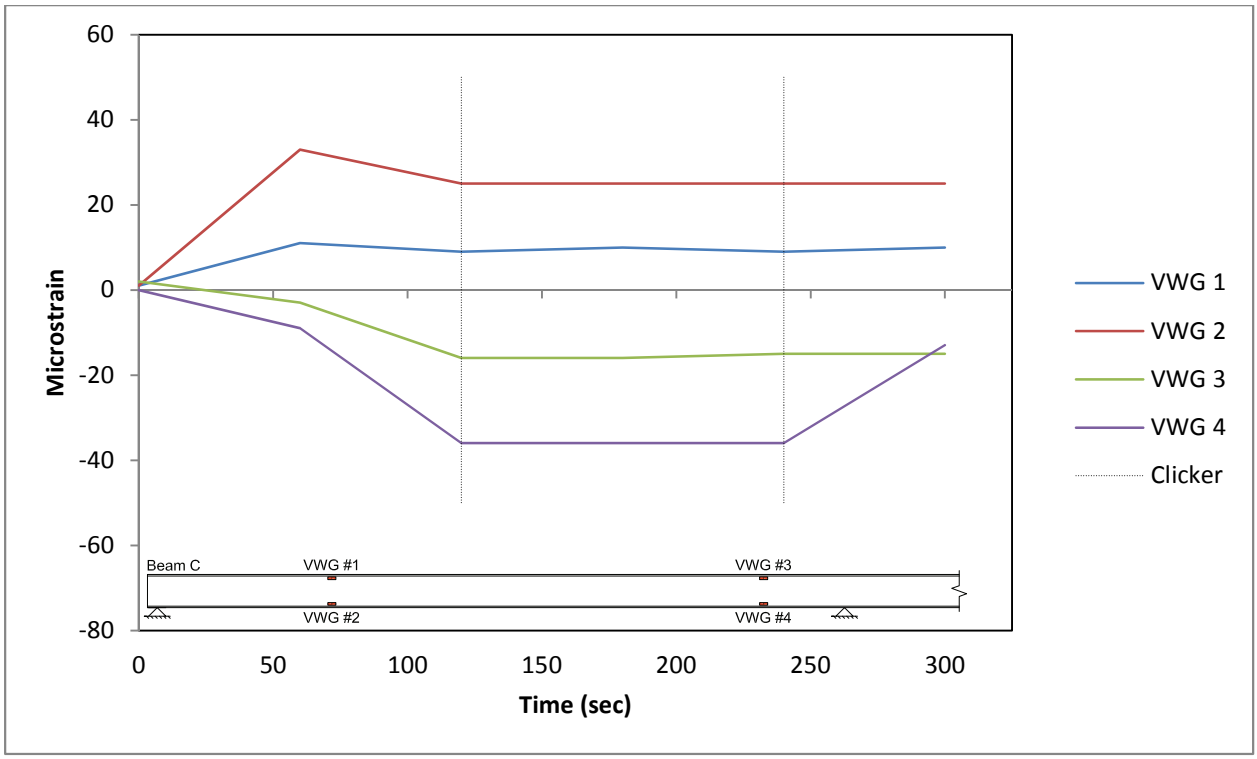

Figure 5-23. Test Run #2 Strain Plot for VWGs 1-4

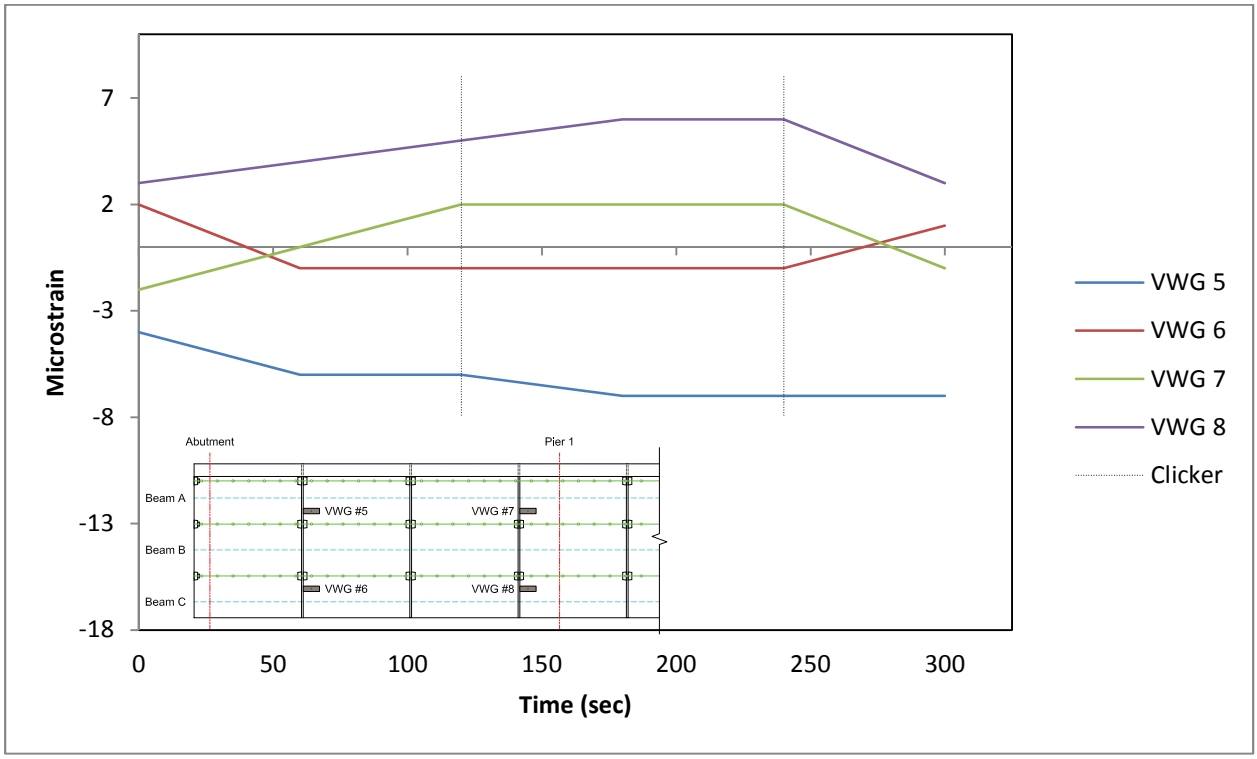

Figure 5-24. Test Run #2 Strain Plot for VWGs 5-8

As shown in Figures Figure 5-23 and Figure 5-24, the CR23X data logger was able to record three data points during the time the trucks were stopped and in position. The strain measurement over this period was taken as an average of those three readings. In order to understand the trends presented in Figures Figure 5-23 and Figure 5-24, Figure 5-25 presents a moment diagram (kip-in.) considering the full axle loads. Note that gauge location #1 represents the position of the gauges located at the panel joint between panels 1A and 2B, which is the joint nearest 0.4L of the span between Abutment A and Pier 1. Gauge location #2 represents the location of the gauges at the panel joint between panels 3C and 4B, which is the joint nearest Pier 1. Gauge location #3 represents the location of the gauges at the panel joint between 5D and 6C, which is the joint at the center of the bridge.

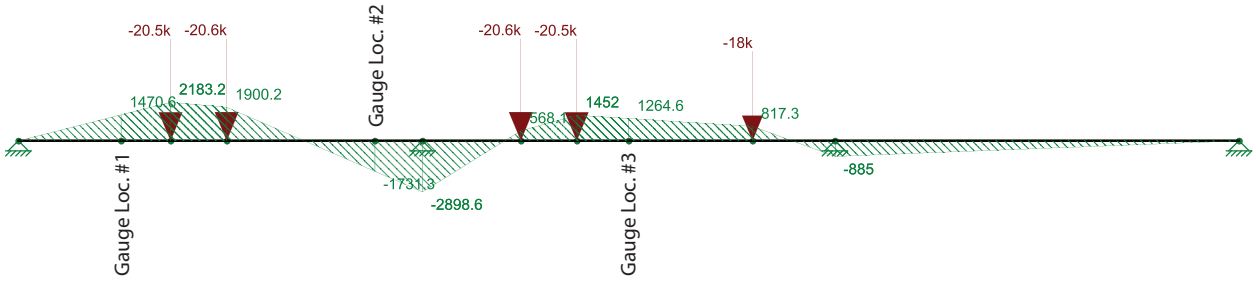

Figure 5-25. Moment Diagram Considering Full Axle Loads

Also necessary to interpret the strains presented in Figure 5-23 and Figure 5-24 is a drawing of the estimated location of the elastic neutral axis, which is presented in Figure 5-26. From this figure, it is assumed that the vibrating wire gauges embedded within the deck panels (VWGs 5-8) and any gauges placed on the top of the deck (LVDT 1 and 2 and BDI gauges 7 and 8) are above the neutral axis. All other gauges, which include VWGs 1-4, are below the neutral axis.

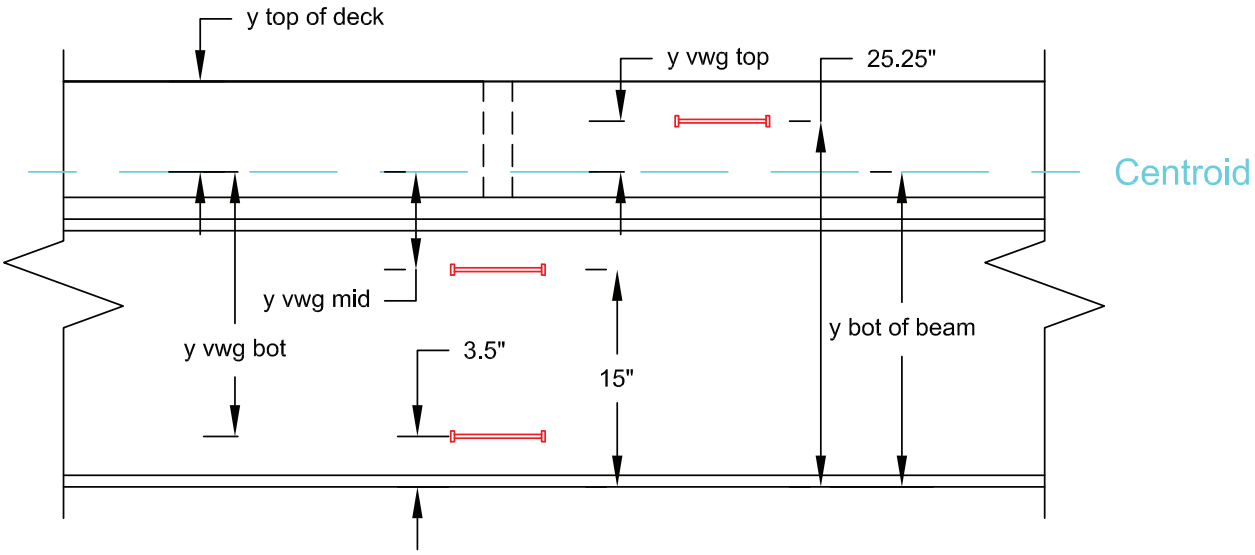

Figure 5-26. Approximate Location of the Composite ENA

In the graph in Figure 5-23, VWGs 1 and 2 exhibit an increase in tensile strain, with VWG 2 displaying a greater increase in strain than VWG 1. This data is consistent with the assumptions and simplifications made in Figure 5-25 and Figure 5-26. VWGs 1 and 2 are located at Gauge Location #1, which is in a zone of positive moment, and both gauges are assumed to be below the neutral axis with VWG 2 farther from the neutral axis than VWG 1. The opposite is true for VWGs 3 and 4 which exhibit an increase in compressive strain. As shown in Figure 5-21, VWGs 3 and 4, which are at Gauge Location #2, are in a zone of negative moment. Therefore, it makes sense that the increase in strains in VWGs 3 and 4 are negative.

The same trends can be viewed in Figure 5-24. In this case, however, all VWGs are assumed to be above the neutral axis, which causes a reversal of the signs of the strains at Gauge Location #1 and #2. Therefore, VWGs 5 and 6, which are within a zone of positive moment exhibit an increase in negative strain and VWGs 7 and 8, which are within a zone of negative moment exhibit an increase in positive strain. It is also consistent with the predicted location of the neutral axis that the strains within the

VWGs in the deck is overall less than the strains within VWGs 1-4 because of how much closer the gauges are to the neutral axis. Similar trends are also present in the data collected from the six BDI strain gauges, presented in Figure 5-27.

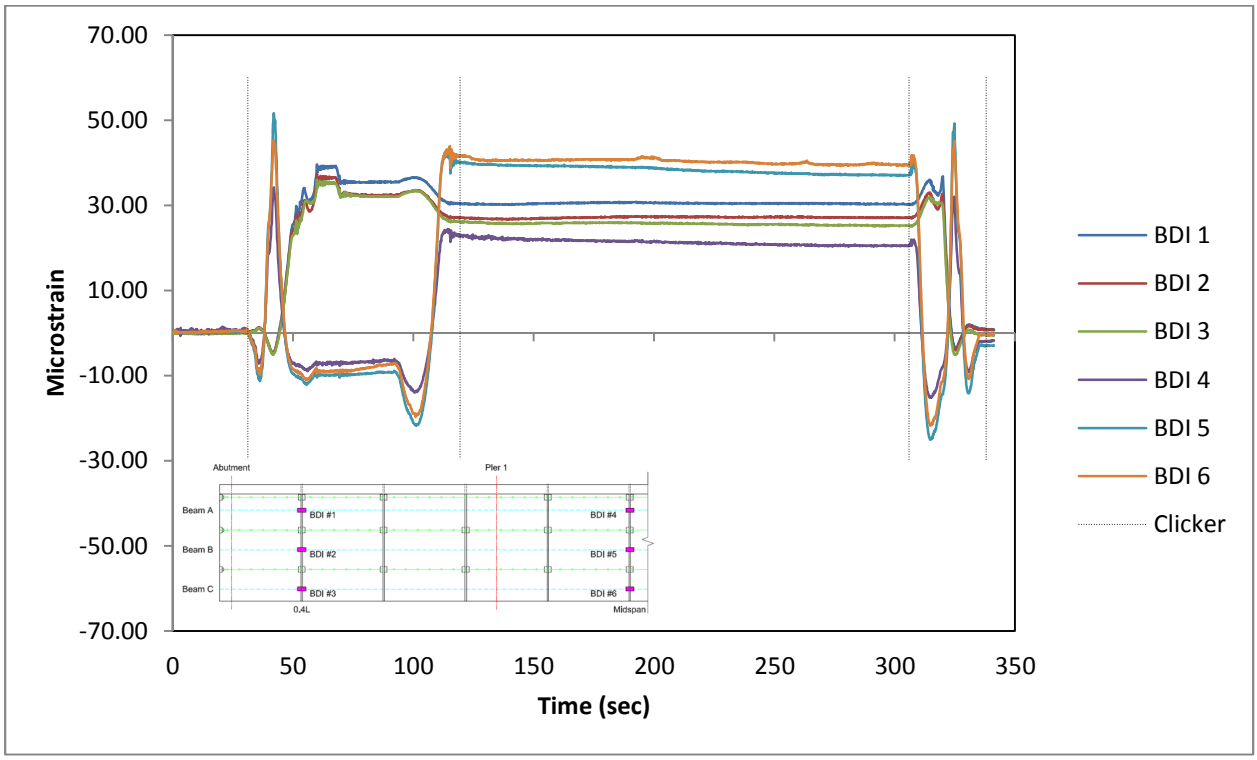

Figure 5-27. Test Run #2 Strain Plot for BDI Gauges 1-6

In this case, all six BDI strain gauges are in locations of positive moment. BDI gauges 1-3 are located at Gauge Location #1, and BDI gauges 4-6 are located at Gauge Location #3 in Figure 5-25. Because all of the gauges are subjected to positive moment and are located below the neutral axis, they all should and did present positive tensile strain measurements. The magnitude of the strains is slightly dissimilar to the model, because according to the model there should be higher tensile strains at Gauge Location #1 than at Gauge Location #3. In the recorded data, BDI gauges 1, 2, and 3 are all tightly grouped at approximately 30 με. BDI gauges 5 and 6 exhibited higher strain measurements, at approximately 40 με,

while BDI gauge 4, which is essentially at the same location as BDI gauges 5 and 6, exhibited much lower strains at approximately 20 με. Overall, however, all six gauges presented strains which were consistent with the predicted values in sign and were of similar magnitudes.

The deflections of Twangers 1-6 were all measured as negative values, which indicate that the bridge was deflecting downwards. Figure 5-28 presents the Twanger deflections recorded during Test Run #2.

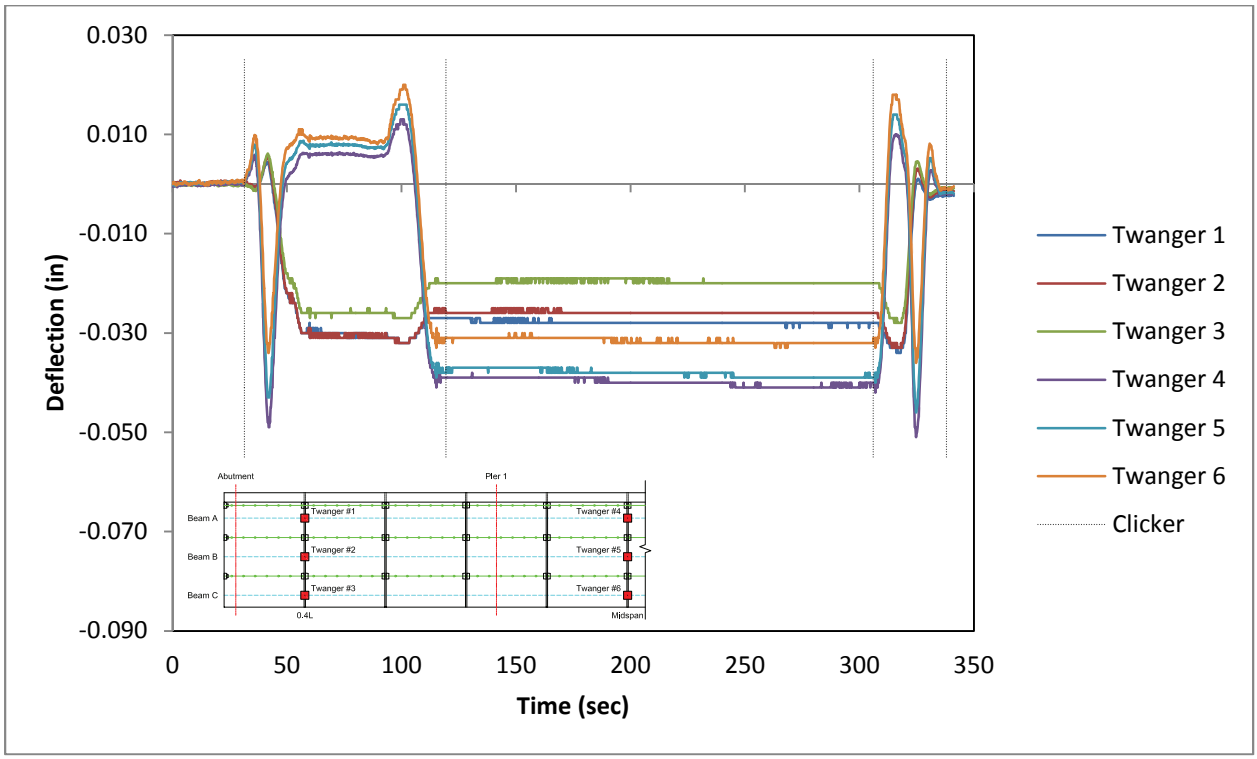

Figure 5-28. Test Run #2 Strain Plot for Twangers 1-6

Similar to the trends presented by BDI gauges 1-6, Twangers 4, 5, and 6 all presented slightly larger deflections than the deflections measured by Twangers 1, 2, and 3. Also, there seems to be a trend that Twangers 3 and 6, which are both located on Beam C, are deflecting less than the other Twangers. This could be explained by the transverse positioning of the trucks, which may have been slightly off-center and with more of the truck weight being supported by Beams A and B.

Of special importance during the negative moment test runs was the data collected by the four gauges located on top of the deck. LVDT 1 and BDI gauge 7 were located on the outside edge of the Phase I lane, and LVDT 2 and BDI gauge 8 were located on the inside edge of the travel lane. The data collected by these gauges is presented in Figure 5-29 and Figure 5-30.

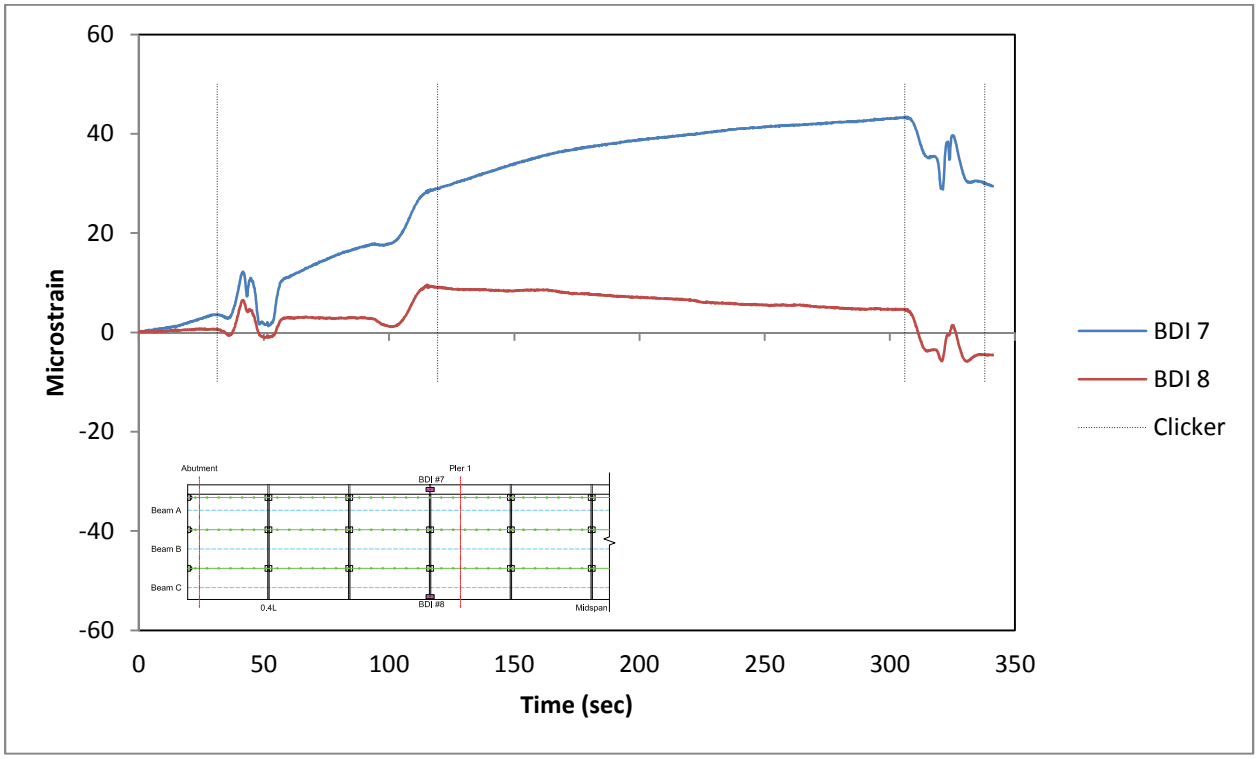

Figure 5-29. Test Run #2 Strain Plot for BDI Gauges 7 and 8

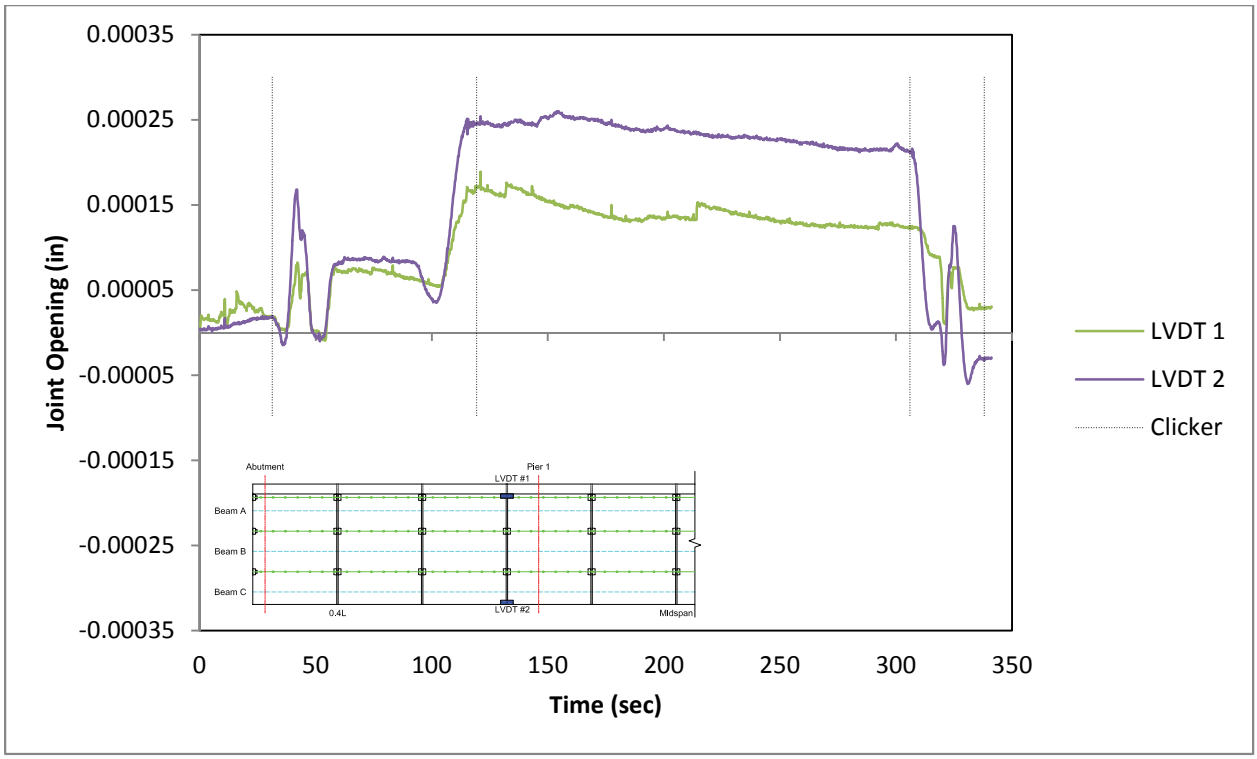

Figure 5-30. Test Run #2 Strain Plot for LVDTs 1 and 2

BDI gauges 7 and 8 show an increase in tensile strains and LVDTs 1 and 2 show a slight increase in positive displacement indicating joint expansion. This trend is consistent with the model's predictions. Note that the LVDT data measurements were all below the calibrated limit of 0.001 in, which means that while the sign convention is correct, the accuracy of the values cannot be verified.

Also of note is the large slope of BDI gauge 7 and its relative magnitude compared to BDI gauge 8. During the time that the truck is stopped the measurement of BDI gauge 7 changes 10 με, while BDI gauge only changes approximately 3 με. This large variation in strains could have been caused by a variety of different things. One possibility was that BDI gauge 7 was not properly secured to the bridge. It is also possible that the gauge was just not functioning properly, or that the gauge was subjected to direct sunlight during the test which heated the gauge and caused it to give incorrect readings. This

trend of BDI gauge 7 increasing in tensile strain can also be seen in test runs 3 and 4, as shown in Figure 5-31 and Figure 5-32. The trend is not, however, present in any other data sets. The increase in strain may just be a product of such a long waiting period in between stops. In runs 1, 2, and 3 the trucks stayed in position for nearly three minutes while the rest of the negative moment tests, the trucks only stayed in position for approximately 30 seconds. For purposes of data comparison and because the cause of this data fluctuation was never fully determined, the measurements were averaged from the time when the truck stopped until it began moving again.

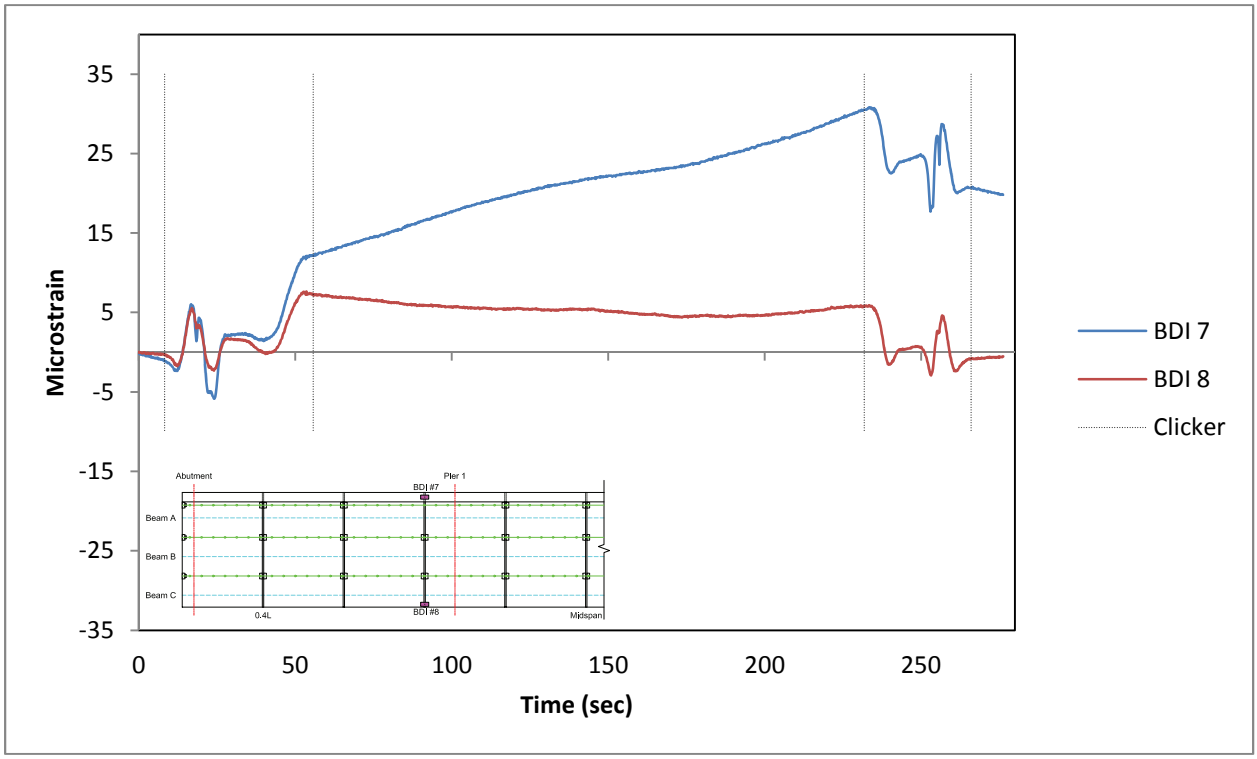

Figure 5-31. Test Run #3 Strain Plot for BDI Gauges 7 and 8

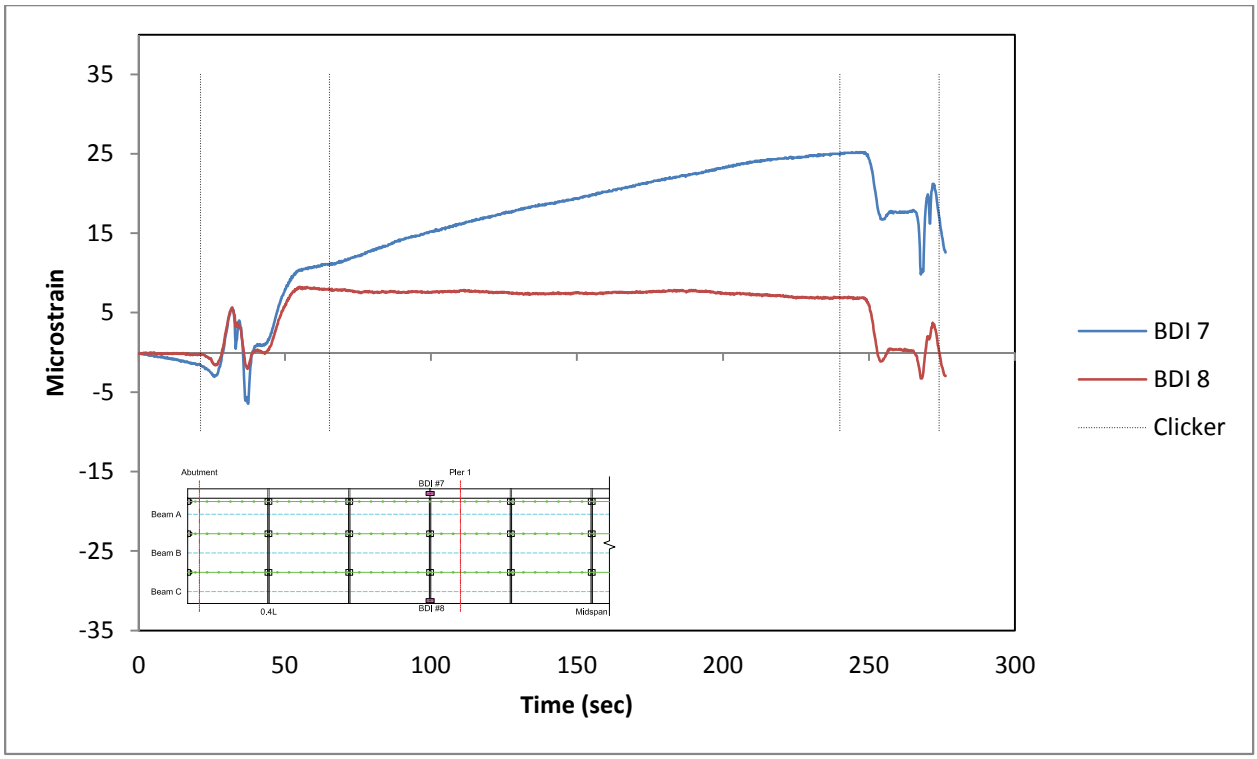

Figure 5-32. Test Run #4 Strain Plot for BDI Gauges 7 and 8

The reason for the difference in BDI 7 and 8 may be a result of the differing tributary widths, the transversely-varying truck positions, or the difference in moment of inertia of the barrier rails.

The individual plots from all of the negative moment test runs are not presented in this section, but exhibit the same patterns as discussed previously in the results from Test Run #2. All of the plots are, however, presented in Appendix I. The final numerical results are presented in Table 5-6. Note that only the gauges of particular interest during the negative moment tests are included. These gauges are VWG 3, 4, 7, and 9; BDI gauges 7 and 8; and LVDTs 1 and 2.

Table 5-6. Negative Moment Test Results

Run #	VWG 3 (με)	VWG 4 (με)	VWG 7 (με)	VWG 8 (με)	BDI 7 (με)	BDI 8 (με)	LVDT 1 (in)	LVDT 2 (in)
2	-16	-36	2	6	38	7	0.000	0.000
3	-13	-33	2	7	21	5	0.000	0.000
4	-15	-35	1	7	19	7	0.000	0.000
6	-17	-35	4	3	14	9	0.000	0.000
7	-15	-32	3	3	12	8	0.000	0.000
8	-17	-37	5	3	12	8	0.000	0.000
Static Average	**-15**	**-35**	**3**	**5**	**20**	**7**	**0.000**	**0.000**
3-Beam Predict.	**-21**	**-48**	**7**	**4**	**15**	**11**	**0.000**	**0.000**
5-Beam Predict.	**-12**	**-29**	**4**	**3**	**9**	**7**	**0.000**	**0.000**
3-Beam % Difference	**25%**	**28%**	**59%**	**-12%**	**-33%**	**33%**	**0%**	**0%**
5-Beam % Difference	**-24%**	**-20%**	**32%**	**-87%**	**-122%**	**-12%**	**0%**	**0%**
	Note: % Difference calculations are based on static average							

Most of the data in Table 5-6 is consistent among all the test runs, and only varies about 3 με. The data from BDI gauge 7, however, varied a lot. If the data from runs 2-4, when the gauge continually increased in strain measurements during the test, were disregarded, the static average would be 12.7 με. This would mean that the average measured strain for BDI gauge 7 would be almost exactly in between the 3-beam and 5-beam predicted values.

Overall, the data fit the model predictions well. The 3-beam prediction tended to over-predict the average strains, while the 5-beam prediction tended to under-predict the average strain. The measurements from VWGs 7 and 8 do not fall exactly within the two predicted values, but they are only off by one microstrain. Also of importance is the fact that LVDT 1 and LVDT 2 showed essentially no deflection due to joint expansion within their range of calibration which was 0.001 in.

5.2.3 Summary of Test Runs 9-12

The results from runs 9-12 were very similar to the results from static runs 1 and 5, except that there were no well-defined plateaus in the data plots where the trucks stopped and the overall test durations were much shorter. Due to the fact that the truck did not stop, the clicker was much more important, as

it was essential in determining the location of the trucks as they moved across the bridge. During these runs, the test duration was so short that the data logger was left running between the time when the first truck drove over the bridge and when the second truck ran over the bridge. The resulting graphs, therefore, show the strains from both trucks running in the same direction over the bridge. The trucks speed was calculated by the amount of time it took the truck to drive from one clicking location to the next. The speeds from runs 9-12 are presented in Table 5-7.

Table 5-7. Truck Speeds from Test Runs 9-12

Run #	ft/sec	mph
9a	1.9	1.3
9b	2.6	1.7
10a	2.1	1.4
10b	3.2	2.2
11a	37.9	25.8
11b	37.3	25.4
12a	34.5	23.5
12b	28.9	19.7

A plot of the BDI strain gauge results from Run 9 is presented in Figure 5-33. It is important to note that the vertical dotted lines, while very similar to the lines placed in the figures from the static tests, there is only one line marking each important location. This is because there is no period of time in when the truck stops at this location, the vertical line represents the point in time when the truck is passing through. To summarize, there are ten vertical lines on each plot, the first five correspond to the first truck and the second five correspond to the second truck. The first line for each truck represents when the truck enters the bridge and the last line represents then the truck leaves the bridge. The three lines in between represent the times in which the truck passes through locations 1-3 presented in Figure 5-16. The order in which the trucks pass through each location is dependent on the direction of travel of the trucks.

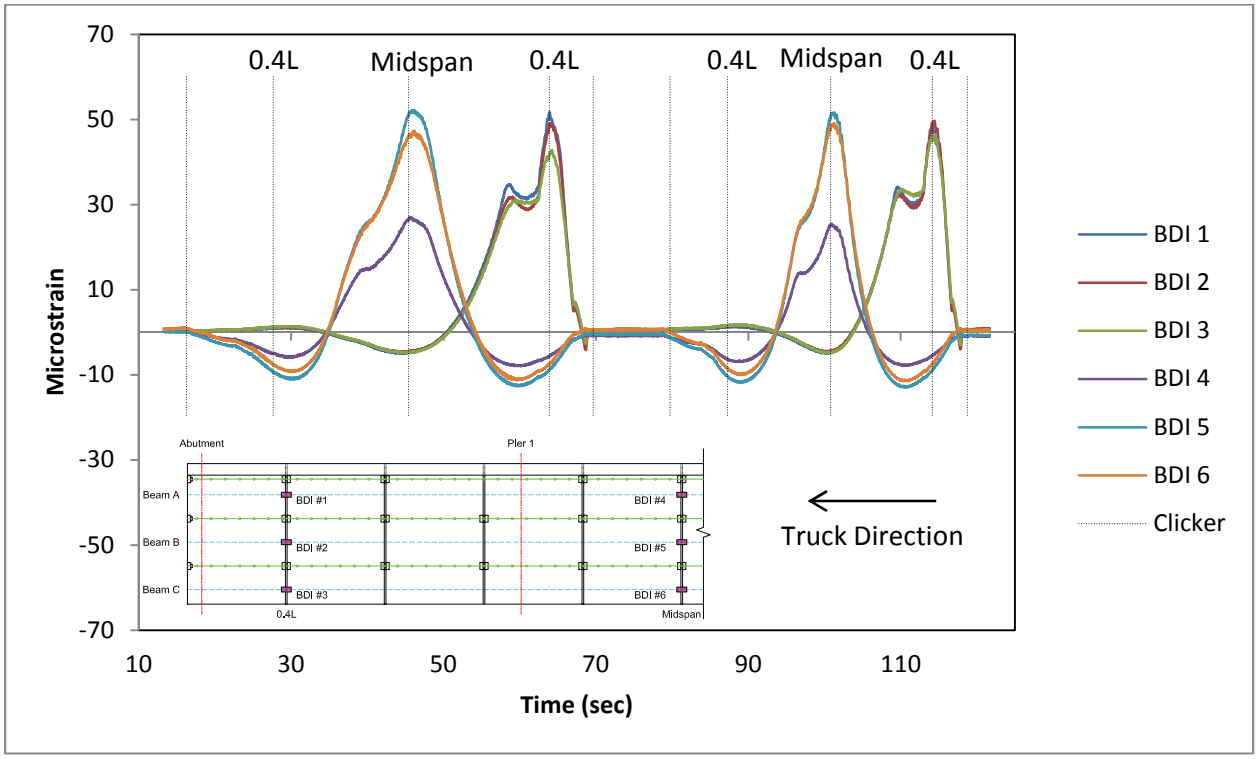

Figure 5-33. Test Run #9 Strain Plot for BDI Gauges 1-6

The graphs all follow the same patterns as described in detail in section 5.2.2. Overall, when comparing the crawling speed tests to the results of the static tests in runs 1 and 5, the difference in strains at gauge locations 1, 2, and 3 are minimal. The crawling tests produced on average 0.71% higher strains. When considering all of the different sources of error, this 0.71% increase in average strains is negligible. When increasing the speeds of the trucks to nearly 25 mph in test runs 11 and 12, the oscillating effects of the dynamic load were much more visible and caused a definite increase in strains and deflections. At location 1 (0.4L of the first span) there was on average a 10% increase in strains and deflections from the crawling speed to the high-speed dynamic test. At location 2 (center of the middle span) the increase in strains was only 5% on average. This decrease in dynamic effects at the center of the bridge may be due to the damping of the trucks' shock absorbers. The oscillating dynamic impacts are typically

initiated by a vehicle driving over the change in grade associated with leaving the pavement and entering the bridge's deck surface. This reduction in oscillations can be seen in the plot of BDI gauges 1-6 from run #11 in Figure 5-34. In this plot, there are fewer vertical clicker lines than on Figure 5-33. This is because at the speed of the trucks it was only possible to mark the points in time when the truck entered the bridge, crossed the center, and exited the bridge.

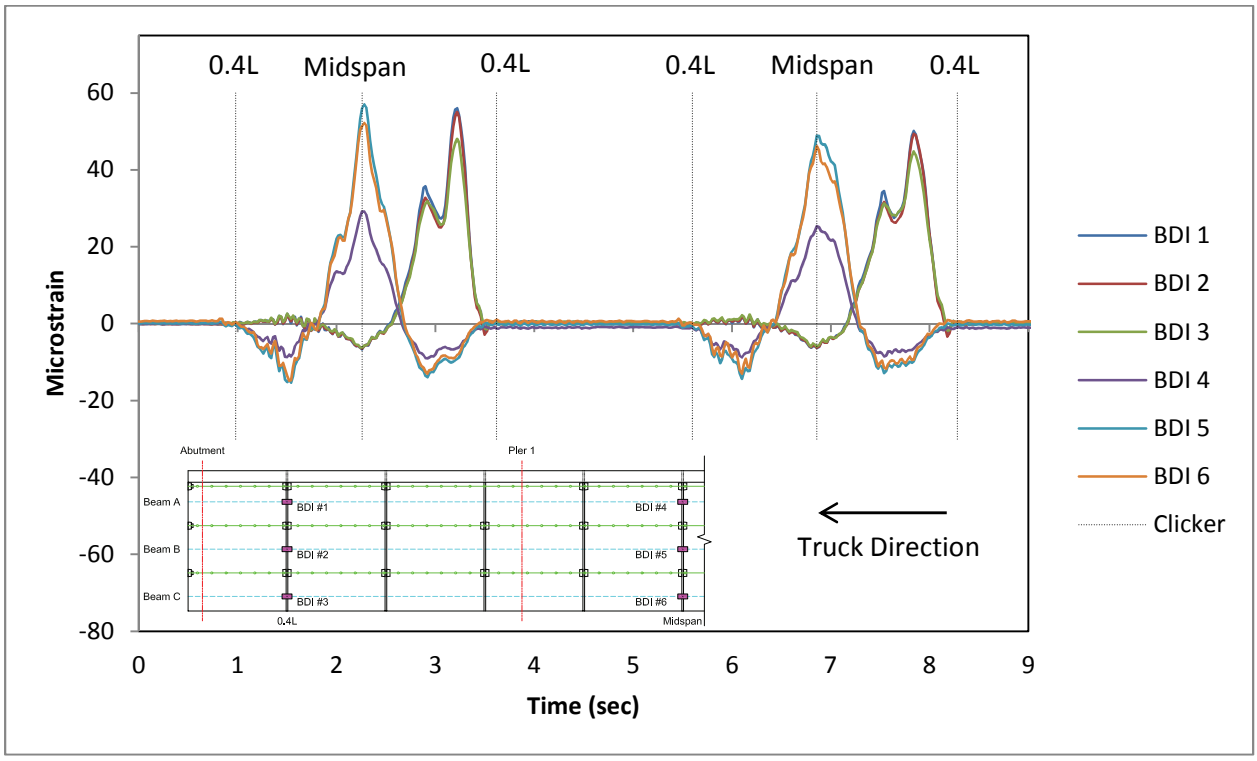

Figure 5-34. Test Run #11 Strain Plot for BDI Gauges 1-6

Notice that when comparing Figure 5-33 to Figure 5-34 the graphs are nearly identical except that Figure 5-34 has lines that are much more jagged than Figure 5-33, especially throughout the first half of the bridge. These jagged lines are directly related to oscillations caused by the truck driving onto the deck surface. The lines on Figure 5-34 do, however, become smooth again and more similar to Figure 5-33 after the center of the truck is past the first pier.

5.2.4 Comparison of Predicted Results and Measurements for Strains at Midspan and 0.4L

Overall, the two prediction models tended to predict an upper bound and a lower bound for the strains and deflections measured during the live load test. Table 5-8 presents the strains and deflections measured at midspan of the center span while the center of gravity of the truck was positioned directly over the gauges. Note that the percent difference calculations at the bottom of the table are calculated comparing the static average to the two predictive models. This value was used because the models do not take into account any effects of dynamic impact and are purely based on static loads.

Table 5-8. Measured and Predicted Strains and Deflections at the Midspan of the Center Span

Run #	BDI 4 (με)	BDI 5 (με)	BDI 6 (με)	Twanger 4 (in)	Twanger 5 (in)	Twanger 6 (in)
1	25	47	45	-0.049	-0.044	-0.035
5	24	51	46	-0.049	-0.045	-0.035
9a	27	51	46	-0.049	-0.045	-0.036
9b	25	51	48	-0.047	-0.044	-0.038
10a	25	52	50	-0.046	-0.045	-0.038
10b	24	49	49	-0.046	-0.045	-0.039
11a	29	56	51	-0.056	-0.051	-0.041
11b	25	49	46	-0.053	-0.047	-0.038
12a	21	38	40	-0.047	-0.044	-0.037
12b	25	47	45	-0.050	-0.046	-0.039
Static Average	**25**	**49**	**45**	**-0.049**	**-0.045**	**-0.035**
Crawling Average	25	51	48	-0.047	-0.045	-0.038
At Speed Average	25	48	46	-0.052	-0.047	-0.039
3-Beam Predict.	**90**	**84**	**81**	**-0.046**	**-0.042**	**-0.040**
5-Beam Predict.	**54**	**51**	**48**	**-0.027**	**-0.025**	**-0.024**
3-Beam % Difference	**73%**	**42%**	**44%**	**-7%**	**-6%**	**13%**
5-Beam % Difference	**54%**	**3%**	**6%**	**-81%**	**-78%**	**-45%**
	Note: % Difference calculations are based on static average					

As displayed in Table 5-8, the values attained through the static runs 1 and 5 are very similar to the values from the crawling speed tests and the high-speed tests. There is no significant trend towards increasing strains as the speed of the trucks increase. The twangers do, however, follow this trend and on average increase 0.003 in. of deflection from the static tests to the high-speed tests. Overall, the predicted values bracket the measured data with most of the values falling somewhere in between the

higher strain and deflection prediction of the 3-beam model and the lower strain and deflection prediction of the 5-beam model. BDI gauges 5 and 6 present values which are closely predicted by the 5-beam model, while the twangers present values which are closely predicted by the 3-beam model. BDI gauge 4 presented values which were much less than both predictive models and much less than the values of strain measured on the other two beams. This anomaly is not present in the deflection data where twanger 4, which is at the same location as BDI gauge 4, actually measured slightly higher deflections than the other twangers. The strain measurement produced by BDI gauge 4 may have been affected by the cross-bracing nearby or may have been attached to the bridge improperly. The twangers are less affected by such local phenomena and are more of a global measurement. Also, as shown in Table 5-8, there is no real increase in strains or deflections between the static/pseudo-static and the dynamic runs. This is due to the fact that, by midspan of the center span, the truck's shock absorbers have sufficiently dampened the oscillations typically observed during dynamic runs.

Table 5-9 and Table 5-10 present the strains and deflections measured at 0.4L of the first span (location #1) while the center of gravity of the truck was positioned directly over the gauges. Table 5-9 presents the measured and predicted strains and deflections at the bottom of the beams, while Table 5-10 presents the measured and predicted strains from the VWGs located on the side of beam A and within the panel.

Table 5-9. Measured and Predicted Strains and Deflections at 0.4L

Run #	BDI 1 (με)	BDI 2 (με)	BDI 3 (με)	Twanger 1 (in)	Twanger 2 (in)	Twanger 3 (in)
1	51	49	43	-0.030	-0.032	-0.027
5	50	48	44	-0.030	-0.031	-0.026
9a	52	49	42	-0.032	-0.031	-0.026
9b	48	49	46	-0.029	-0.032	-0.028
10a	50	52	50	-0.033	-0.036	-0.032
10b	50	52	50	-0.032	-0.036	-0.032
11a	56	55	48	-0.034	-0.035	-0.027
11b	50	49	45	-0.031	-0.033	-0.027
12a	70	77	76	-0.043	-0.050	-0.044
12b	60	58	51	-0.036	-0.039	-0.031
Static Average	**51**	**48**	**43**	**-0.030**	**-0.031**	**-0.027**
Crawling Average	50	51	47	-0.031	-0.034	-0.029
At Speed Average	59	60	55	-0.036	-0.039	-0.032
3-Beam Predict.	**87**	**81**	**78**	**-0.038**	**-0.035**	**-0.033**
5-Beam Predict.	**52**	**49**	**47**	**-0.023**	**-0.021**	**-0.020**
3-Beam % Error	**42%**	**41%**	**44%**	**21%**	**10%**	**20%**
5-Beam % Error	**3%**	**1%**	**7%**	**-30%**	**-50%**	**-33%**
	Note: % Error calculations are based on static average					

Table 5-10. Measured and Predicted Strains and Deflections at 0.4L Continued

Run #	VWG 1 (με)	VWG 2 (με)	VWG 5 (με)	VWG 6 (με)
1	15	40	-6	-3
5	15	39	-2	-4
9a	13	37	-2	-5
9b	16	41	-2	-5
10a	17	45	-2	-5
10b	16	45	-2	-5
11a	16	42	-3	-5
11b	14	36	-2	-5
12a	23	62	-2	-6
12b	18	49	-2	-6
Static Average	**15**	**40**	**-4**	**-4**
Crawling Average	15	42	-2	-5
At Speed Average	18	47	-2	-5
3-Beam Predict.	**28**	**66**	**-10**	**-6**
5-Beam Predict.	**17**	**40**	**-6**	**-3**
3-Beam % Error	**47%**	**40%**	**57%**	**39%**
5-Beam % Error	**12%**	**1%**	**28%**	**-1%**
	Note: % Error calculations are based on static average			

In a similar pattern to the results from the midspan of the center span, the strains much more closely follow the results of the 5-beam model, while the deflections measured by the twangers follow the results of the 3-beam model. The 3-beam and 5-beam models again tend to bracket the actual measured strains fairly well. Unlike the results recorded at midspan location 2, the results presented in Table 5-9 and Table 5-10 are all fairly consistent, with no gauges presenting significantly different strain or deflection measurements. Unlike the measurements from midspan, the gauges at 0.4L show a definite increase in strains from the static tests to the dynamic tests with an average increase in the BDI gauges of 10 με, which represents an increase of 15% on average. The twangers also witnessed an increase in deflection during the dynamic runs with an average increase of 0.007 in., which represents an average increase of 20%.

5.2.5 Joint Compression Results during Live Load Test

One of the most important aspects of this study is looking at the overall ability of the post-tensioning to keep the concrete panels in compression and reduce tension cracks, especially over a pier where there will be an accumulation of negative moment. The following two tables summarize the effects of the trucks on the compression force in the deck during the negative moment tests, which were designed to maximize the negative moment at the joint near the pier, and during the rest of the static and dynamic tests. Table 5-11 presents the results of BDI gauges 7 and 8 and LVDTs 1 and 2, which were all positioned on the top of the deck over the joint near the first pier. Table 5-12 presents the results of VWGs 5-8, which are all of the vibrating wire gauges within the deck.

Table 5-11. Maximum Joint Expansion/Cracking Width

Run #	BDI 7 (με)	BDI 8 (με)	LVDT 1 (in)	LVDT 2 (in)
1	14	11	0.000	0.000
2	43	10	0.000	0.000
3	31	8	0.000	0.000
4	25	8	0.000	0.000
5	9	6	0.000	0.000
6	14	9	0.000	0.000
7	12	9	0.000	0.000
8	13	9	0.000	0.000
9	9	7	0.000	0.000
10	9	10	0.000	0.000
11	9	7	0.000	0.000
12	9	8	0.000	0.000
Max =	**43**	**11**	**0.000**	**0.000**
			*LVDT is only calibrated to 0.001 in	

Table 5-12. Maximum Measured Tension Strain in the Deck

Run #	VWG 5 (με)	VWG 6 (με)	VWG 7 (με)	VWG 8 (με)
1	-1	3	1	4
2	-4	2	2	6
3	1	3	2	7
4	-8	0	1	7
5	1	2	4	2
6	0	0	5	3
7	1	0	5	4
8	0	0	5	4
9	1	1	3	2
10	1	1	3	2
11	1	1	3	2
12	0	1	3	2
Max =	**1**	**3**	**5**	**7**

Table 5-11 shows that while the BDI gauges arranged over the panel joint were able to measure strains up to 43 με, these strains were not nearly large enough to be measured by the LVDTs which are calibrated to measure 0.001 in. With a gauge length of 3 in. the BDI gauges would need to read 333 με before the LVDTs measured 0.001 in. Therefore, it can be determined that there was no measurable cracking occurring at the panel joint nearest the first pier.

Table 5-12 shows that through all of the tests, the maximum tension strain measured near the middle of the panels was 7 με in VWG 8, which was near the pier. According to Swenty's dissertation, it was determined that cracking between panels would occur over a pier when the stress is greater than $1.5\sqrt{f'_c}$. With an E of 6287 ksi, the stress necessary for cracking is 154 psi, which converts to a tensile strain of 18.5 με. Therefore, the maximum tensile strain of 7 με is not enough to cause cracks, especially due to the fact that the strain required to crack is significantly higher than the recorded strains because the tensile force in the panels would need to first exceed the compression force applied to the panels during the post-tensioning. The 7 με measurement is, therefore, not indicative of tensile stress within the concrete but a decrease in compressive stress from post-tensioning. When the concrete panels were post-tensioned, the measured compressive strain averaged nearly 80 με, which means that the strain measurement required to cause cracking would be approximately 95 με. It is also important to note that the reason for the significant difference in strains measured by the VWGs and the BDI gauges is most likely due to the drift in strains caused by direct sunlight, which is not present in the strains measured by the VWGs.

5.2.6 Strain Distribution and Neutral Axis Location

In order to determine whether the deck and beams were acting compositely, it is necessary to look at the strain distribution throughout the beam. Figure 5-35 presents the measured and predicted strain distribution within Beam C at the joint near the first pier. Note that the measurements displayed in this graph are from the point in time when the trucks are in position to cause the maximum negative moment at the joint. Figure 5-36 presents the measured and predicted strain distribution at 0.4L of the first span within Beam C. These measurements were taken from the point in time when the truck is positioned directly over the gauges. Figure 5-37 presents the measured and predicted strain distribution at 0.4L of the first span within Beam C, but the truck is located away from the gauges and is centered at midspan of the center span. This graph was produced in order to determine if the bridge acted compositely even when the loads are not oriented directly over the gauges. When the truck is directly over the gauges, the weight of the truck may actually induce enough friction between the concrete and steel to imitate fully composite behavior. Showing that the beams and deck still act compositely when the truck load is away from the gauges proves that the beams and deck panels are in fact acting together and are fully composite. Note that the following graphs represent the strain distribution between the panel joints, which is approximately half way between shear pockets.

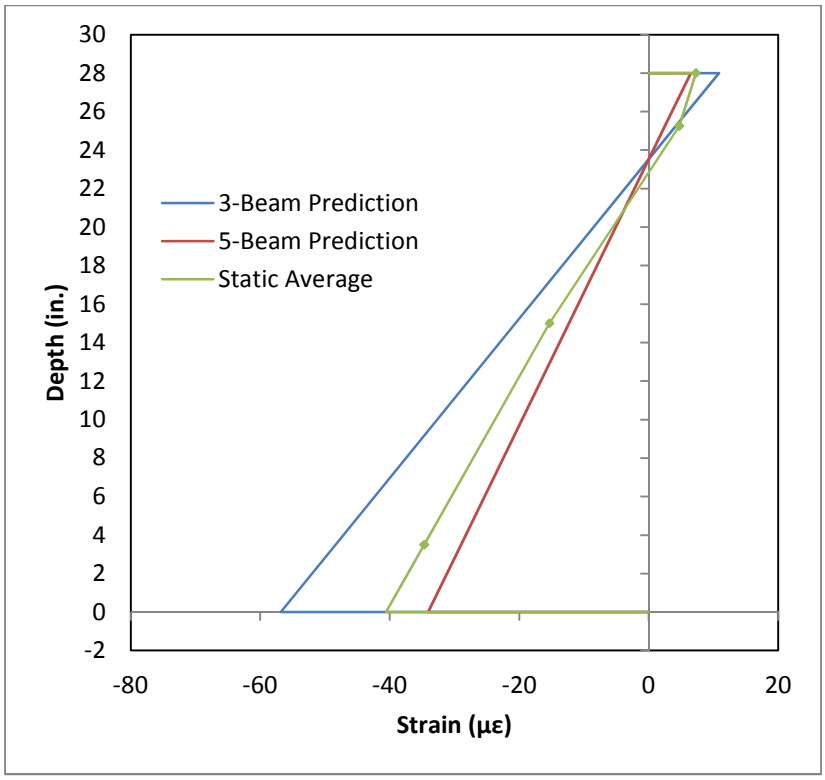

Figure 5-35. Strain Distribution within Beam C During –M Test

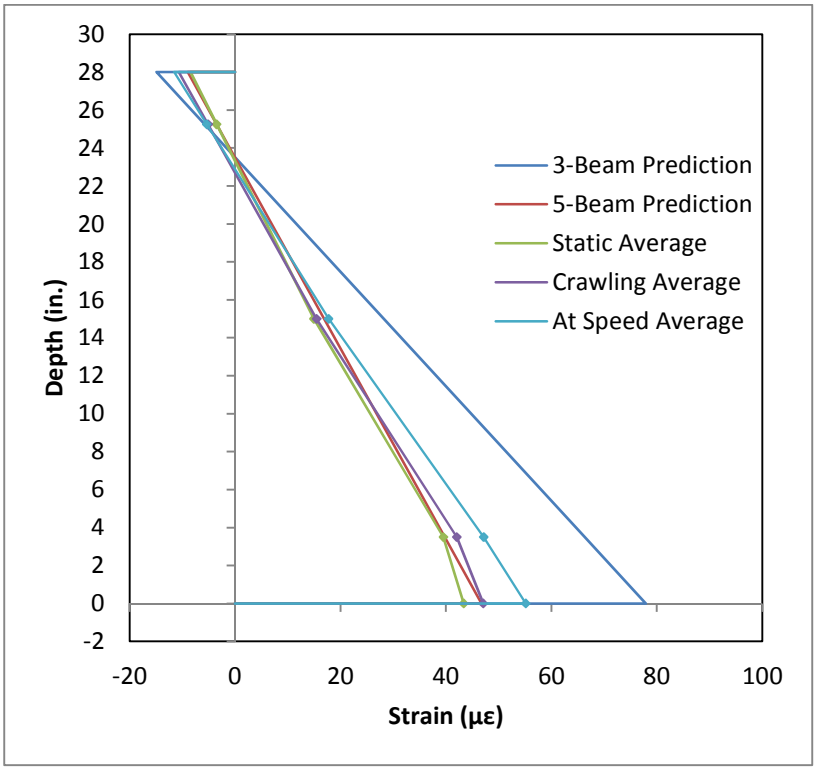

Figure 5-36. Strain Distribution within Beam C at 0.4L when Truck is at 0.4L

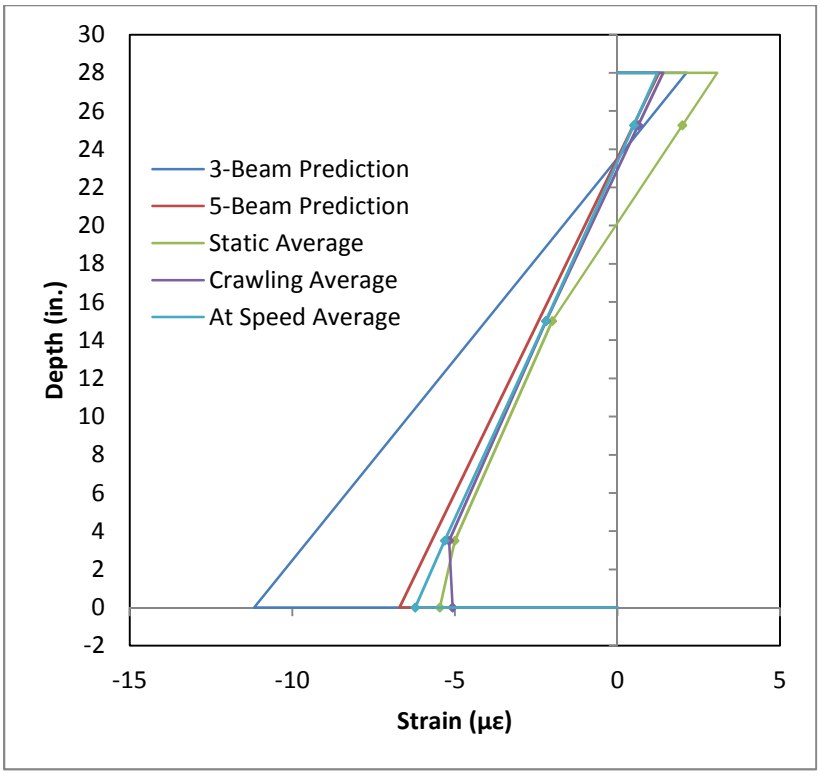

Figure 5-37. Strain Distribution within Beam C at 0.4L when Truck is at Midspan of the Center Span

Figure 5-35 shows that the strain distribution within the joint near the pier is linear and fits right in between the 5-beam and 3-beam predictions for strain. The predicted neutral axis of the fully-composite section was 5.01 in. above the steel for all locations along the length of the bridge. The measured neutral axis was 4.34 in. above the steel, which represents 13% error between the measured and predicted values. Figure 5-36 also shows that the strain distribution at 0.4L is linear. The neutral axis calculated for the static average is 4.81 in. which represents a 4% error between the measured and predicted values. The average measured values again fall between the 5-beam and 3-beam predictions.

Figure 5-37 displays a linear strain distribution throughout the concrete and steel. While the strains are much smaller, the values still fall close to the 5-beam and 3-beam predicted values. The neutral axis location was determined to be at 4.83 in. above the top of the steel. This again represents an error of

4% between the measured and predicted values. The fact that the steel beam and concrete deck are still linear and the measured strains are within the predicted range proves that the deck and beam are acting fully-compositely.

5.2.7 Distribution Factors from the Live Load Test

Distribution factors were calculated using the maximum strains measured by the three BDI gauges at 0.4L. It was determined that beam A supported 34% of the truck load, beam B supported 34%, and beam C supported 32%. These percentages did not vary significantly between tests, and show that the truck load was split evenly among the beams. This proves that the composite deck was stiff enough to spread out the load and make the individual beams act together as a system. These experimentally determined distribution factors very closely matched the assumed value of 33% per beam. Figure 5-38 presents a graph showing the measured strains at 0.4L for runs 1, 5, and 9-12. The AASHTO LRDF Design Manual recommends moment distribution factors of 0.6 (60%) for the exterior beams A and C, and 0.458 (45.8%) for the interior beam B.

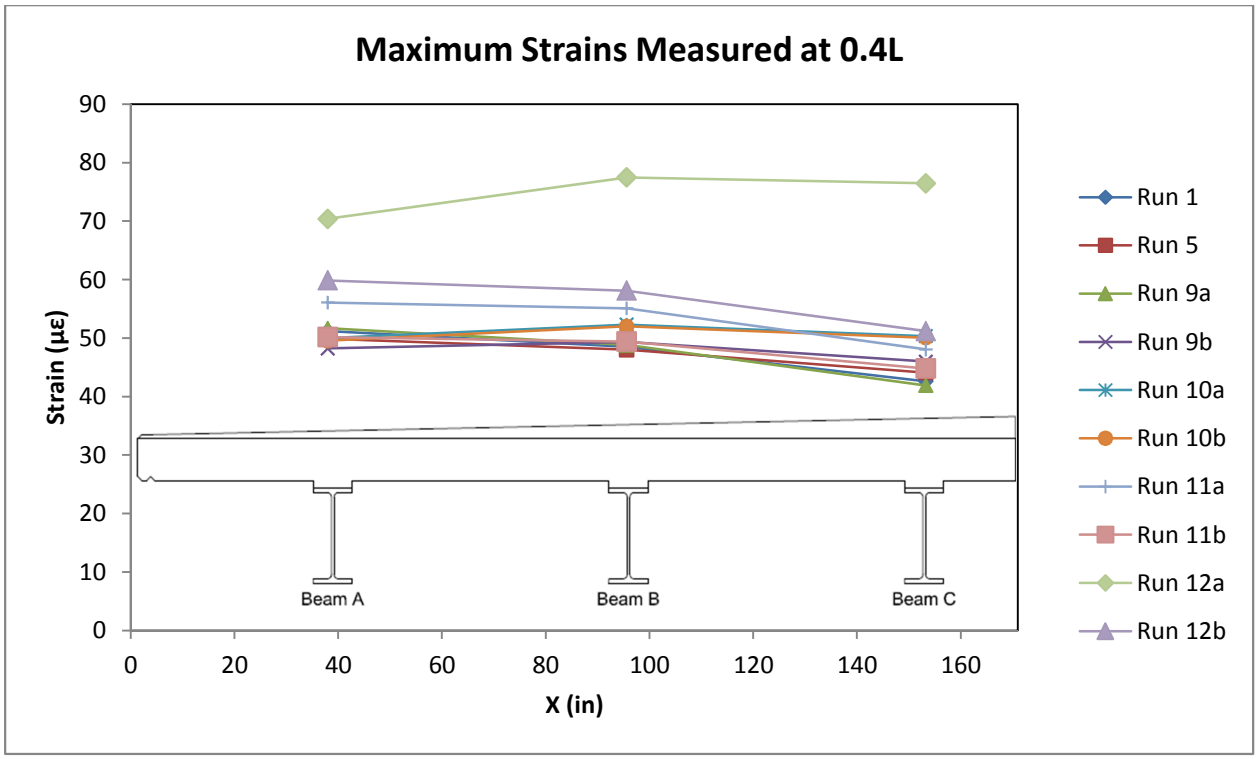

Figure 5-38. Strains Measured at 0.4L by BDI Gauges 1, 2, and 3

Chapter 6: Conclusions and Recommendations

This section of the report presents conclusions and recommendations concerning the results of the live load test and the long-term strain monitoring data.

6.1 Conclusions from Long-Term Testing

- During the setting of the deck panels into the Phase I side of the bridge, the measured strain values matched the predicted values very closely for the gauges located at 0.4L of Beam C with an average error of 4.3%. The strains measured by the gauges near the pier, however, did not match the predicted values as closely with an average error of 32.3%.
- During the post-tensioning, the strain values measured by the embedded VWGs not on the side of the broken strands matched the predicted values very closely with an error of 6.3%. The strains measured by the embedded VWGs on the side of the broken strands were not as close to the predicted values with an average error of 26%.
- During the post-tensioning, the strain values measured by the VWGs on the side of Beam C measured nearly zero change in strain when comparing the strains from before to the post-tensioning to the strains measured after the post-tensioning. This indicates no transfer of force into the beams.
- When comparing the measured long-term strain distributions to the predictions made by Bowers' model, the results do not match very well. The results are, however, within the same magnitude for the measurements taken at 110 and 140 days. The graphs do also present very similar slopes as the predicted values, and exhibit many of the same trends. The results from day 215 are quantitatively very different from the predictions but show that the strains measured within the cross-section are linear, which means that the deck and girders are acting

compositely. It can, therefore, be concluded that due to creep and shrinkage, stresses redistribute qualitatively according to Bowers' model, but it will be necessary for further study of temperature effects to determine if the model is quantitatively accurate as well.

6.2 Conclusions from Short-Term Testing

- The results from test runs 1 and 5, which were identical except that the data was recorded by the CR23X data logger during run 1 and by the CR3000 prototype data logger during run 5, produced comparable results which verified that the CR3000 data logger was working properly.
- The strains measured at the joint during the negative moment tests (runs 2-4 and 6-8) fit the predictions of the 3-beam and 5-beam models fairly well, with most of the data being bracketed between the two predictive models. The gauges which were on top of the bridge exhibited excessive drift during the tests, and also exhibited the greatest difference from the predicted values.
- The strains measured at 0.4L and at midspan presented many of the same trends witnessed during the negative moment test runs. The gauges underneath the bridge were much more accurate and tended to fall within the predicted range of the 3-beam and 5-beam models. The gauges on top of the bridge suffered from significant drift caused by direct sunlight and, therefore, exhibited much greater difference from the predicted values.
- During all of the live load tests, the LVDTs at the top of the joint near the pier measured 0 in. of expansion, while the BDI gauges measured 43 με, which would produce deflection measurements well below the perceptible limits of the LVDTs. The VWGs embedded within the deck measured a maximum tensile strain of 7 με, which is below the limit of 25 με proposed by Swenty's research in order to limit full-depth cracking. This proves that Swenty's joint designs

and recommended level of prestress force across the joint is at least initially adequate to keep the joints in compression during maximum service loads.

- The strains measured during the live load tests show that the strain distribution within the deck and beams was linear. This proves that the deck and the beams were acting fully-compositely. Therefore, the 3 ft 4 in. center-to-center shear pocket spacing was sufficient in keeping the deck and beams together, at least prior to long-term losses occur. This is further supported by the fact that the strains measured during the long-term study were also linear throughout the cross-section, as well.
- The guard rails, which had similar moments of inertia as the actual beams, but were not fully composite with the deck, were modeled as additional supporting beams with the same moments of inertia as the W18x71 beams. Another model was created in which the barriers were assumed to provide no additional stiffness to the bridge. These two models were able to successfully bracket most of the data recorded during the live load test, which demonstrates that this is an acceptable approach to predicting strains when the additional stiffness provided by the barrier rails is unknown. The assumptions and calculations involved in these predictions are located in section 4.3 of this report.

6.3 Recommendations

- Swenty's recommendations regarding a maximum tensile stress of $1.5\sqrt{f'_c}$ across a joint in order to prevent cracks from forming were correct, and can be applied to future precast deck panel bridge designs.
- Bowers' Mathcad model for prestress loss, which utilizes the age-adjusted effective modulus method and AASHTO equations for creep and shrinkage, accurately predicted trends in the data

over the long-term and kept the joints in compression during live load testing. Although further testing may be necessary, Bowers' model can used successfully to determine the level of post-tensioning force required for three span bridges.

- Based on these test results, pocket spacings up to 3 ft 4 in. center-to-center can be used for precast deck panel bridges of similar configuration.

6.4 Future Research

In order to more accurately compare the results of Bowers' model for post-tensioning losses, it would be necessary to investigate the effects of temperature on the strains measured within the bridge. In this research project, there were just not enough temperature measurements recorded along the depth and length of the bridge in order to fully understand the effects of the temperature variations. With a better understanding of these effects, it may be possible to come much closer to the results predicted by Bowers' model, which takes into account no temperature effects at all. It may also be necessary for separate lab tests to be performed in order to determine an accurate expansion coefficient for concrete with reinforcement steel, in order to determine how temperature affects the strains measured throughout the entire bridge.

References

American Association of State Highway and Transportation Officials (AASHTO) [2008]. LRFD Bridge Design Specifications: Fourth Edition. Washington, D.C.

Badie, Sameh S. (2012). "PCI Committee on Bridges Task Force on Extending the Stud Spacing Limit for Full-Depth Precast Concrete Deck Penals from 24 Inches to 48 Inches." *Prestressed Concrete Institute*.

Bowers, Susan E. (2007). “Recommendations for Longitudinal Post-Tensioning in Full-Depth Precast Concrete Bridge Deck Panels.” Thesis. Virginia Polytechnic Institute and State University, Blacksburg, VA.

James, Randy. (2009) "America: Still Stuck in Traffic." <http://www.time.com/time/nation/article/0,8599,1909417,00.html>. (June 27, 2012).

Laman, Jeffrey, J. Sellers, and Jeffrey Schulz. (2012). "Influence of Temperature on Highway Bridge Strain Measurements Using Vibrating Wire Gages."

Menkulasi, F., and Roberts-Wollmann, C. L. (2005). "Behavior of horizontal shear connections for full-depth precast concrete bridge decks on prestressed girders." PCI Journal, 50(3), 60-73.

PCI. (2003). PCI Bridge Design Manual, PCI Institute, Chicago, IL.

"Report Card for American Infrastructure." American Society of Civil Engineers, 2009. <http://www.infrastructurereportcard.org/> (June 27, 2012).

Sproles, John. "Proposed Bridge on Route 65 over Staunton Creek." VDOT Structure and Bridge Division. Bristol, VA. April 12, 2010. pp. 1-18.

Sullivan, Sean. (2007). "Construction and Behavior of Precast Bridge Deck Panel Systems." Dissertation. Virginia Polytechnic Institute and State University, Blacksburg, VA.

Swenty, Matthew K. (2009). "The Investigation of Transverse Joints and Grouts on Full Depth Concrete Bridge Deck Panels." Dissertation. Virginia Polytechnic Institute and State University, Blacksburg, VA.

Appendix A – Newcrete Cylinder Strengths

BeamTracker™

Concrete Testing Results

Pour: Slab-2 P-1

B-1346 VADOT/Scott/Ken Construction Company, Inc.

Spec Mix: **P-36** Release: **4,000** psi 28-Day: **6,000** psi

— Plastic Testing —

Test Date/Time	Pos	Ticket	Mix	D[1]	Temp (°F) Air	Temp (°F) Conc	Air (%)	Spread (in.)	VSI	JRΔ (in.)	U/W (pcf)	W/C	Cyl	
9/8/11 14:19	1	08R081756	P-36	M	70	70	2.30	25.00	1.0		154.2	0.358		Rejected/Air
9/8/11 15:05	1	08R081757	P-36	M	70	72	3.60	24.00	0.0	0.00	152.5	0.361	V-1	Accepted

[1]Delivery mode: [N] Not Recorded [P] Placer [M] Mixer [H] Hopper/Direct
BP in the position column indicates a batch plant test.

— Release Breaks —

Test Date/Time	Cure Hours	Notes*	Beam	Pos	Cyl	Breaks (psi) Actual		Average	
9/9/11 09:00	17.9		BM-2B	1	V-1	4,507	4,723	**4,615**	Release Bed

— Shipping Breaks —

Test Date	Cure Days	Notes*	Beam	Pos	Cyl	Breaks (psi) Actual	Average

[No break tests recorded]

*Move mouse over note to view entire entry, or over status of plastic test to view rejected yards.

Reload for Viewing **Print** **Close**
SnapLink this screen

BeamTracker™

Concrete Testing Results

Pour: Slab-2 P-2

B-1346 VADOT/Scott/Ken Construction Company, Inc.

Spec Mix: **P-36** Release: **4,000** psi 28-Day: **6,000** psi

— Plastic Testing —

Test Date/Time		Pos	Ticket	Mix	D[1]	Temp (°F) Air	Temp (°F) Conc	Air (%)	Spread (in.)	VSI	JRΔ (in.)	U/W (pcf)	W/C	Cyl	
9/12/11	15:53	1	08R081867	P-36	M	75	70	3.00	23.50	0.0	2.00	152.7	0.359	V2	Accepted
9/12/11	15:54	2	08R081867	P-36	M	75	70	3.00	23.50	0.0	2.00	152.7	0.359	V3	Accepted
9/12/11	16:39	3	08R081869	P-36	M	75	71	3.70	24.25	0.0	1.75	151.5	0.359	V4	Accepted
9/12/11	16:40	4	08R081869	P-36	M	75	71	3.70	24.25	0.0	1.75	151.5	0.359	V5	Accepted

[1]Delivery mode: [N] Not Recorded [P] Placer [M] Mixer [H] Hopper/Direct
BP in the position column indicates a batch plant test.

— Release Breaks —

Test Date/Time		Cure Hours	Notes*	Beam	Pos	Cyl	Breaks (psi) Actual		Breaks (psi) Average	
9/14/11	06:30	38.6		BM-2B	1	V2	6,027	5,979	**6,003**	Release Bed
9/14/11	06:30	38.6		BM-4B	2	V3	6,027	5,979	**6,003**	Release Bed
9/14/11	06:30	37.9		BM-12G	3	V4	6,166	6,533	**6,350**	Release Bed
9/14/11	06:30	37.8		BM-16G	4	V5	6,166	6,533	**6,350**	Release Bed

— Shipping Breaks —

Test Date	Cure Days	Notes*	Beam	Pos	Cyl	Breaks (psi) Actual	Breaks (psi) Average

[No break tests recorded]

*Move mouse over note to view entire entry, or over status of plastic test to view rejected yards.

Reload for Viewing Print Close

SnapLink this screen

BeamTracker™

Concrete Testing Results

Pour: Slab-2 P-3

B-1346 VADOT/Scott/Ken Construction Company, Inc.

Spec Mix: **P-36** Release: **4,000** psi 28-Day: **6,000** psi

— Plastic Testing —

Test Date/Time		Pos	Ticket	Mix	D[1]	Temp (°F) Air	Temp (°F) Conc	Air (%)	Spread (in.)	VSI	JRΔ (in.)	U/W (pcf)	W/C	Cyl	
9/15/11	12:30	1	08R082056	P-36	M	64	70	4.80	24.00	0.0	1.00	147.7	0.355	V-6	Accepted
9/15/11	12:31	2	08R082056	P-36	M	64	70	4.80	24.00	0.0	1.00	147.7	0.355	V-7	Accepted
9/15/11	13:09	3	08R082057	P-36	M	64	72	3.40	25.00	1.0	0.50	150.8	0.357	V-8	Accepted
9/15/11	13:10	4	08R082057	P-36	M	64	72	3.40	25.00	1.0	0.50	150.8	0.357	V-9	Accepted

[1]Delivery mode: [N] Not Recorded [P] Placer [M] Mixer [H] Hopper/Direct
BP in the position column indicates a batch plant test.

— Release Breaks —

Test Date/Time		Cure Hours	Notes*	Beam	Pos	Cyl	Breaks (psi) Actual		Average	
9/16/11	10:10	21.7		BM-3C	1	V-6	4,371	4,265	**4,318**	Release Bed
9/16/11	10:10	21.7		BM-7C	2	V-7	4,371	4,265	**4,318**	Release Bed
9/16/11	10:10	21.0		BM-13G	3	V-8	4,621	4,547	**4,584**	Release Bed
9/16/11	10:10	21.0		BM-17G	4	V-9	4,621	4,547	**4,584**	Release Bed

— Shipping Breaks —

Test Date	Cure Days	Notes*	Beam	Pos	Cyl	Breaks (psi) Actual	Average

[No break tests recorded]

*Move mouse over note to view entire entry, or over status of plastic test to view rejected yards.

Reload for Viewing Print Close

SnapLink this screen

BeamTracker™

Concrete Testing Results

Pour: Slab-2 P-4

B-1346 VADOT/Scott/Ken Construction Company, Inc.

Spec Mix: **P-36** Release: **4,000** psi 28-Day: **6,000** psi

— Plastic Testing —

Test Date/Time		Pos	Ticket	Mix	D[1]	Temp (°F) Air	Temp (°F) Conc	Air (%)	Spread (in.)	VSI	JRΔ (in.)	U/W (pcf)	W/C	Cyl	
9/19/11	15:21	1	08R082221	P-36	M	66	64	3.30	24.75	1.0	0.25	149.2	0.358	V-10	Accepted
9/19/11	15:22	2	08R082221	P-36	M	66	64	3.30	24.75	1.0	0.25	149.2	0.358	V-11	Accepted
9/19/11	15:55	3	08R082224	P-36	M	66	66	3.80	25.00	1.0	1.00	149.2	0.357	V-12	Accepted
9/19/11	15:56	4	08R082224	P-36	M	66	66	3.80	25.00	1.0	1.00	149.2	0.357	V-13	Accepted

[1]Delivery mode: [N] Not Recorded [P] Placer [M] Mixer [H] Hopper/Direct
BP in the position column indicates a batch plant test.

— Release Breaks —

Test Date/Time		Cure Hours	Notes*	Beam	Pos	Cyl	Breaks (psi) Actual		Average	
9/20/11	10:00	18.7		BM-6C	1	V-10	3,590	3,406	**3,498**	Break Failed
9/20/11	10:00	18.6		BM-8C	2	V-11	3,590	3,406	**3,498**	Break Failed
9/20/11	10:00	18.1		BM-14G	3	V-12	4,003	3,809	**3,906**	Break Failed
9/20/11	10:00	18.1		BM-18G	4	V-13	4,003	3,809	**3,906**	Break Failed
9/21/11	06:30	39.2		BM-6C	1	V-10	6,052	5,828	**5,940**	Release Bed
9/21/11	06:30	39.1		BM-8C	2	V-11	6,052	5,828	**5,940**	Release Bed
9/21/11	06:30	38.6		BM-14G	3	V-12	6,382	5,919	**6,151**	Release Bed
9/21/11	06:30	38.6		BM-18G	4	V-13	6,382	5,919	**6,151**	Release Bed

— Shipping Breaks —

Test Date	Cure Days	Notes*	Beam	Pos	Cyl	Breaks (psi) Actual	Average

[No break tests recorded]

*Move mouse over note to view entire entry, or over status of plastic test to view rejected yards.

Reload for Viewing **Print** **Close**
SnapLink this screen

BeamTracker™

Concrete Testing Results

Pour: Slab-2 P-5

B-1346 VADOT/Scott/Ken Construction Company, Inc.

Spec Mix: **P-36** Release: **4,000** psi 28-Day: **6,000** psi

— Plastic Testing —

Test Date/Time		Pos	Ticket	Mix	D[1]	Temp (°F) Air	Temp (°F) Conc	Air (%)	Spread (in.)	VSI	JRΔ (in.)	U/W (pcf)	W/C	Cyl	
9/22/11	09:34	1	08R082375	P-36	M	66	70	2.90	22.25	0.0		151.0			Rejected/Air
9/22/11	10:20	1	08R082380	P-36	M	68	71	3.10	22.50	0.0	0.50	149.9	0.359	V-14	Accepted
9/22/11	10:21	2	08R082380	P-36	M	68	71	3.10	22.50	0.0	0.50	149.9	0.359	V-15	Accepted
9/22/11	11:03	3	08R082388	P-36	M	68	72	4.30	22.00	0.0	1.00	148.4	0.359	V-16	Accepted
9/22/11	11:04	4	08R082388	P-36	M	68	72	4.30	22.00	0.0	0.50	148.4	0.359	V-17	Accepted

[1]Delivery mode: [N] Not Recorded [P] Placer [M] Mixer [H] Hopper/Direct
BP in the position column indicates a batch plant test.

— Release Breaks —

Test Date/Time		Cure Hours	Notes*	Beam	Pos	Cyl	Breaks (psi) Actual		Breaks (psi) Average	
9/23/11	12:05	25.7		BM-5D	1	V-14	5,103	4,704	**4,904**	Release Bed
9/23/11	12:05	25.7		BM-9C	2	V-15	5,103	4,704	**4,904**	Release Bed
9/23/11	12:05	25.0		BM-15H	3	V-16	5,120	5,081	**5,101**	Release Bed
9/23/11	12:05	25.0		BM-19G	4	V-17	5,120	5,081	**5,101**	Release Bed

— Shipping Breaks —

Test Date	Cure Days	Notes*	Beam	Pos	Cyl	Breaks (psi) Actual	Breaks (psi) Average

[No break tests recorded]

*Move mouse over note to view entire entry, or over status of plastic test to view rejected yards.

Reload for Viewing **Print** **Close**

SnapLink this screen

Appendix B – CR23X Program Code

Final CR23x Program Description

};CR23X

Program variables

;$
;:VWGs1 :VWGs2 :VWGs3 :VWGs4 :VWGs5
;:VWGs6 :VWGs7 :VWGs8 :VWGt1 :VWGt2
;:VWGt3 :VWGt4 :VWGt5 :VWGt6 :VWGt7
;:VWGt8 :Batt_Volts :PTemp_DegF
;$

Output table setup

;101 Output_Table 3600.00 Sec
;1 101 L
;2 Year_RTM L
;3 Day_RTM L
;4 Hour_Minute_RTM L
;5 VWG_S1 L
;6 VWG_S2 L
;7 VWG_S3 L
;8 VWG_S4 L
;9 VWG_S5 L
;10 VWG_S6 L
;11 VWG_S7 L
;12 VWG_S8 L
;13 VWG_T1 L
;14 VWG_T2 L
;15 VWG_T3 L
;16 VWG_T4 L
;17 VWG_T5 L
;18 VWG_T6 L
;19 VWG_T7 L
;20 VWG_T8 L

MODE 1
SCAN RATE 3600 (seconds between scans)

1:P86 **Do**
1:41 Set Port 1 High (Turns on the AVW1 Vibrating Wire Interface)

2:P87 **Begin loop** (Starts the loop that reads all 8 VWGs)
1:0 Delay
2:8 Count

3:P86 **Do**
1:72 Pulse Port 2

4:P28 **Vibrating Wire (Single Ended)** (Reads the vibrating wire strain gauges)
1:1 Repetitions
2:2 SE Chan
3:1 EX Chan
4:4 Start Frequency of sweep (100's of Hz)
5:10 End Frequency of sweep (100's of Hz)
6:500 Number of cycles
7:500 Delay (0.01 sec.)
8:1-- Location (for data storage)
9:3242 Multiplier
10:0.0 Offset

5:P4 **EX-DEL-DIFF** (Reads the temperatures from the VWG thermistors)
1:1 Repetitions
2:15 Range
3:1 SE Chan.
4:1 EX Chan.
5:100 Delay (0.01 sec.)
6:2500 Excite (mV)
7:9-- Location (for data storage)
8:0.001 Multiplier
9:0.0 Offset

6:P55 **Polynomial** (Changes the thermistor value into Celsius)
1:1 Repetitions
2:9-- X Location
3:9-- F(x) Location
4:-104.78 C0
5:378.11 C1
6:-611.59 C2
7:544.27 C3
8:-240.91 C4
9:43.089 C5

7:P37 **Z = X * F** (Changes the VWG temperature reading from Celsius to Fahrenheit)
1:9-- X
2:1.8 F
3:9-- Z

8:P34 **Z =X + F** (Changes the VWG temperature reading from Celsius to Fahrenheit)
1:9-- X
2:32 F
3:9-- Z

9:P95 **End loop** (Ends the loop that was reading the VWGs)

10:P86 **Do**
1:51 Set Port 1 Low (Turns off the AVW1 Vibrating Wire Interface)

11:P17 **Panel Temperature**
1:18 Location (for data storage)

12:P37 **Z = X * F** (Changes the panel temperature reading from Celsius to Fahrenheit)
1:18 X
2:1.8 F
3:18 Z

13:P34 **Z =X + F** (Changes the panel temperature reading from Celsius to Fahrenheit)
1:18 X
2:32 F
3:18 Z

10:P10 **Battery Voltage**
1:17 Location (for data storage)

11:P86 **Do**
1:10 Set Flag 0 High

12:P77 **Real Time**
1:1110 Option (Year – Day – Hour – Minute)

13:P70 **Sample**
1:18 Repetitions
2:1-- Location (for data storage)

Other information the CR23x needs for the program to run…

MODE 2
SCAN RATE 0.0000

MODE 3

MODE 10
1:61
2:64
3:0

MODE 12
1:0000
2:0000
3:0000

```
};CR23X
;$
;:VWGs1   :VWGs2   :VWGs3   :VWGs4   :VWGs5
;:VWGs6   :VWGs7   :VWGs8   :VWGt1   :VWGt2
;:VWGt3   :VWGt4   :VWGt5   :VWGt6   :VWGt7
;:VWGt8   :Batt_Volts    :PTemp_DegF
;$

;101 Output_Table   3600.00 Sec
;1 101 L
;2 Year_RTM  L
;3 Day_RTM  L
;4 Hour_Minute_RTM  L
;5 VWG_S1 L
;6 VWG_S2 L
;7 VWG_S3 L
;8 VWG_S4 L
;9 VWG_S5 L
;10 VWG_S6 L
;11 VWG_S7 L
;12 VWG_S8 L
;13 VWG_T1 L
;14 VWG_T2 L
;15 VWG_T3 L
;16 VWG_T4 L
;17 VWG_T5 L
;18 VWG_T6 L
;19 VWG_T7 L
;20 VWG_T8 L

MODE 1
SCAN RATE 3600

1:P86

1:41

2:P87
1:0
2:4

3:P86
```

1:72

4:P28
1:1
2:2
3:1
4:4
5:10
6:500
7:500
8:1--
9:4062
10:0.0

5:P4

1:1
2:15
3:1
4:1
5:100
6:2500
7:9--
8:0.001
9:0.0

6:P55
1:1
2:9--
3:9--
4:-104.78
5:378.11
6:-611.59
7:544.27
8:-240.91
9:43.089

7:P37
1:9--
2:1.8
3:9--

8:P34
1:9--
2:32
3:9--

9:P95

10:P87
1:0
2:4

11:P86
1:72

12:P28
1:1
2:2
3:1
4:4
5:10
6:500
7:500
8:5--
9:3304
10:0.0

13:P4

1:1
2:15
3:1
4:1
5:100
6:2500
7:13--
8:0.001
9:0.0

14:P55
1:1
2:13--
3:13--

4:-104.78
5:378.11
6:-611.59
7:544.27
8:-240.91
9:43.089

15:P37
1:13--
2:1.8
3:13--

16:P34
1:13--
2:32
3:13--

17:P95

18:P86
1:51

19:P17
1:18

20:P37
1:18
2:1.8
3:18

21:P34
1:18
2:32
3:18

22:P10
1:17

23:P86
1:10

24:P77

1:1110

25:P70
1:18
2:1--

MODE 2
SCAN RATE 0.0000

MODE 3

MODE 10
1:61
2:64
3:0

MODE 12
1:0000
2:0000
3:0000

Appendix C – Gauge Calibration Data from Live Load Test

Calibration Summary

Gauge Type	Name	BDI #	Original Name	Cal. Factor	Cable Length (ft)
Twanger	Twang 1	T1034	8	180.18	25
Twanger	Twang 2	T1035	5	189.50	25
Twanger	Twang 3	T1036	3	-187.72	25
Twanger	Twang 4	T1037	2	-190.37	25
Twanger	Twang 5	T1038	6	181.62	25
Twanger	Twang 6	T1039	9	174.61	25
Twanger	Twang 7	T1040	13	-189.07	25
LVDT	LVDT 1	T1041	LVDT 8	0.08148	150
LVDT	LVDT 2	T1045	LVDT 3	0.08145	150
LVDT	LVDT 3	T1043	LVDT 2	0.07867	90
BDI	BDI 1	B2007		98920	15
BDI	BDI 2	B2009		100340	15
BDI	BDI 3	B2010		97600	15
BDI	BDI 4	B2011		100000	15
BDI	BDI 5	B2012		98400	20
BDI	BDI 6	B2013		101640	20
BDI	BDI 7	B2014		97700	20
BDI	BDI 8	B2015		96580	20

Twanger Notes:

Positive deflection = bridge is deflecting up away from the ground
Negative deflection = bridge is deflecting downward towards the ground

When you pull down on the twanger attached to the bridge the deflection will be a positive number

LVDT Notes:

LVDT #1:
Zero without it being compressed at all
Set at -0.03"
Zero when beginning the test in order to get 0.03" of measurement in either direction
0.06" effective range

LVDT #2:
Zero without it being compressed at all
Set at -0.05
Zero when beginning the test in order to get 0.05" of measurement in either direction
0.1" effective range

LVDT #3 -- Range = 0.07 -- Same steps as above but set at -0.035"

Negative displacement = LVDT is being compressed
Positive displacement = LVDT is being uncompressed

BDI Notes:

Negative strain = compression
Positive strain = tension

Appendix D – Strains due to Deck Panels and Post-Tensioning

Predicted Girder 3 Strain Due to Panel Dead Load

Panel weight: $wt := 15000$ lbs

****Calculations assume that the panel dead load is distributed evenly among the supporting girders**

Load divided evenly to the three girders: $load := \frac{wt}{3} = 5000$ lbs

Linearly distributed load on each girder: $line\_load := \frac{load}{10 \cdot 12 \cdot 1000} = 0.042 \ \frac{k}{in}$

Strain gauge position #1 (102.5" from outside support):

Moment at position 1 calculated in SAP 2000: $M_1 := 485.5$ kip·in

Strain gauge position #2 (342.5" from outside support):

Moment at position 2 calculated in SAP 2000: $M_2 := -236.6$ kip·in

Formula used to calculate strain at gauge locations: $\varepsilon = \frac{M \cdot c}{E \cdot I}$

Modulus of elasticity of steel: $E := 29000$ ksi

Moment of inertia of W18X71 beam: $I := 1170$ in^4

Distance from centroid of beam to location of strain gauge: $c := 5.75$ in

VWG #1 predicted strain due to panel loads:

$$\varepsilon_1 := \frac{M_1 \cdot -c}{E \cdot I} \cdot 10^6 = -82.276 \ \mu\varepsilon$$

VWG #2 predicted strain due to panel loads:

$$\varepsilon_2 := \frac{M_1 \cdot c}{E \cdot I} \cdot 10^6 = 82.276 \ \mu\varepsilon$$

VWG #1 predicted strain due to panel loads:

$$\varepsilon_3 := \frac{M_2 \cdot -c}{E \cdot I} \cdot 10^6 = 40.096 \ \mu\varepsilon$$

VWG #2 predicted strain due to panel loads:

$$\varepsilon_4 := \frac{M_2 \cdot c}{E \cdot I} \cdot 10^6 = -40.096 \ \mu\varepsilon$$

Predicted Girder 3 Strain Due to Panel Dead Load

Comparison of predicted strains to measured strains due to panel placement:

****Calculations assume that the panel dead load is distributed evenly among the supporting girders**

Vibrating-wire gauge #1:

Measured strain: $\varepsilon m_1 := -88 \quad \mu\varepsilon$ Predicted strain: $\varepsilon_1 = -82.276 \quad \mu\varepsilon$

Percent difference: $e_1 := \frac{\varepsilon m_1 - \varepsilon_1}{\varepsilon m_1} = 6.505 \cdot \%$ $e_1 = 6.505 \cdot \%$

Vibrating-wire gauge #2:

Measured strain: $\varepsilon m_2 := 84 \quad \mu\varepsilon$ Predicted strain: $\varepsilon_2 = 82.276 \quad \mu\varepsilon$

Percent difference: $e_2 := \frac{\varepsilon m_2 - \varepsilon_2}{\varepsilon m_2} = 2.052 \cdot \%$ $e_2 = 2.052 \cdot \%$

Vibrating-wire gauge #3:

Measured strain: $\varepsilon m_3 := 51 \quad \mu\varepsilon$ Predicted strain: $\varepsilon_3 = 40.096 \quad \mu\varepsilon$

Percent difference: $e_3 := \frac{\varepsilon m_3 - \varepsilon_3}{\varepsilon m_3} = 21.381 \cdot \%$ $e_3 = 21.381 \cdot \%$

Vibrating-wire gauge #4:

Measured strain: $\varepsilon m_4 := -28 \quad \mu\varepsilon$ Predicted strain: $\varepsilon_4 = -40.096 \quad \mu\varepsilon$

Percent difference: $e_4 := \frac{\varepsilon m_4 - \varepsilon_4}{\varepsilon m_4} = -43.199 \cdot \%$ $e_4 = -43.199 \cdot \%$

$\varepsilon m_1 = -88 \quad \mu\varepsilon$ $\varepsilon m_2 = 84 \quad \mu\varepsilon$ $\varepsilon m_3 = 51 \quad \mu\varepsilon$ $\varepsilon m_4 = -28 \quad \mu\varepsilon$

$\varepsilon_1 = -82.276 \quad \mu\varepsilon$ $\varepsilon_2 = 82.276 \quad \mu\varepsilon$ $\varepsilon_3 = 40.096 \quad \mu\varepsilon$ $\varepsilon_4 = -40.096 \quad \mu\varepsilon$

Predicted Girder 3 Strain Due to Panel Dead Load

Panel weight: $wt := 15000 \quad lbs$

****Panel load is distributed proportionally between supporting girders**

Distributed load along width of panel: $width\_load := \frac{wt}{171 \cdot 1000} = 0.088 \quad \frac{k}{in}$

Load supported by girder 3: $load := 4.027 \quad kips$

Linearly distributed load on each girder: $line\_load := \frac{load}{10 \cdot 12} = 0.03356 \quad \frac{k}{in}$

Strain gauge position #1 (102.5" from outside support):

Moment at position 1 calculated in SAP 2000: $M_1 := 421.484 \quad kip \cdot in$

Strain gauge position #2 (342.5" from outside support):

Moment at position 2 calculated in SAP 2000: $M_2 := -205.398 \quad kip \cdot in$

Formula used to calculate strain at gauge locations: $\varepsilon = \frac{M \cdot c}{E \cdot I}$

Modulus of elasticity of steel: $E := 29000 \quad ksi$

Moment of inertia of W18X71 beam: $I := 1170 \quad in^4$

Distance from centroid of beam to location of strain gauge: $c := 5.75 \quad in$

VWG #1 predicted strain due to panel loads:

$$\varepsilon_1 := \frac{M_1 \cdot -c}{E \cdot I} \cdot 10^6 = -71.427 \quad \mu\varepsilon$$

VWG #2 predicted strain due to panel loads:

$$\varepsilon_2 := \frac{M_1 \cdot c}{E \cdot I} \cdot 10^6 = 71.427 \quad \mu\varepsilon$$

VWG #1 predicted strain due to panel loads:

$$\varepsilon_3 := \frac{M_2 \cdot -c}{E \cdot I} \cdot 10^6 = 34.808 \quad \mu\varepsilon$$

VWG #2 predicted strain due to panel loads:

$$\varepsilon_4 := \frac{M_2 \cdot c}{E \cdot I} \cdot 10^6 = -34.808 \quad \mu\varepsilon$$

Predicted Girder 3 Strain Due to Panel Dead Load

Comparison of predicted strains to measured strains due to panel placement:

****Panel load is distributed proportionally between supporting girders**

Vibrating-wire gauge #1:

Measured strain: $\varepsilon m_1 = -88 \quad \mu\varepsilon$ Predicted strain: $\varepsilon_1 = -71.427 \quad \mu\varepsilon$

Percent difference: $e_1 := \frac{\varepsilon m_1 - \varepsilon_1}{\varepsilon m_1} = 18.832 \cdot \%$ $e_1 = 18.832 \cdot \%$

Vibrating-wire gauge #2:

Measured strain: $\varepsilon m_2 = 84 \quad \mu\varepsilon$ Predicted strain: $\varepsilon_2 = 71.427 \quad \mu\varepsilon$

Percent difference: $e_2 := \frac{\varepsilon m_2 - \varepsilon_2}{\varepsilon m_2} = 14.967 \cdot \%$ $e_2 = 14.967 \cdot \%$

Vibrating-wire gauge #3:

Measured strain: $\varepsilon m_3 = 51 \quad \mu\varepsilon$ Predicted strain: $\varepsilon_3 = 34.808 \quad \mu\varepsilon$

Percent difference: $e_3 := \frac{\varepsilon m_3 - \varepsilon_3}{\varepsilon m_3} = 31.749 \cdot \%$ $e_3 = 31.749 \cdot \%$

Vibrating-wire gauge #4:

Measured strain: $\varepsilon m_4 = -28 \quad \mu\varepsilon$ Predicted strain: $\varepsilon_4 = -34.808 \quad \mu\varepsilon$

Percent difference: $e_4 := \frac{\varepsilon m_4 - \varepsilon_4}{\varepsilon m_4} = -24.315 \cdot \%$ $e_4 = -24.315 \cdot \%$

Predicted Prestressing Strain in Embedded VWGs - With Ruptured Strands

All measurements are made from the bottom (inner edge) of the drawing below:

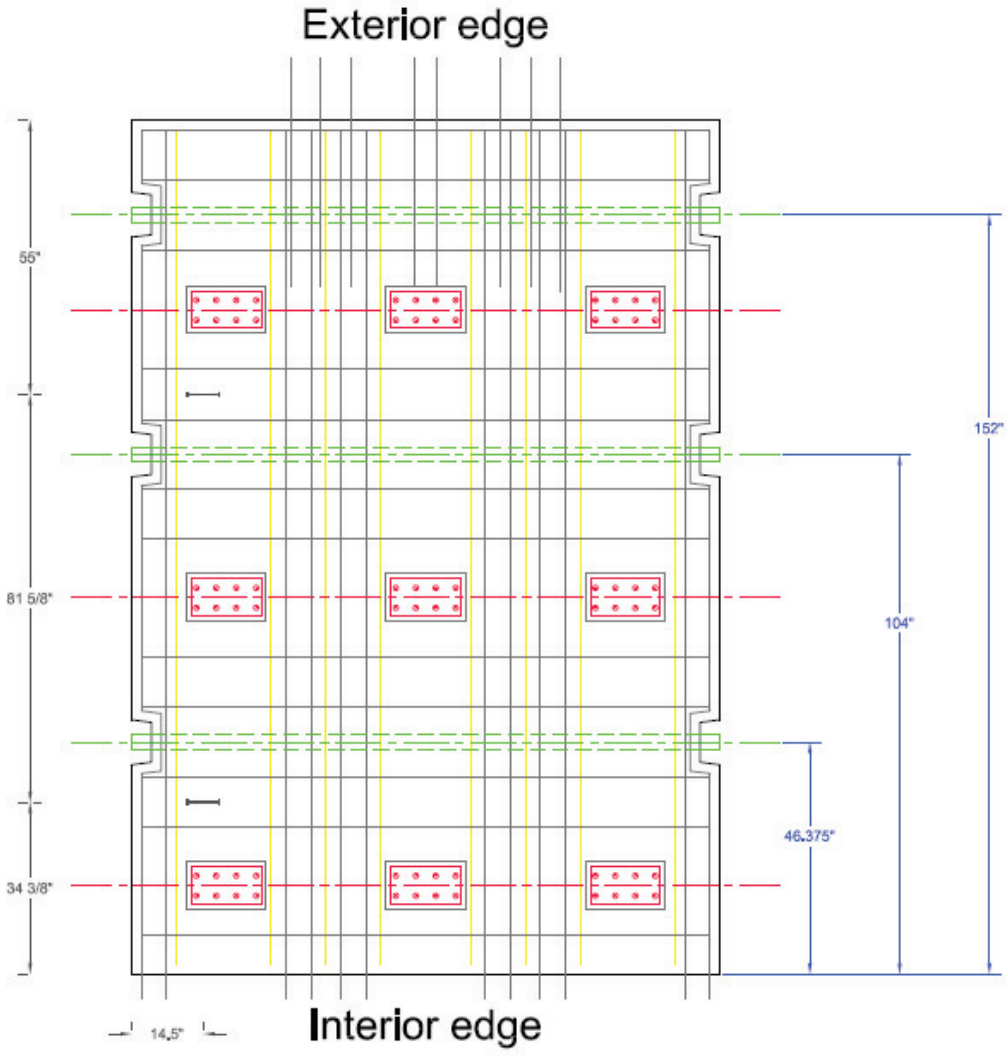

Locations of post-tensioning strand ducts:

Strand duct #1: All 4 strands ruptured

Strand duct #2: $duct_2 := 104$ in

Strand duct #3: $duct_3 := 152$ in

Predicted Prestressing Strain in Embedded VWGs - With Ruptured Strands

Location of equivalent point load from post-tensioning strands:

$$F_{loc} := \frac{duct_2 + duct_3}{2} = 128 \quad \text{in}$$

Eccentricity of equivalent point load from middle of panel:

$$F_{ecc} := F_{loc} - \frac{171}{2} = 42.5 \quad \text{in}$$

Eccentricity of upper VWG from middle of panel:

$$VWG_{top\_loc} := 34 + \frac{3}{8} + 81 + \frac{5}{8} - \frac{171}{2} = 30.5 \quad \text{in}$$

Eccentricity of lower VWG from middle of panel:

$$VWG_{bot\_loc} := 34 + \frac{3}{8} - \frac{171}{2} = -51.125 \quad \text{in}$$

Equation for calculating stress:

$$\sigma = \frac{P}{A} + \frac{P \cdot e \cdot y}{I}$$

Material properties:

Total post-tensioning axial force: $P_{avg} := 37.10 \cdot 8 = 296.8$ kips (***Average force in each strand)

Cross-sectional area of panel: $A := 171 \cdot 8 = 1368$ in^2

Moment of inertia of the panel: $I := \frac{1}{12} \cdot 8 \cdot 171^3 = 3333474$ in^4

Modulus of panel: $E := 57 \cdot \sqrt{6000} = 4415.201$ ksi

Predicted Prestressing Strain in Embedded VWGs - With Ruptured Strands

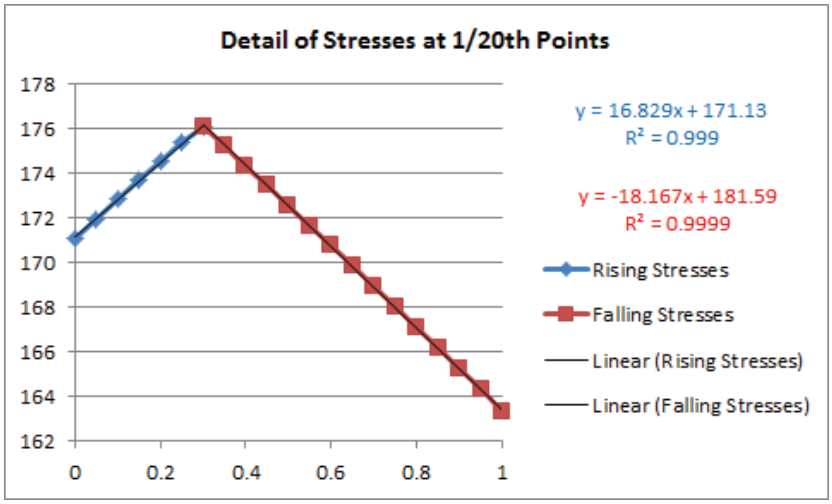

VWGs 5 and 6 are located 135.5" from dead end and 1064.5" from live end (0.887*X/L)

$$P_{56} := (-18.167 \cdot 0.887 + 181.59) \cdot 0.217 \cdot 8 = 287.266 \quad \text{kips}$$

VWGs 7 and 8 are located 375.5" from dead end and 824.5" from live end (0.687*X/L)

$$P_{78} := (-18.167 \cdot 0.687 + 181.59) \cdot 0.217 \cdot 8 = 293.574 \quad \text{kips}$$

Stress at VWG #5:

$$\sigma_5 := \frac{P_{56}}{A} + \frac{P_{56} \cdot F_{ecc} \cdot VWG_{top\_loc}}{I} = 0.322 \quad \text{ksi}$$

Stress at VWG #6:

$$\sigma_6 := \frac{P_{56}}{A} + \frac{P_{56} \cdot F_{ecc} \cdot VWG_{bot\_loc}}{I} = 0.023 \quad \text{ksi}$$

Predicted strain measurement at VWG 5:

$$\varepsilon_5 := -\frac{\sigma_5}{E} \cdot 10^6 = -72.861 \quad \mu\varepsilon$$

Predicted Prestressing Strain in Embedded VWGs - With Ruptured Strands

Predicted strain measurement at VWG 6:

$$\varepsilon_6 := -\frac{\sigma_6}{E}\cdot 10^6 = -5.152 \quad \mu\varepsilon$$

Stress at VWG #7:

$$\sigma_7 := \frac{P_{78}}{A} + \frac{P_{78}\cdot F_{ecc}\cdot VWG_{top\_loc}}{I} = 0.329 \quad ksi$$

Stress at VWG #8:

$$\sigma_8 := \frac{P_{78}}{A} + \frac{P_{78}\cdot F_{ecc}\cdot VWG_{bot\_loc}}{I} = 0.023 \quad ksi$$

Predicted strain measurement at VWG 7:

$$\varepsilon_7 := -\frac{\sigma_7}{E}\cdot 10^6 = -74.461 \quad \mu\varepsilon$$

Predicted strain measurement at VWG 8:

$$\varepsilon_8 := -\frac{\sigma_8}{E}\cdot 10^6 = -5.265 \quad \mu\varepsilon$$

Measured changes in strain:

$\varepsilon m_5 := -54 \quad \mu\varepsilon$ $\varepsilon m_6 := -3 \quad \mu\varepsilon$ $\varepsilon m_7 := -57 \quad \mu\varepsilon$ $\varepsilon m_8 := -10 \quad \mu\varepsilon$

Percent error of measured values compared to predicted values of strain:

$$e_5 := \frac{\varepsilon_5 - \varepsilon m_5}{\varepsilon m_5} = 34.928\cdot\%$$

$$e_6 := \frac{\varepsilon_6 - \varepsilon m_6}{\varepsilon m_6} = 71.718\cdot\%$$

$$e_7 := \frac{\varepsilon_7 - \varepsilon m_7}{\varepsilon m_7} = 30.633\cdot\%$$

$$e_7 := \frac{\varepsilon_8 - \varepsilon m_8}{\varepsilon m_8} = -47.353\cdot\%$$

Positive value = measured strain is higher than predicted strain
Negative value = measured strain is lower than predicted strain

Predicted Prestressing Strain in Embedded VWGs

All measurements are made from the bottom (inner edge) of the drawing below:

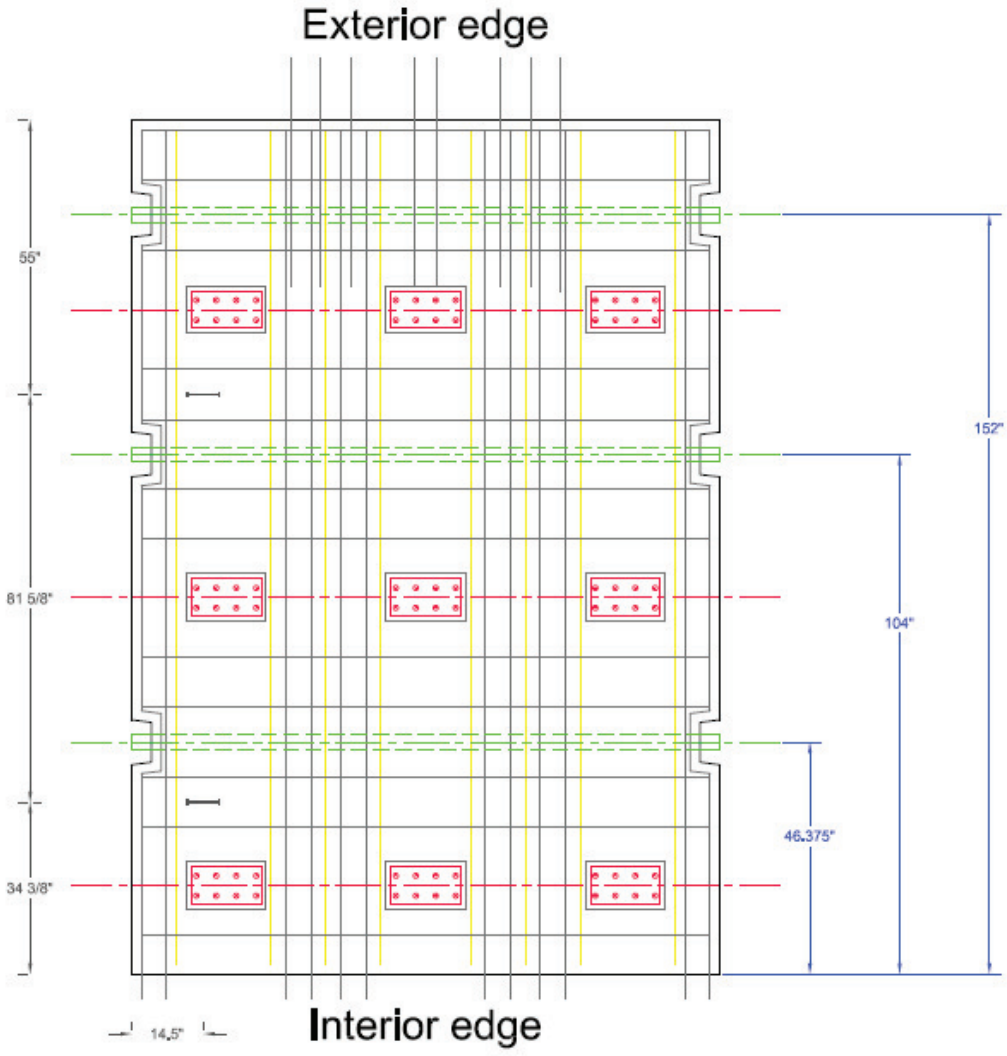

Locations of post-tensioning strand ducts:

Strand duct #1: $duct_1 := 46.375$ in

Strand duct #2: $duct_2 := 104$ in

Strand duct #3: $duct_3 := 152$ in

Predicted Prestressing Strain in Embedded VWGs

Location of equivalent point load from post-tensioning strands:

$$F_{loc} := \frac{duct_1 + duct_2 + duct_3}{3} = 100.792 \quad in$$

Eccentricity of equivalent point load from middle of panel:

$$F_{ecc} := F_{loc} - \frac{171}{2} = 15.292 \quad in$$

Eccentricity of upper VWG from middle of panel:

$$VWG_{top\_loc} := 34 + \frac{3}{8} + 81 + \frac{5}{8} - \frac{171}{2} = 30.5 \quad in$$

Eccentricity of lower VWG from middle of panel:

$$VWG_{bot\_loc} := 34 + \frac{3}{8} - \frac{171}{2} = -51.125 \quad in$$

Equation for calculating stress:

$$\sigma = \frac{P}{A} + \frac{P \cdot e \cdot y}{I}$$

Material properties:

Total post-tensioning axial force: $P_{avg} := 37.10 \cdot 12 = 445.2$ kips (***Average force in each strand)

Cross-sectional area of panel: $A := 171 \cdot 8 = 1368$ in^2

Moment of inertia of the panel: $I := \frac{1}{12} \cdot 8 \cdot 171^3 = 3333474$ in^4

Modulus of panel: $E := 57 \cdot \sqrt{6000} = 4415.201$ ksi

Predicted Prestressing Strain in Embedded VWGs

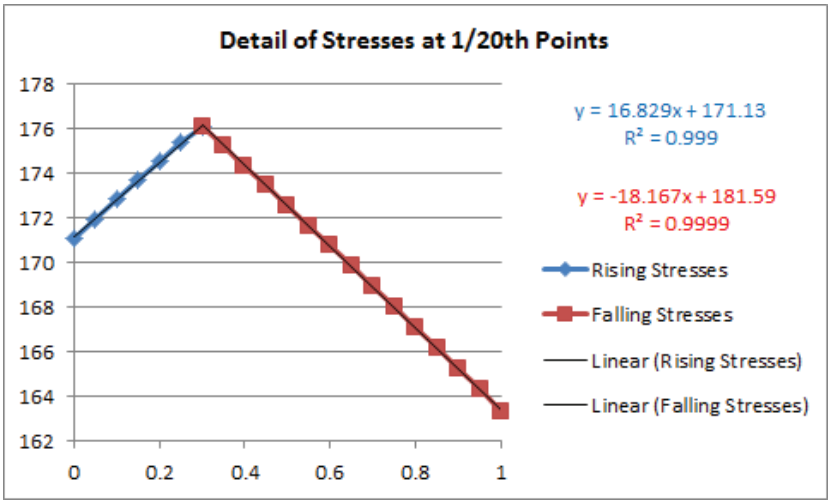

VWGs 5 and 6 are located 135.5" from dead end and 1064.5" from live end (0.887*X/L)

$$P_{56} := (-18.167 \cdot 0.887 + 181.59) \cdot 0.217 \cdot 12 = 430.899 \text{ kips}$$

VWGs 7 and 8 are located 375.5" from dead end and 824.5" from live end (0.687*X/L)

$$P_{78} := (-18.167 \cdot 0.687 + 181.59) \cdot 0.217 \cdot 12 = 440.361 \text{ kips}$$

Stress at VWG #5:

$$\sigma_5 := \frac{P_{56}}{A} + \frac{P_{56} \cdot F_{ecc} \cdot VWG_{top\_loc}}{I} = 0.375 \quad \text{ksi}$$

Stress at VWG #6:

$$\sigma_6 := \frac{P_{56}}{A} + \frac{P_{56} \cdot F_{ecc} \cdot VWG_{bot\_loc}}{I} = 0.214 \quad \text{ksi}$$

Predicted strain measurement at VWG 5:

$$\varepsilon_5 := -\frac{\sigma_5}{E} \cdot 10^6 = -84.996 \quad \mu\varepsilon$$

Predicted Prestressing Strain in Embedded VWGs

Predicted strain measurement at VWG 6:

$$\varepsilon_6 := -\frac{\sigma_6}{E}\cdot 10^6 = -48.453 \quad \mu\varepsilon$$

Stress at VWG #7:

$$\sigma_7 := \frac{P_{78}}{A} + \frac{P_{78}\cdot F_{ecc}\cdot VWG_{top\_loc}}{I} = 0.384 \quad ksi$$

Stress at VWG #8:

$$\sigma_8 := \frac{P_{78}}{A} + \frac{P_{78}\cdot F_{ecc}\cdot VWG_{bot\_loc}}{I} = 0.219 \quad ksi$$

Predicted strain measurement at VWG 7:

$$\varepsilon_7 := -\frac{\sigma_7}{E}\cdot 10^6 = -86.862 \quad \mu\varepsilon$$

Predicted strain measurement at VWG 8:

$$\varepsilon_8 := -\frac{\sigma_8}{E}\cdot 10^6 = -49.516 \quad \mu\varepsilon$$

Measured changes in strain:

$\varepsilon m_5 := -68 \quad \mu\varepsilon$ $\quad \varepsilon_5 = -84.996$

$\varepsilon m_6 := -53 \quad \mu\varepsilon$ $\quad \varepsilon_6 = -48.453$

$\varepsilon m_7 := -72 \quad \mu\varepsilon$ $\quad \varepsilon_7 = -86.862$

$\varepsilon m_8 := -43 \quad \mu\varepsilon$ $\quad \varepsilon_8 = -49.516$

Percent error of measured values compared to predicted values of strain:

$$e_5 := \frac{\varepsilon_5 - \varepsilon m_5}{\varepsilon m_5} = 24.994\cdot\%$$

$$e_6 := \frac{\varepsilon_6 - \varepsilon m_6}{\varepsilon m_6} = -8.58\cdot\%$$

$$e_7 := \frac{\varepsilon_7 - \varepsilon m_7}{\varepsilon m_7} = 20.642\cdot\%$$

$$e_7 := \frac{\varepsilon_8 - \varepsilon m_8}{\varepsilon m_8} = 15.154\cdot\%$$

Positive value = measured strain is lower than predicted strain
Negative value = measured strain is higher than predicted strain

Predicted Prestressing Strain in Embedded VWGs

$$strains_{56} := \begin{pmatrix} 34.375 & \varepsilon_5 & \varepsilon m_5 \\ 116 & \varepsilon_6 & \varepsilon m_6 \end{pmatrix} = \begin{pmatrix} 34.375 & -84.996 & -68 \\ 116 & -48.453 & -53 \end{pmatrix}$$

$$strains_{78} := \begin{pmatrix} 34.375 & \varepsilon_7 & \varepsilon m_7 \\ 116 & \varepsilon_8 & \varepsilon m_8 \end{pmatrix} = \begin{pmatrix} 34.375 & -86.862 & -72 \\ 116 & -49.516 & -43 \end{pmatrix}$$

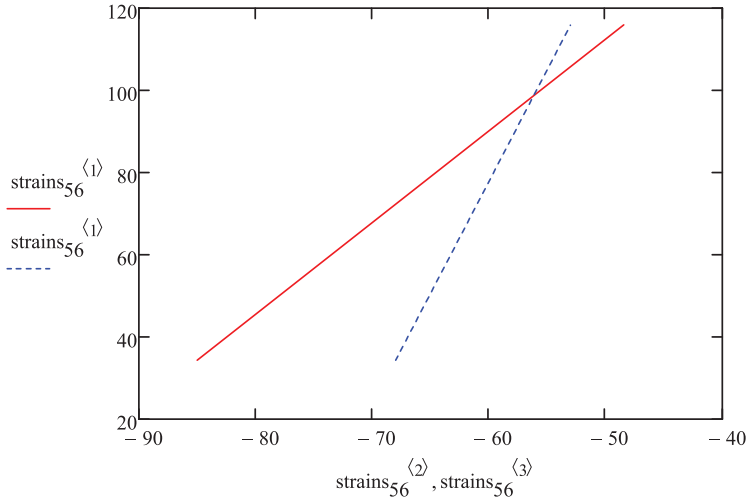

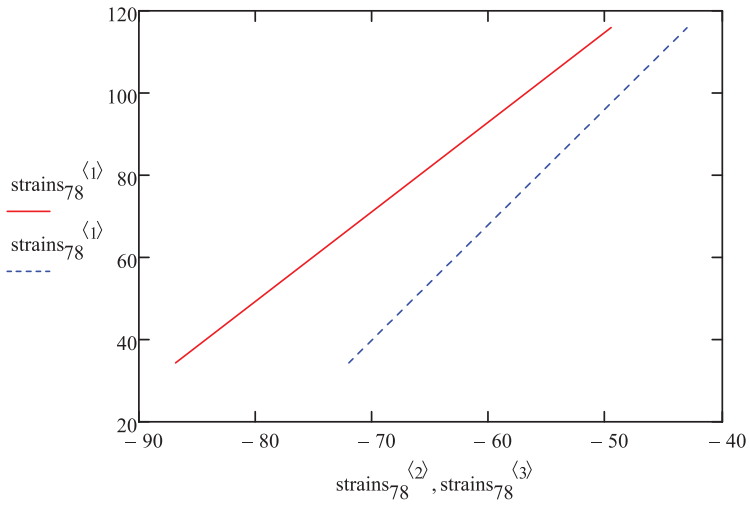

Appendix E – Strand Elongation Reports

8006 Haute Ct.
Springfield, Va 22150
Phone : (703) 451 4300
Fax : (703)451 0862

Children's Hospital of Philadelphia

MULTISTRAND STRESSING RECORD

Location: Rt 65 Over Staunton Creek
Element: Panels 1A, 1B, 2
Date:
Ram Number: 6MR074
Gauge Number: 6MR074 A

	Tendon #	Jacking			Elongation			Theoretical Elongation					Remarks
		Force (Kips)	Gauge Pressure 20%	Gauge Pressure 100%	20%	100%	Net	Net	-5%	5%			
Panels	1	41	1059	5333			6 5/8	6 1/4	5 15/16	6 9/16			
1A, 1B, 2	2	41	1059	5333			6 3/8	6 1/4	5 15/16	6 9/16			
	3	41	1059	5333			6 1/2	6 1/4	5 15/16	6 9/16			
	4	41	1059	5333			6 3/8	6 1/4	5 15/16	6 9/16			
	5	41	1059	5333			6 3/8	6 1/4	5 15/16	6 9/16			
	6	41	1059	5333			6 3/8	6 1/4	5 15/16	6 9/16			
	7	41	1059	5333			6 3/8	6 1/4	5 15/16	6 9/16			
	8	41	1059	5333			6 3/8	6 1/4	5 15/16	6 9/16			
	9	41	1059	5333			6 1/4	6 1/4	5 15/16	6 9/16			
	10	41	1059	5333			6 1/4	6 1/4	5 15/16	6 9/16			
	11	41	1059	5333			6 5/16	6 1/4	5 15/16	6 9/16			
	12	41	1059	5333			6 1/4	6 1/4	5 15/16	6 9/16			

Comments

GAUGE PRESSURES (Assume Gauge A)

MULTI-STRAND RAM INFORMATION

Stressed by
(Print name and signature)

Mike Wilkerson Mike Wilkerson VSL

8006 Haute Ct.
Springfield, Va 22150
Phone : (703) 451 4300
Fax : (703)451 0862

MULTISTRAND STRESSING RECORD

Location: Rt 65 Over Staunton Creek
Ram Number: 6MR089
Element: **Panels 3A, 3B, 4**
Gauge Number: 6MR089 A
Date: 2-9-12

	Tendon #	Jacking Force (Kips)	Jacking Gauge Pressure 20%	Jacking Gauge Pressure 100%	Elongation 20%	Elongation 100%	Elongation Net	Theoretical Elongation Net	Theoretical Elongation -5%	Theoretical Elongation 5%			Remarks
Panels	1	41	1066	5328			6 1/2	6 1/4	5 15/16	6 9/16			
3A,3B,4	2	41	1066	5328			6 1/4	6 1/4	5 15/16	6 9/16			
	3	41	1066	5328			6 5/8	6 1/4	5 15/16	6 9/16			
	4	41	1066	5328			6 3/8	6 1/4	5 15/16	6 9/16			
	5	41	1066	5328			6 3/8	6 1/4	5 15/16	6 9/16			
	6	41	1066	5328			6 3/8	6 1/4	5 15/16	6 9/16			
	7	41	1066	5328			6 3/8	6 1/4	5 15/16	6 9/16			
	8	41	1066	5328			6 1/2	6 1/4	5 15/16	6 9/16			
	9	41	1066	5328			6 3/8	6 1/4	5 15/16	6 9/16			
	10	41	1066	5328			6 3/8	6 1/4	5 15/16	6 9/16			
	11	41	1066	5328			6 1/4	6 1/4	5 15/16	6 9/16			
	12	41	1066	5328			6 1/4	6 1/4	5 15/16	6 9/16			
	13	41	1066	5328			6 1/2	6 1/4	5 15/16	6 9/16			
	14	41	1066	5328			6 1/2	6 1/4	5 15/16	6 9/16			
	15	41	1066	5328			6 3/8	6 1/4	5 15/16	6 9/16			
	16	41	1066	5328			6 1/2	6 1/4	5 15/16	6 9/16			

Comments

GAUGE PRESSURES (Assume Gauge A)

MULTI-STRAND RAM INFORMATION

Stressed by
(Print name and signature)

Zack McKenzie
Bruce Osborn

PROJECT

V Structural LLC
8006 Haute Court
Springfield, Virginia 22150
Phone : (703) 451 4300
Fax : (703) 451 0862

GROUTING REPORT

Location: Piles over Staunton Creek 3A, B, & 4
Date: 2-9-12
Weather: cold breezy 34
Grout Mix Formula: Water: gallons per LB
Admixture bags lb/bag
Mix 2-3 mins
Mixing Duration Time: 3 mins 00 secs

Ambient Temperature: 34 °F
Admixture Temperature: — °F
Cement Temperature: 45 °F
Water Temperature: 40 °F
Grout Temperature: 76 °F
Brand Name:

Start Time: 1225
Finish Time: 118

Comments: Flow 14 sec. Deck temp 35°
Mud Bal. - 1.85

Grouting Operator (Print name and signature): Bruce Osborn
Grouting Crew Member (Print name and signature): Zack McKenzie
Bryan Hall

Date 2-9-12

Verified by (Print name and signature): Glen Zidek
Date

Notes

Bruce Osborn

Appendix F – Live Load Test Predicted Strains

Composite Section Properties for Beam A:

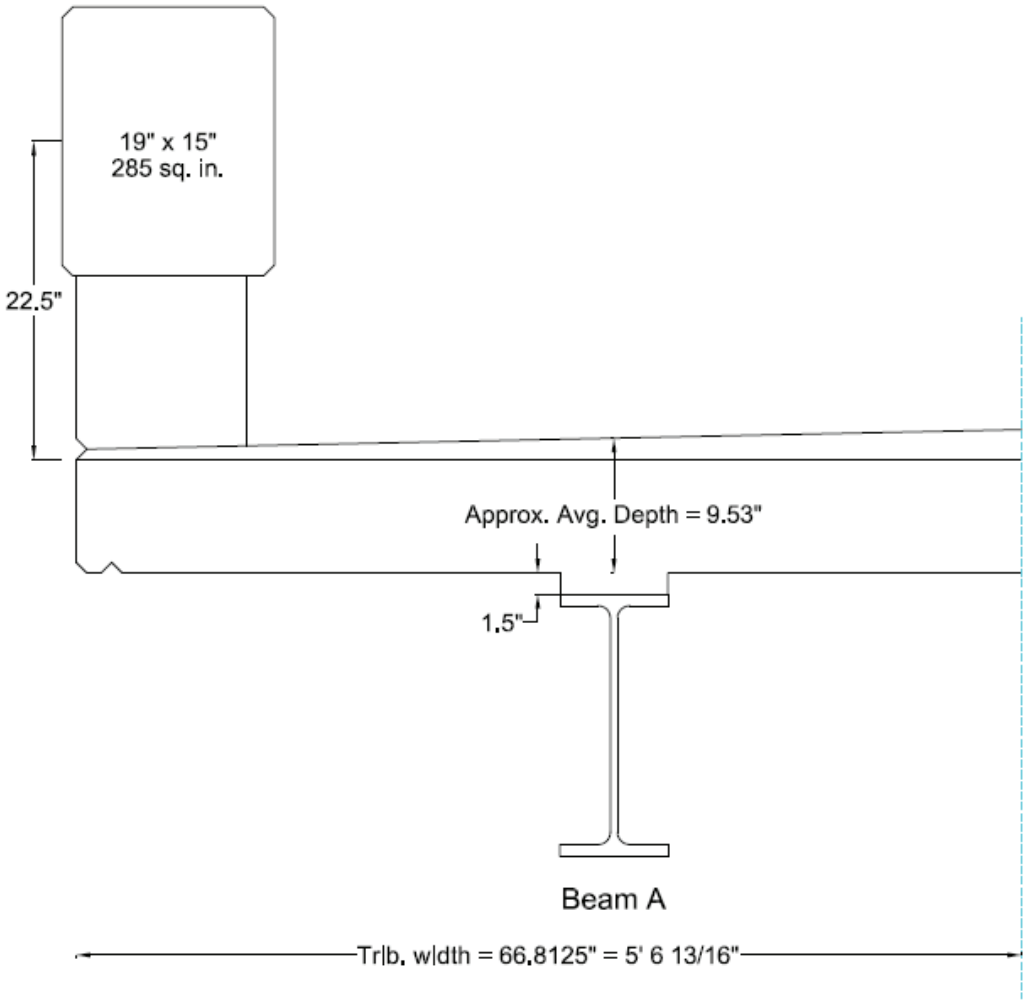

Slab properties:

Avg. Concrete slab depth:	$d := 9.53$	in
Modular ratio:	$n := 4.61$	
Haunch depth:	$H := 1.5$	in
Effective width:	$b_s := 66.8125$	in

Composite Section Property Calculations:

Beam properties:

Top Flange	thickness	$tf_t := 0.81$ in
	width	$tf_w := 7.64$ in
Web	thickness	$w_t := 0.495$ in
	depth	$w_d := 18.5 - 2 \cdot tf_t = 16.88$ in
Bottom flange	thickness	$bf_t := 0.81$ in
	width	$bf_w := 7.64$ in

Moment of inertia: $I_{NA} := 1170 \ in^4$

Section modulus: $S_{top\_of\_steel} := 127 \ in^3$

$S_{bot\_of\_steel} := 127 \ in^3$

Distance to centroid: $d_{top\_of\_steel} := 9.25$ in

$d_{bot\_of\_steel} := 9.25$ in

Gross steel area: $A_{g\_s} := 20.8 \ in^2$

Distance to centroid from center: $d_{s\_s} := 0$ in

Concrete barrier properties:

Area of concrete: $A_{c\_barr} := 285 \ in^2$

Height of barrier: $h_{barr} := 19$ in

Width of barrier: $w_{barr} := 15$ in

Height of centroid of barrier to top of deck: $d_{ts\_barr} := 22.5$ in

Composite Section Property Calculations:

Short-term (n) Composite Section:

Steel Section:

$A_s := A_{g\_s} = 20.8$ in^2 $\quad d_s := d_{s\_s} = 0$ in

$Ad_s := A_s \cdot d_s = 0$ in^3 $\quad Ad2_s := A_s \cdot d_s^{\,2} = 0$ in^4

$I_{os} := I_{NA} = 1170$ in^4 $\quad I_s := I_{os} + Ad2_s = 1170$ in^4

Concrete Slab:

$A_c := d \cdot \frac{b_s}{n} = 138.118$ in^2 $\quad d_c := \frac{d}{2} + H + \frac{w_d}{2} + tf_t = 15.515$ in

$Ad_c := A_c \cdot d_c = 2142.898$ in^3 $\quad Ad2_c := A_c \cdot d_c^{\,2} = 33247.061$ in^4

$I_{oc} := \frac{1}{12} \cdot \left(\frac{b_s}{n}\right) \cdot d^3 = 1045.332$ in^4 $\quad I_c := I_{oc} + Ad2_c = 34292.393$ in^4

Concrete Barrier:

$A_{c\_barr} := h_{barr} \cdot \frac{w_{barr}}{n} = 61.822$ in^2 $\quad d_{c\_barr} := d + H + \frac{w_d}{2} + tf_t + d_{ts\_barr} = 42.78$ in

$Ad_{c\_barr} := A_{c\_barr} \cdot d_{c\_barr} = 2644.751$ in^3 $\quad Ad2_{c\_barr} := A_{c\_barr} \cdot d_{c\_barr}^{\,2} = 113142.428$ in^4

$I_{oc\_barr} := \frac{1}{12} \cdot \left(\frac{w_{barr}}{n}\right) \cdot h_{barr}^{\,3} = 1859.816$ in^4 $\quad I_{c\_barr} := I_{oc\_barr} + Ad2_{c\_barr} = 115002.244$ in^4

Section Property Calculations (Considering Barrier's Contribution to Strength):

$A_{sum} := A_s + A_c + A_{c\_barr} = 220.74$ in^2 $\quad Ad_{sum} := Ad_s + Ad_c + Ad_{c\_barr} = 4787.648$ in^3

$I_{sum} := I_s + I_c + I_{c\_barr} = 150464.637$ in^4 $\quad d_{s\_stc} := \frac{Ad_{sum}}{A_{sum}} = 21.689$

$imbal := -d_{s\_stc} \cdot Ad_{sum} = -103839.738$ in^4

$I_{NA\_stc} := I_{sum} + imbal = 46624.899$ in^4

$d_{top\_of\_steel\_stc} := \frac{w_d}{2} + tf_t - d_{s\_stc} = -12.439$ in $\quad S_{top\_of\_steel\_stc} := \frac{I_{NA\_stc}}{d_{top\_of\_steel\_stc}} = -3748.256$ in^3

$d_{bot\_of\_steel\_stc} := \frac{w_d}{2} + bf_t + d_{s\_stc} = 30.939$ in $\quad S_{bot\_of\_steel\_stc} := \frac{I_{NA\_stc}}{d_{bot\_of\_steel\_stc}} = 1506.99$ in^3

Results (Considering Barrier's Contribution to Strength):

Moment of inertia of the composite section: $I_{NA\_stc} = 46624.899$ in^4

Distance to the centroid from the top of the steel section: $d_{top\_of\_steel\_stc} = -12.439$ in

Distance to the centroid from the bottom of the steel section: $d_{bot\_of\_steel\_stc} = 30.939$ in

Section modulus about the top of the steel: $S_{top\_of\_steel\_stc} = -3748.256$ in^3

Section modulus about the bottom of the steel: $S_{bot\_of\_steel\_stc} = 1506.99$ in^3

Composite Section Property Calculations:

Section Property Calculations (Not Considering Barrier's Contribution to Strength):

$A_{sum} := A_s + A_c = 158.918 \quad in^2$

$Ad_{sum} := Ad_s + Ad_c = 2142.898 \quad in^3$

$I_{sum} := I_s + I_c = 35462.393 \quad in^4$

$d_{s\_stc} := \frac{Ad_{sum}}{A_{sum}} = 13.484$

$imbal := -d_{s\_stc} \cdot Ad_{sum} = -28895.51 \quad in^4$

$I_{NA\_stc} := I_{sum} + imbal = 6566.882 \quad in^4$

$d_{top\_of\_steel\_stc} := \frac{w_d}{2} + tf_t - d_{s\_stc} = -4.234 \quad in$

$S_{top\_of\_steel\_stc} := \frac{I_{NA\_stc}}{d_{top\_of\_steel\_stc}} = -1550.872 \quad in^3$

$d_{bot\_of\_steel\_stc} := \frac{w_d}{2} + bf_t + d_{s\_stc} = 22.734 \quad in$

$S_{bot\_of\_steel\_stc} := \frac{I_{NA\_stc}}{d_{bot\_of\_steel\_stc}} = 288.853 \quad in^3$

Results (Not Considering Barrier's Contribution to Strength):

Moment of inertia of the composite section: $I_{NA\_stc} = 6566.882 \quad in^4$

Distance to the centroid from the top of the steel section: $d_{top\_of\_steel\_stc} = -4.234 \quad in$

Distance to the centroid from the bottom of the steel section: $d_{bot\_of\_steel\_stc} = 22.734 \quad in$

Section modulus about the top of the steel: $S_{top\_of\_steel\_stc} = -1550.872 \quad in^3$

Section modulus about the bottom of the steel: $S_{bot\_of\_steel\_stc} = 288.853 \quad in^3$

Composite Section Properties for Beam B:

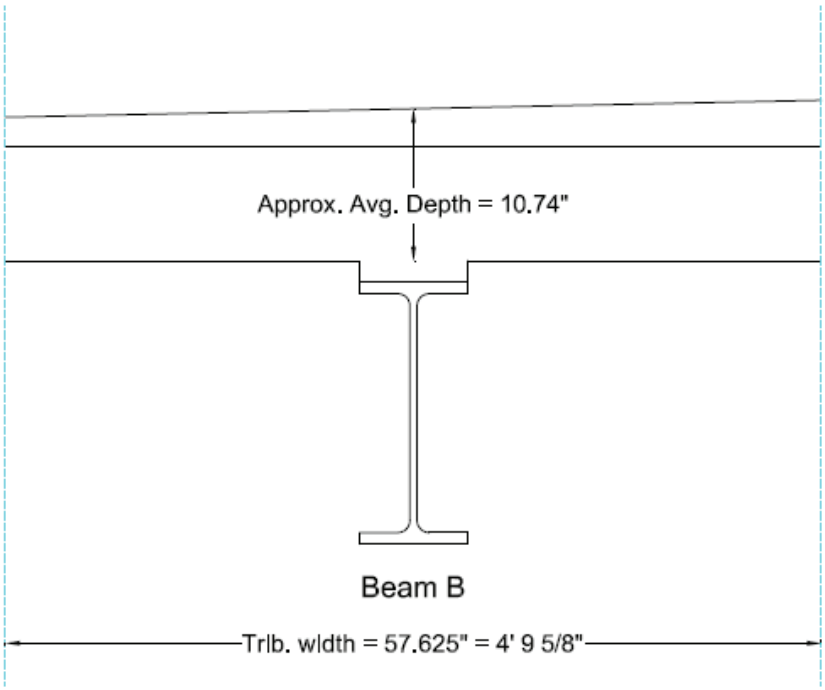

Slab properties:

Avg. concrete slab depth:	$d := 10.74$	in
Modular ratio:	$n := 4.61$	
Haunch depth:	$H := 1.5$	in
Effective width:	$b_s := 57.625$	in

Composite Section Property Calculations:

Beam properties:

Top Flange	thickness	$tf_t := 0.81$ in
	width	$tf_w := 7.64$ in
Web	thickness	$w_t := 0.495$ in
	depth	$w_d := 18.5 - 2 \cdot tf_t = 16.88$ in
Bottom flange	thickness	$bf_t := 0.81$ in
	width	$bf_w := 7.64$ in

Moment of inertia: $I_{NA} := 1170 \ in^4$

Section modulus: $S_{top\_of\_steel} := 127 \ in^3$

$S_{bot\_of\_steel} := 127 \ in^3$

Distance to centroid: $d_{top\_of\_steel} := 9.25$ in

$d_{bot\_of\_steel} := 9.25$ in

Gross steel area: $A_{g\_s} := 20.8 \ in^2$

Distance to centroid from center: $d_{s\_s} := 0$ in

Composite Section Property Calculations:

Short-term (n) Composite Section:

Steel Section:

$A_s := A_{g\_s} = 20.8$ in^2 $\quad d_s := d_{s\_s} = 0$ in

$Ad_s := A_s \cdot d_s = 0$ in^3 $\quad Ad2_s := A_s \cdot d_s^{\,2} = 0$ in^4

$I_{os} := I_{NA} = 1170$ in^4 $\quad I_s := I_{os} + Ad2_s = 1170$ in^4

Concrete Slab:

$A_c := d \cdot \frac{b_s}{n} = 134.25$ in^2 $\quad d_c := \frac{d}{2} + H + \frac{w_d}{2} + tf_t = 16.12$ in

$Ad_c := A_c \cdot d_c = 2164.11$ in^3 $\quad Ad2_c := A_c \cdot d_c^{\,2} = 34885.453$ in^4

$I_{oc} := \frac{1}{12} \cdot \left(\frac{b_s}{n}\right) \cdot d^3 = 1290.451$ in^4 $\quad I_c := I_{oc} + Ad2_c = 36175.904$ in^4

Section Property Calculations:

$A_{sum} := A_s + A_c = 155.05$ in^2 $\quad Ad_{sum} := Ad_s + Ad_c = 2164.11$ in^3

$I_{sum} := I_s + I_c = 37345.904$ in^4 $\quad d_{s\_stc} := \frac{Ad_{sum}}{A_{sum}} = 13.957$

$imbal := -d_{s\_stc} \cdot Ad_{sum} = -30205.56$ in^4

$I_{NA\_stc} := I_{sum} + imbal = 7140.344$ in^4

$d_{top\_of\_steel\_stc} := \frac{w_d}{2} + tf_t - d_{s\_stc} = -4.707$ in $\quad S_{top\_of\_steel\_stc} := \frac{I_{NA\_stc}}{d_{top\_of\_steel\_stc}} = -1516.803$ in^3

$d_{bot\_of\_steel\_stc} := \frac{w_d}{2} + bf_t + d_{s\_stc} = 23.207$ in $\quad S_{bot\_of\_steel\_stc} := \frac{I_{NA\_stc}}{d_{bot\_of\_steel\_stc}} = 307.674$ in^3

Results:

Moment of inertia of the composite section: $I_{NA\_stc} = 7140.344$ in^4

Distance to the centroid from the top of the steel section: $d_{top\_of\_steel\_stc} = -4.707$ in

Distance to the centroid from the bottom of the steel section: $d_{bot\_of\_steel\_stc} = 23.207$ in

Section modulus about the top of the steel: $S_{top\_of\_steel\_stc} = -1516.803$ in^3

Section modulus about the bottom of the steel: $S_{bot\_of\_steel\_stc} = 307.674$ in^3

Composite Section Properties for Beam C:

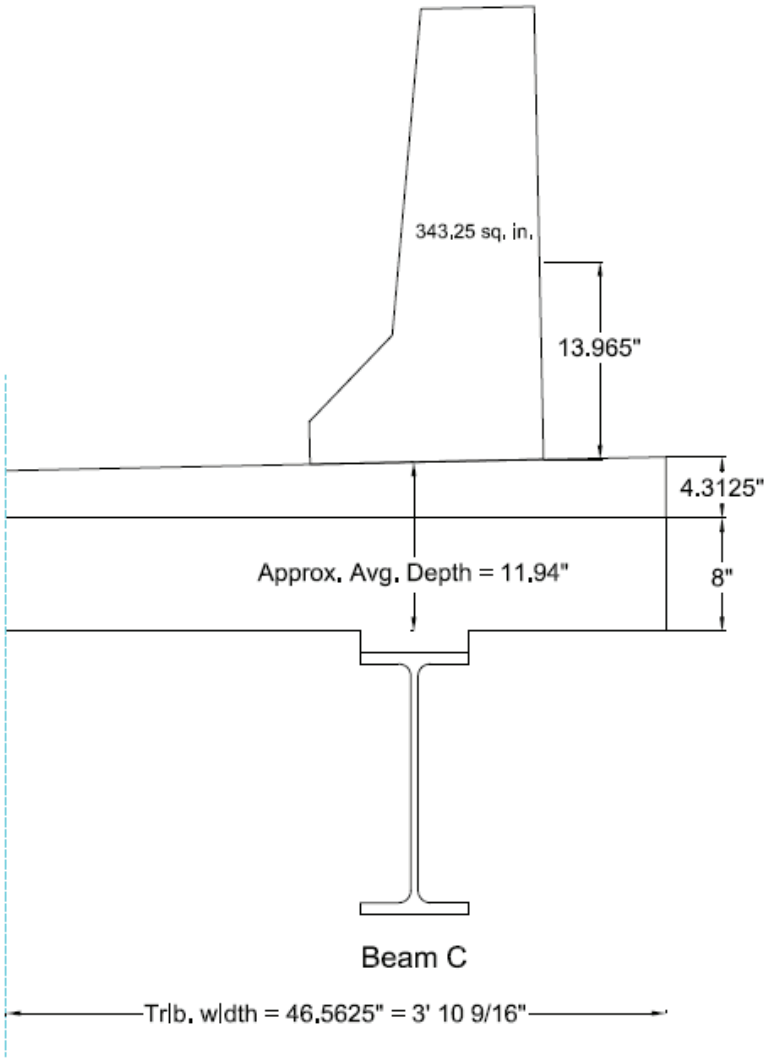

Slab properties:

Avg. concrete slab depth:	$d := 11.94$	in
Modular ratio:	$n := 4.61$	
Haunch depth:	$H := 1.5$	in
Effective width:	$b_s := 46.5625$	in

Composite Section Property Calculations:

Beam properties:

Top Flange	thickness	$tf_t := 0.81$ in
	width	$tf_w := 7.64$ in
Web	thickness	$w_t := 0.495$ in
	depth	$w_d := 18.5 - 2 \cdot tf_t = 16.88$ in
Bottom flange	thickness	$bf_t := 0.81$ in
	width	$bf_w := 7.64$ in

Moment of inertia: $I_{NA} := 1170 \ in^4$

Section modulus: $S_{top\_of\_steel} := 127 \ in^3$

$S_{bot\_of\_steel} := 127 \ in^3$

Distance to centroid: $d_{top\_of\_steel} := 9.25 \ in$

$d_{bot\_of\_steel} := 9.25 \ in$

Gross steel area: $A_{g\_s} := 20.8 \ in^2$

Distance to centroid from center: $d_{s\_s} := 0 \ in$

Concrete barrier properties:

Area of concrete: $A_{c\_barr} := \frac{(212.75 + 81 + 49.5)}{n} = 74.458 \ in^2$

Approximated shape of barrier

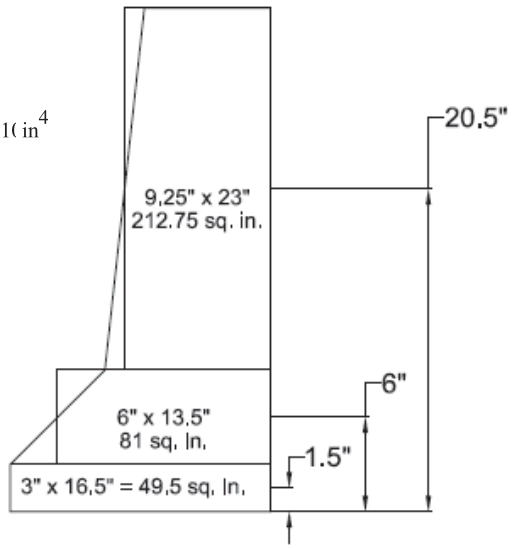

Moment of inertia of barrier (from center of steel):

$$I_{c\_barr1} := \frac{1}{12} \cdot \frac{9.25}{n} \cdot 23^3 + 212.75 \cdot \left(20.5 + H + tf_t + \frac{w_d}{2}\right)^2 = 209798.1 \ in^4$$

$$I_{c\_barr2} := \frac{1}{12} \cdot \frac{6}{n} \cdot 13.5^3 + 81 \cdot \left(6 + H + tf_t + \frac{w_d}{2}\right)^2 = 22992.414 \ in^4$$

$$I_{c\_barr3} := \frac{1}{12} \cdot \frac{3}{n} \cdot 16.5^3 + 49.5 \cdot \left(1.5 + H + tf_t + \frac{w_d}{2}\right)^2 = 7671.701 \ in^4$$

$$I_{c\_barr} := I_{c\_barr1} + I_{c\_barr2} + I_{c\_barr3} = 240462.219 \ in^4$$

Height of centroid of barrier from center of steel:

$$d_{c\_barr} := \frac{49.5 \cdot 1.5 + 81 \cdot 6 + 212.75 \cdot 20.5}{212.75 + 81 + 49.5} + H + tf_t + \frac{w_d}{2} = 25.088 \ in$$

Composite Section Property Calculations:

Short-term (n) Composite Section:

Steel Section:

$A_s := A_{g\_s} = \blacksquare$ in^2 $\quad d_s := d_{s\_s} = 0$ in

$Ad_s := A_s \cdot d_s = 0$ in^3 $\quad Ad2_s := A_s \cdot d_s^{\,2} = 0$ in^4

$I_{os} := I_{NA} = 1170$ in^4 $\quad I_s := I_{os} + Ad2_s = 1170$ in^4

Concrete Slab:

$A_c := d \cdot \frac{b_s}{n} = 120.598$ in^2 $\quad d_c := \frac{d}{2} + H + \frac{w_d}{2} + tf_t = 16.72$ in

$Ad_c := A_c \cdot d_c = 2016.397$ in^3 $\quad Ad2_c := A_c \cdot d_c^{\,2} = 33714.152$ in^4

$I_{oc} := \frac{1}{12} \cdot \left(\frac{b_s}{n}\right) \cdot d^3 = 1432.739$ in^4 $\quad I_c := I_{oc} + Ad2_c = 35146.891$ in^4

Concrete Barrier:

$A_{c\_barr} = 74.458$ in^2 $\quad d_{c\_barr} = 25.088$ in

$Ad_{c\_barr} := A_{c\_barr} \cdot d_{c\_barr} = 1868.018$ in^3 $\quad Ad2_{c\_barr} := A_{c\_barr} \cdot d_{c\_barr}^{\,2} = 46865.413$ in^4

$I_{c\_barr} = 240462.219$ in^4

Section Property Calculations (Considering Barrier's Contribution to Strength):

$A_{sum} := A_s + A_c + A_{c\_barr} = 215.856$ in^2 $\quad Ad_{sum} := Ad_s + Ad_c + Ad_{c\_barr} = 3884.415$ in^3

$I_{sum} := I_s + I_c + I_{c\_barr} = 276779.11$ in^4 $\quad d_{s\_stc} := \frac{Ad_{sum}}{A_{sum}} = 17.995$

$imbal := -d_{s\_stc} \cdot Ad_{sum} = -69901.718$ in^4

$I_{NA\_stc} := I_{sum} + imbal = 206877.392$ in^4

$d_{top\_of\_steel\_stc} := \frac{w_d}{2} + tf_t - d_{s\_stc} = -8.745$ in $\quad S_{top\_of\_steel\_stc} := \frac{I_{NA\_stc}}{d_{top\_of\_steel\_stc}} = -23655.48$ in^3

$d_{bot\_of\_steel\_stc} := \frac{w_d}{2} + bf_t + d_{s\_stc} = 27.245$ in $\quad S_{bot\_of\_steel\_stc} := \frac{I_{NA\_stc}}{d_{bot\_of\_steel\_stc}} = 7593.104$ in^3

Results (Considering Barrier's Contribution to Strength):

Moment of inertia of the composite section: $I_{NA\_stc} = 206877.392$ in^4

Distance to the centroid from the top of the steel section: $d_{top\_of\_steel\_stc} = -8.745$ in

Distance to the centroid from the bottom of the steel section: $d_{bot\_of\_steel\_stc} = 27.245$ in

Section modulus about the top of the steel: $S_{top\_of\_steel\_stc} = -23655.48$ in^3

Section modulus about the bottom of the steel: $S_{bot\_of\_steel\_stc} = 7593.104$ in^3

Composite Section Property Calculations:

Section Property Calculations (Not Considering Barrier's Contribution to Strength):

$A_{sum} := A_s + A_c = 141.398$ in^2

$Ad_{sum} := Ad_s + Ad_c = 2016.397$ in^3

$I_{sum} := I_s + I_c = 36316.891$ in^4

$d_{s\_stc} := \frac{Ad_{sum}}{A_{sum}} = 14.26$

$imbal := -d_{s\_stc} \cdot Ad_{sum} = -28754.712$ in^4

$I_{NA\_stc} := I_{sum} + imbal = 7562.179$ in^4

$d_{top\_of\_steel\_stc} := \frac{w_d}{2} + tf_t - d_{s\_stc} = -5.01$ in

$S_{top\_of\_steel\_stc} := \frac{I_{NA\_stc}}{d_{top\_of\_steel\_stc}} = -1509.283$ in^3

$d_{bot\_of\_steel\_stc} := \frac{w_d}{2} + bf_t + d_{s\_stc} = 23.51$ in

$S_{bot\_of\_steel\_stc} := \frac{I_{NA\_stc}}{d_{bot\_of\_steel\_stc}} = 321.652$ in^3

Results (Not Considering Barrier's Contribution to Strength):

Moment of inertia of the composite section: $I_{NA\_stc} = 7562.179$ in^4

Distance to the centroid from the top of the steel section: $d_{top\_of\_steel\_stc} = -5.01$ in

Distance to the centroid from the bottom of the steel section: $d_{bot\_of\_steel\_stc} = 23.51$ in

Section modulus about the top of the steel: $S_{top\_of\_steel\_stc} = -1509.283$ in^3

Section modulus about the bottom of the steel: $S_{bot\_of\_steel\_stc} = 321.652$ in^3

Stresses and Strains at Gauge Locations on Beam A:

Composite section properties (not considering barriers):

Moment of inertia of the composite section:	$I_{NA\_stc} = 6566.882$ in^4	$I := I_{NA\_stc}$
Distance to the centroid from the top of the steel section:	$d_{top\_of\_steel\_stc} = -4.234$ in	
Distance to the centroid from the bottom of the steel section:	$d_{bot\_of\_steel\_stc} = 22.734$ in	
Section modulus about the top of the steel:	$S_{top\_of\_steel\_stc} = -1550.872$ in^3	
Section modulus about the bottom of the steel:	$S_{bot\_of\_steel\_stc} = 288.853$ in^3	

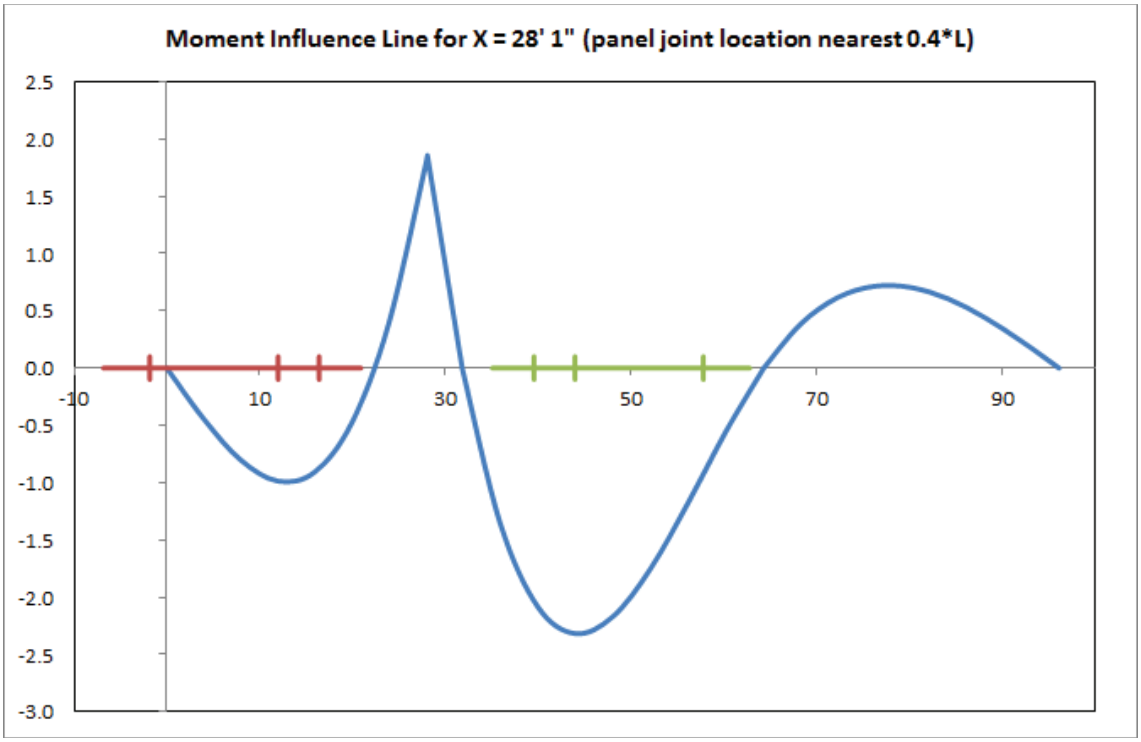

Note: the red and green lines represent the two dump trucks and the locations of their respective axels

Distribution factor: $distbf := \frac{1}{3}$ *Assuming that the load distributes evenly into the 3 beams

Front axel weight: $f\_axel_{wt} := 15500 \cdot distbf = 5166.667$ lbs

Middle axel weight: $m\_axel_{wt} := 19500 \cdot distbf = 6500$ lbs

Back axel weight: $b\_axel_{wt} := 18750 \cdot distbf = 6250$ lbs

Influence line magnitudes at axel locations:

Truck 1:	$truck1_{f\_axel} := 0$	$truck1_{m\_axel} := -0.9855$	$truck1_{b\_axel} := -0.8547$
Truck 2:	$truck2_{f\_axel} := -0.9236$	$truck2_{m\_axel} := -2.3165$	$truck2_{b\_axel} := -2.0125$

Stresses and Strains at Gauge Locations on Beam A:

Total moment developed at the panel interface (divided into the three girders):

$$M_{total} := \frac{truck1_{f\_axel} \cdot f\_axel_{wt} + truck1_{m\_axel} \cdot m\_axel_{wt} + truck1_{b\_axel} \cdot b\_axel_{wt} \cdots}{+ truck2_{f\_axel} \cdot f\_axel_{wt} + truck2_{m\_axel} \cdot m\_axel_{wt} + truck2_{b\_axel} \cdot b\_axel_{wt}} = -44.155$$

$$1000$$

$M_{total} = -44.155$ kip·ft $M := M_{total} \cdot 12 = -529.859$ kip·in

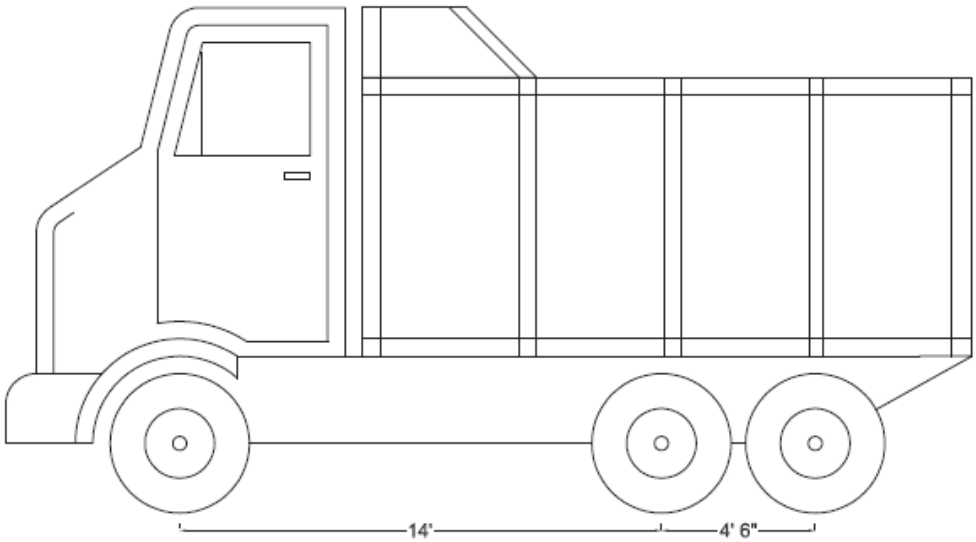

Total area (converted into steel) of the composite beam and slab system: $A_{tot} := A_{sum} = 158.918$ in^2

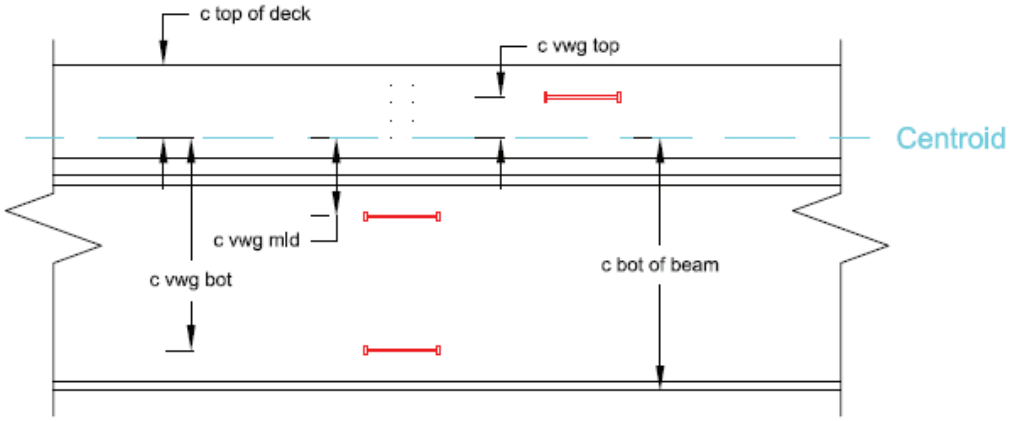

Stresses and Strains at Gauge Locations on Beam A:

Distances from centroid of composite section to gauge locations:

$c_{top\_deck} := -\left(H + 8 + d_{top\_of\_steel\_stc}\right) = -5.266$ in $\qquad c_{bot\_beam} := d_{bot\_of\_steel\_stc} = 22.734$ in

$c_{vwg\_top} := -\left(-c_{top\_deck} - 2.75\right) = -2.516$ in $\qquad c_{vwg\_mid} := 2.6875 - d_{top\_of\_steel\_stc} + 0.81 = 7.732$ in

$c_{vwg\_bot} := 2.6875 + 0.81 + 11.5 - d_{top\_of\_steel\_stc} = 19.232$ in

Modulus of elasticity:

$E_s := 29000$ ksi $\qquad E_c := 6287$ ksi $\qquad n := \frac{E_s}{E_c} = 4.613$

Predicted stresses at gauge loactions during static load test:

Stress at top of the deck: $\sigma_{top\_deck} := \frac{M \cdot c_{top\_deck}}{I \cdot n} = 0.092$ ksi

Stress at top vwg in deck: $\sigma_{vwg\_top} := \frac{M \cdot c_{vwg\_top}}{I \cdot n} = 0.044$ ksi

Stress at middle vwg on beam: $\sigma_{vwg\_mid} := \frac{M \cdot c_{vwg\_mid}}{I} = -0.624$ ksi

Positive stress = tension
Negative stress = compression

Stress at bottom vwg on beam: $\sigma_{vwg\_bot} := \frac{M \cdot c_{vwg\_bot}}{I} = -1.552$ ksi

Stress at bottom of the beam: $\sigma_{bot\_beam} := \frac{M \cdot c_{bot\_beam}}{I} = -1.834$ ksi

Predicted strains at gauge locations during static load test:

Strain at top of the deck: $\varepsilon_{top\_deck} := \frac{\sigma_{top\_deck}}{E_c} \cdot 10^6 = 14.6507$ με $\qquad \varepsilon_{bdi7} := \varepsilon_{top\_deck}$

Strain at top vwg in deck: $\varepsilon_{vwg\_top} := \frac{\sigma_{vwg\_top}}{E_c} \cdot 10^6 = 6.9994$ με $\qquad \varepsilon_{vwg7} := \varepsilon_{vwg\_top}$

Strain at middle vwg on beam: $\varepsilon_{vwg\_mid} := \frac{\sigma_{vwg\_mid}}{E_s} \cdot 10^6 = -21.5122$ με

Strain at bottom vwg on beam: $\varepsilon_{vwg\_bot} := \frac{\sigma_{vwg\_bot}}{E_s} \cdot 10^6 = -53.5086$ με

Strain at bottom of the beam: $\varepsilon_{bot\_beam} := \frac{\sigma_{bot\_beam}}{E_s} \cdot 10^6 = -63.2536$ με

Stresses and Strains at Gauge Locations on Beam A:

Strains and stresses with truck at midspan:

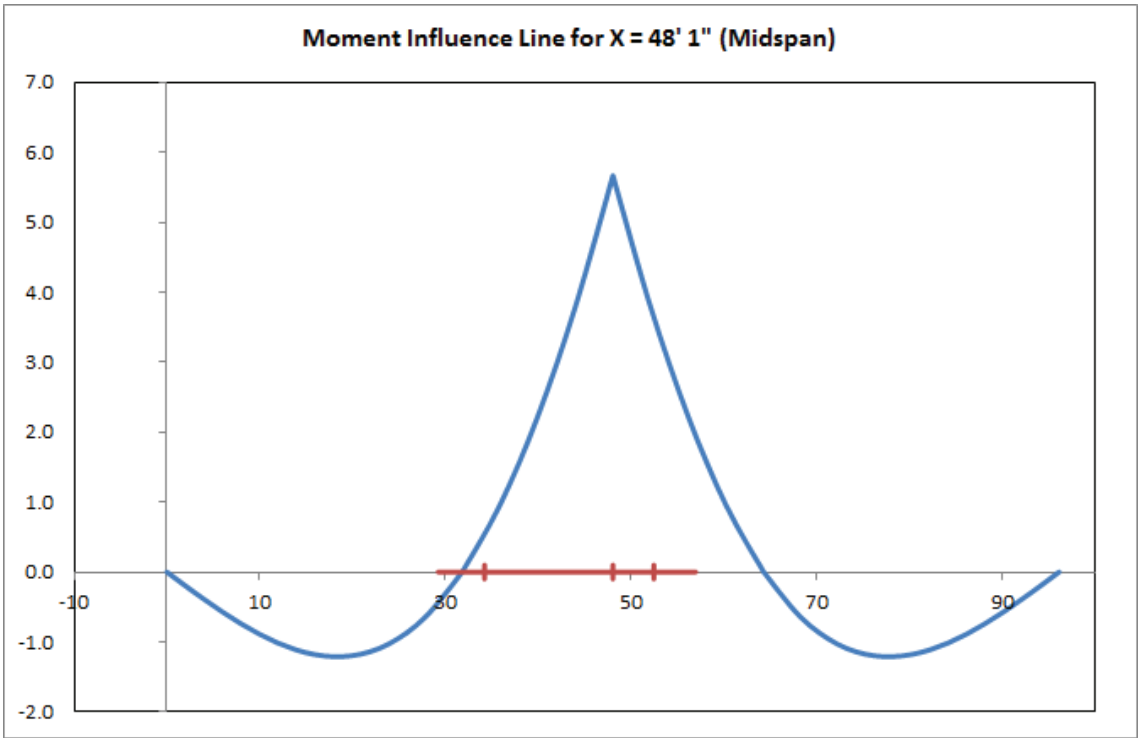

Influence line magnitudes at axel locations:

Truck 1: $truck1_{f\_axel} := 0.569$ $truck1_{m\_axel} := 5.667$ $truck1_{b\_axel} := 3.653$

Total moment developed at the panel interface (divided into the three girders):

$$M_{total} := \frac{truck1_{f\_axel} \cdot f\_axel_{wt} + truck1_{m\_axel} \cdot m\_axel_{wt} + truck1_{b\_axel} \cdot b\_axel_{wt}}{1000} = 62.607$$

$M_{total} = 62.607$ kip·ft $M := M_{total} \cdot 12 = 751.279$ kip·in

Stresses and Strains at Gauge Locations on Beam A:

Predicted max stresses at midspan gauge loactions during moving tests:

Stress at bottom of the beam: $\sigma_{bot\_beam} := \frac{M \cdot c_{bot\_beam}}{I} = 2.601$ ksi

Positive stress = tension
Negative stress = compression

Predicted max strains at midspan gauge locations during moving tests:

Strain at bottom of the beam: $\varepsilon_{bot\_beam} := \frac{\sigma_{bot\_beam}}{E_s} \cdot 10^6 = 89.6863$ με

$\varepsilon_{bdi4} := \varepsilon_{bot\_beam}$

Max deflection at midspan:

$\Delta_{max} := -0.04571$ in Calculated using Mastan2

$\Delta_{twang4} := \Delta_{max}$

Deflected shape produced by Mastan2:

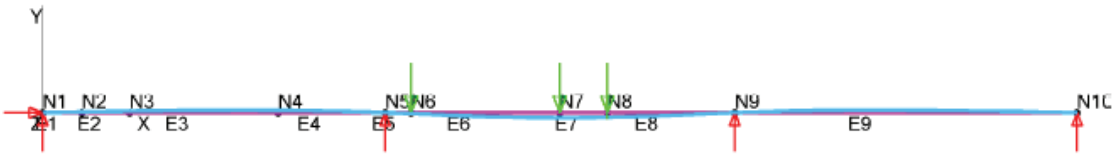

Moment diagram produced by Mastan2:

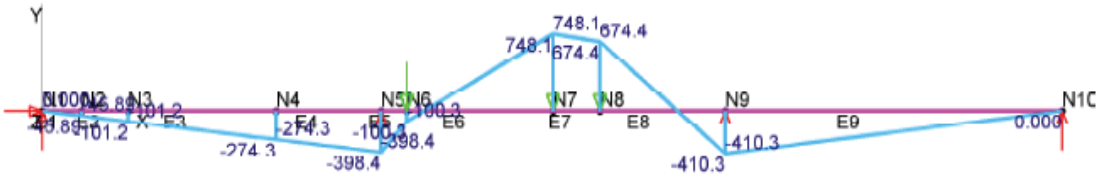

Stresses and Strains at Gauge Locations on Beam A:

Strains and stresses with truck at 0.4*L of first span:

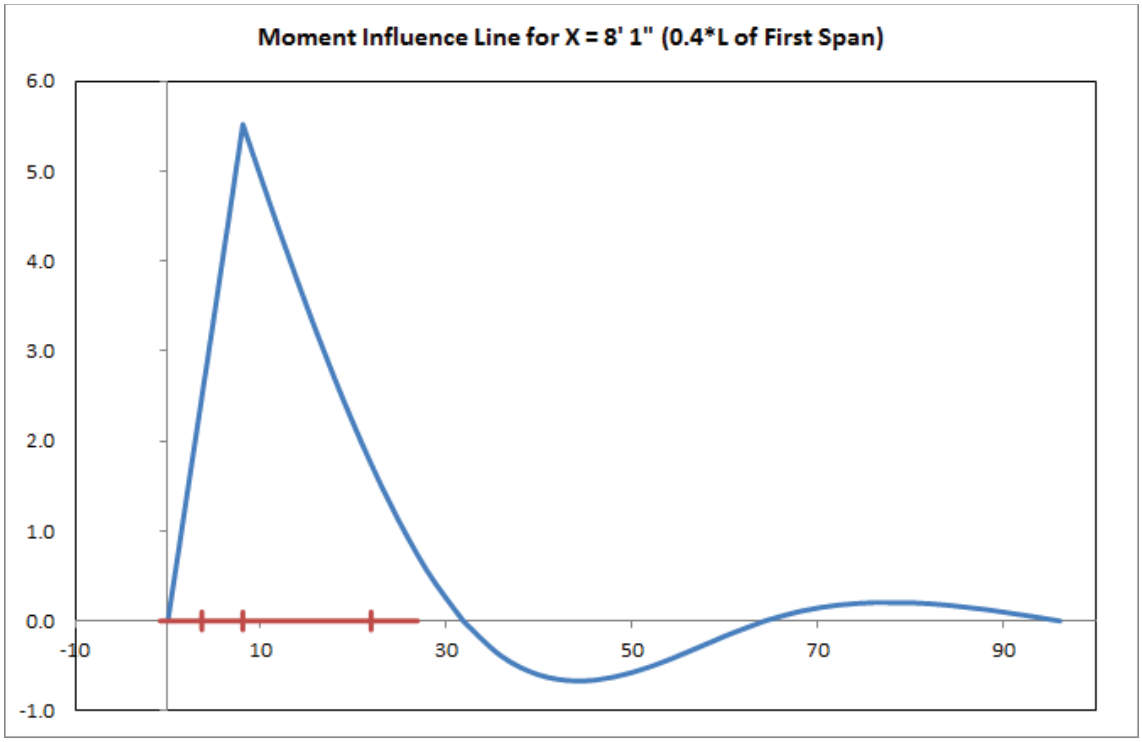

Influence line magnitudes at axel locations:

Truck 1: $truck1_{f\_axel} := 1.7617$ $truck1_{m\_axel} := 5.523$ $truck1_{b\_axel} := 2.493$

Total moment developed at the panel interface (divided into the three girders):

$$M_{total} := \frac{truck1_{f\_axel} \cdot f\_axel_{wt} + truck1_{m\_axel} \cdot m\_axel_{wt} + truck1_{b\_axel} \cdot b\_axel_{wt}}{1000} = 60.583$$

$M_{total} = 60.583$ kip·ft $M := M_{total} \cdot 12 = 726.994$ kip·in

Stresses and Strains at Gauge Locations on Beam A:

Predicted max stresses at midspan gauge loactions during moving tests:

Stress at top of the deck: $\sigma_{top\_deck} := \frac{M \cdot c_{top\_deck}}{I \cdot n} = -0.126$ ksi

Stress at top vwg in deck: $\sigma_{vwg\_top} := \frac{M \cdot c_{vwg\_top}}{I \cdot n} = -0.06$ ksi

Stress at middle vwg on beam: $\sigma_{vwg\_mid} := \frac{M \cdot c_{vwg\_mid}}{I} = 0.856$ ksi

Positive stress = tension
Negative stress = compression

Stress at bottom vwg on beam: $\sigma_{vwg\_bot} := \frac{M \cdot c_{vwg\_bot}}{I} = 2.129$ ksi

Stress at bottom of the beam: $\sigma_{bot\_beam} := \frac{M \cdot c_{bot\_beam}}{I} = 2.517$ ksi

Predicted max strains at midspan gauge locations during moving tests:

Strain at top of the deck: $\varepsilon_{top\_deck} := \frac{\sigma_{top\_deck}}{E_c} \cdot 10^6 = -20.1015$ με

Strain at top vwg in deck: $\varepsilon_{vwg\_top} := \frac{\sigma_{vwg\_top}}{E_c} \cdot 10^6 = -9.6035$ με $\quad \varepsilon_{vwg5} := \varepsilon_{vwg\_top}$

Strain at middle vwg on beam: $\varepsilon_{vwg\_mid} := \frac{\sigma_{vwg\_mid}}{E_s} \cdot 10^6 = 29.5159$ με

Strain at bottom vwg on beam: $\varepsilon_{vwg\_bot} := \frac{\sigma_{vwg\_bot}}{E_s} \cdot 10^6 = 73.4166$ με

Strain at bottom of the beam: $\varepsilon_{bot\_beam} := \frac{\sigma_{bot\_beam}}{E_s} \cdot 10^6 = 86.7872$ με $\quad \varepsilon_{bdi1} := \varepsilon_{bot\_beam}$

Max deflection at midspan:

$\Delta_{max} := -0.03811$ in Calculated using Mastan2 $\quad \Delta_{twang1} := \Delta_{max}$

Deflected shape produced by Mastan2:

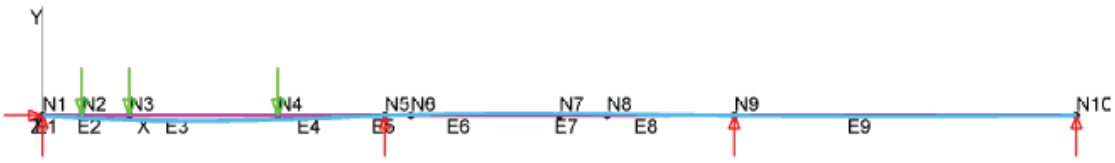

Moment diagram produced by Mastan2:

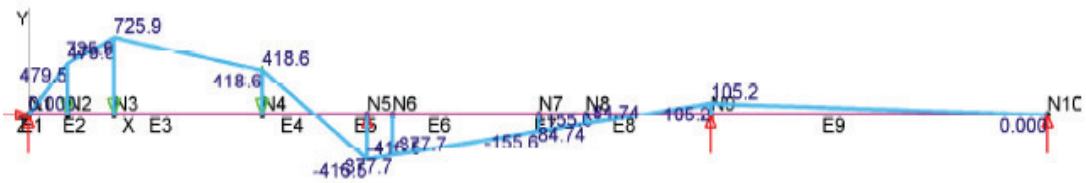

Stresses and Strains at Gauge Locations on Beam A:

Summary of Approximate Field Strains and Deflections:

Static Load Test:

At gauge location near pier:

LVDT #1:	$\Delta_{LVDT1} := 0$	in
BDI #7:	$\varepsilon_{bdi7} = 14.651$	με
VWG #7:	$\varepsilon_{vwg7} = 6.999$	με

Moving Load Tests:

At gauge location midspan:

BDI #4:	$\varepsilon_{bdi4} = 89.686$	με
Twanger #4:	$\Delta_{twang4} = -0.046$	in

At gauge location 0.4*L of first span:

VWG #5:	$\varepsilon_{vwg5} = -9.604$	με
BDI #1:	$\varepsilon_{bdi1} = 86.787$	με
Twanger #1:	$\Delta_{twang1} = -0.038$	in

Stresses and Strains at Gauge Locations on Beam B:

Composite section properties (not considering barriers):

Moment of inertia of the composite section: $I_{NA\_stc} = 7140.344$ in^4 $I := I_{NA\_stc}$

Distance to the centroid from the top of the steel section: $d_{top\_of\_steel\_stc} = -4.707$ in

Distance to the centroid from the bottom of the steel section: $d_{bot\_of\_steel\_stc} = 23.207$ in

Section modulus about the top of the steel: $S_{top\_of\_steel\_stc} = -1516.803$ in^3

Section modulus about the bottom of the steel: $S_{bot\_of\_steel\_stc} = 307.674$ in^3

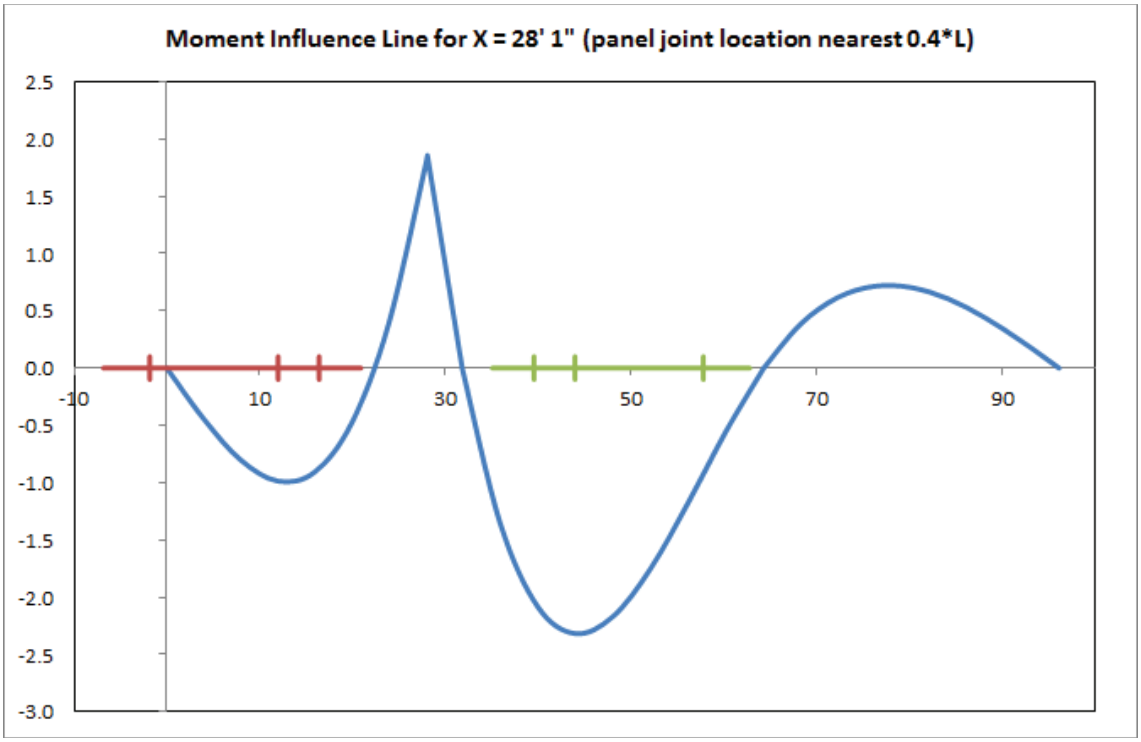

Note: the red and green lines represent the two dump trucks and the locations of their respective axels

Distribution factor: $distbf := \frac{1}{3}$ *Assuming that the load distributes evenly into the 3 beams

Front axel weight: $f\_axel_{wt} := 15500 \cdot distbf = 5166.667$ lbs

Middle axel weight: $m\_axel_{wt} := 19500 \cdot distbf = 6500$ lbs

Back axel weight: $b\_axel_{wt} := 18750 \cdot distbf = 6250$ lbs

Influence line magnitudes at axel locations:

Truck 1: $truck1_{f\_axel} := 0$ $truck1_{m\_axel} := -0.9855$ $truck1_{b\_axel} := -0.8547$

Truck 2: $truck2_{f\_axel} := -0.9236$ $truck2_{m\_axel} := -2.3165$ $truck2_{b\_axel} := -2.0125$

Stresses and Strains at Gauge Locations on Beam B:

Total moment developed at the panel interface (divided into the three girders):

$$M_{total} := \frac{truck1_{f\_axel} \cdot f\_axel_{wt} + truck1_{m\_axel} \cdot m\_axel_{wt} + truck1_{b\_axel} \cdot b\_axel_{wt} \cdots}{+ truck2_{f\_axel} \cdot f\_axel_{wt} + truck2_{m\_axel} \cdot m\_axel_{wt} + truck2_{b\_axel} \cdot b\_axel_{wt}} = -44.155$$

$$1000$$

$M_{total} = -44.155$ kip·ft $M := M_{total} \cdot 12 = -529.859$ kip·in

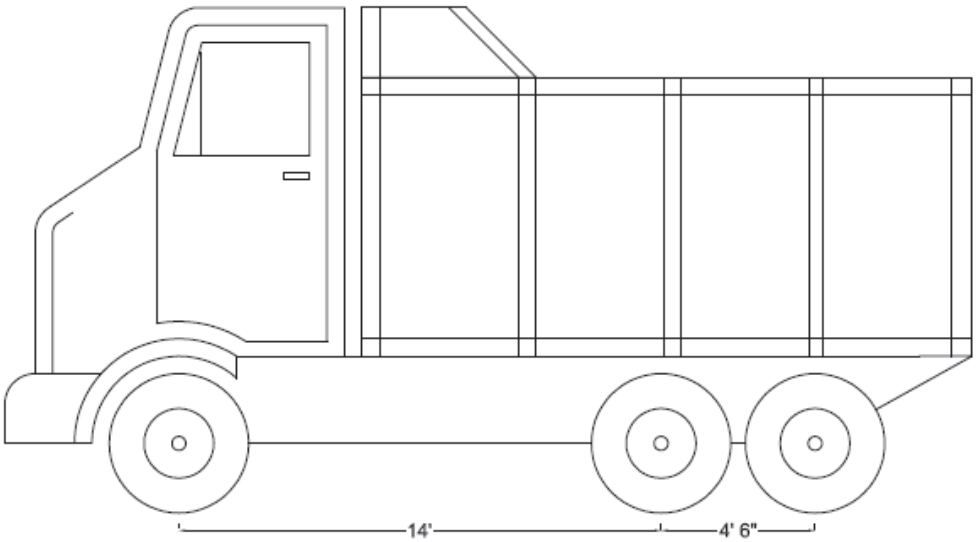

Total area (converted into steel) of the composite beam and slab system: $A_{tot} := A_{sum} = 155.05$ in^2

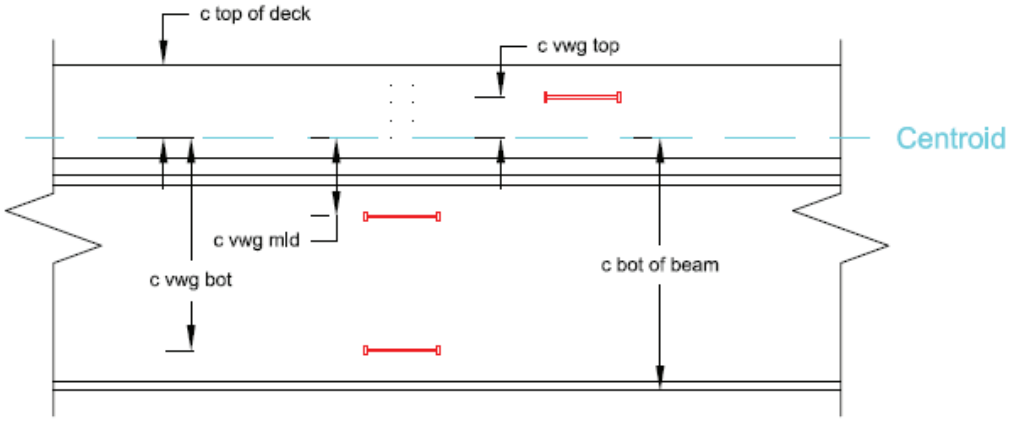

Stresses and Strains at Gauge Locations on Beam B:

Distances from centroid of composite section to gauge locations:

$c_{top\_deck} := -\left(H + 8 + d_{top\_of\_steel\_stc}\right) = -4.793$ in

$c_{bot\_beam} := d_{bot\_of\_steel\_stc} = 23.207$ in

$c_{vwg\_top} := -\left(-c_{top\_deck} - 2.75\right) = -2.043$ in

$c_{vwg\_mid} := 2.6875 - d_{top\_of\_steel\_stc} + 0.81 = 8.205$ in

$c_{vwg\_bot} := 2.6875 + 0.81 + 11.5 - d_{top\_of\_steel\_stc} = 19.705$ in

Modulus of elasticity:

$E_s := 29000$ ksi $\quad E_c := 6287$ ksi $\quad n := \frac{E_s}{E_c} = 4.613$

Predicted stresses at gauge loactions during static load test:

Stress at top of the deck: $\sigma_{top\_deck} := \frac{M \cdot c_{top\_deck}}{I \cdot n} = 0.077$ ksi

Stress at top vwg in deck: $\sigma_{vwg\_top} := \frac{M \cdot c_{vwg\_top}}{I \cdot n} = 0.033$ ksi

Stress at middle vwg on beam: $\sigma_{vwg\_mid} := \frac{M \cdot c_{vwg\_mid}}{I} = -0.609$ ksi

Positive stress = tension
Negative stress = compression

Stress at bottom vwg on beam: $\sigma_{vwg\_bot} := \frac{M \cdot c_{vwg\_bot}}{I} = -1.462$ ksi

Stress at bottom of the beam: $\sigma_{bot\_beam} := \frac{M \cdot c_{bot\_beam}}{I} = -1.722$ ksi

Predicted strains at gauge locations during static load test:

Strain at top of the deck: $\varepsilon_{top\_deck} := \frac{\sigma_{top\_deck}}{E_c} \cdot 10^6 = 12.2633$ με

Strain at top vwg in deck: $\varepsilon_{vwg\_top} := \frac{\sigma_{vwg\_top}}{E_c} \cdot 10^6 = 5.2264$ με

Strain at middle vwg on beam: $\varepsilon_{vwg\_mid} := \frac{\sigma_{vwg\_mid}}{E_s} \cdot 10^6 = -20.9953$ με

Strain at bottom vwg on beam: $\varepsilon_{vwg\_bot} := \frac{\sigma_{vwg\_bot}}{E_s} \cdot 10^6 = -50.422$ με

Strain at bottom of the beam: $\varepsilon_{bot\_beam} := \frac{\sigma_{bot\_beam}}{E_s} \cdot 10^6 = -59.3843$ με

Stresses and Strains at Gauge Locations on Beam B:

Strains and stresses with truck at midspan:

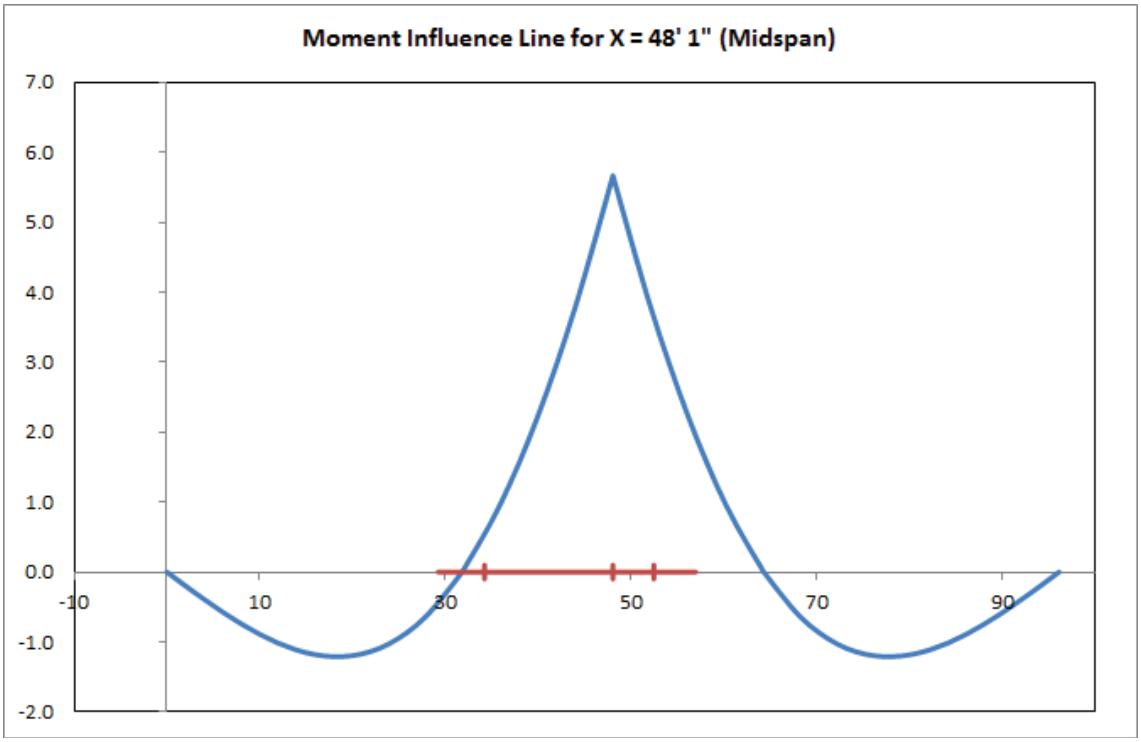

Influence line magnitudes at axel locations:

Truck 1: $truck1_{f\_axel} := 0.569$ $truck1_{m\_axel} := 5.667$ $truck1_{b\_axel} := 3.653$

Total moment developed at the panel interface (divided into the three girders):

$$M_{total} := \frac{truck1_{f\_axel} \cdot f\_axel_{wt} + truck1_{m\_axel} \cdot m\_axel_{wt} + truck1_{b\_axel} \cdot b\_axel_{wt}}{1000} = 62.607$$

$M_{total} = 62.607$ kip·ft $M := M_{total} \cdot 12 = 751.279$ kip·in

Stresses and Strains at Gauge Locations on Beam B:

Predicted max stresses at midspan gauge loactions during moving tests:

Stress at bottom of the beam: $\sigma_{bot\_beam} := \frac{M \cdot c_{bot\_beam}}{I} = 2.442$ ksi

Positive stress = tension
Negative stress = compression

Predicted max strains at midspan gauge locations during moving tests:

Strain at bottom of the beam: $\varepsilon_{bot\_beam} := \frac{\sigma_{bot\_beam}}{E_s} \cdot 10^6 = 84.2001$ με

$\varepsilon_{bdi5} := \varepsilon_{bot\_beam}$

Max deflection at midspan:

$\Delta_{max} := -0.04204$ in Calculated using Mastan2

$\Delta_{twang5} := \Delta_{max}$

Deflected shape produced by Mastan2:

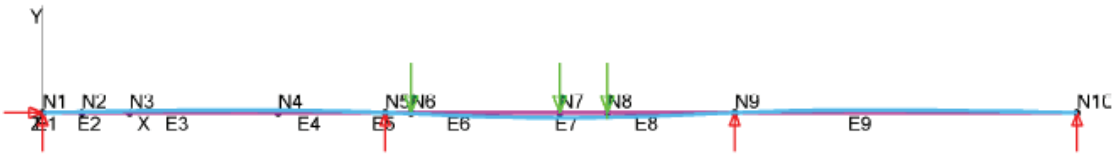

Moment diagram produced by Mastan2:

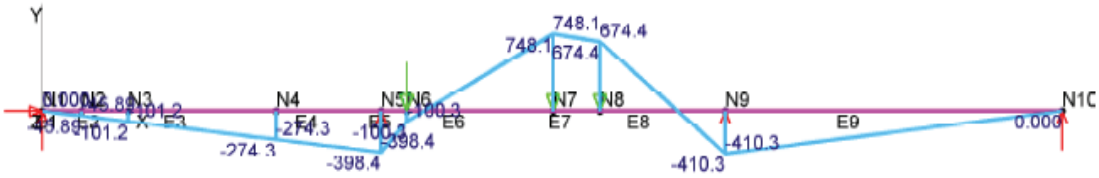

Stresses and Strains at Gauge Locations on Beam B:

Strains and stresses with truck at 0.4*L of first span:

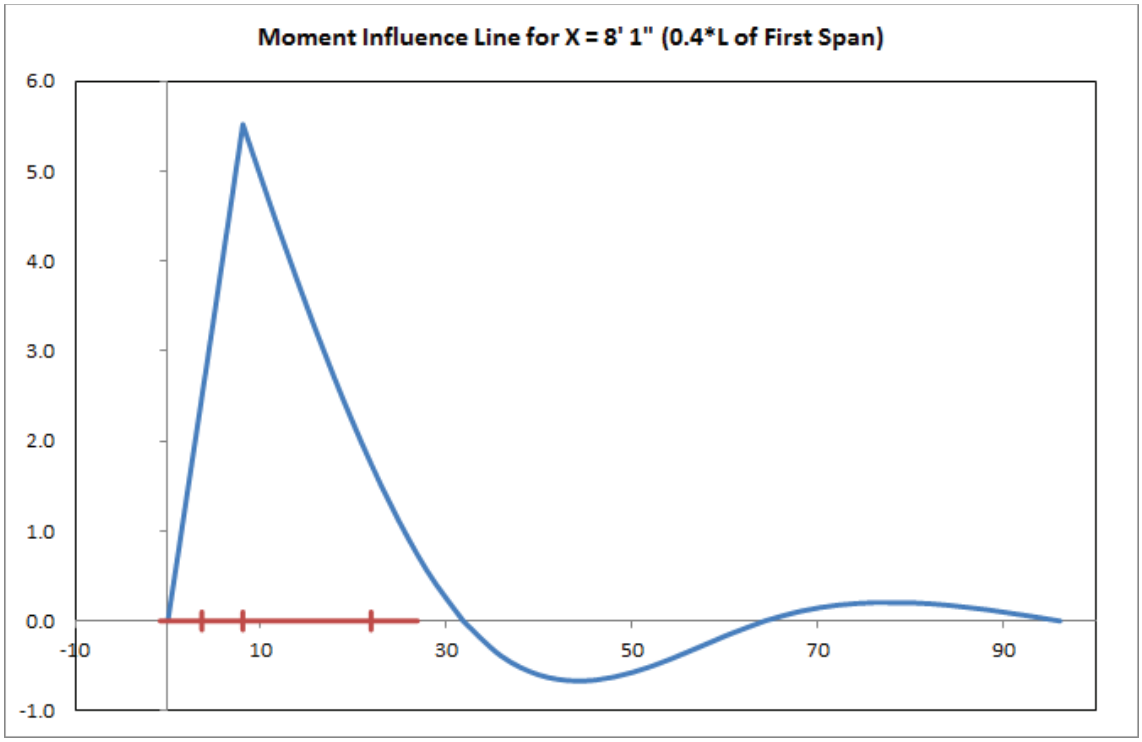

Influence line magnitudes at axel locations:

Truck 1: $truck1_{f\_axel} := 1.7617$ $truck1_{m\_axel} := 5.523$ $truck1_{b\_axel} := 2.493$

Total moment developed at the panel interface (divided into the three girders):

$$M_{total} := \frac{truck1_{f\_axel} \cdot f\_axel_{wt} + truck1_{m\_axel} \cdot m\_axel_{wt} + truck1_{b\_axel} \cdot b\_axel_{wt}}{1000} = 60.583$$

$M_{total} = 60.583$ kip·ft $M := M_{total} \cdot 12 = 726.994$ kip·in

Stresses and Strains at Gauge Locations on Beam B:

Predicted max stresses at midspan gauge loactions during moving tests:

Stress at top of the deck: $\sigma_{top\_deck} := \frac{M \cdot c_{top\_deck}}{I \cdot n} = -0.106$ ksi

Stress at top vwg in deck: $\sigma_{vwg\_top} := \frac{M \cdot c_{vwg\_top}}{I \cdot n} = -0.045$ ksi

Stress at middle vwg on beam: $\sigma_{vwg\_mid} := \frac{M \cdot c_{vwg\_mid}}{I} = 0.835$ ksi

Positive stress = tension
Negative stress = compression

Stress at bottom vwg on beam: $\sigma_{vwg\_bot} := \frac{M \cdot c_{vwg\_bot}}{I} = 2.006$ ksi

Stress at bottom of the beam: $\sigma_{bot\_beam} := \frac{M \cdot c_{bot\_beam}}{I} = 2.363$ ksi

Predicted max strains at midspan gauge locations during moving tests:

Strain at top of the deck: $\varepsilon_{top\_deck} := \frac{\sigma_{top\_deck}}{E_c} \cdot 10^6 = -16.8258$ με

Strain at top vwg in deck: $\varepsilon_{vwg\_top} := \frac{\sigma_{vwg\_top}}{E_c} \cdot 10^6 = -7.1709$ με

Strain at middle vwg on beam: $\varepsilon_{vwg\_mid} := \frac{\sigma_{vwg\_mid}}{E_s} \cdot 10^6 = 28.8066$ με

Strain at bottom vwg on beam: $\varepsilon_{vwg\_bot} := \frac{\sigma_{vwg\_bot}}{E_s} \cdot 10^6 = 69.1816$ με

Strain at bottom of the beam: $\varepsilon_{bot\_beam} := \frac{\sigma_{bot\_beam}}{E_s} \cdot 10^6 = 81.4783$ με

$\varepsilon_{bdi2} := \varepsilon_{bot\_beam}$

Max deflection at midspan:

$\Delta_{max} := -0.03505$ in Calculated using Mastan2

$\Delta_{twang2} := \Delta_{max}$

Deflected shape produced by Mastan2:

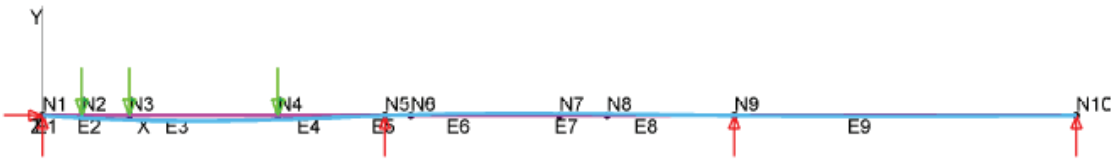

Moment diagram produced by Mastan2:

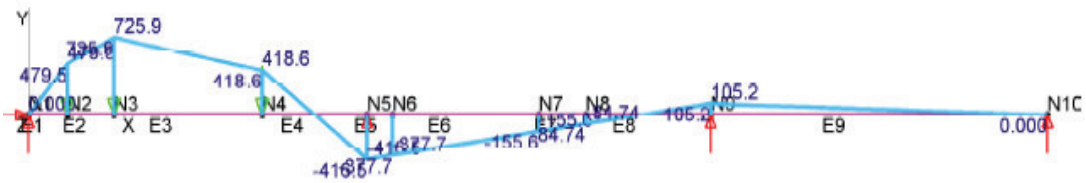

Stresses and Strains at Gauge Locations on Beam B:

Summary of Approximate Field Strains and Deflections:

Moving Load Tests:

At gauge location midspan:

BDI #5: $\varepsilon_{bdi5} = 84.2$ με

Twanger #5: $\Delta_{twang5} = -0.042$ in

At gauge location 0.4*L of first span:

BDI #2: $\varepsilon_{bdi2} = 81.478$ με

Twanger #2: $\Delta_{twang2} = -0.035$ in

Stresses and Strains at Gauge Locations on Beam C:

Composite section properties (not considering barriers):

Moment of inertia of the composite section: $I_{NA\_stc} = 7562.179$ in^4 $I := I_{NA\_stc}$

Distance to the centroid from the top of the steel section: $d_{top\_of\_steel\_stc} = -5.01$ in

Distance to the centroid from the bottom of the steel section: $d_{bot\_of\_steel\_stc} = 23.51$ in

Section modulus about the top of the steel: $S_{top\_of\_steel\_stc} = -1509.283$ in^3

Section modulus about the bottom of the steel: $S_{bot\_of\_steel\_stc} = 321.652$ in^3

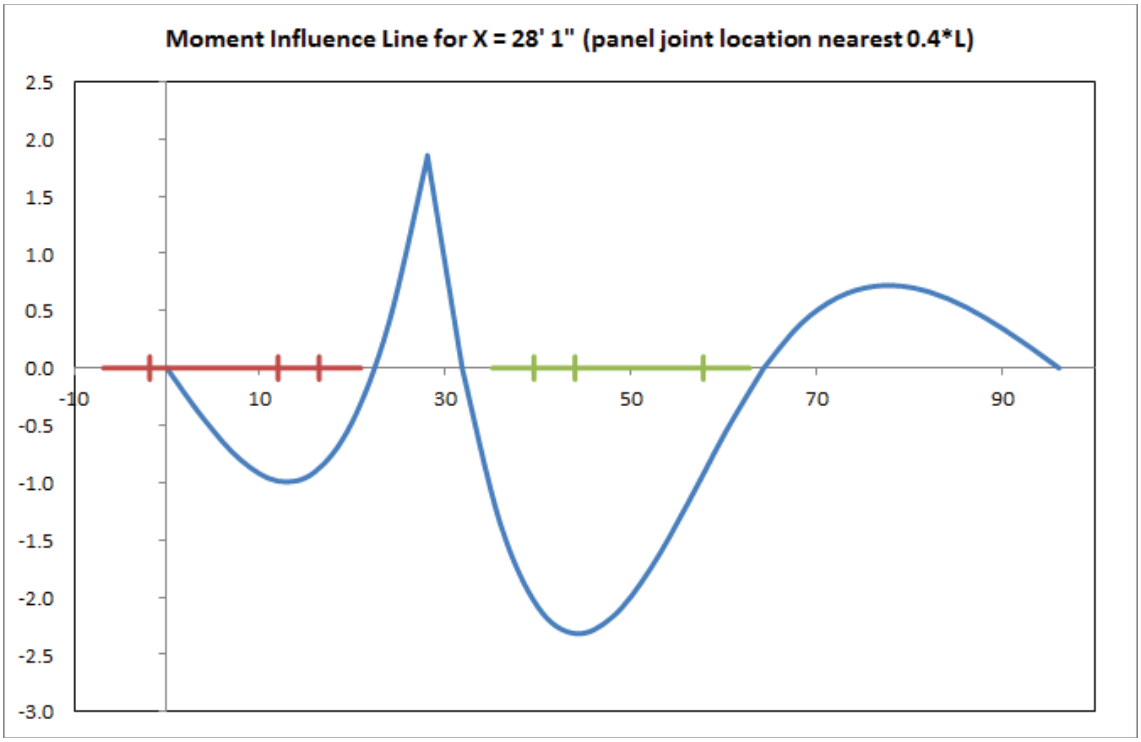

Note: the red and green lines represent the two dump trucks and the locations of their respective axels

Distribution factor: $distbf := \frac{1}{3}$ *Assuming that the load distributes evenly into the 3 beams

Front axel weight: $f\_axel_{wt} := 15500 \cdot distbf = 5166.667$ lbs

Middle axel weight: $m\_axel_{wt} := 19500 \cdot distbf = 6500$ lbs

Back axel weight: $b\_axel_{wt} := 18750 \cdot distbf = 6250$ lbs

Influence line magnitudes at axel locations:

Truck 1: $truck1_{f\_axel} := 0$ $truck1_{m\_axel} := -0.9855$ $truck1_{b\_axel} := -0.8547$

Truck 2: $truck2_{f\_axel} := -0.9236$ $truck2_{m\_axel} := -2.3165$ $truck2_{b\_axel} := -2.0125$

Stresses and Strains at Gauge Locations on Beam C:

Total moment developed at the panel interface (divided into the three girders):

$$M_{total} := \frac{truck1_{f\_axel} \cdot f\_axel_{wt} + truck1_{m\_axel} \cdot m\_axel_{wt} + truck1_{b\_axel} \cdot b\_axel_{wt} \cdots}{+ truck2_{f\_axel} \cdot f\_axel_{wt} + truck2_{m\_axel} \cdot m\_axel_{wt} + truck2_{b\_axel} \cdot b\_axel_{wt}} = -44.155$$

$$1000$$

$M_{total} = -44.155$ kip·ft $M := M_{total} \cdot 12 = -529.859$ kip·in

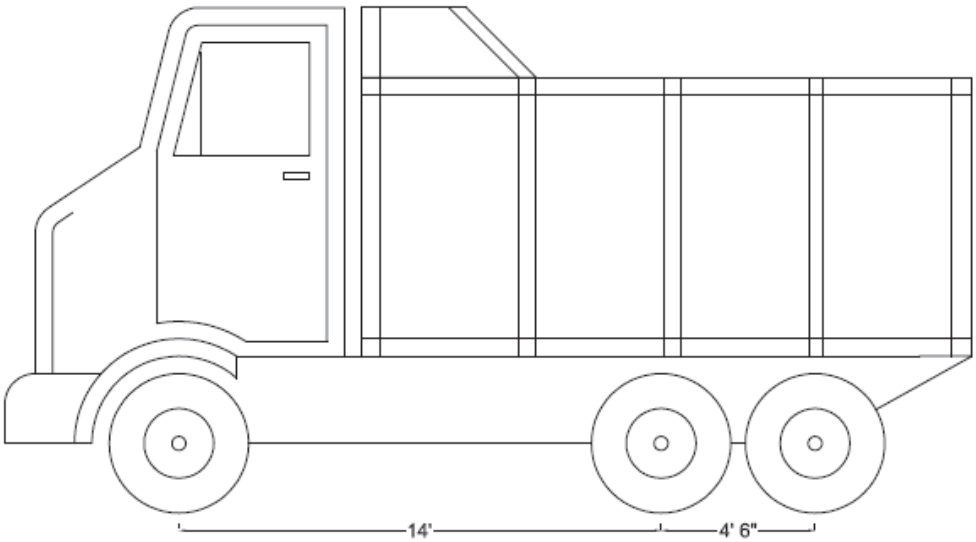

Total area (converted into steel) of the composite beam and slab system: $A_{tot} := A_{sum} = 141.398$ in^2

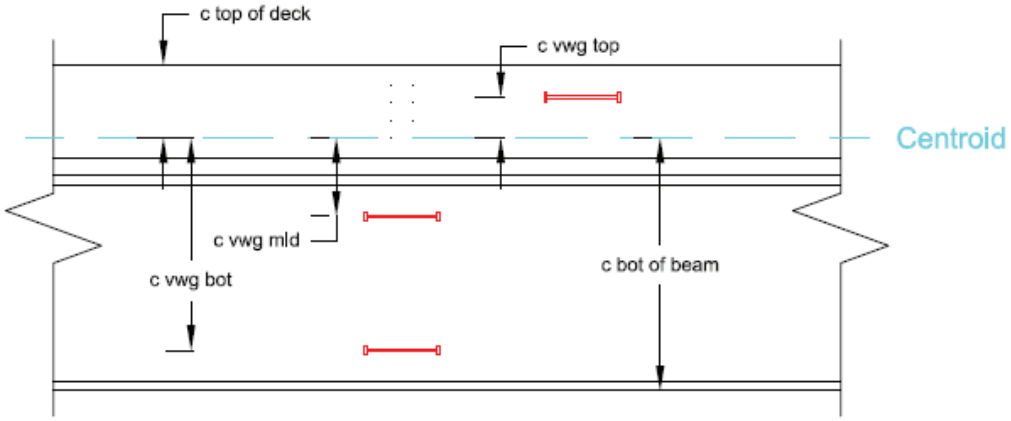

Stresses and Strains at Gauge Locations on Beam C:

Distances from centroid of composite section to gauge locations:

$c_{top\_deck} := -\left(H + 8 + d_{top\_of\_steel\_stc}\right) = -4.49$ in

$c_{bot\_beam} := d_{bot\_of\_steel\_stc} = 23.51$ in

$c_{vwg\_top} := -\left(-c_{top\_deck} - 2.75\right) = -1.74$ in

$c_{vwg\_mid} := 2.6875 - d_{top\_of\_steel\_stc} + 0.81 = 8.508$ in

$c_{vwg\_bot} := 2.6875 + 0.81 + 11.5 - d_{top\_of\_steel\_stc} = 20.008$ in

Modulus of elasticity:

$E_s := 29000$ ksi $\quad E_c := 6287$ ksi $\quad n := \frac{E_s}{E_c} = 4.613$

Predicted stresses at gauge loactions during static load test:

Stress at top of the deck: $\sigma_{top\_deck} := \frac{M \cdot c_{top\_deck}}{I \cdot n} = 0.068$ ksi

Stress at top vwg in deck: $\sigma_{vwg\_top} := \frac{M \cdot c_{vwg\_top}}{I \cdot n} = 0.026$ ksi

Stress at middle vwg on beam: $\sigma_{vwg\_mid} := \frac{M \cdot c_{vwg\_mid}}{I} = -0.596$ ksi

Positive stress = tension
Negative stress = compression

Stress at bottom vwg on beam: $\sigma_{vwg\_bot} := \frac{M \cdot c_{vwg\_bot}}{I} = -1.402$ ksi

Stress at bottom of the beam: $\sigma_{bot\_beam} := \frac{M \cdot c_{bot\_beam}}{I} = -1.647$ ksi

Predicted strains at gauge locations during static load test:

Strain at top of the deck: $\varepsilon_{top\_deck} := \frac{\sigma_{top\_deck}}{E_c} \cdot 10^6 = 10.8472$ με $\quad \varepsilon_{bdi8} := \varepsilon_{top\_deck}$

Strain at top vwg in deck: $\varepsilon_{vwg\_top} := \frac{\sigma_{vwg\_top}}{E_c} \cdot 10^6 = 4.2029$ με $\quad \varepsilon_{vwg8} := \varepsilon_{vwg\_top}$

Strain at middle vwg on beam: $\varepsilon_{vwg\_mid} := \frac{\sigma_{vwg\_mid}}{E_s} \cdot 10^6 = -20.5561$ με $\quad \varepsilon_{vwg3} := \varepsilon_{vwg\_mid}$

Strain at bottom vwg on beam: $\varepsilon_{vwg\_bot} := \frac{\sigma_{vwg\_bot}}{E_s} \cdot 10^6 = -48.3413$ με $\quad \varepsilon_{vwg4} := \varepsilon_{vwg\_bot}$

Strain at bottom of the beam: $\varepsilon_{bot\_beam} := \frac{\sigma_{bot\_beam}}{E_s} \cdot 10^6 = -56.8037$ με

Stresses and Strains at Gauge Locations on Beam C:

Strains and stresses with truck at midspan:

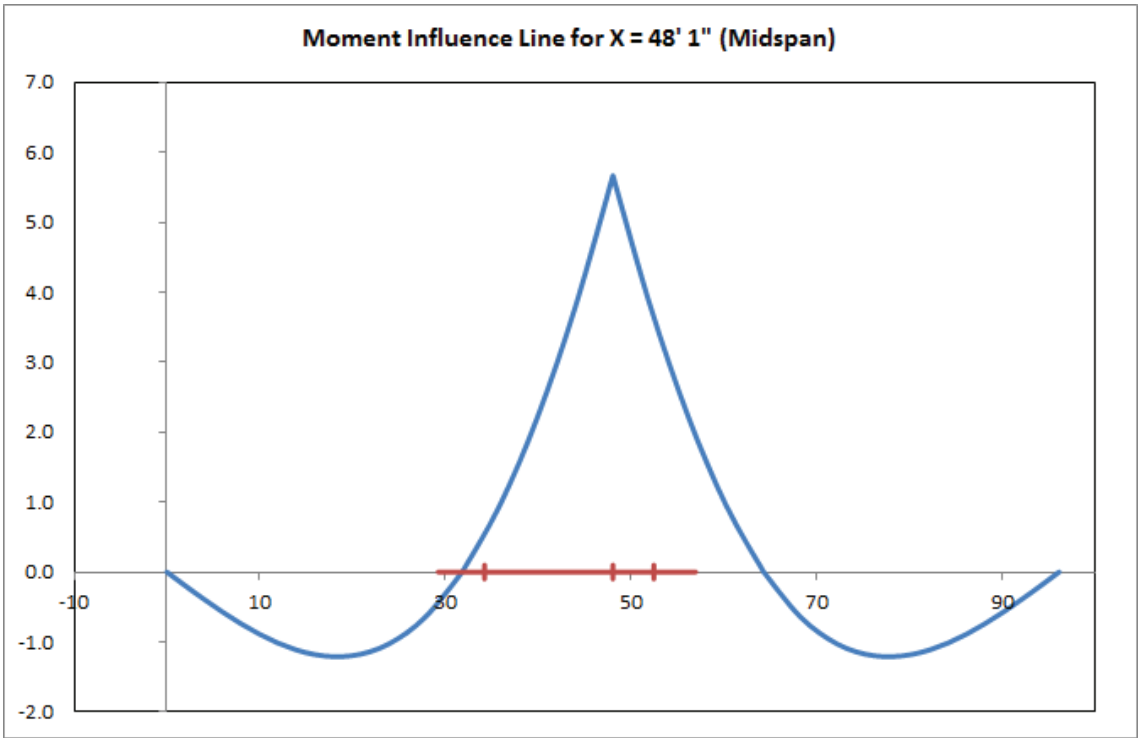

Influence line magnitudes at axel locations:

Truck 1: $truck1_{f\_axel} := 0.569$ $truck1_{m\_axel} := 5.667$ $truck1_{b\_axel} := 3.653$

Total moment developed at the panel interface (divided into the three girders):

$$M_{total} := \frac{truck1_{f\_axel} \cdot f\_axel_{wt} + truck1_{m\_axel} \cdot m\_axel_{wt} + truck1_{b\_axel} \cdot b\_axel_{wt}}{1000} = 62.607$$

$M_{total} = 62.607$ kip·ft $M := M_{total} \cdot 12 = 751.279$ kip·in

Stresses and Strains at Gauge Locations on Beam C:

Predicted max stresses at midspan gauge loactions during moving tests:

Stress at bottom of the beam: $\sigma_{bot\_beam} := \frac{M \cdot c_{bot\_beam}}{I} = 2.336$ ksi

Positive stress = tension
Negative stress = compression

Predicted max strains at midspan gauge locations during moving tests:

Strain at bottom of the beam: $\varepsilon_{bot\_beam} := \frac{\sigma_{bot\_beam}}{E_s} \cdot 10^6 = 80.541$ με

$\varepsilon_{bdi6} := \varepsilon_{bot\_beam}$

Max deflection at midspan:

$\Delta_{max} := -0.03969$ in Calculated using Mastan2

$\Delta_{twang6} := \Delta_{max}$

Deflected shape produced by Mastan2:

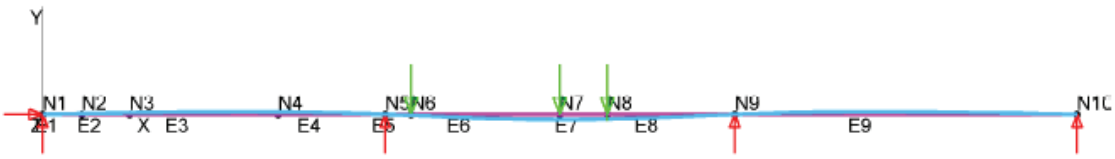

Moment diagram produced by Mastan2:

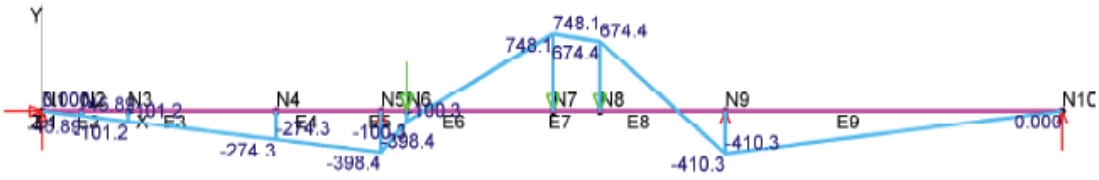

Stresses and Strains at Gauge Locations on Beam C:

Strains and stresses with truck at 0.4*L of first span:

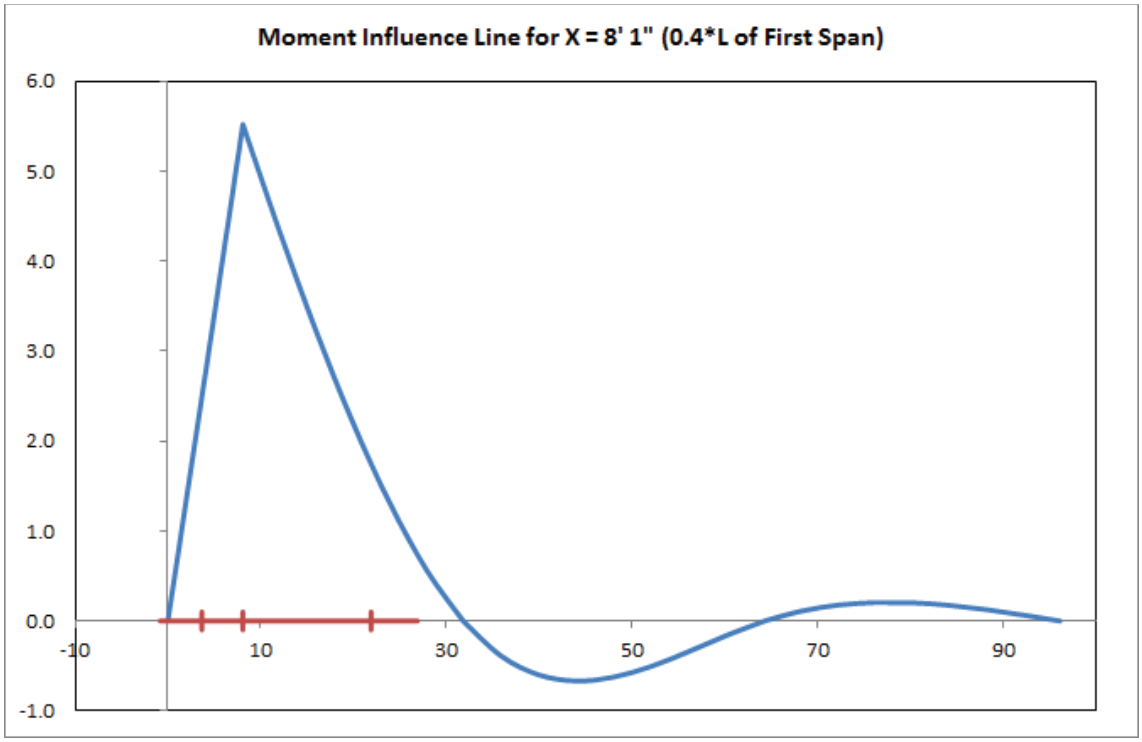

Influence line magnitudes at axel locations:

Truck 1: $truck1_{f\_axel} := 1.7617$ $truck1_{m\_axel} := 5.523$ $truck1_{b\_axel} := 2.493$

Total moment developed at the panel interface (divided into the three girders):

$$M_{total} := \frac{truck1_{f\_axel} \cdot f\_axel_{wt} + truck1_{m\_axel} \cdot m\_axel_{wt} + truck1_{b\_axel} \cdot b\_axel_{wt}}{1000} = 60.583$$

$M_{total} = 60.583$ kip·ft $M := M_{total} \cdot 12 = 726.994$ kip·in

Stresses and Strains at Gauge Locations on Beam C:

Predicted max stresses at midspan gauge loactions during moving tests:

Stress at top of the deck: $\sigma_{top\_deck} := \frac{M \cdot c_{top\_deck}}{I \cdot n} = -0.094$ ksi

Stress at top vwg in deck: $\sigma_{vwg\_top} := \frac{M \cdot c_{vwg\_top}}{I \cdot n} = -0.036$ ksi

Stress at middle vwg on beam: $\sigma_{vwg\_mid} := \frac{M \cdot c_{vwg\_mid}}{I} = 0.818$ ksi

Positive stress = tension
Negative stress = compression

Stress at bottom vwg on beam: $\sigma_{vwg\_bot} := \frac{M \cdot c_{vwg\_bot}}{I} = 1.923$ ksi

Stress at bottom of the beam: $\sigma_{bot\_beam} := \frac{M \cdot c_{bot\_beam}}{I} = 2.26$ ksi

Predicted max strains at midspan gauge locations during moving tests:

Strain at top of the deck: $\varepsilon_{top\_deck} := \frac{\sigma_{top\_deck}}{E_c} \cdot 10^6 = -14.883$ με

Strain at top vwg in deck: $\varepsilon_{vwg\_top} := \frac{\sigma_{vwg\_top}}{E_c} \cdot 10^6 = -5.7667$ με $\quad \varepsilon_{vwg6} := \varepsilon_{vwg\_top}$

Strain at middle vwg on beam: $\varepsilon_{vwg\_mid} := \frac{\sigma_{vwg\_mid}}{E_s} \cdot 10^6 = 28.204$ με $\quad \varepsilon_{vwg1} := \varepsilon_{vwg\_mid}$

Strain at bottom vwg on beam: $\varepsilon_{vwg\_bot} := \frac{\sigma_{vwg\_bot}}{E_s} \cdot 10^6 = 66.3267$ με $\quad \varepsilon_{vwg2} := \varepsilon_{vwg\_bot}$

Strain at bottom of the beam: $\varepsilon_{bot\_beam} := \frac{\sigma_{bot\_beam}}{E_s} \cdot 10^6 = 77.9376$ με $\quad \varepsilon_{bdi3} := \varepsilon_{bot\_beam}$

Max deflection at midspan:

$\Delta_{max} := -0.0331$ in Calculated using Mastan2 $\quad \Delta_{twang3} := \Delta_{max}$

Deflected shape produced by Mastan2:

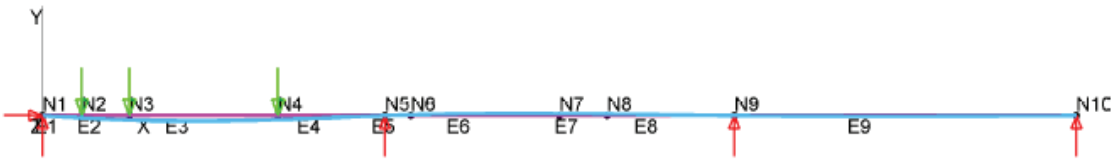

Moment diagram produced by Mastan2:

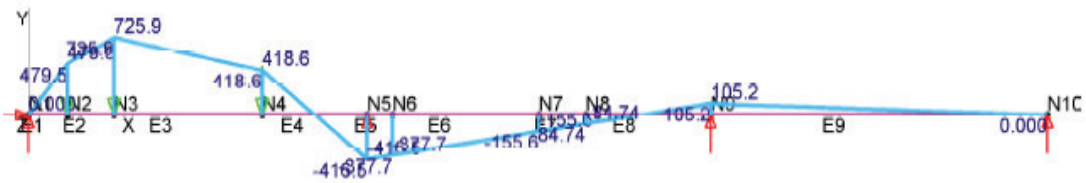

Stresses and Strains at Gauge Locations on Beam C:

Summary of Approximate Field Strains and Deflections:

Static Load Test:

At gauge location near pier:

LVDT #2:	$\Delta_{LVDT2} := 0$	in
BDI #8:	$\varepsilon_{bdi8} = 10.847$	με
VWG #8:	$\varepsilon_{vwg8} = 4.203$	με
VWG #3:	$\varepsilon_{vwg3} = -20.556$	με
VWG #4:	$\varepsilon_{vwg4} = -48.341$	με

Moving Load Tests:

At gauge location midspan:

BDI #6:	$\varepsilon_{bdi6} = 80.541$	με
Twanger #6:	$\Delta_{twang6} = -0.04$	in

At gauge location 0.4*L of first span:

VWG #6:	$\varepsilon_{vwg6} = -5.767$	με
VWG #1:	$\varepsilon_{vwg1} = 28.204$	με
VWG #2:	$\varepsilon_{vwg2} = 66.327$	με
BDI #3:	$\varepsilon_{bdi3} = 77.938$	με
Twanger #3:	$\Delta_{twang3} = -0.033$	in

Stresses and Strains at Gauge Locations on Beam A:

Composite section properties (considering barriers):

Moment of inertia of the composite section:	$I_{NA\_stc} = 6566.882$ in^4	$I := I_{NA\_stc}$
Distance to the centroid from the top of the steel section:	$d_{top\_of\_steel\_stc} = -4.234$ in	
Distance to the centroid from the bottom of the steel section:	$d_{bot\_of\_steel\_stc} = 22.734$ in	
Section modulus about the top of the steel:	$S_{top\_of\_steel\_stc} = -1550.872$ in^3	
Section modulus about the bottom of the steel:	$S_{bot\_of\_steel\_stc} = 288.853$ in^3	

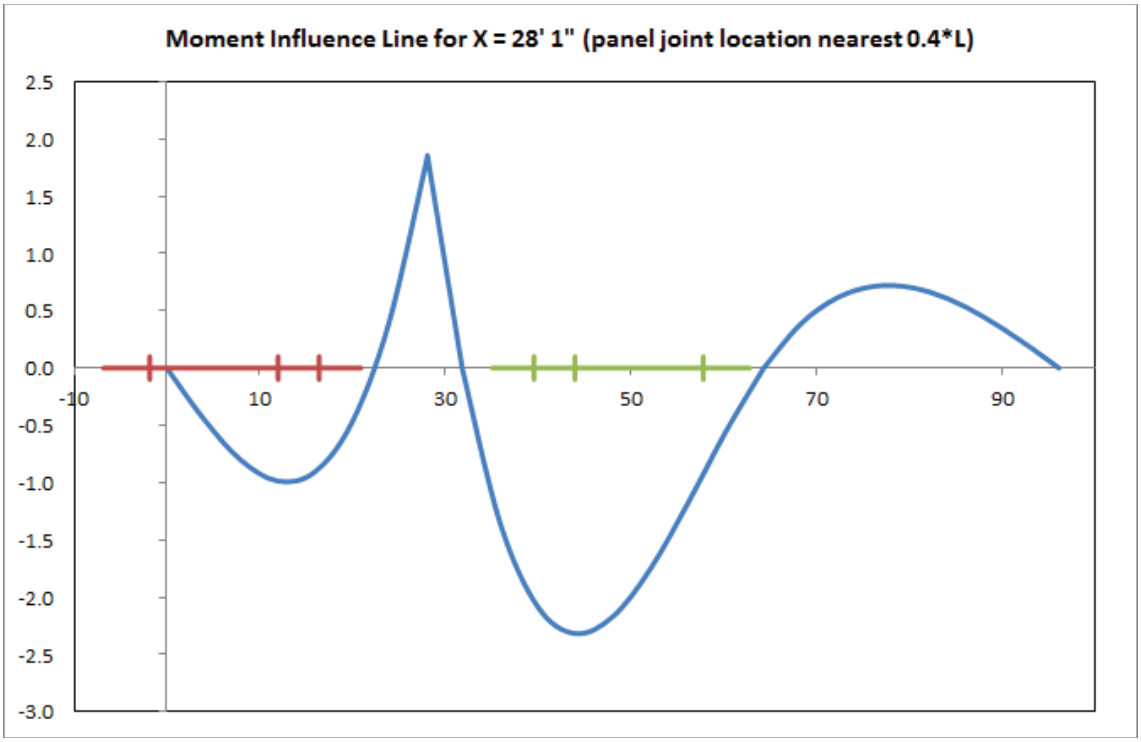

Note: the red and green lines represent the two dump trucks and the locations of their respective axels

Distribution factor: $distbf := \frac{1}{5}$ *Assuming that the load distributes evenly into the 3 beams and 2 barriers

Front axel weight: $f\_axel_{wt} := 15500 \cdot distbf = 3100$ lbs

Middle axel weight: $m\_axel_{wt} := 19500 \cdot distbf = 3900$ lbs

Back axel weight: $b\_axel_{wt} := 18750 \cdot distbf = 3750$ lbs

Influence line magnitudes at axel locations:

Truck 1:	$truck1_{f\_axel} := 0$	$truck1_{m\_axel} := -0.9855$	$truck1_{b\_axel} := -0.8547$
Truck 2:	$truck2_{f\_axel} := -0.9236$	$truck2_{m\_axel} := -2.3165$	$truck2_{b\_axel} := -2.0125$

Stresses and Strains at Gauge Locations on Beam A:

Total moment developed at the panel interface (divided into the three girders):

$$M_{total} := \frac{truck1_{f\_axel} \cdot f\_axel_{wt} + truck1_{m\_axel} \cdot m\_axel_{wt} + truck1_{b\_axel} \cdot b\_axel_{wt} \cdots}{+ truck2_{f\_axel} \cdot f\_axel_{wt} + truck2_{m\_axel} \cdot m\_axel_{wt} + truck2_{b\_axel} \cdot b\_axel_{wt}} = -26.493$$

$$1000$$

$M_{total} = -26.493 \quad kip \cdot ft \qquad M := M_{total} \cdot 12 = -317.916 \quad kip \cdot in$

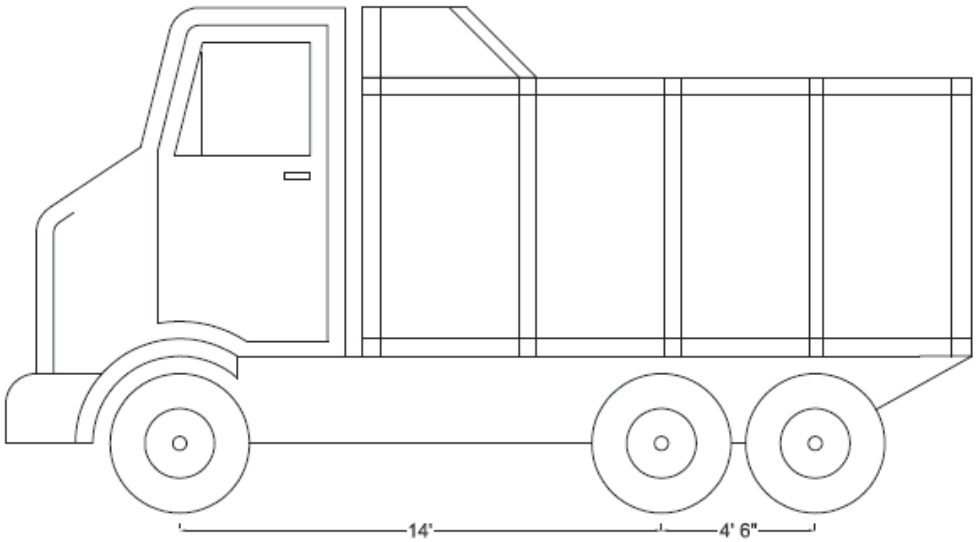

Total area (converted into steel) of the composite beam and slab system: $A_{tot} := A_{sum} = 158.918 \quad in^2$

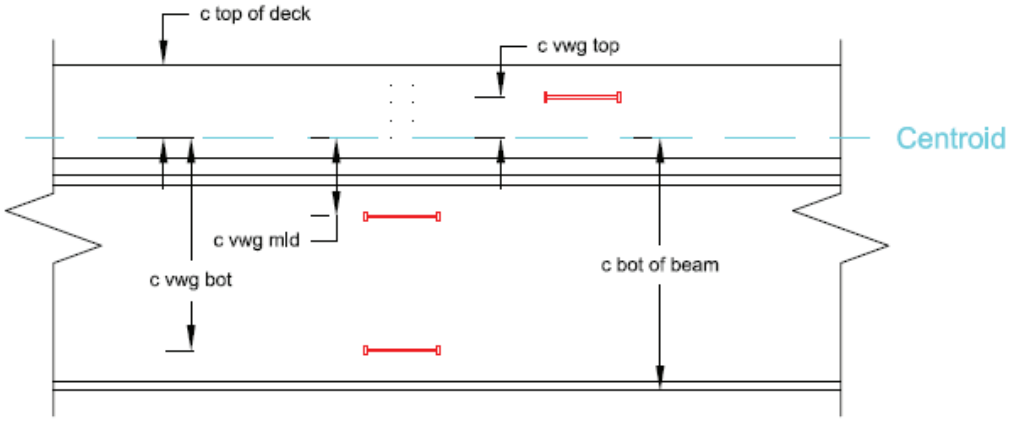

Stresses and Strains at Gauge Locations on Beam A:

Distances from centroid of composite section to gauge locations:

$c_{top\_deck} := -\left(H + 8 + d_{top\_of\_steel\_stc}\right) = -5.266$ in

$c_{bot\_beam} := d_{bot\_of\_steel\_stc} = 22.734$ in

$c_{vwg\_top} := -\left(-c_{top\_deck} - 2.75\right) = -2.516$ in

$c_{vwg\_mid} := 2.6875 - d_{top\_of\_steel\_stc} + 0.81 = 7.732$ in

$c_{vwg\_bot} := 2.6875 + 0.81 + 11.5 - d_{top\_of\_steel\_stc} = 19.232$ in

Modulus of elasticity:

$E_s := 29000$ ksi $\quad E_c := 6287$ ksi $\quad n := \frac{E_s}{E_c} = 4.613$

Predicted stresses at gauge loactions during static load test:

Stress at top of the deck: $\sigma_{top\_deck} := \frac{M \cdot c_{top\_deck}}{I \cdot n} = 0.055$ ksi

Stress at top vwg in deck: $\sigma_{vwg\_top} := \frac{M \cdot c_{vwg\_top}}{I \cdot n} = 0.026$ ksi

Stress at middle vwg on beam: $\sigma_{vwg\_mid} := \frac{M \cdot c_{vwg\_mid}}{I} = -0.374$ ksi

Positive stress = tension
Negative stress = compression

Stress at bottom vwg on beam: $\sigma_{vwg\_bot} := \frac{M \cdot c_{vwg\_bot}}{I} = -0.931$ ksi

Stress at bottom of the beam: $\sigma_{bot\_beam} := \frac{M \cdot c_{bot\_beam}}{I} = -1.101$ ksi

Predicted strains at gauge locations during static load test:

Strain at top of the deck: $\varepsilon_{top\_deck} := \frac{\sigma_{top\_deck}}{E_c} \cdot 10^6 = 8.7904$ με $\quad \varepsilon_{bdi7} := \varepsilon_{top\_deck}$

Strain at top vwg in deck: $\varepsilon_{vwg\_top} := \frac{\sigma_{vwg\_top}}{E_c} \cdot 10^6 = 4.1996$ με $\quad \varepsilon_{vwg7} := \varepsilon_{vwg\_top}$

Strain at middle vwg on beam: $\varepsilon_{vwg\_mid} := \frac{\sigma_{vwg\_mid}}{E_s} \cdot 10^6 = -12.9073$ με

Strain at bottom vwg on beam: $\varepsilon_{vwg\_bot} := \frac{\sigma_{vwg\_bot}}{E_s} \cdot 10^6 = -32.1052$ με

Strain at bottom of the beam: $\varepsilon_{bot\_beam} := \frac{\sigma_{bot\_beam}}{E_s} \cdot 10^6 = -37.9521$ με

Stresses and Strains at Gauge Locations on Beam A:

Strains and stresses with truck at midspan:

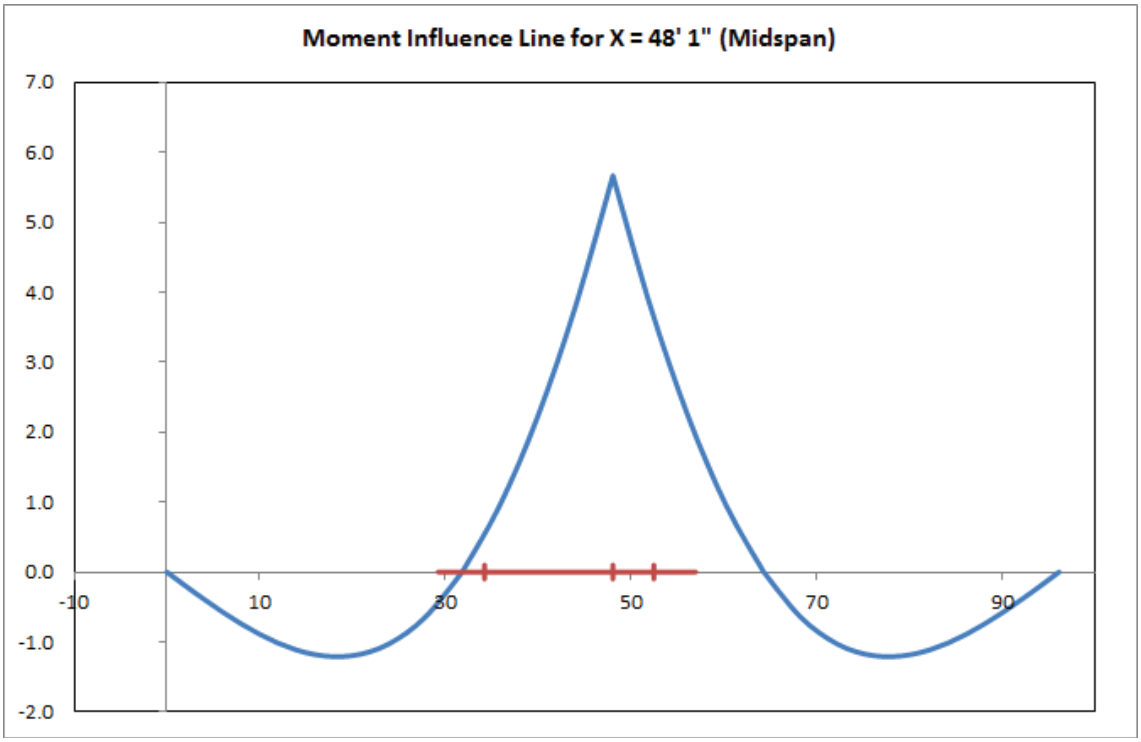

Influence line magnitudes at axel locations:

Truck 1: $truck1_{f\_axel} := 0.569$ $truck1_{m\_axel} := 5.667$ $truck1_{b\_axel} := 3.653$

Total moment developed at the panel interface (divided into the three girders):

$$M_{total} := \frac{truck1_{f\_axel} \cdot f\_axel_{wt} + truck1_{m\_axel} \cdot m\_axel_{wt} + truck1_{b\_axel} \cdot b\_axel_{wt}}{1000} = 37.564$$

$M_{total} = 37.564$ kip·ft $M := M_{total} \cdot 12 = 450.767$ kip·in

Stresses and Strains at Gauge Locations on Beam A:

Predicted max stresses at midspan gauge loactions during moving tests:

Stress at bottom of the beam: $\sigma_{bot\_beam} := \frac{M \cdot c_{bot\_beam}}{I} = 1.561$ ksi

Positive stress = tension
Negative stress = compression

Predicted max strains at midspan gauge locations during moving tests:

Strain at bottom of the beam: $\varepsilon_{bot\_beam} := \frac{\sigma_{bot\_beam}}{E_s} \cdot 10^6 = 53.8118$ με

$\varepsilon_{bdi4} := \varepsilon_{bot\_beam}$

Max deflection at midspan:

$\Delta_{max} := -0.02742$ in Calculated using Mastan2

$\Delta_{twang4} := \Delta_{max}$

Deflected shape produced by Mastan2:

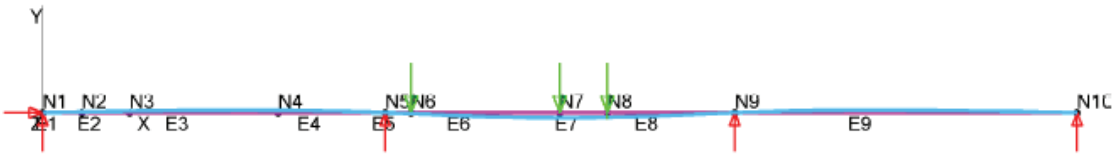

Moment diagram produced by Mastan2:

Stresses and Strains at Gauge Locations on Beam A:

Strains and stresses with truck at 0.4*L of first span:

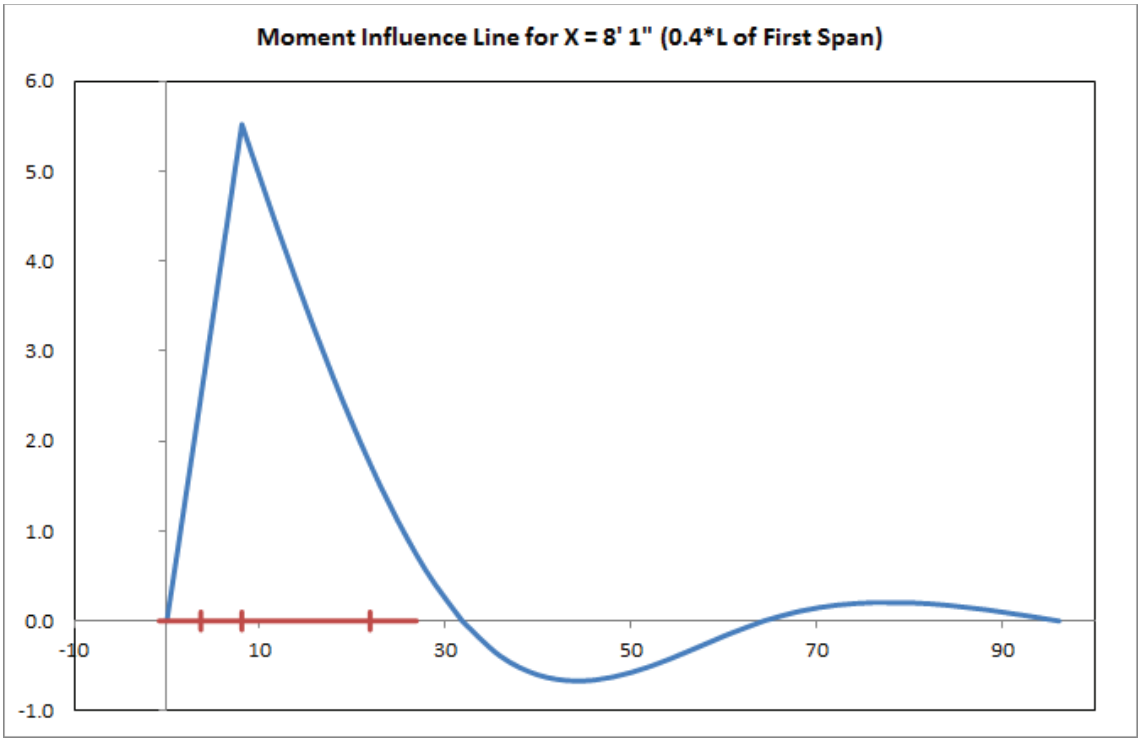

Influence line magnitudes at axel locations:

Truck 1: $truck1_{f\_axel} := 1.7617$ $truck1_{m\_axel} := 5.523$ $truck1_{b\_axel} := 2.493$

Total moment developed at the panel interface (divided into the three girders):

$$M_{total} := \frac{truck1_{f\_axel} \cdot f\_axel_{wt} + truck1_{m\_axel} \cdot m\_axel_{wt} + truck1_{b\_axel} \cdot b\_axel_{wt}}{1000} = 36.35$$

$M_{total} = 36.35$ kip·ft $M := M_{total} \cdot 12 = 436.197$ kip·in

Stresses and Strains at Gauge Locations on Beam A:

Predicted max stresses at midspan gauge loactions during moving tests:

Stress at top of the deck: $\sigma_{top\_deck} := \frac{M \cdot c_{top\_deck}}{I \cdot n} = -0.076$ ksi

Stress at top vwg in deck: $\sigma_{vwg\_top} := \frac{M \cdot c_{vwg\_top}}{I \cdot n} = -0.036$ ksi

Stress at middle vwg on beam: $\sigma_{vwg\_mid} := \frac{M \cdot c_{vwg\_mid}}{I} = 0.514$ ksi

Positive stress = tension
Negative stress = compression

Stress at bottom vwg on beam: $\sigma_{vwg\_bot} := \frac{M \cdot c_{vwg\_bot}}{I} = 1.277$ ksi

Stress at bottom of the beam: $\sigma_{bot\_beam} := \frac{M \cdot c_{bot\_beam}}{I} = 1.51$ ksi

Predicted max strains at midspan gauge locations during moving tests:

Strain at top of the deck: $\varepsilon_{top\_deck} := \frac{\sigma_{top\_deck}}{E_c} \cdot 10^6 = -12.0609$ με

Strain at top vwg in deck: $\varepsilon_{vwg\_top} := \frac{\sigma_{vwg\_top}}{E_c} \cdot 10^6 = -5.7621$ με $\quad \varepsilon_{vwg5} := \varepsilon_{vwg\_top}$

Strain at middle vwg on beam: $\varepsilon_{vwg\_mid} := \frac{\sigma_{vwg\_mid}}{E_s} \cdot 10^6 = 17.7095$ με

Strain at bottom vwg on beam: $\varepsilon_{vwg\_bot} := \frac{\sigma_{vwg\_bot}}{E_s} \cdot 10^6 = 44.0499$ με

Strain at bottom of the beam: $\varepsilon_{bot\_beam} := \frac{\sigma_{bot\_beam}}{E_s} \cdot 10^6 = 52.0723$ με $\quad \varepsilon_{bdi1} := \varepsilon_{bot\_beam}$

Max deflection at midspan:

$\Delta_{max} := -0.02287$ in Calculated using Mastan2 $\quad \Delta_{twang1} := \Delta_{max}$

Deflected shape produced by Mastan2:

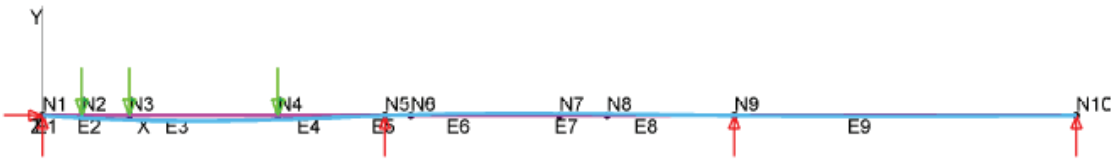

Moment diagram produced by Mastan2:

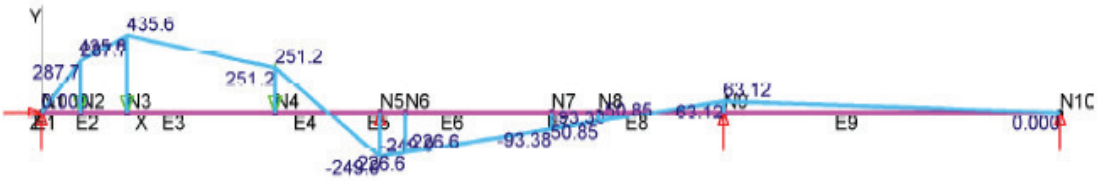

Stresses and Strains at Gauge Locations on Beam A:

Summary of Approximate Field Strains and Deflections:

Static Load Test:

At gauge location near pier:

LVDT #1:	$\Delta_{LVDT1} := 0$	in
BDI #7:	$\varepsilon_{bdi7} = 8.79$	με
VWG #7:	$\varepsilon_{vwg7} = 4.2$	με

Moving Load Tests:

At gauge location midspan:

BDI #4:	$\varepsilon_{bdi4} = 53.812$	με
Twanger #4:	$\Delta_{twang4} = -0.027$	in

At gauge location 0.4*L of first span:

VWG #5:	$\varepsilon_{vwg5} = -5.762$	με
BDI #1:	$\varepsilon_{bdi1} = 52.072$	με
Twanger #1:	$\Delta_{twang1} = -0.023$	in

Stresses and Strains at Gauge Locations on Beam B:

Composite section properties (considering barriers):

Moment of inertia of the composite section: $I_{NA\_stc} = 7140.344$ in^4 $I := I_{NA\_stc}$

Distance to the centroid from the top of the steel section: $d_{top\_of\_steel\_stc} = -4.707$ in

Distance to the centroid from the bottom of the steel section: $d_{bot\_of\_steel\_stc} = 23.207$ in

Section modulus about the top of the steel: $S_{top\_of\_steel\_stc} = -1516.803$ in^3

Section modulus about the bottom of the steel: $S_{bot\_of\_steel\_stc} = 307.674$ in^3

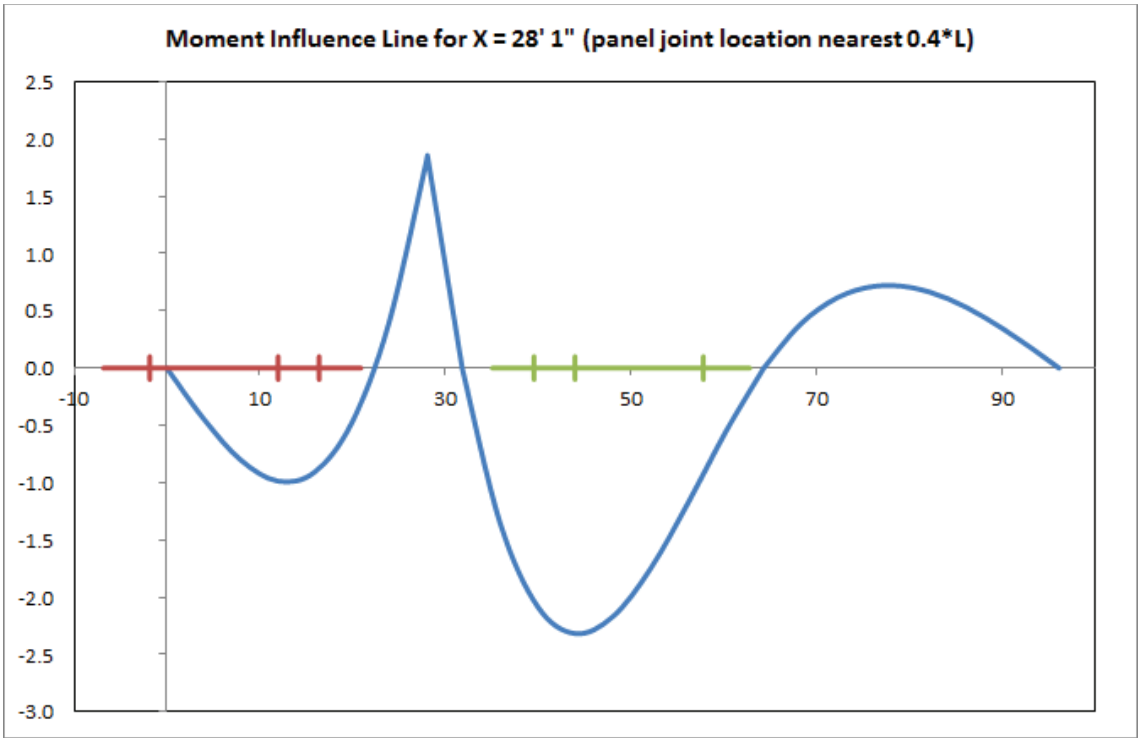

Note: the red and green lines represent the two dump trucks and the locations of their respective axels

Distribution factor: $distbf := \frac{1}{5}$ *Assuming that the load distributes evenly into the 3 beams and 2 barriers

Front axel weight: $f\_axel_{wt} := 15500 \cdot distbf = 3100$ lbs

Middle axel weight: $m\_axel_{wt} := 19500 \cdot distbf = 3900$ lbs

Back axel weight: $b\_axel_{wt} := 18750 \cdot distbf = 3750$ lbs

Influence line magnitudes at axel locations:

Truck 1: $truck1_{f\_axel} := 0$ $truck1_{m\_axel} := -0.9855$ $truck1_{b\_axel} := -0.8547$

Truck 2: $truck2_{f\_axel} := -0.9236$ $truck2_{m\_axel} := -2.3165$ $truck2_{b\_axel} := -2.0125$

Stresses and Strains at Gauge Locations on Beam B:

Total moment developed at the panel interface (divided into the three girders):

$$M_{total} := \frac{truck1_{f\_axel} \cdot f\_axel_{wt} + truck1_{m\_axel} \cdot m\_axel_{wt} + truck1_{b\_axel} \cdot b\_axel_{wt} \cdots}{+ truck2_{f\_axel} \cdot f\_axel_{wt} + truck2_{m\_axel} \cdot m\_axel_{wt} + truck2_{b\_axel} \cdot b\_axel_{wt}} = -26.493$$

$$1000$$

$M_{total} = -26.493 \quad kip \cdot ft \qquad M := M_{total} \cdot 12 = -317.916 \quad kip \cdot in$

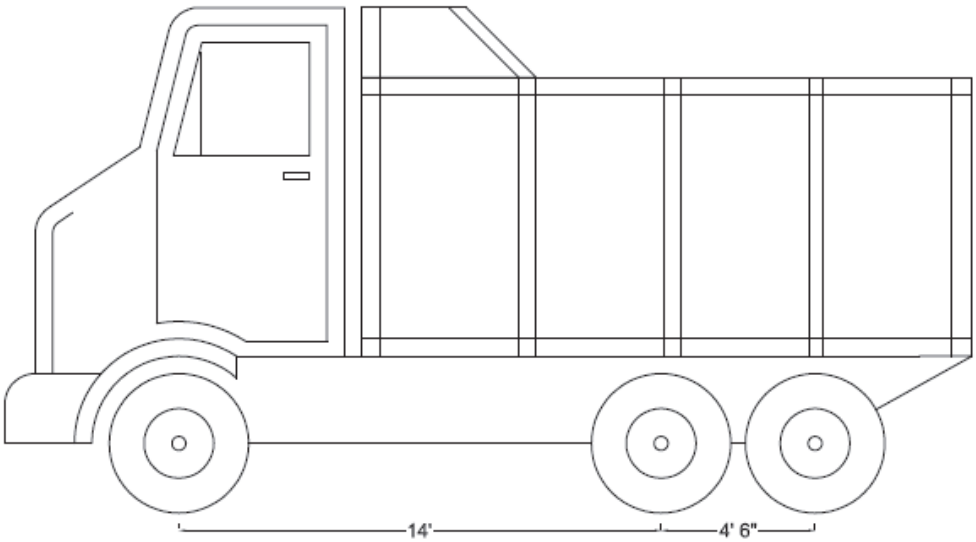

Total area (converted into steel) of the composite beam and slab system: $A_{tot} := A_{sum} = 155.05 \quad in^2$

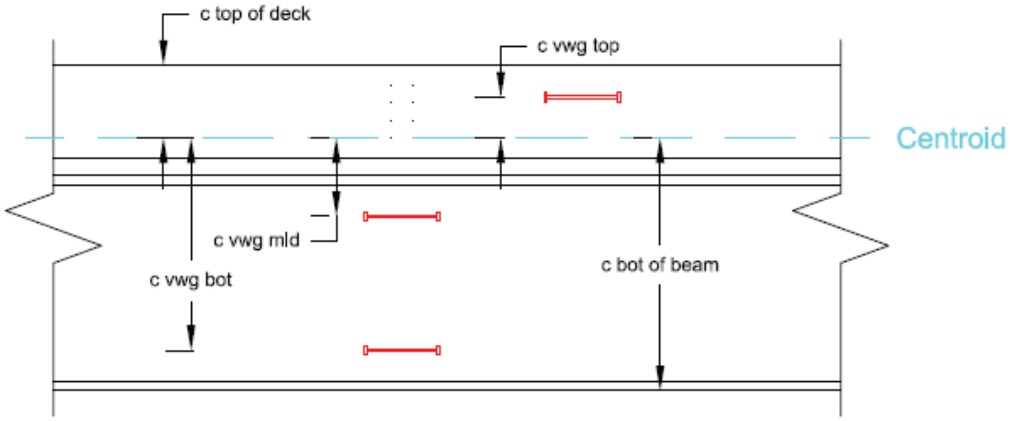

Stresses and Strains at Gauge Locations on Beam B:

Distances from centroid of composite section to gauge locations:

$c_{top\_deck} := -\left(H + 8 + d_{top\_of\_steel\_stc}\right) = -4.793$ in

$c_{bot\_beam} := d_{bot\_of\_steel\_stc} = 23.207$ in

$c_{vwg\_top} := -\left(-c_{top\_deck} - 2.75\right) = -2.043$ in

$c_{vwg\_mid} := 2.6875 - d_{top\_of\_steel\_stc} + 0.81 = 8.205$ in

$c_{vwg\_bot} := 2.6875 + 0.81 + 11.5 - d_{top\_of\_steel\_stc} = 19.705$ in

Modulus of elasticity:

$E_s := 29000$ ksi $\quad E_c := 6287$ ksi $\quad n := \frac{E_s}{E_c} = 4.613$

Predicted stresses at gauge loactions during static load test:

Stress at top of the deck: $\sigma_{top\_deck} := \frac{M \cdot c_{top\_deck}}{I \cdot n} = 0.046$ ksi

Stress at top vwg in deck: $\sigma_{vwg\_top} := \frac{M \cdot c_{vwg\_top}}{I \cdot n} = 0.02$ ksi

Stress at middle vwg on beam: $\sigma_{vwg\_mid} := \frac{M \cdot c_{vwg\_mid}}{I} = -0.365$ ksi

Positive stress = tension
Negative stress = compression

Stress at bottom vwg on beam: $\sigma_{vwg\_bot} := \frac{M \cdot c_{vwg\_bot}}{I} = -0.877$ ksi

Stress at bottom of the beam: $\sigma_{bot\_beam} := \frac{M \cdot c_{bot\_beam}}{I} = -1.033$ ksi

Predicted strains at gauge locations during static load test:

Strain at top of the deck: $\varepsilon_{top\_deck} := \frac{\sigma_{top\_deck}}{E_c} \cdot 10^6 = 7.358$ με

Strain at top vwg in deck: $\varepsilon_{vwg\_top} := \frac{\sigma_{vwg\_top}}{E_c} \cdot 10^6 = 3.1359$ με

Strain at middle vwg on beam: $\varepsilon_{vwg\_mid} := \frac{\sigma_{vwg\_mid}}{E_s} \cdot 10^6 = -12.5972$ με

Strain at bottom vwg on beam: $\varepsilon_{vwg\_bot} := \frac{\sigma_{vwg\_bot}}{E_s} \cdot 10^6 = -30.2532$ με

Strain at bottom of the beam: $\varepsilon_{bot\_beam} := \frac{\sigma_{bot\_beam}}{E_s} \cdot 10^6 = -35.6306$ με

Stresses and Strains at Gauge Locations on Beam B:

Strains and stresses with truck at midspan:

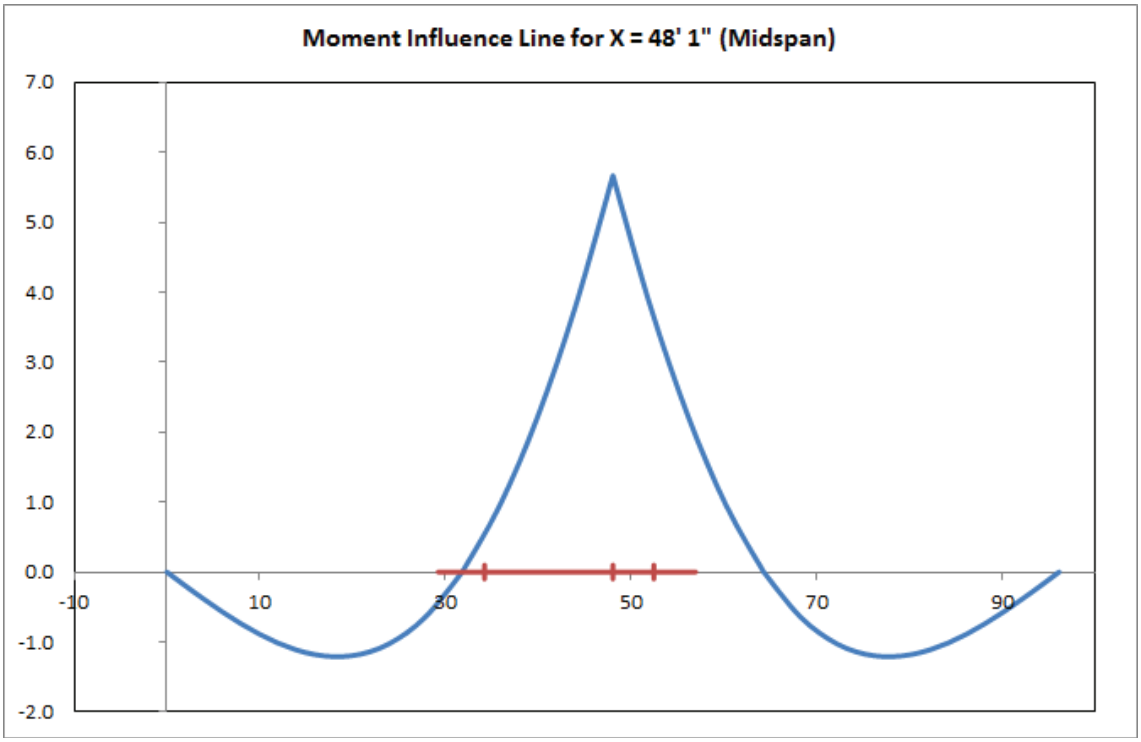

Influence line magnitudes at axel locations:

Truck 1: $truck1_{f\_axel} := 0.569$ $truck1_{m\_axel} := 5.667$ $truck1_{b\_axel} := 3.653$

Total moment developed at the panel interface (divided into the three girders):

$$M_{total} := \frac{truck1_{f\_axel} \cdot f\_axel_{wt} + truck1_{m\_axel} \cdot m\_axel_{wt} + truck1_{b\_axel} \cdot b\_axel_{wt}}{1000} = 37.564$$

$M_{total} = 37.564$ kip·ft $M := M_{total} \cdot 12 = 450.767$ kip·in

Stresses and Strains at Gauge Locations on Beam B:

Predicted max stresses at midspan gauge loactions during moving tests:

Stress at bottom of the beam: $\sigma_{bot\_beam} := \frac{M \cdot c_{bot\_beam}}{I} = 1.465$ ksi

Positive stress = tension
Negative stress = compression

Predicted max strains at midspan gauge locations during moving tests:

Strain at bottom of the beam: $\varepsilon_{bot\_beam} := \frac{\sigma_{bot\_beam}}{E_s} \cdot 10^6 = 50.52$ με

$\varepsilon_{bdi5} := \varepsilon_{bot\_beam}$

Max deflection at midspan:

$\Delta_{max} := -0.02522$ in Calculated using Mastan2

$\Delta_{twang5} := \Delta_{max}$

Deflected shape produced by Mastan2:

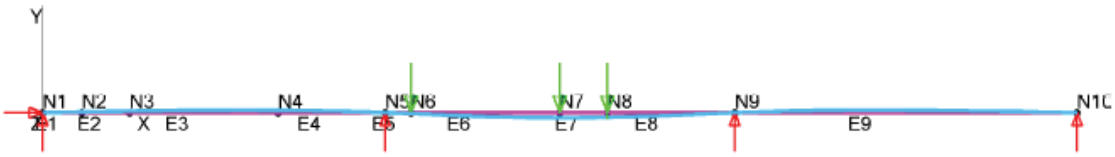

Moment diagram produced by Mastan2:

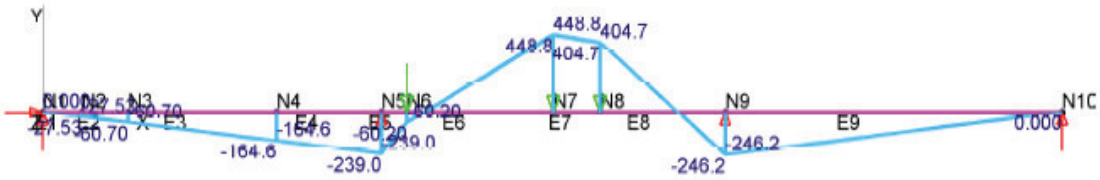

Stresses and Strains at Gauge Locations on Beam B:

Strains and stresses with truck at 0.4*L of first span:

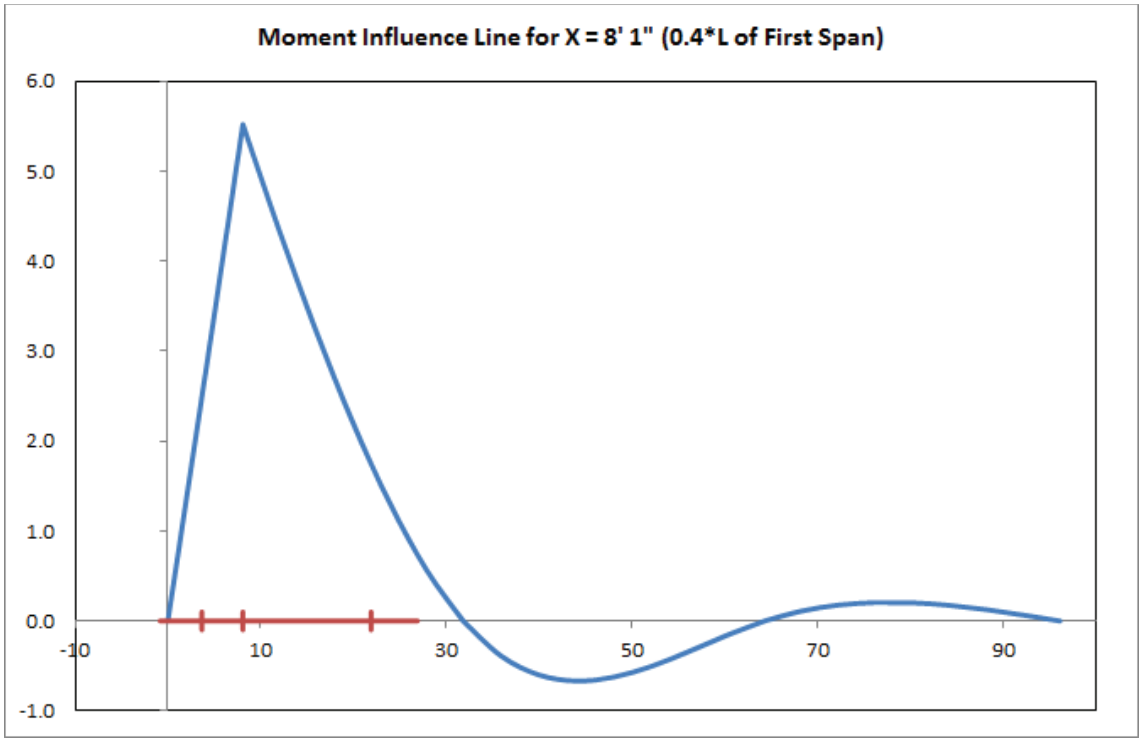

Influence line magnitudes at axel locations:

Truck 1: $truck1_{f\_axel} := 1.7617$ $truck1_{m\_axel} := 5.523$ $truck1_{b\_axel} := 2.493$

Total moment developed at the panel interface (divided into the three girders):

$$M_{total} := \frac{truck1_{f\_axel} \cdot f\_axel_{wt} + truck1_{m\_axel} \cdot m\_axel_{wt} + truck1_{b\_axel} \cdot b\_axel_{wt}}{1000} = 36.35$$

$M_{total} = 36.35$ kip·ft $M := M_{total} \cdot 12 = 436.197$ kip·in

Stresses and Strains at Gauge Locations on Beam B:

Predicted max stresses at midspan gauge loactions during moving tests:

Stress at top of the deck: $\sigma_{top\_deck} := \frac{M \cdot c_{top\_deck}}{I \cdot n} = -0.063$ ksi

Stress at top vwg in deck: $\sigma_{vwg\_top} := \frac{M \cdot c_{vwg\_top}}{I \cdot n} = -0.027$ ksi

Stress at middle vwg on beam: $\sigma_{vwg\_mid} := \frac{M \cdot c_{vwg\_mid}}{I} = 0.501$ ksi

Positive stress = tension
Negative stress = compression

Stress at bottom vwg on beam: $\sigma_{vwg\_bot} := \frac{M \cdot c_{vwg\_bot}}{I} = 1.204$ ksi

Stress at bottom of the beam: $\sigma_{bot\_beam} := \frac{M \cdot c_{bot\_beam}}{I} = 1.418$ ksi

Predicted max strains at midspan gauge locations during moving tests:

Strain at top of the deck: $\varepsilon_{top\_deck} := \frac{\sigma_{top\_deck}}{E_c} \cdot 10^6 = -10.0955$ με

Strain at top vwg in deck: $\varepsilon_{vwg\_top} := \frac{\sigma_{vwg\_top}}{E_c} \cdot 10^6 = -4.3026$ με

Strain at middle vwg on beam: $\varepsilon_{vwg\_mid} := \frac{\sigma_{vwg\_mid}}{E_s} \cdot 10^6 = 17.284$ με

Strain at bottom vwg on beam: $\varepsilon_{vwg\_bot} := \frac{\sigma_{vwg\_bot}}{E_s} \cdot 10^6 = 41.5089$ με

Strain at bottom of the beam: $\varepsilon_{bot\_beam} := \frac{\sigma_{bot\_beam}}{E_s} \cdot 10^6 = 48.887$ με

$\varepsilon_{bdi2} := \varepsilon_{bot\_beam}$

Max deflection at midspan:

$\Delta_{max} := -0.02103$ in Calculated using Mastan2

$\Delta_{twang2} := \Delta_{max}$

Deflected shape produced by Mastan2:

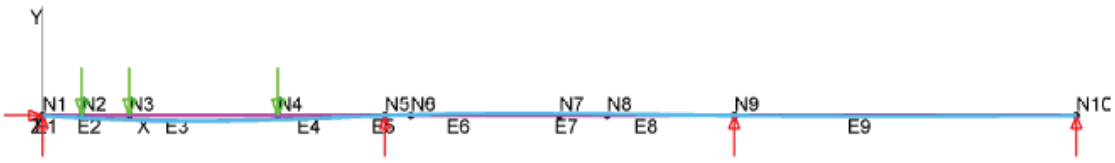

Moment diagram produced by Mastan2:

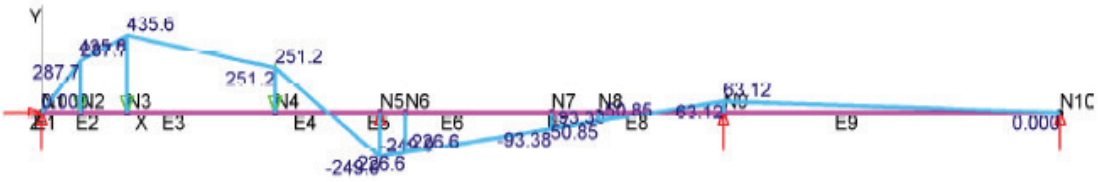

Stresses and Strains at Gauge Locations on Beam B:

Summary of Approximate Field Strains and Deflections:

Moving Load Tests:

At gauge location midspan:

BDI #5:	$\varepsilon_{bdi5} = 50.52$	με
Twanger #5:	$\Delta_{twang5} = -0.025$	in

At gauge location 0.4*L of first span:

BDI #2:	$\varepsilon_{bdi2} = 48.887$	με
Twanger #2:	$\Delta_{twang2} = -0.021$	in

Stresses and Strains at Gauge Locations on Beam C:

Composite section properties (considering barriers):

Moment of inertia of the composite section: $I_{NA\_stc} = 7562.179$ in^4 $I := I_{NA\_stc}$

Distance to the centroid from the top of the steel section: $d_{top\_of\_steel\_stc} = -5.01$ in

Distance to the centroid from the bottom of the steel section: $d_{bot\_of\_steel\_stc} = 23.51$ in

Section modulus about the top of the steel: $S_{top\_of\_steel\_stc} = -1509.283$ in^3

Section modulus about the bottom of the steel: $S_{bot\_of\_steel\_stc} = 321.652$ in^3

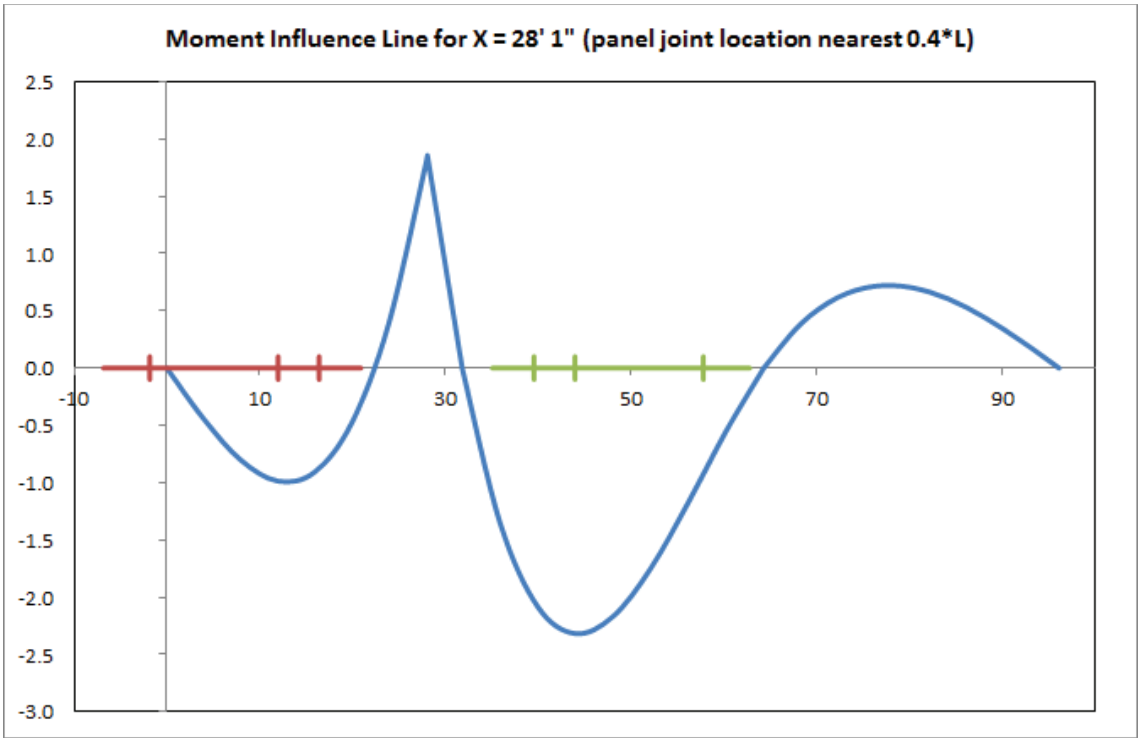

Note: the red and green lines represent the two dump trucks and the locations of their respective axels

Distribution factor: $distbf := \frac{1}{5}$ *Assuming that the load distributes evenly into the 3 beams and 2 barriers

Front axel weight: $f\_axel_{wt} := 15500 \cdot distbf = 3100$ lbs

Middle axel weight: $m\_axel_{wt} := 19500 \cdot distbf = 3900$ lbs

Back axel weight: $b\_axel_{wt} := 18750 \cdot distbf = 3750$ lbs

Influence line magnitudes at axel locations:

Truck 1: $truck1_{f\_axel} := 0$ $truck1_{m\_axel} := -0.9855$ $truck1_{b\_axel} := -0.8547$

Truck 2: $truck2_{f\_axel} := -0.9236$ $truck2_{m\_axel} := -2.3165$ $truck2_{b\_axel} := -2.0125$

Stresses and Strains at Gauge Locations on Beam C:

Total moment developed at the panel interface (divided into the three girders):

$$M_{total} := \frac{truck1_{f\_axel} \cdot f\_axel_{wt} + truck1_{m\_axel} \cdot m\_axel_{wt} + truck1_{b\_axel} \cdot b\_axel_{wt} \cdots}{+ truck2_{f\_axel} \cdot f\_axel_{wt} + truck2_{m\_axel} \cdot m\_axel_{wt} + truck2_{b\_axel} \cdot b\_axel_{wt}} = -26.493$$

$$1000$$

$M_{total} = -26.493 \quad kip \cdot ft \qquad M := M_{total} \cdot 12 = -317.916 \quad kip \cdot in$

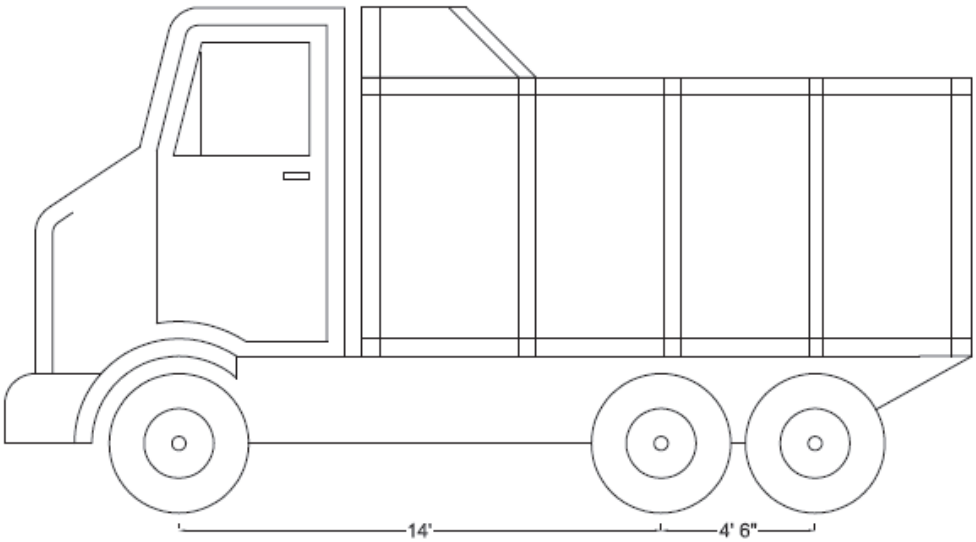

Total area (converted into steel) of the composite beam and slab system: $A_{tot} := A_{sum} = 141.398 \quad in^2$

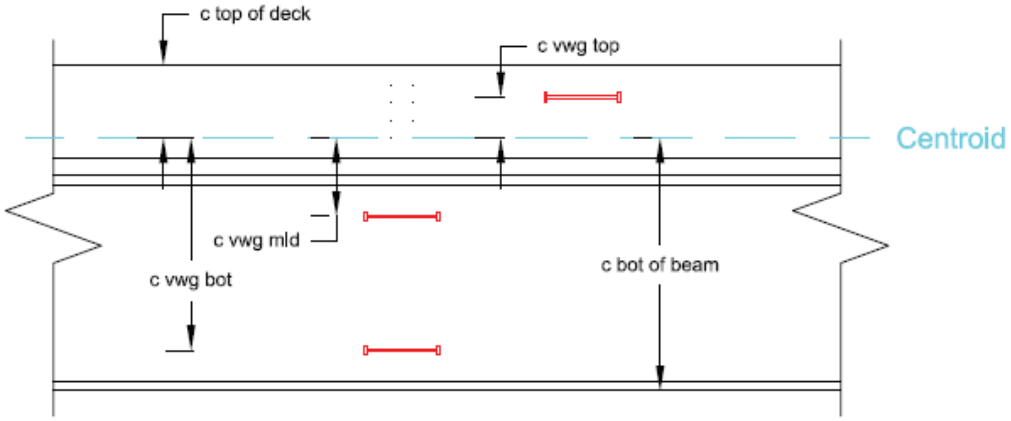

Stresses and Strains at Gauge Locations on Beam C:

Distances from centroid of composite section to gauge locations:

$c_{top\_deck} := -\left(H + 8 + d_{top\_of\_steel\_stc}\right) = -4.49$ in

$c_{bot\_beam} := d_{bot\_of\_steel\_stc} = 23.51$ in

$c_{vwg\_top} := -\left(-c_{top\_deck} - 2.75\right) = -1.74$ in

$c_{vwg\_mid} := 2.6875 - d_{top\_of\_steel\_stc} + 0.81 = 8.508$ in

$c_{vwg\_bot} := 2.6875 + 0.81 + 11.5 - d_{top\_of\_steel\_stc} = 20.008$ in

Modulus of elasticity:

$E_s := 29000$ ksi $\quad E_c := 6287$ ksi $\quad n := \frac{E_s}{E_c} = 4.613$

Predicted stresses at gauge loactions during static load test:

Stress at top of the deck: $\sigma_{top\_deck} := \frac{M \cdot c_{top\_deck}}{I \cdot n} = 0.041$ ksi

Stress at top vwg in deck: $\sigma_{vwg\_top} := \frac{M \cdot c_{vwg\_top}}{I \cdot n} = 0.016$ ksi

Stress at middle vwg on beam: $\sigma_{vwg\_mid} := \frac{M \cdot c_{vwg\_mid}}{I} = -0.358$ ksi

Positive stress = tension
Negative stress = compression

Stress at bottom vwg on beam: $\sigma_{vwg\_bot} := \frac{M \cdot c_{vwg\_bot}}{I} = -0.841$ ksi

Stress at bottom of the beam: $\sigma_{bot\_beam} := \frac{M \cdot c_{bot\_beam}}{I} = -0.988$ ksi

Predicted strains at gauge locations during static load test:

Strain at top of the deck: $\varepsilon_{top\_deck} := \frac{\sigma_{top\_deck}}{E_c} \cdot 10^6 = 6.5083$ με $\quad \varepsilon_{bdi8} := \varepsilon_{top\_deck}$

Strain at top vwg in deck: $\varepsilon_{vwg\_top} := \frac{\sigma_{vwg\_top}}{E_c} \cdot 10^6 = 2.5218$ με $\quad \varepsilon_{vwg8} := \varepsilon_{vwg\_top}$

Strain at middle vwg on beam: $\varepsilon_{vwg\_mid} := \frac{\sigma_{vwg\_mid}}{E_s} \cdot 10^6 = -12.3336$ με $\quad \varepsilon_{vwg3} := \varepsilon_{vwg\_mid}$

Strain at bottom vwg on beam: $\varepsilon_{vwg\_bot} := \frac{\sigma_{vwg\_bot}}{E_s} \cdot 10^6 = -29.0048$ με $\quad \varepsilon_{vwg4} := \varepsilon_{vwg\_bot}$

Strain at bottom of the beam: $\varepsilon_{bot\_beam} := \frac{\sigma_{bot\_beam}}{E_s} \cdot 10^6 = -34.0822$ με

Stresses and Strains at Gauge Locations on Beam C:

Strains and stresses with truck at midspan:

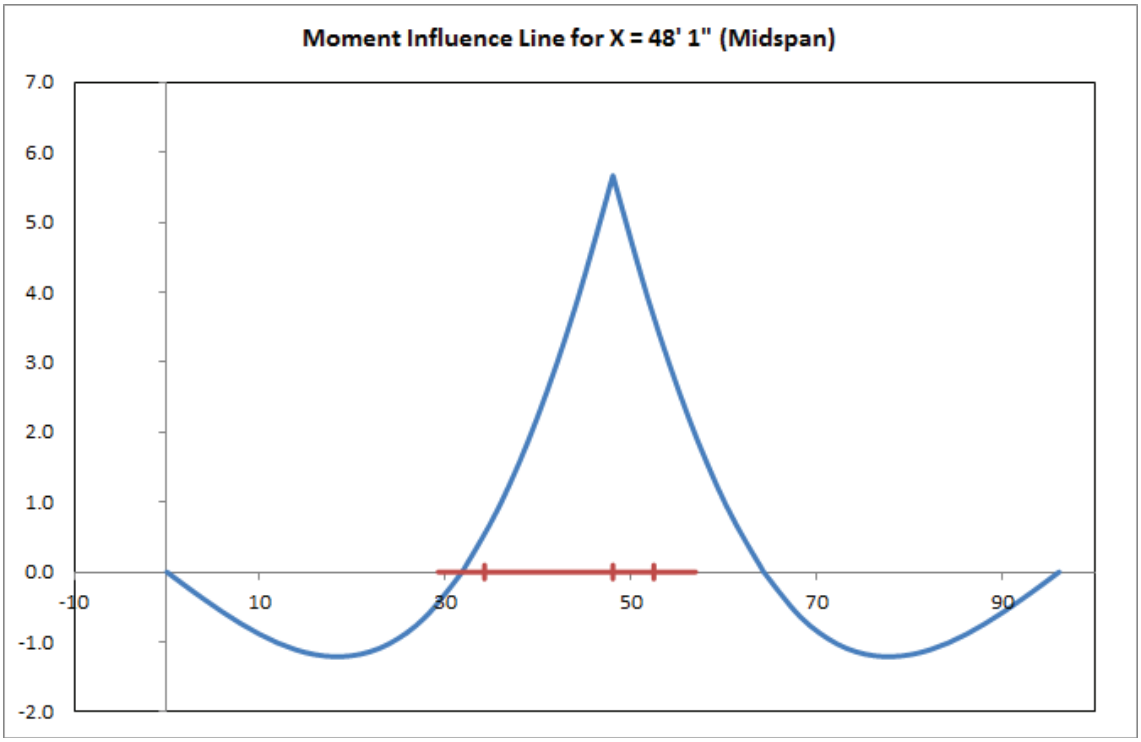

Influence line magnitudes at axel locations:

Truck 1: $truck1_{f\_axel} := 0.569$ $truck1_{m\_axel} := 5.667$ $truck1_{b\_axel} := 3.653$

Total moment developed at the panel interface (divided into the three girders):

$$M_{total} := \frac{truck1_{f\_axel} \cdot f\_axel_{wt} + truck1_{m\_axel} \cdot m\_axel_{wt} + truck1_{b\_axel} \cdot b\_axel_{wt}}{1000} = 37.564$$

$M_{total} = 37.564$ kip·ft $M := M_{total} \cdot 12 = 450.767$ kip·in

Stresses and Strains at Gauge Locations on Beam C:

Predicted max stresses at midspan gauge loactions during moving tests:

Stress at bottom of the beam: $\sigma_{bot\_beam} := \frac{M \cdot c_{bot\_beam}}{I} = 1.401$ ksi

Positive stress = tension
Negative stress = compression

Predicted max strains at midspan gauge locations during moving tests:

Strain at bottom of the beam: $\varepsilon_{bot\_beam} := \frac{\sigma_{bot\_beam}}{E_s} \cdot 10^6 = 48.3246$ με

$\varepsilon_{bdi6} := \varepsilon_{bot\_beam}$

Max deflection at midspan:

$\Delta_{max} := -0.02381$ in Calculated using Mastan2

$\Delta_{twang6} := \Delta_{max}$

Deflected shape produced by Mastan2:

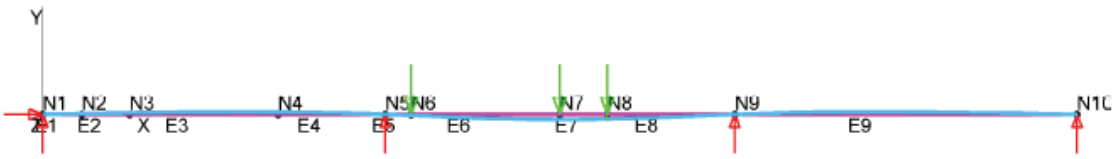

Moment diagram produced by Mastan2:

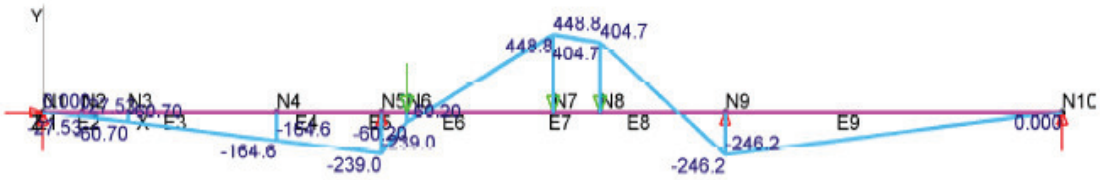

Stresses and Strains at Gauge Locations on Beam C:

Strains and stresses with truck at 0.4*L of first span:

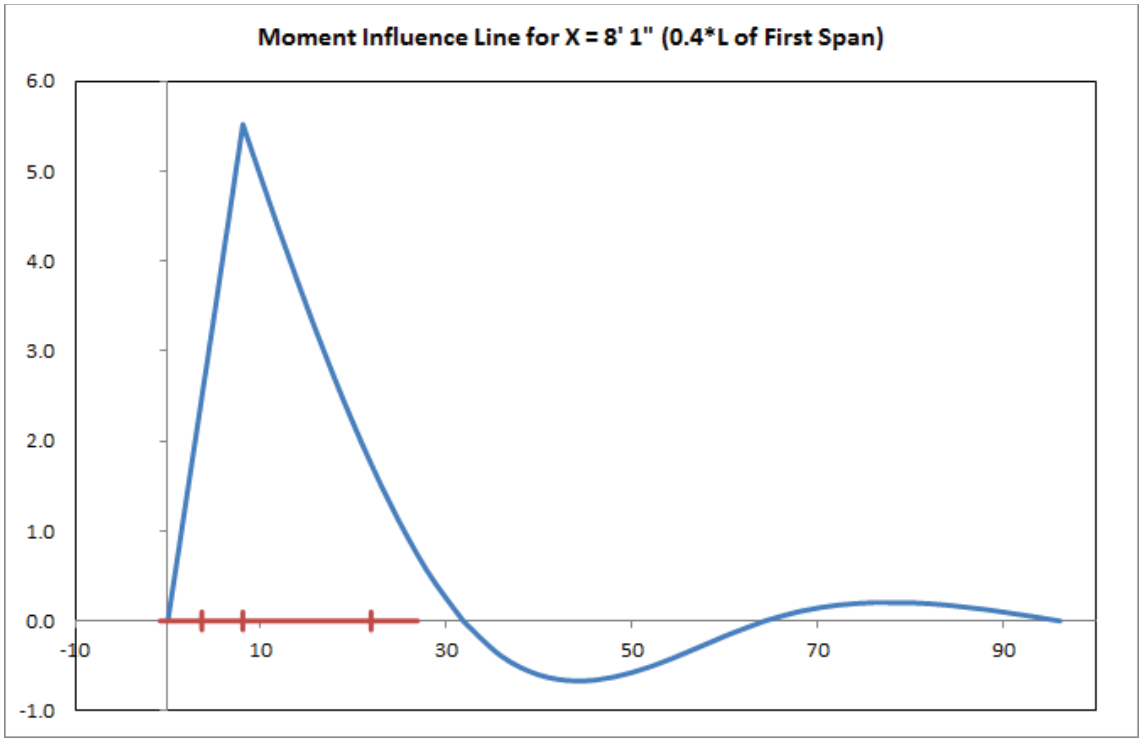

Influence line magnitudes at axel locations:

Truck 1: $truck1_{f\_axel} := 1.7617$ $truck1_{m\_axel} := 5.523$ $truck1_{b\_axel} := 2.493$

Total moment developed at the panel interface (divided into the three girders):

$$M_{total} := \frac{truck1_{f\_axel} \cdot f\_axel_{wt} + truck1_{m\_axel} \cdot m\_axel_{wt} + truck1_{b\_axel} \cdot b\_axel_{wt}}{1000} = 36.35$$

$M_{total} = 36.35$ kip·ft $M := M_{total} \cdot 12 = 436.197$ kip·in

Stresses and Strains at Gauge Locations on Beam C:

Predicted max stresses at midspan gauge loactions during moving tests:

Stress at top of the deck: $\sigma_{top\_deck} := \frac{M \cdot c_{top\_deck}}{I \cdot n} = -0.056$ ksi

Stress at top vwg in deck: $\sigma_{vwg\_top} := \frac{M \cdot c_{vwg\_top}}{I \cdot n} = -0.022$ ksi

Stress at middle vwg on beam: $\sigma_{vwg\_mid} := \frac{M \cdot c_{vwg\_mid}}{I} = 0.491$ ksi

Positive stress = tension
Negative stress = compression

Stress at bottom vwg on beam: $\sigma_{vwg\_bot} := \frac{M \cdot c_{vwg\_bot}}{I} = 1.154$ ksi

Stress at bottom of the beam: $\sigma_{bot\_beam} := \frac{M \cdot c_{bot\_beam}}{I} = 1.356$ ksi

Predicted max strains at midspan gauge locations during moving tests:

Strain at top of the deck: $\varepsilon_{top\_deck} := \frac{\sigma_{top\_deck}}{E_c} \cdot 10^6 = -8.9298$ με

Strain at top vwg in deck: $\varepsilon_{vwg\_top} := \frac{\sigma_{vwg\_top}}{E_c} \cdot 10^6 = -3.46$ με $\quad \varepsilon_{vwg6} := \varepsilon_{vwg\_top}$

Strain at middle vwg on beam: $\varepsilon_{vwg\_mid} := \frac{\sigma_{vwg\_mid}}{E_s} \cdot 10^6 = 16.9224$ με $\quad \varepsilon_{vwg1} := \varepsilon_{vwg\_mid}$

Strain at bottom vwg on beam: $\varepsilon_{vwg\_bot} := \frac{\sigma_{vwg\_bot}}{E_s} \cdot 10^6 = 39.796$ με $\quad \varepsilon_{vwg2} := \varepsilon_{vwg\_bot}$

Strain at bottom of the beam: $\varepsilon_{bot\_beam} := \frac{\sigma_{bot\_beam}}{E_s} \cdot 10^6 = 46.7625$ με $\quad \varepsilon_{bdi3} := \varepsilon_{bot\_beam}$

Max deflection at midspan:

$\Delta_{max} := -0.01986$ in Calculated using Mastan2 $\quad \Delta_{twang3} := \Delta_{max}$

Deflected shape produced by Mastan2:

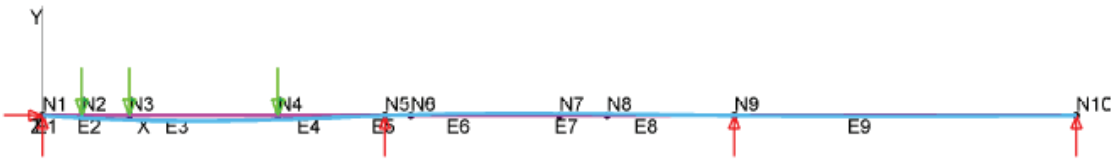

Moment diagram produced by Mastan2:

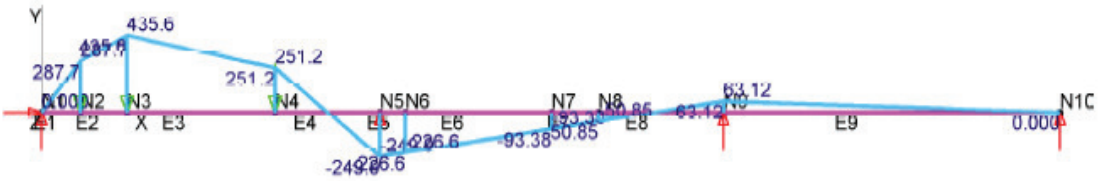

Stresses and Strains at Gauge Locations on Beam C:

Summary of Approximate Field Strains and Deflections:

Static Load Test:

At gauge location near pier:

LVDT #2:	$\Delta_{LVDT2} := 0$	in
BDI #8:	$\varepsilon_{bdi8} = 6.508$	με
VWG #8:	$\varepsilon_{vwg8} = 2.522$	με
VWG #3:	$\varepsilon_{vwg3} = -12.334$	με
VWG #4:	$\varepsilon_{vwg4} = -29.005$	με

Moving Load Tests:

At gauge location midspan:

BDI #6:	$\varepsilon_{bdi6} = 48.325$	με
Twanger #6:	$\Delta_{twang6} = -0.024$	in

At gauge location 0.4*L of first span:

VWG #6:	$\varepsilon_{vwg6} = -3.46$	με
VWG #1:	$\varepsilon_{vwg1} = 16.922$	με
VWG #2:	$\varepsilon_{vwg2} = 39.796$	με
BDI #3:	$\varepsilon_{bdi3} = 46.763$	με
Twanger #3:	$\Delta_{twang3} = -0.02$	in

Appendix G – ACI 209 Creep and Shrinkage Calculations

ACI 209 Shrinkage Calculations

Shrinkage bar properties:

25 x 25 mm rectangular prism $ht := 25 \cdot 0.0393700787 = 0.984$ in $len := 250 \cdot 0.0393700787 = 9.843$ in

Concrete strength: $fc := 6000$ psi

Steam cure duration: $t_c := 1$ days

Never loaded

Humidity = 50% $h := 0.50$

Air content = 3.6% $\alpha := 3.6$

Ultimate shrinkage strain equation:

$\varepsilon_{shu} = 780 \cdot \gamma_{sh} \cdot 10^{-6}$ Equation A-4

$\gamma_{sh} = \gamma_{shtc} \cdot \gamma_{shRH} \cdot \gamma_{shvs} \cdot \gamma_{shs} \cdot \gamma_{sh\psi} \cdot \gamma_{shc} \cdot \gamma_{sh\alpha}$ Equation A-5

Initial moist curing coefficient γ_{shtc}: $t_c = 1$

For curing times different from 7 days for moist-cured concrete or 1 to 3 days for steam-cured concrete:

$\gamma_{shtc} = 1.202 - 0.2337 \cdot \log(t_c)$ Equation A-6

Otherwise: $\gamma_{shtc} := 1$

Ambient relative humidity coefficient γ_{shRH}:

h = relative humidity in decimal form

$$\gamma_{shRH} := \begin{cases} 1.40 - 1.02 \cdot h & \text{if } 0.4 \le h \le 0.8 \\ 3.00 - 3.0 \cdot h & \text{if } 0.8 < h \le 1 \end{cases} = 0.89$$ Equation A-6

$\gamma_{shRH} = 0.89$

Volume to surface ratio coefficient γ_{shvs}:

$VS := \frac{ht^2 \cdot len}{\left(4 \cdot ht \cdot len + 2 \cdot ht^2\right)} = 0.234$ in *Note: VS = V/S but cannot be shown correctly in Mathcad

$\gamma_{shvs} := 1.2 \cdot e^{(-0.12 \cdot VS)} = 1.167$ Equation A-8

ACI 209 Shrinkage Calculations - CONTINUED

Slump coefficient γ_{shs}:

s = slump in inches

$\gamma_{shs} = 0.89 + 0.041 \cdot s$ Equation A-11

But since slump is unknown: $\gamma_{shs} := 1$

Fine aggregate coefficient $\gamma_{sh\psi}$:

ψ = ratio of fine aggregate by weight expressed as percentage

$$\gamma_{sh\psi} = \begin{cases} 0.30 + 0.014 \cdot \psi & \text{if } \psi \le 50\% \\ 0.90 + 0.002 \cdot \psi & \text{if } \psi > 50\% \end{cases}$$ Equation A-12

But since fine aggregate ratio is unknown: $\gamma_{sh\psi} := 1$

Cement content coefficient γ_{shc}:

c = the cement content in lb/yd^3

$\gamma_{shc} = 0.75 + 0.00036 \cdot c$ Equation A-12

But since the cement content is unknown: $\gamma_{shc} := 1$

Air content coefficient $\gamma_{sh\alpha}$:

α = air content in percent

$\gamma_{sh\alpha} := (0.95 + 0.008 \cdot \alpha \ge 1)$ Equation A-12

$\gamma_{sh\alpha} := 1$

Ultimate shrinkage strain:

$\gamma_{sh} := \gamma_{shtc} \cdot \gamma_{shRH} \cdot \gamma_{shvs} \cdot \gamma_{shs} \cdot \gamma_{sh\psi} \cdot \gamma_{shc} \cdot \gamma_{sh\alpha} = 1.038$ Equation A-4

$\varepsilon_{shu} := 780 \cdot \gamma_{sh} = 809.94$ με Equation A-5

ACI 209 Shrinkage Calculations - CONTINUED

ACI 209 shrinkage strain development with time:

$$\varepsilon_{sh}(t,t_c) = \frac{(t-t_c)^{\alpha}}{f+(t-t_c)^{\alpha}}\cdot\varepsilon_{shu}$$ Equation A-1

$t_c := 1$ days of steam curing $f := 55$ for 1 days of steam cure $\alpha := 1$ $\varepsilon_{shu} = 809.94$ με

$$\varepsilon_{sh\_ACI}(t,t_c) := \frac{(t-t_c)^{\alpha}}{f+(t-t_c)^{\alpha}}\cdot\varepsilon_{shu} \rightarrow \frac{809.94\cdot(t-t_c)}{t-t_c+55}$$ Equation A-1

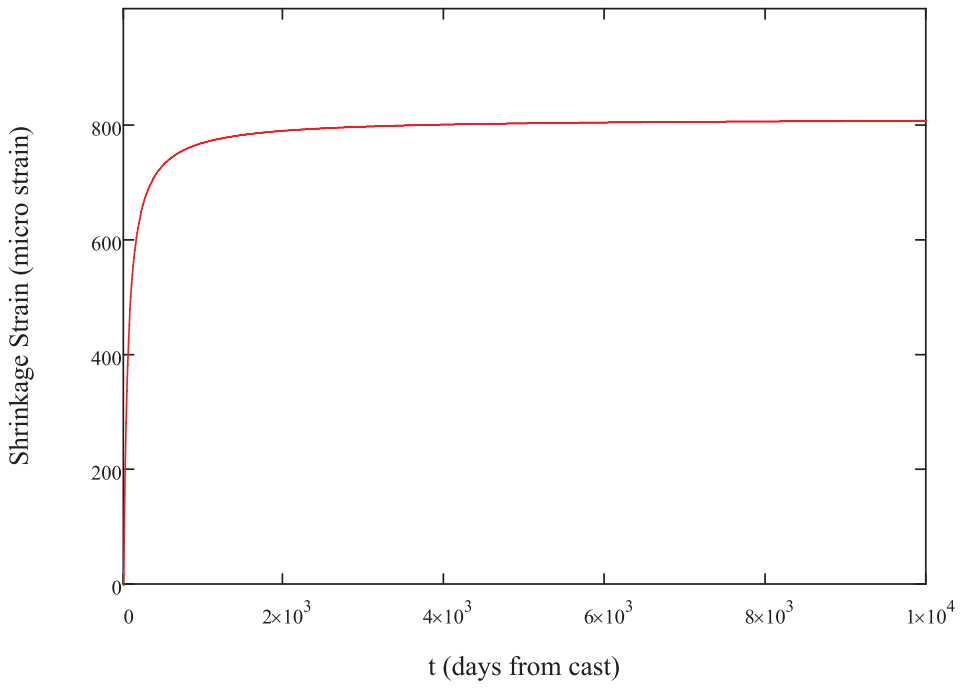

ACI 209 Shrinkage Calculations:

Panel properties:

8 x 171 in. slab $ht := 8$ in $wd := 171$ in

Concrete strength: $fc := 6000$ psi

Steam cure duration: $t_c := 1$ days

Never loaded

Ultimate shrinkage strain equation:

$$\varepsilon_{shu} = 780 \cdot \gamma_{sh} \cdot 10^{-6}$$ Equation A-4

$$\gamma_{sh} = \gamma_{shtc} \cdot \gamma_{shRH} \cdot \gamma_{shvs} \cdot \gamma_{shs} \cdot \gamma_{sh\psi} \cdot \gamma_{shc} \cdot \gamma_{sh\alpha}$$ Equation A-5

Initial moist curing coefficient γ_{shtc}: $t_c = 1$

For curing times different from 7 days for moist-cured concrete or 1 to 3 days for steam-cured concrete:

$$\gamma_{shtc} = 1.202 - 0.2337 \cdot \log(t_c)$$ Equation A-6

Otherwise: $\gamma_{shtc} := 1$

Ambient relative humidity coefficient γ_{shRH}:

h = relative humidity in decimal form

$$\gamma_{shRH} := \begin{cases} 1.40 - 1.02 \cdot h & \text{if } 0.4 \le h \le 0.8 \\ 3.00 - 3.0 \cdot h & \text{if } 0.8 < h \le 1 \end{cases} =$$ Equation A-6

$\gamma_{shRH} := 1$

Volume to surface ratio coefficient γ_{shvs}:

$VS := \frac{ht \cdot wd}{(2 \cdot ht + 2 \cdot wd)} = 3.821$ in *Note: VS = V/S but cannot be shown correctly in Mathcad

$\gamma_{shvs} := 1.2 \cdot e^{(-0.12 \cdot VS)} = 0.759$ Equation A-8

ACI 209 Shrinkage Calculations - CONTINUED:

Slump coefficient γ_{shs}:

s = slump in inches

$$\gamma_{shs} = 0.89 + 0.041 \cdot s$$ Equation A-11

But since slump is unknown: $\gamma_{shs} := 1$

Fine aggregate coefficient $\gamma_{sh\psi}$:

ψ = ratio of fine aggregate by weight expressed as percentage

$$\gamma_{sh\psi} = \begin{cases} 0.30 + 0.014 \cdot \psi & \text{if } \psi \le 50\% \\ 0.90 + 0.002 \cdot \psi & \text{if } \psi > 50\% \end{cases}$$ Equation A-12

But since fine aggregate ratio is unknown: $\gamma_{sh\psi} := 1$

Cement content coefficient γ_{shc}:

c = the cement content in lb/yd^3

$$\gamma_{shc} = 0.75 + 0.00036 \cdot c$$ Equation A-12

But since the cement content is unknown: $\gamma_{shc} := 1$

Air content coefficient $\gamma_{sh\alpha}$:

$\alpha := 3.6 \quad \%$

$\gamma_{sh\alpha} := (0.95 + 0.008 \cdot \alpha \ge 1) = 0$ Equation A-12

$\gamma_{sh\alpha} := 1$

Ultimate shrinkage strain:

$\gamma_{sh} := \gamma_{shtc} \cdot \gamma_{shRH} \cdot \gamma_{shvs} \cdot \gamma_{shs} \cdot \gamma_{sh\psi} \cdot \gamma_{shc} \cdot \gamma_{sh\alpha} = 0.759$ Equation A-4

$\varepsilon_{shu} := 780 \cdot \gamma_{sh} = 591.74 \quad \mu\varepsilon$ Equation A-5

ACI 209 Shrinkage Calculations - CONTINUED:

ACI 209 shrinkage strain development with time:

$$\varepsilon_{sh}(t,t_c) = \frac{(t-t_c)^{\alpha}}{f+(t-t_c)^{\alpha}}\cdot\varepsilon_{shu}$$ Equation A-1

$t_c := 1$ days of steam curing $f := 55$ for 1 days of steam cure $\alpha := 1$ $\varepsilon_{shu} = 591.74$ με

$$\varepsilon_{sh\_ACI}(t,t_c) := \frac{(t-t_c)^{\alpha}}{f+(t-t_c)^{\alpha}}\cdot\varepsilon_{shu} \rightarrow \frac{591.74\cdot(t-t_c)}{t-t_c+55}$$ Equation A-1

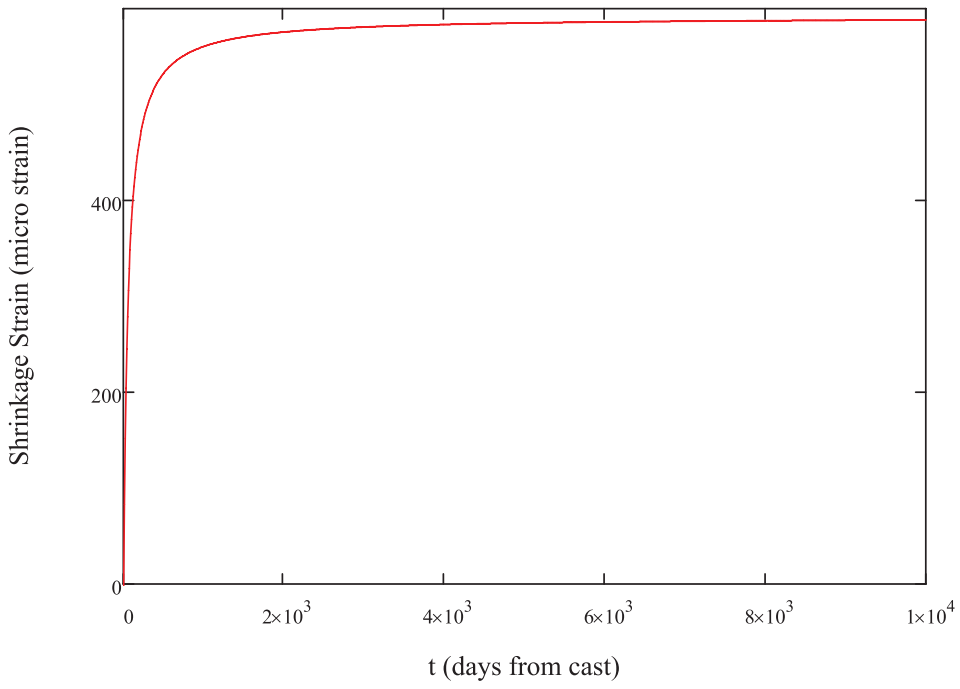

ACI 209 Creep Strain Calculations:

Ultimate creep coefficient:

$\phi_u = 2.35 \cdot \gamma_c$ Equation A-20

$\gamma_c = \gamma_{cto} \cdot \gamma_{cRH} \cdot \gamma_{cvs} \cdot \gamma_{cs} \cdot \gamma_{c\psi} \cdot \gamma_{c\alpha}$ Equation A-21

Load application coefficient γ_{cto}:

For load applied 7 or more days after moist curing:

$\gamma_{cto} = 1.25 \cdot t_o^{-0.118}$ Equation A-22

For load applied more than 1 to 3 days after steam curing: $t_o := 1$

$\gamma_{cto} := 1.13 \cdot t_o^{-0.094} = 1.13$ Equation A-23

Ambient humidity coefficient γ_{cRH}:

$h \geq 0.4 \qquad \gamma_{cRH} := 1.27 - 0.67 \cdot h \qquad \gamma_{cRH} := 1$ Equation A-24

Volume to surface area coefficient γ_{cvs}: $VS = 3.821$ in

$\gamma_{cvs} := \frac{2}{3} \cdot \left(1 + 1.13 \cdot e^{-0.54 \cdot VS}\right) = 0.762$ Equation A-25

Air content coefficient $\gamma_{c\alpha}$:

$\gamma_{c\alpha} := 0.46 + 0.09 \cdot \alpha \geq 1 = 0$

$\gamma_{c\alpha} := 1$

Slump coefficient and fine aggregate coefficient factors are set to the standard value of 1 due to a lack of information.

$\gamma_{cs} := 1 \qquad \gamma_{c\psi} := 1$

Ultimate creep coefficient:

$\gamma_c := \gamma_{cto} \cdot \gamma_{cRH} \cdot \gamma_{cvs} \cdot \gamma_{cs} \cdot \gamma_{c\psi} \cdot \gamma_{c\alpha} = 0.861$ Equation A-21

$\phi_u := 2.35 \cdot \gamma_c = 2.024$ Equation A-20

ACI 209 Creep Strain Calculations - CONTINUED:

ACI 209 creep coefficient development with time:

$$\phi(t,t_o) = \frac{(t-t_o)^{\psi}}{d+(t-t_o)^{\psi}}\cdot\phi_u$$ Equation A-18

$\psi := 0.6$ $d := 10$ $t_o := 1$ days load is applied $\phi_u = 2.024$

$$\phi_{ACI}(t,t_o) := \frac{(t-t_o)^{\psi}}{d+(t-t_o)^{\psi}}\cdot\phi_u \rightarrow \frac{2.024\cdot(t-t_o)^{0.6}}{(t-t_o)^{0.6}+10}$$ Equation A-18

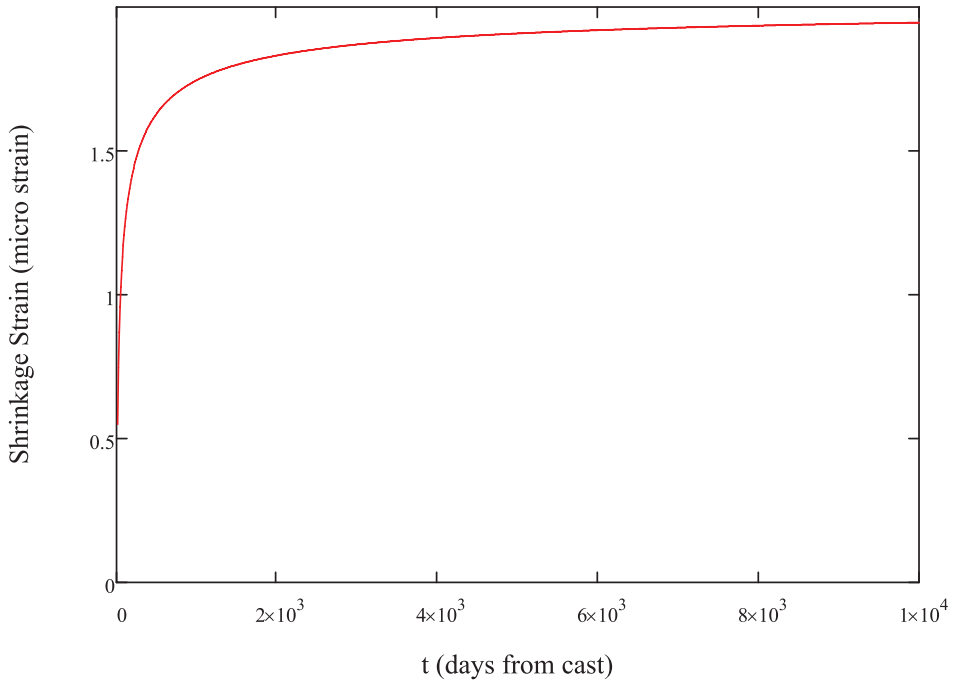

Appendix H – Bowers' Prestress Loss Mathcad Calculations

Deck Panel Prestress Losses

Phase I precast panels:
Three 32.5 ft spans, W18x71, 8" precast deck panels, 7000 psi concrete, 4 strands per girder line

Inputs

Steel girder properties:

$A_g := 20.8$	in^2	Gross cross-sectional area of the girder
$I_g := 1170$	in^4	Moment of inertia of the girder (x-dir)
$E_g := 29000$	ksi	Modulus of elasticity of the girder
$depth_g := 18.5$	in	Depth of the girder
$topw_g := 7.64$	in	Girder top flange width
$L_g := 32.5 \cdot 12$	in	Length of the single span
$c_g := \frac{18.5}{2}$	in	Centroid of the girder measured from the bottom

Deck section properties:

$t_d := 8$	in	Thickness of the deck
$w_d := 46.5625$	in	Effective width of the deck (interior girder spacing)
$\mu_d := 0.7$		Aging coefficient for the deck
$fc_d := 7000$	psi	Compressive strength of the deck concrete
$numspans := 3$		Number of continuous spans

Post-tensioning strand properties:

$numstr_{dpt} := 4$		Number of post-tensioning strands in the **effective** deck
$Astr_d := 0.217$	in^2	Area of each post-tensioning strand in the deck
$Ept_d := 28500$	ksi	Modulus of elasticity of deck post-tensioning strands
$f_{pu} := 270$	ksi	Ultimate strength of prestressing and post-tensioning strands
$K_{Lpr} := 30$		Factor indicating low relaxation strands

Inputs (Continued)

Deck time intervals:

$t_{dpt} := 65$ days — Time the deck is post-tensioned relative to the age of the precast deck panel

$t_{dcomp} := 80$ days — Time the deck is made composite relative to the age of the precast deck panel

$t_{dinf} := 10000$ days — Time considered as the end of bridge service life

Haunch section properties:

$t_h := 1.5$ in — Thickness of the haunch

$\mu_h := 0.7$ — Aging coefficient for the haunch

$fc_h := fc_d$ psi — Compressive strength of haunch material

Haunch time intervals:

$t_{hcomp} := 0.75$ days — Time the haunch is placed (relative to haunch material age), which makes the deck and girders composite

$t_{hinf} := t_{dinf}$ days — Time considered as end of bridge service life

General bridge properties:

$hum := 70$ % — Relative humidity

Calculated Properties

Deck properties:

$len := numspans \cdot \frac{L_g}{12} = 97.5$ ft — Total length of the bridge

$A_d := t_d \cdot w_d = 372.5$ in^2 — Cross-sectional area of the effective deck

$I_d := \frac{1}{12} \cdot w_d \cdot t_d^3 = 1986.667$ in^4 — Moment of inertial of the effective deck

$E_d := 6287$ ksi — Modulus of elasticity of the deck

$perim_d := 2 \cdot w_d = 93.125$ in — Perimeter of the effective deck

Calculated Properties (Continued)

Post-tensioning strand properties:

$Apt_d := numstr_{dpt} \cdot Astr_d = 0.868$ in^2 Total area of post-tensioning strands in deck

$f_{py} := 0.9 \cdot f_{pu} = 243$ ksi Yield stress of prestressing and post-tensioning strands

Haunch properties:

$w_h := topw_g = 7.64$ in Width of the haunch

$A_h := t_h \cdot topw_g = 11.46$ in^2 Cross-sectional area of the haunch

$I_h := \frac{1}{12} \cdot w_h \cdot t_h^3 = 2.149$ in^4 Moment of intertia of the haunch

$E_h := E_d = 6287$ ksi Modulus of elasticity of the haunch

$perim_h := 2 \cdot t_h = 3$ in Section of the haunch perimeter open to the atmosphere

Composite section properties:

$y_h := depth_g + \frac{t_h}{2} = 19.25$ in Centriod of the haunch in comp. section measured from bottom of girder

$y_d := depth_g + t_h + \frac{t_d}{2} = 24$ in Centriod of the deck in the comp. section measured from bottom of girder

$y_{ps} := y_d = 24$ in Centriod of the deck post-tensioning in the comp. section measured from the bottom of the girder

$depth_t := depth_g + t_h + t_d = 28$ in Total depth of the composite section

Creep and Shrinkage Models (from AASHTO LRFD 2006 Interims)

AASHTO Eqn. 5.4.2.3.2-1:

$$\text{CREEP}(fci, t1, t2, hum, area, perim) := \begin{bmatrix} ktd \leftarrow \dfrac{(t2 - t1)}{61 - \left(\dfrac{4 \cdot fci}{1000}\right) + (t2 - t1)} \\ kla \leftarrow t1^{-0.118} \\ khc \leftarrow 1.56 - (0.008 \cdot hum) \\ kvs \leftarrow \max\left[1.45 - 0.13 \cdot \left(\dfrac{area}{perim}\right), 1.0\right] \\ kf \leftarrow \dfrac{5}{1 + \dfrac{fci}{1000}} \\ creep \leftarrow 1.90 \cdot ktd \cdot kla \cdot kvs \cdot khc \cdot kf \\ creep \end{bmatrix}$$

AASHTO Eqn. 5.4.2.3.3-1:

$$\text{SHRINKAGE}(fci, t1, t2, hum, area, perim) := \begin{bmatrix} ktd1 \leftarrow \dfrac{t1}{61 - \left(\dfrac{4 \cdot fci}{1000}\right) + t1} \\ ktd2 \leftarrow \dfrac{t2}{61 - \left(\dfrac{4 \cdot fci}{1000}\right) + t2} \\ khs \leftarrow 2 - (0.014 \cdot hum) \\ kvs \leftarrow \max\left[1.45 - 0.13 \cdot \left(\dfrac{area}{perim}\right), 1.0\right] \\ kf \leftarrow \dfrac{5}{1 + \dfrac{fci}{1000}} \\ shrink \leftarrow -480 \cdot 10^{-6} \cdot (ktd2 - ktd1) \cdot kvs \cdot khs \cdot kf \\ shrink \end{bmatrix}$$

Sign Convention: Tension = Lengthening (+)
Compression = Shortening (-)

Note: Equations were checked with AASHTO 2009 on 7/20/11

Calculate redistribution of stresses in deck from post-tensioning to composite action

Compute state of stress immediately following stressing (use average force in tendons):

$P_{jack} := 0.70 \cdot f_{pu} \cdot numstr_{dpt} \cdot Astr_d = 164.052$ kips

Compute seating losses: **Note:** Post-tensioning tendons are straight, so they only have wobble losses (k*l term)

$\alpha := 0$ $\mu := 0$ $k := 0.001$ per foot of length

$\Delta S := 0.38$ in $len = 97.5$ ft $P_{dead} := P_{jack} \cdot e^{-(\mu \cdot \alpha + k \cdot len)} = 148.812$ kips

$m := \frac{P_{jack} - P_{dead}}{len \cdot 12} = 0.013$ kips/inch $P_{SL} := \frac{\Delta S \cdot Apt_d \cdot Ept_d}{len \cdot 12} = 8.035$ kips

$x_{AS} := \frac{\sqrt{\frac{\Delta S \cdot Apt_d \cdot Ept_d}{m}}}{12} = 70.793$ ft $len = 97.5$ ft

The calculation of P_{avg} depends on whether xAS is greater or less than the total bridge length:

$P_{avg} :=$ if $x_{AS} > len$ = 148.397

- $area_{tris} \leftarrow \frac{1}{2} \cdot (P_{jack} - P_{dead}) \cdot len \cdot 12 \cdot 2$
- $rh \leftarrow \frac{\Delta S \cdot Apt_d \cdot Ept_d - area_{tris}}{len \cdot 12}$
- $P_{sl} \leftarrow rh + 2 \cdot (P_{jack} - P_{dead})$
- $P_{live} \leftarrow P_{jack} - P_{sl}$
- $P_{dead2} \leftarrow P_{dead} - rh$
- $P_{avg} \leftarrow \frac{P_{live} + P_{dead2}}{2}$
- P_{avg}

if $x_{AS} < len$

- $P_{sl} \leftarrow 2 \cdot m \cdot x_{AS} \cdot 12$
- $P_{live} \leftarrow P_{jack} - P_{sl}$
- $P_{mid} \leftarrow P_{jack} - \frac{P_{sl}}{2}$
- $P_{avg} \leftarrow \frac{\left(\frac{P_{live} + P_{mid}}{2}\right) \cdot x_{AS} + \left(\frac{P_{mid} + P_{dead}}{2}\right) \cdot (len - x_{AS})}{len}$
- P_{avg}

P_{avg}

Calculate redistribution of stresses in deck from post-tensioning to composite action

Initial state of internal equilibrium, assuming no tendon eccentricity and that self-wt. causes no significant stresses:

$$Nd_o + Nptd_o = 0$$

$Nptd_o := P_{avg} = 148.397$ kips $\qquad Nd_o := -Nptd_o = -148.397$ kips

Relaxation in deck post-tensioning strands from transfter to composite action:

Average stress in tendons: $f_{pt} := \frac{P_{avg}}{Apt_d} = 170.965$ ksi

$t_i := t_{hcomp} = 0.75 \qquad t := t_{dcomp} - t_{dpt} = 15$

$$\Delta f_{pR1} := \frac{-f_{pt}}{K_{Lpr}} \cdot \left(\frac{f_{pt}}{f_{py}} - 0.55 \right) \cdot \frac{\log(24 \cdot t)}{\log(24 \cdot t_i)} = -1.782$$

$$\varepsilon sh_{d1} := SHRINKAGE(fc_d, t_{dpt}, t_{dcomp}, hum, A_d, perim_d) = -1.368 \times 10^{-5}$$

$$\phi_{d1} := CREEP(fc_d, t_{dpt}, t_{dcomp}, hum, A_d, perim_d) = 0.227$$

$$deqns1 := \begin{bmatrix} \frac{-(1 + \mu_d \cdot \phi_{d1})}{A_d \cdot E_d} & 0 & 1 & 0 \\ 0 & -1 & 0 & Apt_d \cdot Ept_d \\ 1 & 1 & 0 & 0 \\ 0 & 0 & 1 & -1 \end{bmatrix} = \begin{pmatrix} -4.948 \times 10^{-7} & 0 & 1 & 0 \\ 0 & -1 & 0 & 2.474 \times 10^{4} \\ 1 & 1 & 0 & 0 \\ 0 & 0 & 1 & -1 \end{pmatrix} \qquad dvar := \begin{pmatrix} \Delta Nd_1 \\ \Delta Nptd_1 \\ \Delta \varepsilon d_1 \\ \Delta \varepsilon ptd_1 \end{pmatrix}$$

$$dans1 := \begin{pmatrix} \frac{Nd_o}{A_d \cdot E_d} \cdot \phi_{d1} + \varepsilon sh_{d1} \\ -\Delta f_{pR1} \cdot Apt_d \\ 0 \\ 0 \end{pmatrix} \qquad dvalues1 := deqns1^{-1} \cdot dans1 = \begin{pmatrix} 2.214 \\ -2.214 \\ -2.695 \times 10^{-5} \\ -2.695 \times 10^{-5} \end{pmatrix}$$

Results:

$\Delta Nd_1 := dvalues1_1 = 2.214$

$\Delta Nptd_1 := dvalues1_2 = -2.214$

$\Delta \varepsilon d_1 := dvalues1_3 = -2.695 \times 10^{-5}$

$\Delta \varepsilon ptd_1 := dvalues1_4 = -2.695 \times 10^{-5}$

Note: Deck should be losing compression (+)
Post-tensioning strands should be losing tension (-)

Calculate redistribution of stresses in deck from post-tensioning to composite action

$$\varepsilon sh_{h2} := \text{SHRINKAGE}\left(fc_h, t_{hcomp}, t_{hinf}, hum, A_h, perim_h\right) = -2.982 \times 10^{-4}$$

$$\phi_{h2} := \text{CREEP}\left(fc_h, t_{hcomp}, t_{hinf}, hum, A_h, perim_h\right) = 1.224$$

$$\varepsilon sh_{d2} := \text{SHRINKAGE}\left(fc_d, t_{dcomp}, t_{dinf}, hum, A_d, perim_d\right) = -8.836 \times 10^{-5}$$

$$\phi_{d2} := \text{CREEP}\left(fc_d, t_{dcomp}, t_{dinf}, hum, A_d, perim_d\right) = 0.706$$

Need to establish all starting values based on results of previous stages: variables with "oc" indicate starting values for composite stage:

Initial moment at midspan of steel girder due to self-weight only:

$$w_g := A_g \cdot \frac{0.490}{12^3} = 0.006 \quad \text{kip/in}$$

$$Mg_{self} := \frac{w_g \cdot L_g^{\,2}}{8} = 112.139 \quad \text{kip/in}$$

Add deck weight moment to girder:

$$w_{dself} := A_d \cdot \frac{0.150}{12^3} = 0.032 \quad \text{kip/in}$$

$$Md_{self} := \frac{w_{dself} \cdot L_g^{\,2}}{8} = 614.771 \quad \text{kip/in}$$

Stresses in girder due to deck weight only:

$$\sigma_{top} := -\frac{Md_{self} \cdot \left(depth_g - c_g\right)}{I_g} = -4.86 \quad \text{ksi}$$

$$\sigma_{bot} := \frac{Md_{self} \cdot c_g}{I_g} = 4.86 \quad \text{ksi}$$

Strains in girder due to deck weight only:

$$\varepsilon_{top} := \frac{\sigma_{top}}{E_g} \cdot 10^6 = -167.599 \quad \mu\varepsilon/\text{in}$$

$$\varepsilon_{bot} := \frac{\sigma_{bot}}{E_g} \cdot 10^6 = 167.599 \quad \mu\varepsilon/\text{in}$$

Calculate redistribution of stresses in deck from post-tensioning to composite action

Moment in girder due to deck weight only:

$$\phi_d := \frac{\varepsilon_{bot} - \varepsilon_{top}}{depth_g} = 18.119$$

$$Mg_{fromdeck} := \phi_d \cdot 10^{-6} \cdot E_g \cdot I_g = 614.771 \ \ kip \cdot in$$

Revise starting values for composite analysis to include girder and deck weights:

$$Mg_{oc} := Mg_{self} + Mg_{fromdeck} = 726.909$$

$$Nd_{oc} := Nd_o + \Delta Nd_1 = -146.184$$

$$Nptd_{oc} := Nptd_o + \Delta Nptd_1 = 146.184$$

Relaxation in deck post-tensioning strands from composite action to end of service life:

$$f_{pt2} := Nptd_{oc} = 146.184$$

$$t := t_{dinf} - t_{dcomp} = 9920$$

$$t_i := t_{dcomp} = 80$$

$$\Delta f_{pR2} := \frac{-f_{pt2}}{K_{Lpr}} \cdot \left(\frac{f_{pt2}}{f_{py}} - 0.55 \right) \cdot \frac{\log(24 \cdot t)}{\log(24 \cdot t_i)} = -0.412$$

Calculations for system after it becomes composite:

$$a := \frac{t_d}{2} + \frac{t_h}{2} = 4.75$$

$$b := \frac{t_d}{2} + t_h + (depth_g - c_g) = 14.75$$

Calculate redistribution of stresses in deck from post-tensioning to composite action

$$coeff1 := \begin{bmatrix} 1 & 1 & 1 & 1 & 0 & 0 & 0 & 0 & 0 & 0 & 0 & 0 \\ 0 & a & b & 0 & 1 & 1 & 1 & 0 & 0 & 0 & 0 & 0 \\ 0 & 0 & 0 & 0 & 0 & 0 & 0 & 1 & 0 & 0 & -1 & 0 \\ 0 & 0 & 0 & 0 & 0 & 0 & 0 & 1 & -1 & 0 & 0 & a \\ 0 & 0 & 0 & 0 & 0 & 0 & 0 & 1 & 0 & -1 & 0 & b \\ \frac{-(1+\mu_d\cdot\phi_{d2})}{A_d\cdot E_d} & 0 & 0 & 0 & 0 & 0 & 0 & 1 & 0 & 0 & 0 & 0 \\ 0 & 0 & \frac{-1}{A_g\cdot E_g} & 0 & 0 & 0 & 0 & 0 & 0 & 1 & 0 & 0 \\ 0 & \frac{-(1+\mu_h\cdot\phi_{h2})}{A_h\cdot E_h} & 0 & 0 & 0 & 0 & 0 & 0 & 1 & 0 & 0 & 0 \end{bmatrix}$$

$$coeff2 := \begin{bmatrix} 0 & 0 & 0 & -1 & 0 & 0 & 0 & 0 & 0 & 0 & Apt_d\cdot Ept_d & 0 \\ 0 & 0 & 0 & 0 & \frac{-(1+\mu_d\cdot\phi_{d2})}{I_d\cdot E_d} & 0 & 0 & 0 & 0 & 0 & 0 & 1 \\ 0 & 0 & 0 & 0 & 0 & \frac{-(1+\mu_h\cdot\phi_{h2})}{I_h\cdot E_h} & 0 & 0 & 0 & 0 & 0 & 1 \\ 0 & 0 & 0 & 0 & 0 & 0 & \frac{-1}{I_g\cdot E_g} & 0 & 0 & 0 & 0 & 1 \end{bmatrix}$$

$coeffs := stack(coeff1, coeff2)$

$$vars12 := \begin{pmatrix} \Delta N_d \\ \Delta N_h \\ \Delta N_g \\ \Delta N_{ptd} \\ \Delta M_d \\ \Delta M_h \\ \Delta M_g \\ \Delta \varepsilon_d \\ \Delta \varepsilon_h \\ \Delta \varepsilon_g \\ \Delta \varepsilon_{ptd} \\ \Delta \chi \end{pmatrix}$$

$$values12 := \begin{pmatrix} 0 \\ 0 \\ 0 \\ 0 \\ 0 \\ \frac{Nd_{oc}}{A_d\cdot E_d}\cdot\phi_{d2} + \varepsilon sh_{d2} \\ 0 \\ \varepsilon sh_{h2} \\ -\Delta f_{pR2}\cdot Apt_d \\ 0 \\ 0 \\ 0 \end{pmatrix}$$

$$values12 = \begin{pmatrix} 0 \\ 0 \\ 0 \\ 0 \\ 0 \\ -1.324\times 10^{-4} \\ 0 \\ -2.982\times 10^{-4} \\ 0.357 \\ 0 \\ 0 \\ 0 \end{pmatrix}$$

$answers := coeffs^{-1}\cdot values12$

Calculate redistribution of stresses in deck from post-tensioning to composite action

$$answers = \begin{pmatrix} 15.412 \\ 7.931 \\ -19.954 \\ -3.39 \\ 50.726 \\ 0.044 \\ 205.871 \\ -1.226 \times 10^{-4} \\ -9.375 \times 10^{-5} \\ -3.308 \times 10^{-5} \\ -1.226 \times 10^{-4} \\ 6.068 \times 10^{-6} \end{pmatrix}$$

$Mg_f := Mg_{oc} + answers_7 = 932.78$ kip·in

$Nd_f := Nd_{oc} + answers_1 = -130.772$ kips

$Nptd_f := Nptd_{oc} + answers_4 = 142.794$ kips

$\chi_f := answers_{12} = 6.068 \times 10^{-6}$ strain/in

Define values for plot of strain throughout composite cross-section:

$\Delta\varepsilon_d := answers_8 = -1.226 \times 10^{-4}$

$\Delta\varepsilon_h := answers_9 = -9.375 \times 10^{-5}$

$\Delta\varepsilon_g := answers_{10} = -3.308 \times 10^{-5}$

$\Delta\varepsilon_{botg} := \Delta\varepsilon_g + \chi_f \cdot c_g = 2.305 \times 10^{-5}$

$\Delta\varepsilon_{topg} := \Delta\varepsilon_g - \chi_f \cdot (depth_g - c_g) = -8.92 \times 10^{-5}$

$\Delta\varepsilon_{both} := \Delta\varepsilon_h + \chi_f \cdot \frac{t_h}{2} = -8.92 \times 10^{-5}$

$\Delta\varepsilon_{toph} := \Delta\varepsilon_h - \chi_f \cdot \frac{t_h}{2} = -9.831 \times 10^{-5}$

$\Delta\varepsilon_{botd} := \Delta\varepsilon_d + \chi_f \cdot \frac{t_d}{2} = -9.831 \times 10^{-5}$

$\Delta\varepsilon_{topd} := \Delta\varepsilon_d - \chi_f \cdot \frac{t_d}{2} = -1.468 \times 10^{-4}$

$y_{botg} := 0$

$y_{topg} := depth_g = 18.5$

$y_{both} := y_{topg} = 18.5$

$y_{toph} := y_{topg} + t_h = 20$

$y_{botd} := depth_g + t_h = 20$

$y_{topd} := depth_t = 28$

Calculate redistribution of stresses in deck from post-tensioning to composite action

$$\text{microstrains} := 10^6 \cdot \begin{pmatrix} \Delta\varepsilon_{topd} \\ \Delta\varepsilon_{d} \\ \Delta\varepsilon_{botd} \\ \Delta\varepsilon_{h} \\ \Delta\varepsilon_{g} \\ \Delta\varepsilon_{botg} \end{pmatrix} = \begin{pmatrix} -146.846 \\ -122.576 \\ -98.306 \\ -93.755 \\ -33.08 \\ 23.045 \end{pmatrix} \qquad \text{depth} := \begin{pmatrix} y_{topd} \\ y_{d} \\ y_{botd} \\ y_{h} \\ c_{g} \\ y_{botg} \end{pmatrix}$$

$$\text{ms2} := \begin{pmatrix} \text{microstrains}_1 \\ 0 \end{pmatrix} = \begin{pmatrix} -146.846 \\ 0 \end{pmatrix} \qquad \text{depth2} := \begin{pmatrix} y_{topd} \\ y_{topd} \end{pmatrix} = \begin{pmatrix} 28 \\ 28 \end{pmatrix}$$

Graph of change in strains in composite section:

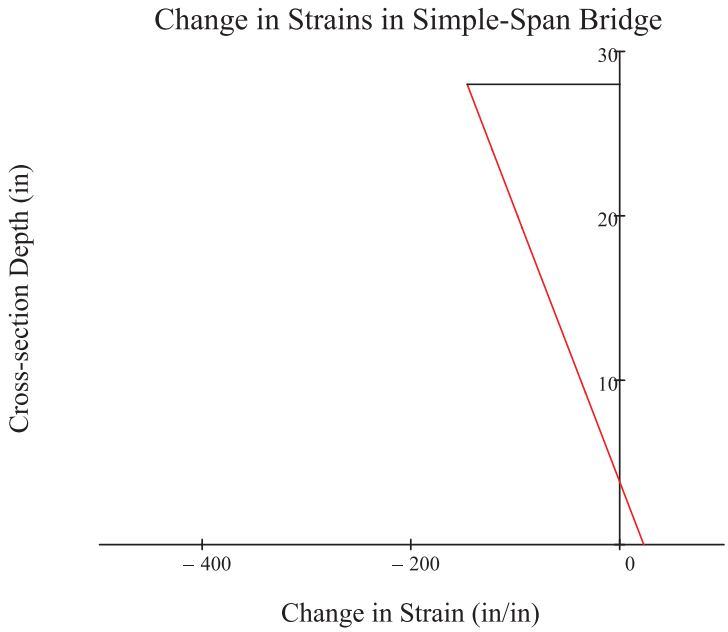

Calculate redistribution of stresses in deck from post-tensioning to composite action

Define values for plot of stress throughout composite cross-section:

$$stress_g := \begin{pmatrix} \Delta\varepsilon_{topg}\cdot E_g \\ \Delta\varepsilon_g\cdot E_g \\ \Delta\varepsilon_{botg}\cdot E_g \end{pmatrix} = \begin{pmatrix} -2.587 \\ -0.959 \\ 0.668 \end{pmatrix} \qquad depths_g := \begin{pmatrix} y_{topg} \\ c_g \\ y_{botg} \end{pmatrix} = \begin{pmatrix} 18.5 \\ 9.25 \\ 0 \end{pmatrix}$$

$\Delta N_d := answers_1 = 15.412$

$\Delta N_h := answers_2 = 7.931$ $\qquad Nd_o = -148.397$

$\Delta M_d := answers_5 = 50.726$ $\qquad Nd_{oc} = -146.184$

$\Delta M_h := answers_6 = 0.044$ $\qquad Nd_f = -130.772$

Stresses in the concrete:

$$stress_d := \begin{bmatrix} \frac{Nd_{oc} + \Delta N_d}{A_d} - \frac{\Delta M_d\cdot\left(\frac{t_d}{2}\right)}{I_d} \\ \frac{Nd_{oc} + \Delta N_d}{A_d} + 0 \\ \frac{Nd_{oc} + \Delta N_d}{A_d} + \frac{\Delta M_d\cdot\left(\frac{t_d}{2}\right)}{I_d} \end{bmatrix} = \begin{pmatrix} -0.453 \\ -0.351 \\ -0.249 \end{pmatrix} \qquad depths_d := \begin{pmatrix} y_{topd} \\ y_d \\ y_{botd} \end{pmatrix} = \begin{pmatrix} 28 \\ 24 \\ 20 \end{pmatrix}$$

$$stress_h := \begin{bmatrix} \frac{\Delta N_h}{A_h} - \frac{\Delta M_h\cdot\left(\frac{t_h}{2}\right)}{I_h} \\ \frac{\Delta N_h}{A_h} + 0 \\ \frac{\Delta N_h}{A_h} + \frac{\Delta M_h\cdot\left(\frac{t_h}{2}\right)}{I_h} \end{bmatrix} = \begin{pmatrix} 0.677 \\ 0.692 \\ 0.708 \end{pmatrix} \qquad depths_h := \begin{pmatrix} y_{toph} \\ y_h \\ y_{both} \end{pmatrix} = \begin{pmatrix} 20 \\ 19.25 \\ 18.5 \end{pmatrix}$$

$$depths_{hz1} := \begin{pmatrix} y_{topd} \\ y_{topd} \end{pmatrix} \qquad depths_{hz2} := \begin{pmatrix} y_{botd} \\ y_{toph} \end{pmatrix} \qquad depths_{hz3} := \begin{pmatrix} y_{both} \\ y_{topg} \end{pmatrix}$$

$$stress_{hz1} := \begin{pmatrix} stress_{d_1} \\ 0 \end{pmatrix} \qquad stress_{hz2} := \begin{pmatrix} stress_{d_3} \\ stress_{h_1} \end{pmatrix} \qquad stress_{hz3} := \begin{pmatrix} stress_{h_3} \\ stress_{g_1} \end{pmatrix}$$

Calculate redistribution of stresses in deck from post-tensioning to composite action

Graph of stresses in composite section (ksi):

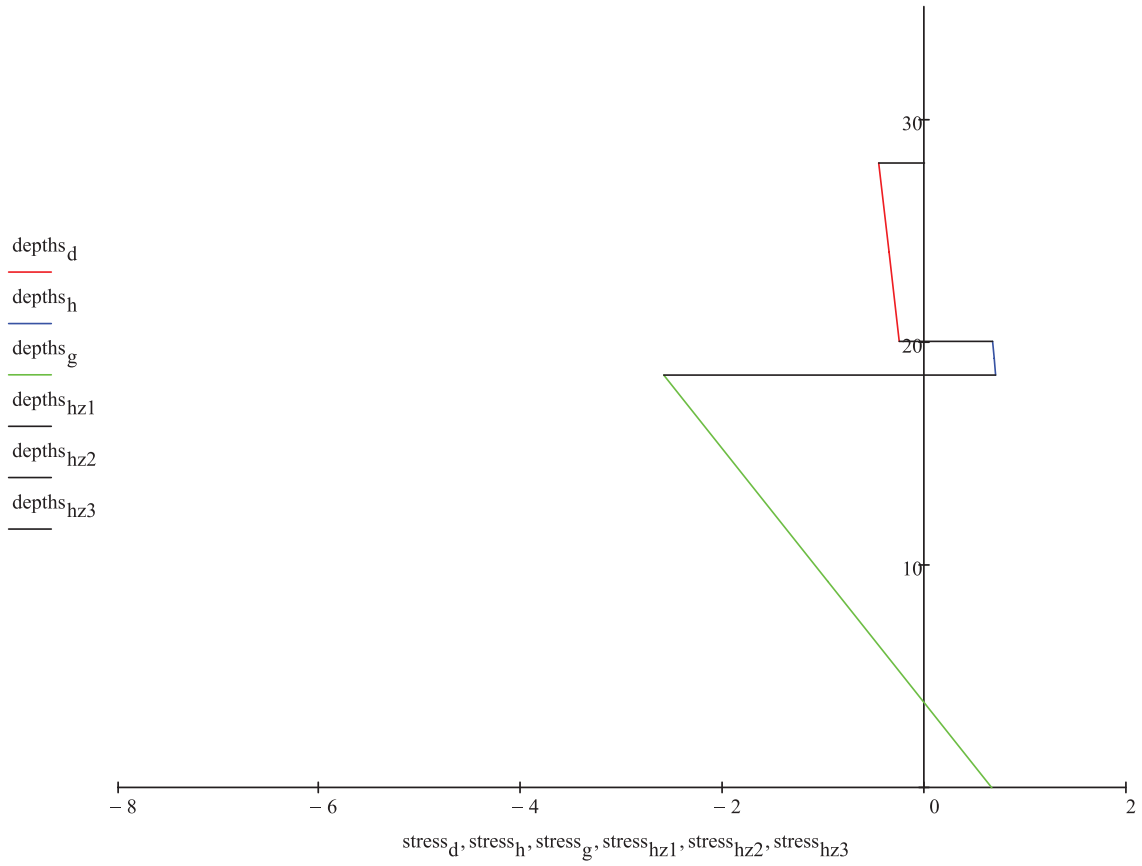

Conclusions for simple span with steel girder:

Initial compression in deck: $\sigma simple_{initial} := \frac{Nd_o}{A_d} = -0.398$ ksi

Final compression at top, middle, and bottom of the deck: $stress_d = \begin{pmatrix} -0.453 \\ -0.351 \\ -0.249 \end{pmatrix}$ ksi

Calculate redistribution of stresses in deck from post-tensioning to composite action

Transformed section properties for composite section including haunch:

$$\phi_{dc} := \text{CREEP}\left(fc_d, t_{dcomp}, t_{dinf}, hum, A_d, perim_d\right) = 0.706$$

$$\phi_{hc} := \text{CREEP}\left(fc_h, t_{hcomp}, t_{hinf}, hum, A_h, perim_h\right) = 1.224$$

Transformed section properties:

Deck: $n_{dg} := \frac{E_d}{E_g} = 0.217$ $\quad Ad_{tr} := n_{dg} \cdot A_d = 80.75\ in^2$

P/T Strands: $n_{pg} := \frac{Ept_d}{E_g} = 0.983$ $\quad Aps_{tr} := n_{pg} \cdot Apt_d = 0.853$

Haunch: $n_{hg} := \frac{E_h}{E_g} = 0.217$ $\quad Ah_{tr} := n_{hg} \cdot A_h = 2.484$

$$A_{tr} := A_g + Aps_{tr} + Ad_{tr} + Ah_{tr} = 104.893$$

$$c_{tr} := \frac{A_g \cdot c_g + Aps_{tr} \cdot y_{ps} + Ad_{tr} \cdot y_d + Ah_{tr} \cdot y_h}{A_{tr}} = 20.963$$

$$I_{tr} := I_g + A_g \cdot \left(c_{tr} - c_g\right)^2 + Aps_{tr} \cdot \left(y_{ps} - c_{tr}\right)^2 + I_d \cdot n_{dg} + Ad_{tr} \cdot \left(y_d - c_{tr}\right)^2 + I_h \cdot n_{hg} + Ah_{tr} \cdot \left(y_h - c_{tr}\right)^2 = 5214.8$$

Age-adjusted transformed section:

$$E_{daatr} := \frac{E_d}{1 + \mu_d \cdot \phi_{dc}} = 4208.173 \qquad E_{haatr} := \frac{E_h}{1 + \mu_h \cdot \phi_{hc}} = 3385.343$$

Deck: $n_{dga} := \frac{E_{daatr}}{E_g} = 0.145$ $\quad Ad_{atr} := n_{dga} \cdot A_d = 54.053$

P/T Strands: $n_{pga} := \frac{Ept_d}{E_g} = 0.983$ $\quad Aps_{atr} := n_{pga} \cdot Apt_d = 0.853$

Haunch: $n_{hga} := \frac{E_{haatr}}{E_g} = 0.117$ $\quad Ah_{atr} := n_{hga} \cdot A_h = 1.338$

$$A_{atr} := A_g + Aps_{atr} + Ad_{atr} + Ah_{atr} = 77.044$$

$$c_{atr} := \frac{A_g \cdot c_g + Aps_{atr} \cdot y_{ps} + Ad_{atr} \cdot y_d + Ah_{atr} \cdot y_h}{A_{atr}} = 19.935$$

$$I_{atr} := I_g + A_g \cdot \left(c_{atr} - c_g\right)^2 + Aps_{atr} \cdot \left(y_{ps} - c_{atr}\right)^2 + I_d \cdot n_{dga} + Ad_{atr} \cdot \left(y_d - c_{atr}\right)^2 + I_h \cdot n_{hga} + Ah_{atr} \cdot \left(y_h - c_{atr}\right)^2$$

$$I_{atr} = 4741.166$$

Add continuity to the three span structure (CONTINUED):

Third point deflection (downward) due to constant curvature:

$$\Delta = \chi \cdot \frac{L^2}{9}$$

Third point deflection (upward) due to restoring forces P:

$$\Delta = \frac{P \cdot L^3}{28 \cdot E \cdot I}$$

Values necessary for deflection calculation:

$E_g = 2.9 \times 10^4$ $\quad I_{atr} = 4741.166$ $\quad L_t := len \cdot 12 = 1170$ $\quad \chi_f = 6.068 \times 10^{-6}$

Solve for P: $P := \frac{28 \cdot E_g \cdot I_{atr} \cdot \chi_f \cdot L_t^2}{9 \cdot L_t^3} = 2.218$ kips

Maximum negative moment: $M_{third} := \frac{P \cdot L_t}{3} = 865.146$ kip·in

$$MGraph := \begin{pmatrix} 0 & 0 \\ \frac{L_g}{12} & -M_{third} \\ \frac{2 \cdot L_g}{12} & -M_{third} \\ \frac{3 \cdot L_g}{12} & 0 \end{pmatrix}$$

$stress_{d_1} = -0.453$

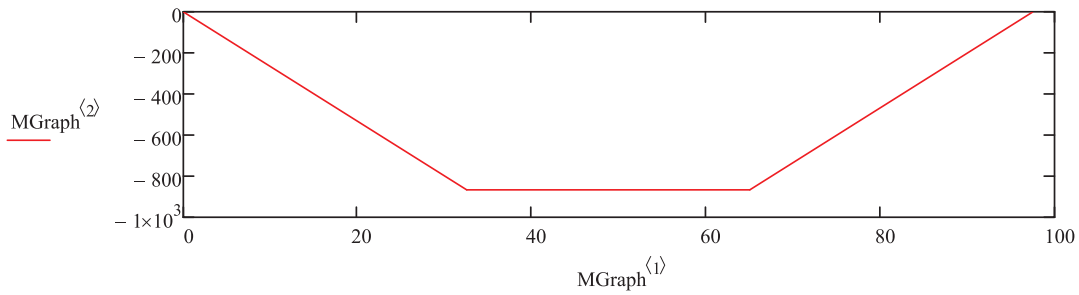

Calculate redistribution of stresses in deck from post-tensioning to composite action

Stress at top, middle, and bottom of the deck in the composite section over a support:

$$\sigma comp_{Mt} := \frac{M_{third} \cdot (depth_t - c_{atr})}{I_{atr}} \cdot n_{dga} = 0.214 \quad ksi$$

$$\sigma comp_{Mm} := \frac{M_{third} \cdot \left(depth_t - c_{atr} - \frac{t_d}{2}\right)}{I_{atr}} \cdot n_{dga} = 0.108 \quad ksi$$

$$\sigma comp_{Mb} := \frac{M_{third} \cdot (depth_t - c_{atr} - t_d)}{I_{atr}} \cdot n_{dga} = 0.002 \quad ksi$$

Strains due to secondary moment effects of 3-span bridge analysis at vwg locations:

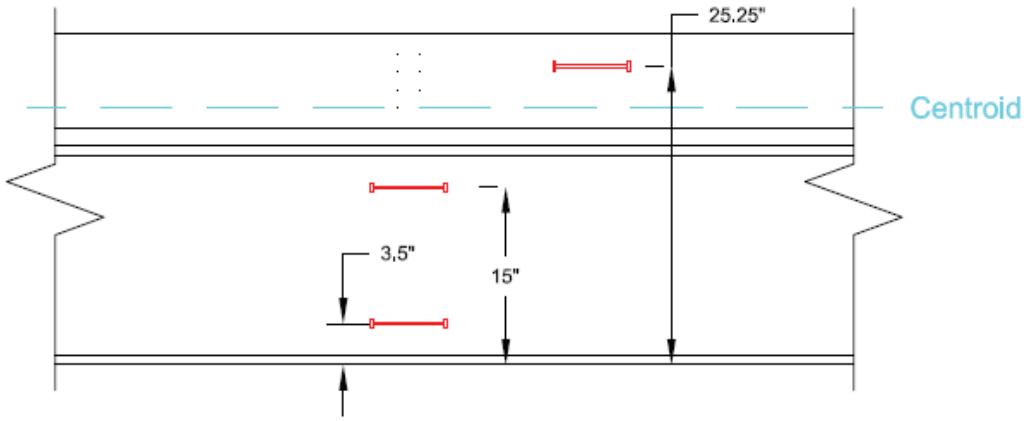

At gauge location 3.75 ft from interior pier: $c_{atr} = 19.935 \quad in$

$$\varepsilon 1_{vwgt} := \frac{M_{third} \cdot \left(\frac{32.5 - 3.75}{32.5}\right) \cdot (25.25 - c_{atr})}{I_{atr} \cdot E_g} = 2.958 \times 10^{-5}$$

$$\varepsilon 1_{vwgm} := \frac{M_{third} \cdot \left(\frac{32.5 - 3.75}{32.5}\right) \cdot (15 - c_{atr})}{I_{atr} \cdot E_g} = -2.747 \times 10^{-5}$$

$$\varepsilon 1_{vwgb} := \frac{M_{third} \cdot \left(\frac{32.5 - 3.75}{32.5}\right) \cdot (3.5 - c_{atr})}{I_{atr} \cdot E_g} = -9.148 \times 10^{-5}$$

Calculate redistribution of stresses in deck from post-tensioning to composite action

At gauge location 23.75 ft from interior pier: $c_{atr} = 19.935 \text{ in}$

$$\varepsilon 2_{vwgt} := \frac{M_{third}\cdot\left(\frac{32.5 - 23.75}{32.5}\right)\cdot(25.25 - c_{atr})}{I_{atr}\cdot E_g} = 9.003 \times 10^{-6}$$

$$\varepsilon 2_{vwgm} := \frac{M_{third}\cdot\left(\frac{32.5 - 23.75}{32.5}\right)\cdot(15 - c_{atr})}{I_{atr}\cdot E_g} = -8.361 \times 10^{-6}$$

$$\varepsilon 2_{vwgb} := \frac{M_{third}\cdot\left(\frac{32.5 - 23.75}{32.5}\right)\cdot(3.5 - c_{atr})}{I_{atr}\cdot E_g} = -2.784 \times 10^{-5}$$

Strains in simple span composite section at vwg locations:

$\Delta\varepsilon_{topd} = -1.468 \times 10^{-4}$ $\Delta\varepsilon_{botg} = 2.305 \times 10^{-5}$

$$slope := \frac{(\Delta\varepsilon_{topd} - \Delta\varepsilon_{botg})}{depth_t} = -6.068 \times 10^{-6}$$

$\varepsilon_{initial}(ht) := \Delta\varepsilon_{botg} + ht\cdot slope$

$\varepsilon i_{vwgt} := \varepsilon_{initial}(25.25) = -1.302 \times 10^{-4}$

$\varepsilon i_{vwgm} := \varepsilon_{initial}(15) = -6.797 \times 10^{-5}$

$\varepsilon i_{vwgb} := \varepsilon_{initial}(3.5) = 1.809 \times 10^{-6}$

Calculate redistribution of stresses in deck from post-tensioning to composite action

Strain Plots:

$$\varepsilon 2nd_1 := \begin{pmatrix} 0 & 25.25 \\ \varepsilon 1_{vwgt} & 25.25 \\ \varepsilon 1_{vwgm} & 15 \\ \varepsilon 1_{vwgb} & 3.5 \\ 0 & 3.5 \end{pmatrix} \qquad \varepsilon 2nd_2 := \begin{pmatrix} 0 & 25.25 \\ \varepsilon 2_{vwgt} & 25.25 \\ \varepsilon 2_{vwgm} & 15 \\ \varepsilon 2_{vwgb} & 3.5 \\ 0 & 3.5 \end{pmatrix} \qquad \varepsilon 1st := \begin{pmatrix} 0 & 25.25 \\ \varepsilon i_{vwgt} & 25.25 \\ \varepsilon i_{vwgm} & 15 \\ \varepsilon i_{vwgb} & 3.5 \\ 0 & 3.5 \end{pmatrix}$$

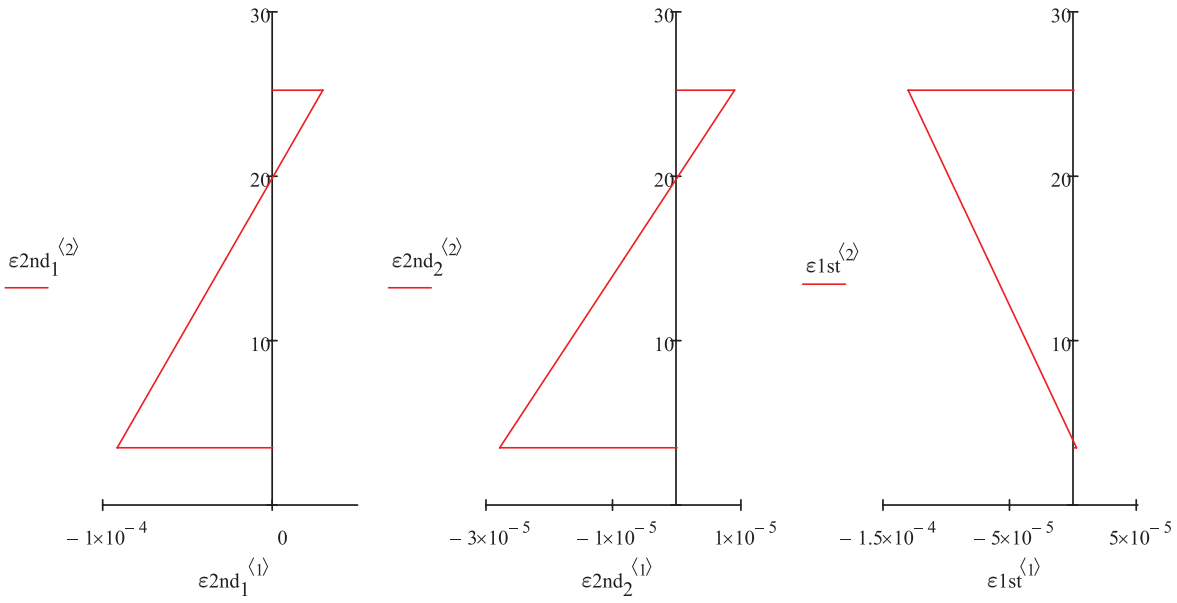

Calculate redistribution of stresses in deck from post-tensioning to composite action

Change in strain at gauge locations:

At gauge location 3.75 ft from interior pier:

$\varepsilon 1f_{vwgt} := \left(\varepsilon i_{vwgt} + \varepsilon 1_{vwgt}\right)\cdot 10^{6} = -100.578$ με VWG 8

$\varepsilon 1f_{vwgm} := \left(\varepsilon i_{vwgm} + \varepsilon 1_{vwgm}\right)\cdot 10^{6} = -95.439$ με VWG 3

$\varepsilon 1f_{vwgb} := \left(\varepsilon i_{vwgb} + \varepsilon 1_{vwgb}\right)\cdot 10^{6} = -89.674$ με VWG 4

At gauge location 23.75 ft from interior pier:

$\varepsilon 2f_{vwgt} := \left(\varepsilon i_{vwgt} + \varepsilon 2_{vwgt}\right)\cdot 10^{6} = -121.157$ με VWG 6

$\varepsilon 2f_{vwgm} := \left(\varepsilon i_{vwgm} + \varepsilon 2_{vwgm}\right)\cdot 10^{6} = -76.329$ με VWG 1

$\varepsilon 2f_{vwgb} := \left(\varepsilon i_{vwgb} + \varepsilon 2_{vwgb}\right)\cdot 10^{6} = -26.034$ με VWG 2

Initial predicted strains at gauge locations:

At gauge location 3.75 ft from interior pier:

$\varepsilon p1_{vwgt} := -49.516$ με VWG 8

$\varepsilon p1_{vwgm} := 34.808$ με VWG 3

$\varepsilon p1_{vwgb} := -34.808$ με VWG 4

At gauge location 23.75 ft from interior pier:

$\varepsilon p2_{vwgt} := -48.453$ με VWG 6

$\varepsilon p2_{vwgm} := -71.427$ με VWG 1

$\varepsilon p2_{vwgb} := 71.427$ με VWG 2

Stress limit (tension): $\frac{1.5\cdot\sqrt{fc_d}}{1000} = 0.125$ ksi

Calculate redistribution of stresses in deck from post-tensioning to composite action

Extrapolated strains at the top and bottom of the composite section:

$$slope1 := \frac{\left(\varepsilon 1f_{vwgm} - \varepsilon 1f_{vwgb}\right)}{11.5} = -0.501 \qquad \varepsilon 1_{final}(ht) := \varepsilon 1f_{vwgb} + ht \cdot slope1$$

$$\varepsilon 1f_{top} := \varepsilon 1_{final}(24.5) = -101.956 \qquad \varepsilon 1f_{bot} := \varepsilon 1_{final}(-3.5) = -87.92$$

$$slope2 := \frac{\left(\varepsilon 2f_{vwgm} - \varepsilon 2f_{vwgb}\right)}{11.5} = -4.373 \qquad \varepsilon 2_{final}(ht) := \varepsilon 2f_{vwgb} + ht \cdot slope2$$

$$\varepsilon 2f_{top} := \varepsilon 2_{final}(24.5) = -133.184 \qquad \varepsilon 2f_{bot} := \varepsilon 2_{final}(-3.5) = -10.727$$

$$slope3 := \frac{\left(\varepsilon p1_{vwgm} - \varepsilon p1_{vwgb}\right)}{11.5} = 6.054 \qquad \varepsilon 3_{pred}(ht) := \varepsilon p1_{vwgb} + ht \cdot slope3$$

$$\varepsilon 1p_{top} := \varepsilon 3_{pred}(15) = 55.995 \qquad \varepsilon 1p_{bot} := \varepsilon 3_{pred}(-3.5) = -55.995$$

$$slope4 := \frac{\left(\varepsilon p2_{vwgm} - \varepsilon p2_{vwgb}\right)}{11.5} = -12.422 \qquad \varepsilon 4_{pred}(ht) := \varepsilon p2_{vwgb} + ht \cdot slope4$$

$$\varepsilon 2p_{top} := \varepsilon 4_{pred}(15) = -114.904 \qquad \varepsilon 2p_{bot} := \varepsilon 4_{pred}(-3.5) = 114.904$$

Calculate redistribution of stresses in deck from post-tensioning to composite action

Tables to export into Excel:

Predicted initial strain gradient:

$$pred1 := \begin{pmatrix} 28 & 0 \\ 28 & \varepsilon p1_{vwgt} \\ 25.25 & \varepsilon p1_{vwgt} \\ 20 & \varepsilon p1_{vwgt} \\ 20 & 0 \\ 18.5 & 0 \\ 18.5 & \varepsilon 1p_{top} \\ 15 & \varepsilon p1_{vwgm} \\ 3.5 & \varepsilon p1_{vwgb} \\ 0 & \varepsilon 1p_{bot} \\ 0 & 0 \end{pmatrix} = \begin{pmatrix} 28 & 0 \\ 28 & -49.516 \\ 25.25 & -49.516 \\ 20 & -49.516 \\ 20 & 0 \\ 18.5 & 0 \\ 18.5 & 55.995 \\ 15 & 34.808 \\ 3.5 & -34.808 \\ 0 & -55.995 \\ 0 & 0 \end{pmatrix}$$

$$pred2 := \begin{pmatrix} 28 & 0 \\ 28 & \varepsilon p2_{vwgt} \\ 25.25 & \varepsilon p2_{vwgt} \\ 20 & \varepsilon p2_{vwgt} \\ 20 & 0 \\ 18.5 & 0 \\ 18.5 & \varepsilon 2p_{top} \\ 15 & \varepsilon p2_{vwgm} \\ 3.5 & \varepsilon p2_{vwgb} \\ 0 & \varepsilon 2p_{bot} \\ 0 & 0 \end{pmatrix} = \begin{pmatrix} 28 & 0 \\ 28 & -48.453 \\ 25.25 & -48.453 \\ 20 & -48.453 \\ 20 & 0 \\ 18.5 & 0 \\ 18.5 & -114.904 \\ 15 & -71.427 \\ 3.5 & 71.427 \\ 0 & 114.904 \\ 0 & 0 \end{pmatrix}$$

Final change in strain gradient:

$$meas1 := \begin{pmatrix} 28 & 0 \\ 28 & \varepsilon 1f_{top} \\ 25.25 & \varepsilon 1f_{vwgt} \\ 15 & \varepsilon 1f_{vwgm} \\ 3.5 & \varepsilon 1f_{vwgb} \\ 0 & \varepsilon 1f_{bot} \\ 0 & 0 \end{pmatrix} = \begin{pmatrix} 28 & 0 \\ 28 & -101.956 \\ 25.25 & -100.578 \\ 15 & -95.439 \\ 3.5 & -89.674 \\ 0 & -87.92 \\ 0 & 0 \end{pmatrix}$$

$$meas2 := \begin{pmatrix} 28 & 0 \\ 28 & \varepsilon 2f_{top} \\ 25.25 & \varepsilon 2f_{vwgt} \\ 15 & \varepsilon 2f_{vwgm} \\ 3.5 & \varepsilon 2f_{vwgb} \\ 0 & \varepsilon 2f_{bot} \\ 0 & 0 \end{pmatrix} = \begin{pmatrix} 28 & 0 \\ 28 & -133.184 \\ 25.25 & -121.157 \\ 15 & -76.329 \\ 3.5 & -26.034 \\ 0 & -10.727 \\ 0 & 0 \end{pmatrix}$$

Calculate redistribution of stresses in deck from post-tensioning to composite action

Final Strain Plots:

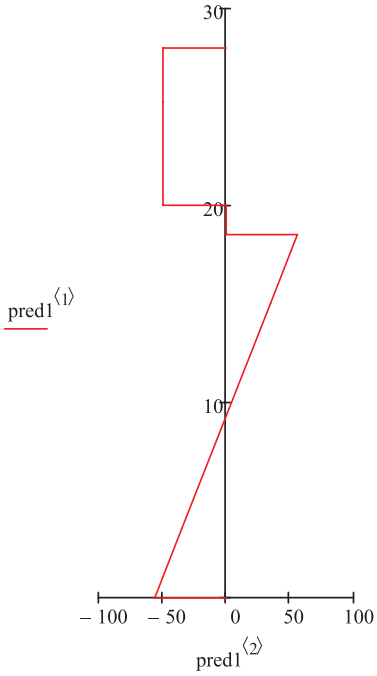

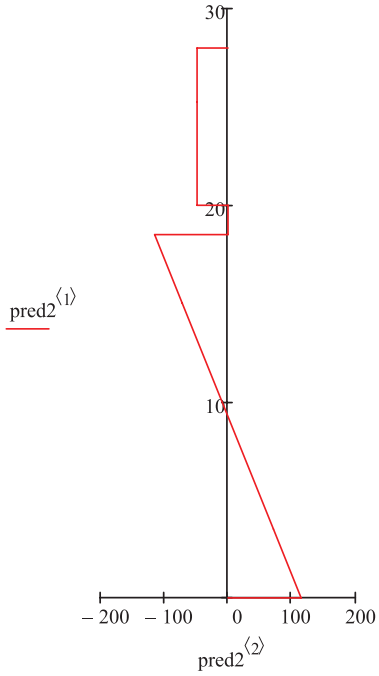

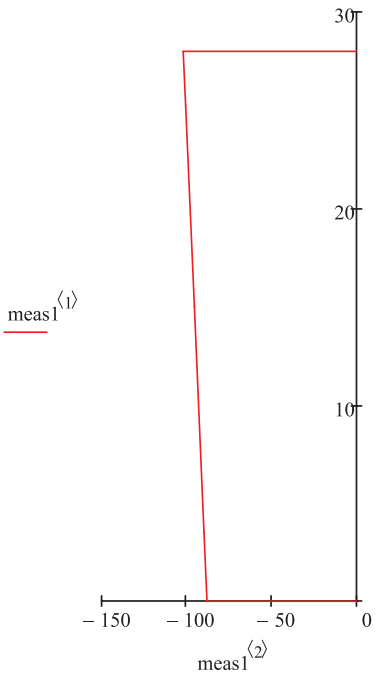

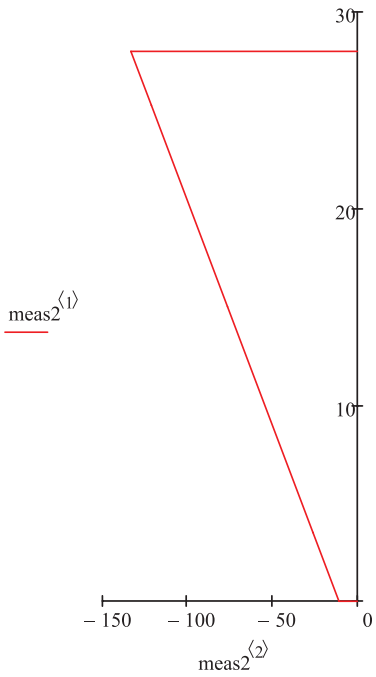

Calculate redistribution of stresses in deck from post-tensioning to composite action

Stress in top fiber due to force redistribution over time at midspan of a single span:

$\sigma comp_{Fredist} := stress_{d_1} = -0.453$ ksi

Obtain live load negative moment over a support from QCon Bridge:

$M_{QCon} := 330347$ ft·lbs

$M_{neg} := M_{QCon} \cdot \frac{12}{1000} = 3964.164$ kip·in

Stress at top of composite section due to live loads (tension):

$$\sigma comp_{LL} := \frac{\left|M_{neg}\right| \cdot \left(depth_t - c_{tr}\right)}{I_{tr}} \cdot n_{dg} = 1.16 \quad \text{ksi}$$

Factor LL using DFM and 0.8 Service III factor:

$$e_g := \frac{t_d}{2} + t_h + \frac{depth_g}{2} = 14.75 \qquad n := \frac{E_g}{E_d} = 4.613 \qquad K_g := n \cdot \left[I_g + \left(A_g \cdot e_g^{\,2}\right)\right] = 2.627 \times 10^4$$

$$DFM_2 := 0.075 + \left[\left(\frac{\frac{w_d}{12}}{9.5}\right)^{0.6} \left(\frac{w_d}{L_g}\right)^{0.2} \left(\frac{K_g}{L_g \cdot t_d^{\,3}}\right)^{0.1}\right] = 0.387$$

$$DFM_1 := 0.06 + \left[\left(\frac{\frac{w_d}{12}}{14}\right)^{0.4} \left(\frac{w_d}{L_g}\right)^{0.3} \left(\frac{K_g}{L_g \cdot t_d^{\,3}}\right)^{0.1}\right] = 0.318$$

$mp := 1 \qquad DFM_f := \frac{DFM_1}{mp} = 0.318 \qquad DFM := \max\left(DFM_2, DFM_1, DFM_f\right) = 0.387$

$\sigma comp_{LLf} := \sigma comp_{LL} \cdot DFM \cdot 0.8 = 0.359$ ksi

Initial compression in deck: $\sigma comp_{initial} := \frac{Nd_o}{A_d} = -0.398$ ksi

Final stress in top of deck: $\sigma comp_{final} := \sigma comp_{Fredist} + \sigma comp_{Mt} + \sigma comp_{LLf} = 0.119$ ksi

Cracking stress at panel joint: $f_c := 7000 \qquad \frac{1.5 \cdot \sqrt{f_c}}{1000} = 0.125$ ksi

Appendix I – Graphs from Live Load Test Runs

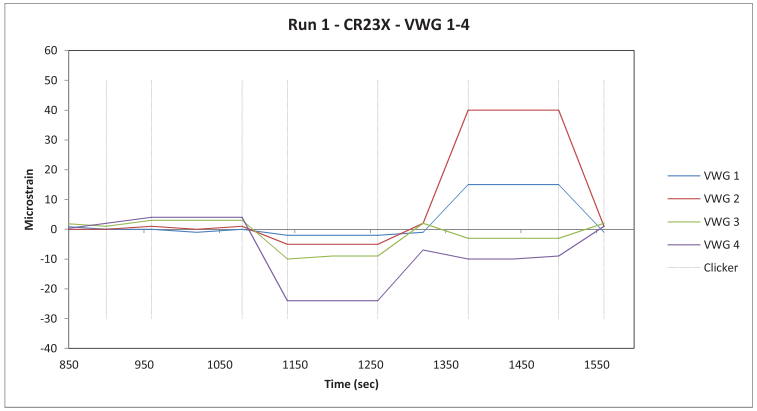
Run 1 - CR23X - VWG 1-4
Microstrain
Time (sec)
VWG 1
VWG 2
VWG 3
VWG 4
Clicker

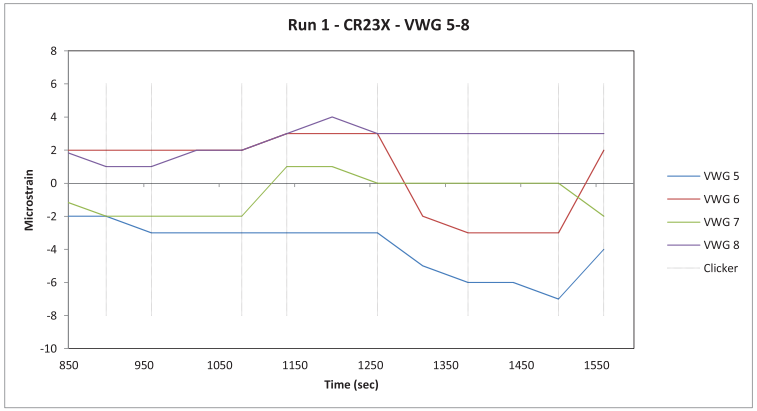
Run 1 - CR23X - VWG 5-8
Microstrain
Time (sec)
VWG 5
VWG 6
VWG 7
VWG 8
Clicker

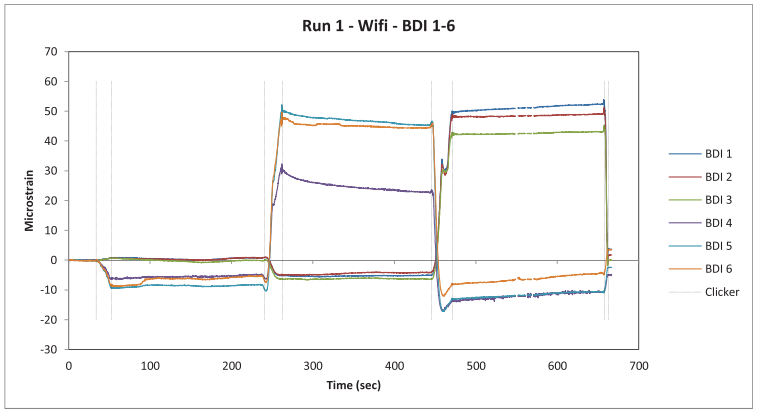
Run 1 - Wifi - BDI 1-6
Microstrain
Time (sec)
BDI 1
BDI 2
BDI 3
BDI 4
BDI 5
BDI 6
Clicker

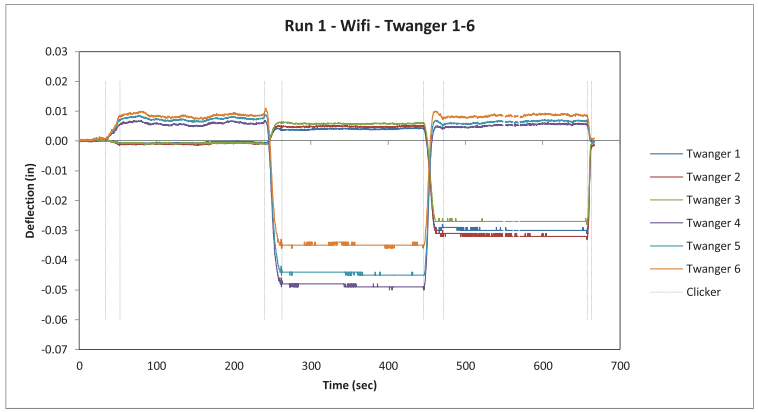
Run 1 - Wifi - Twanger 1-6
Deflection (in)
Time (sec)
Twanger 1
Twanger 2
Twanger 3
Twanger 4
Twanger 5
Twanger 6
Clicker

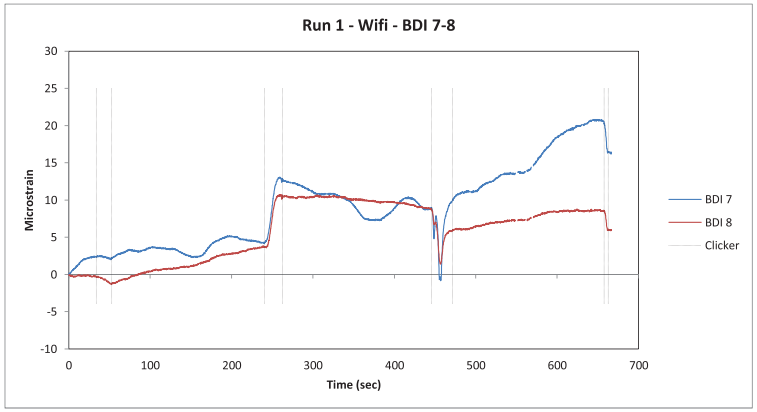
Run 1 - Wifi - BDI 7-8
Microstrain
Time (sec)
BDI 7
BDI 8
Clicker

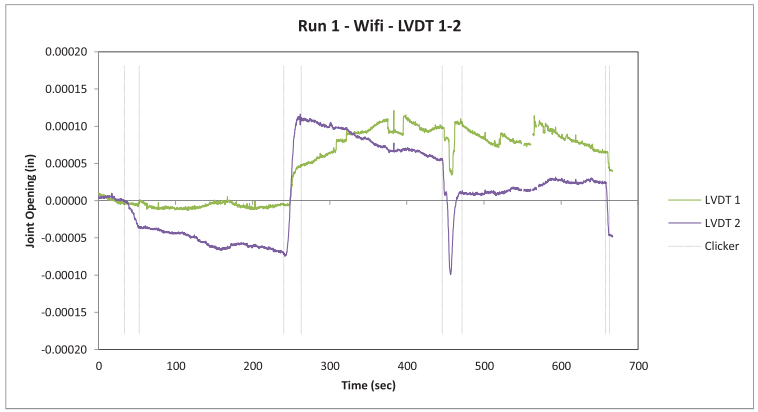
Run 1 - Wifi - LVDT 1-2
Joint Opening (in)
Time (sec)
LVDT 1
LVDT 2
Clicker

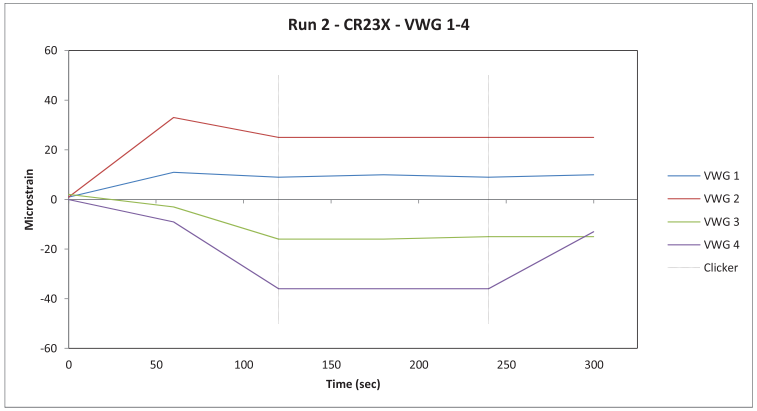
Run 2 - CR23X - VWG 1-4
Microstrain
Time (sec)
VWG 1
VWG 2
VWG 3
VWG 4
Clicker

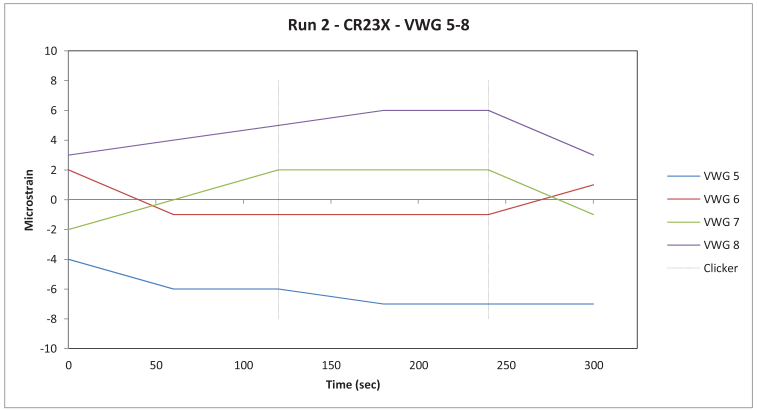
Run 2 - CR23X - VWG 5-8
Microstrain
Time (sec)
VWG 5
VWG 6
VWG 7
VWG 8
Clicker

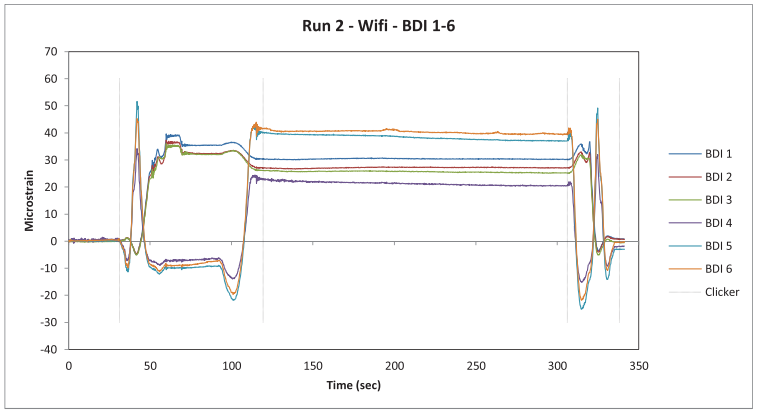
Run 2 - Wifi - BDI 1-6
Microstrain
Time (sec)
BDI 1
BDI 2
BDI 3
BDI 4
BDI 5
BDI 6
Clicker

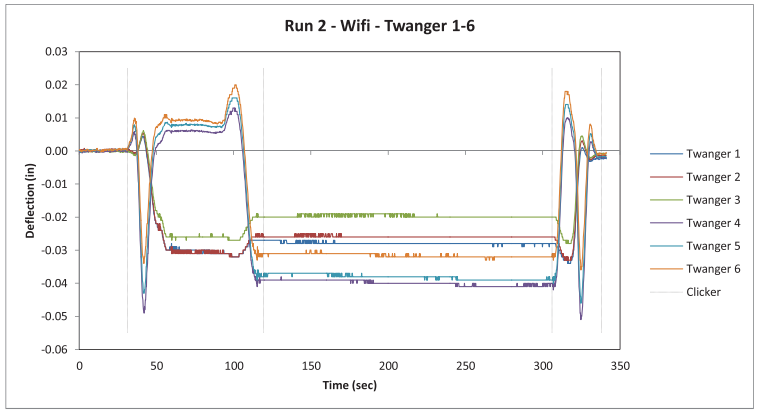
Run 2 - Wifi - Twanger 1-6
Deflection (in)
Time (sec)
Twanger 1
Twanger 2
Twanger 3
Twanger 4
Twanger 5
Twanger 6
Clicker

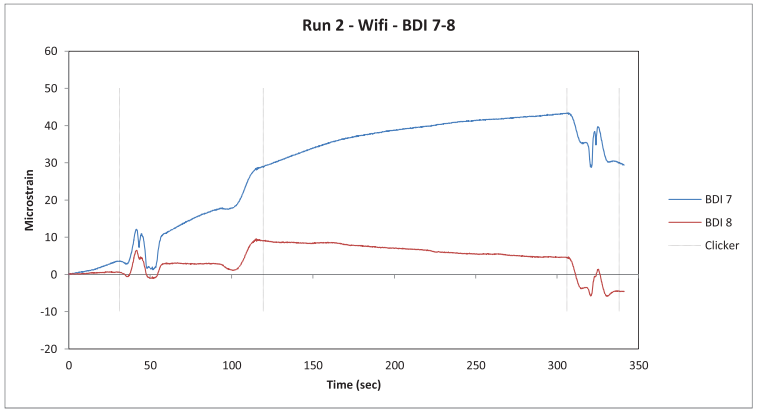
Run 2 - Wifi - BDI 7-8
Microstrain
Time (sec)
BDI 7
BDI 8
Clicker

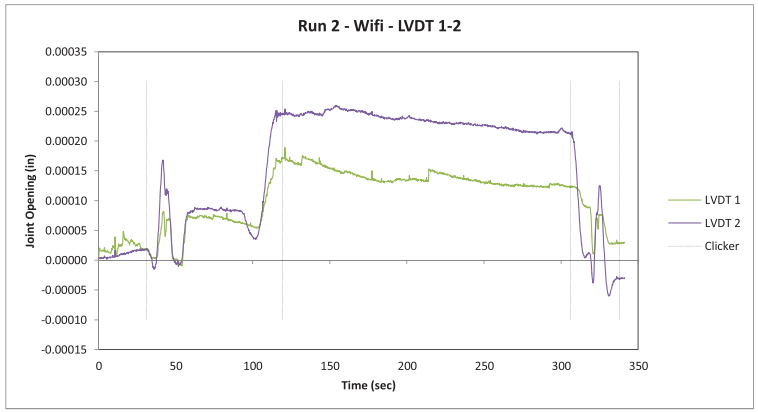
Run 2 - Wifi - LVDT 1-2
Joint Opening (in)
Time (sec)
LVDT 1
LVDT 2
Clicker

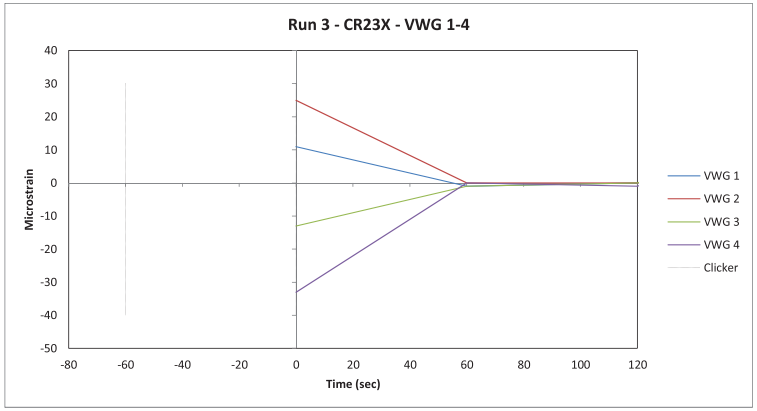
Run 3 - CR23X - VWG 1-4
Microstrain
Time (sec)
VWG 1
VWG 2
VWG 3
VWG 4
Clicker

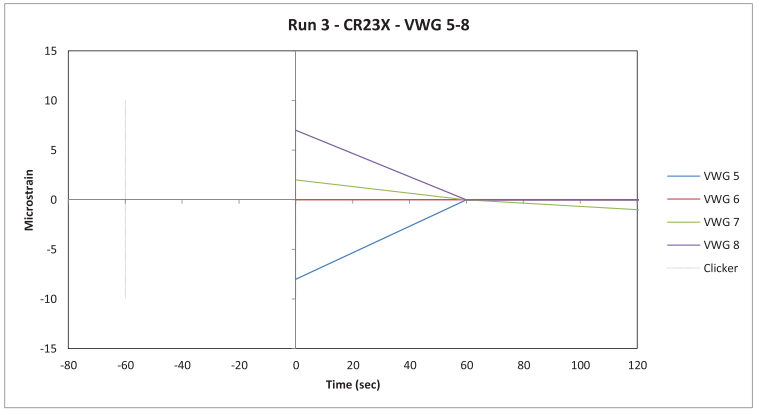
Run 3 - CR23X - VWG 5-8
Microstrain
Time (sec)
VWG 5
VWG 6
VWG 7
VWG 8
Clicker

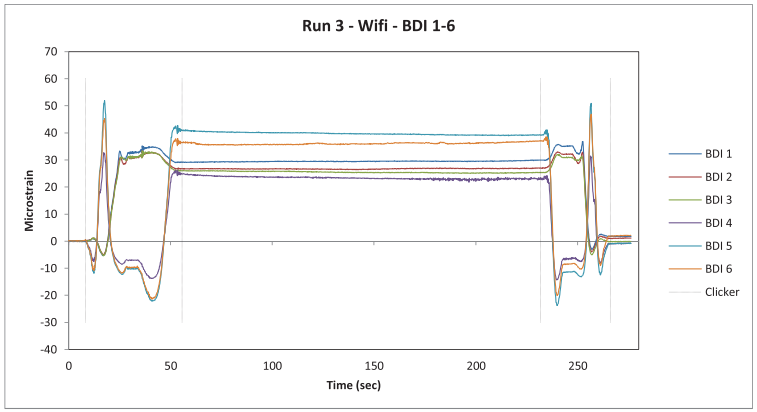
Run 3 - Wifi - BDI 1-6
Microstrain
Time (sec)
BDI 1
BDI 2
BDI 3
BDI 4
BDI 5
BDI 6
Clicker

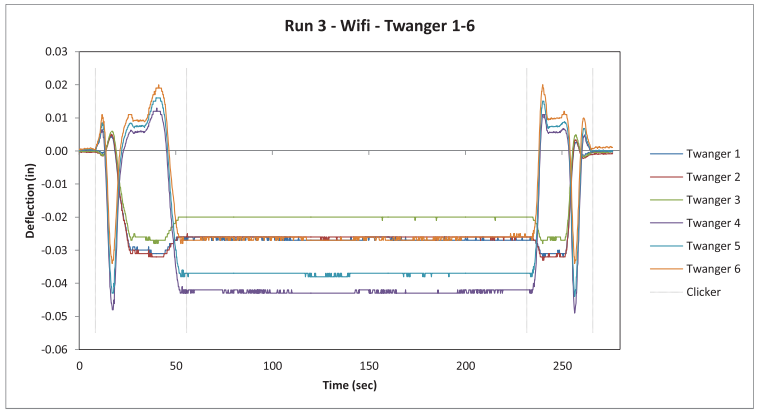
Run 3 - Wifi - Twanger 1-6
Deflection (in)
Time (sec)
Twanger 1
Twanger 2
Twanger 3
Twanger 4
Twanger 5
Twanger 6
Clicker

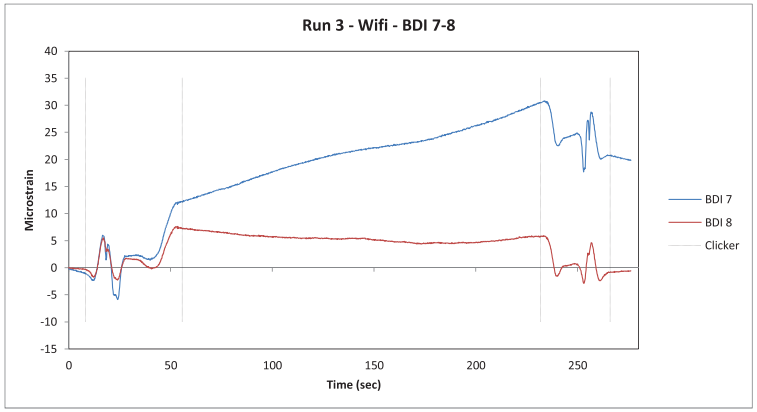
Run 3 - Wifi - BDI 7-8
Microstrain
Time (sec)
BDI 7
BDI 8
Clicker

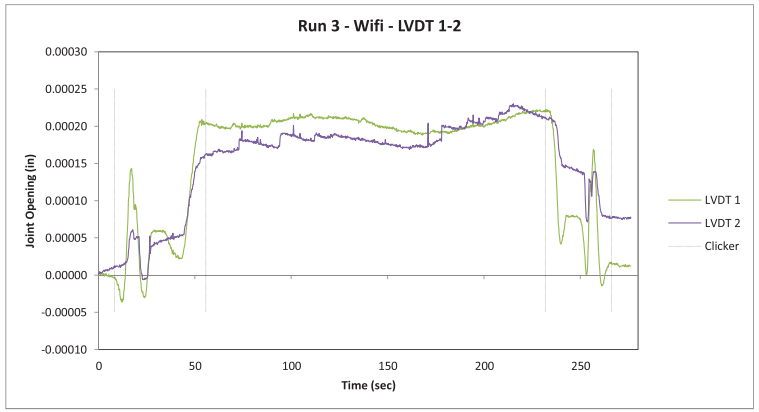
Run 3 - Wifi - LVDT 1-2
Joint Opening (in)
Time (sec)
LVDT 1
LVDT 2
Clicker

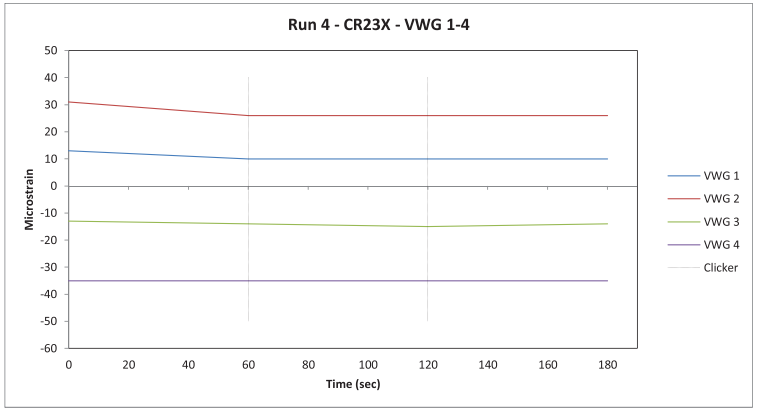
Run 4 - CR23X - VWG 1-4
Microstrain
Time (sec)
VWG 1
VWG 2
VWG 3
VWG 4
Clicker

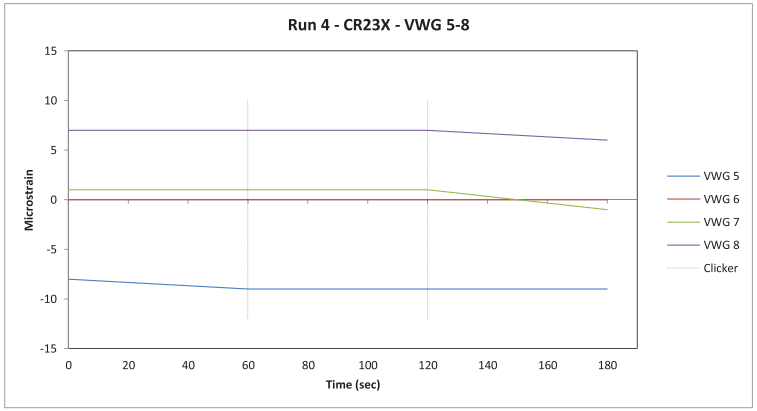
Run 4 - CR23X - VWG 5-8
Microstrain
Time (sec)
VWG 5
VWG 6
VWG 7
VWG 8
Clicker

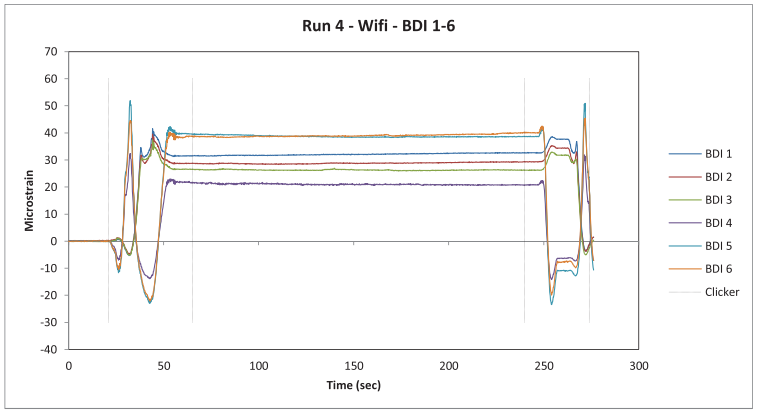
Run 4 - Wifi - BDI 1-6
Microstrain
Time (sec)
BDI 1
BDI 2
BDI 3
BDI 4
BDI 5
BDI 6
Clicker

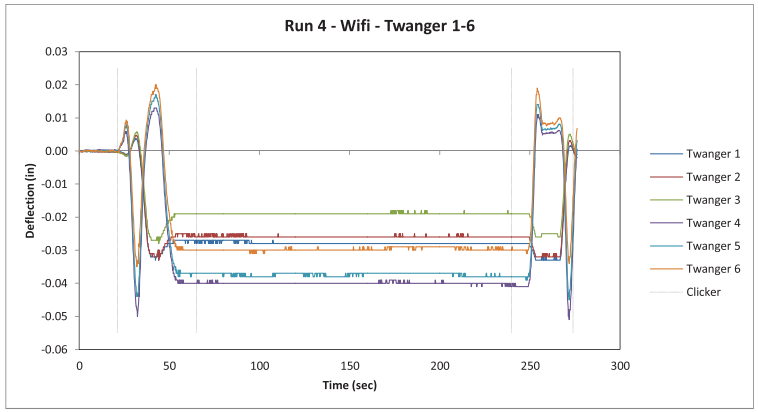
Run 4 - Wifi - Twanger 1-6
Deflection (in)
Time (sec)
Twanger 1
Twanger 2
Twanger 3
Twanger 4
Twanger 5
Twanger 6
Clicker

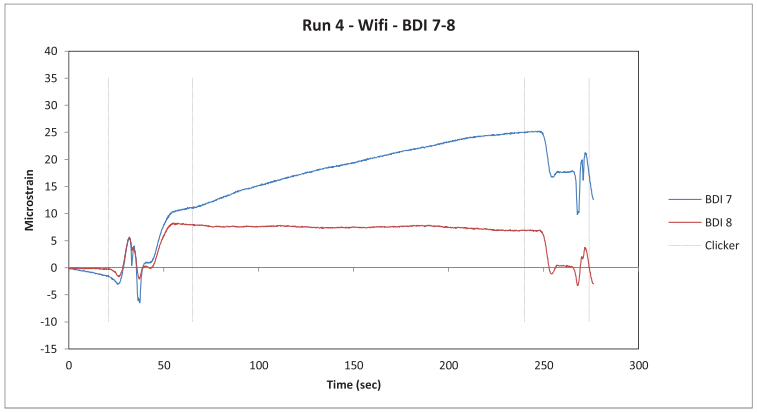
Run 4 - Wifi - BDI 7-8
Microstrain
Time (sec)
BDI 7
BDI 8
Clicker


Run 4 - Wifi - LVDT 1-2
Joint Opening (in)
Time (sec)
LVDT 1
LVDT 2
Clicker

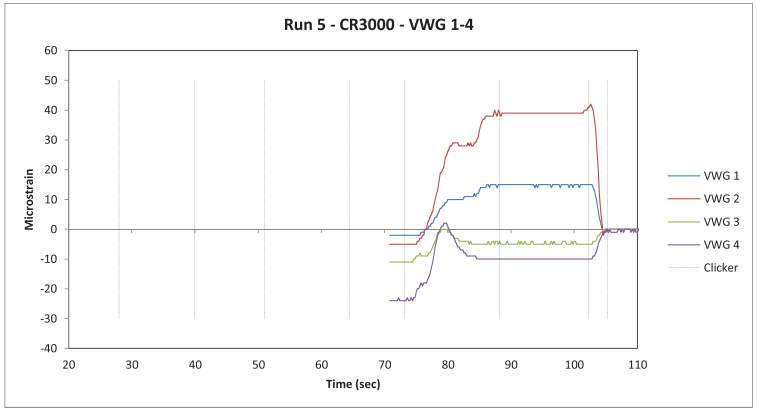
Run 5 - CR3000 - VWG 1-4
Microstrain
Time (sec)
VWG 1
VWG 2
VWG 3
VWG 4
Clicker


Run 5 - CR3000 - VWG 5-8
Microstrain
Time (sec)
VWG 5
VWG 6
VWG 7
VWG 8
Clicker

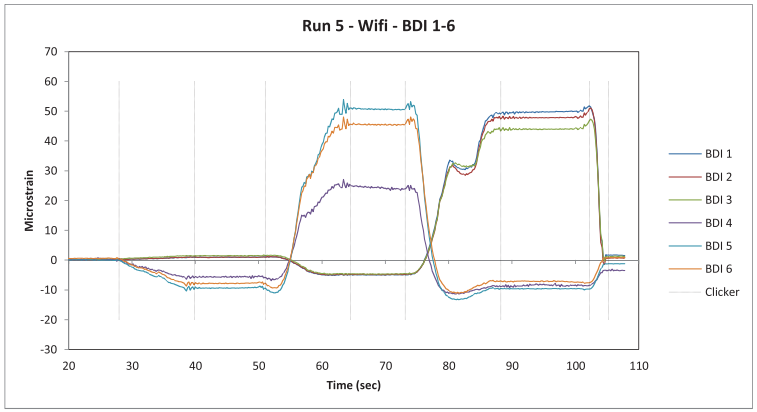
Run 5 - Wifi - BDI 1-6
Microstrain
Time (sec)
BDI 1
BDI 2
BDI 3
BDI 4
BDI 5
BDI 6
Clicker

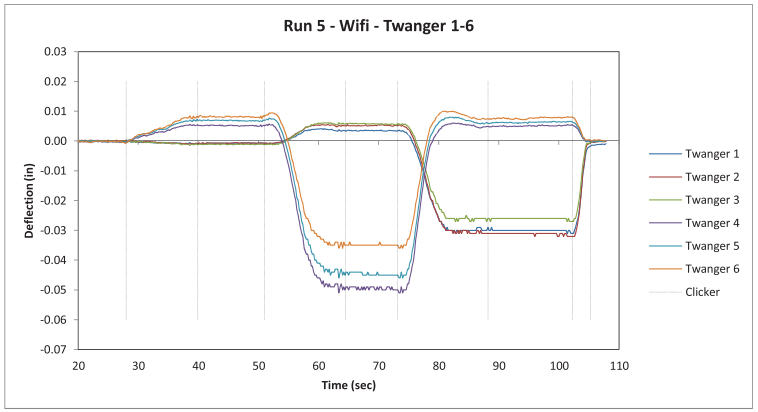
Run 5 - Wifi - Twanger 1-6
Deflection (in)
Time (sec)
Twanger 1
Twanger 2
Twanger 3
Twanger 4
Twanger 5
Twanger 6
Clicker

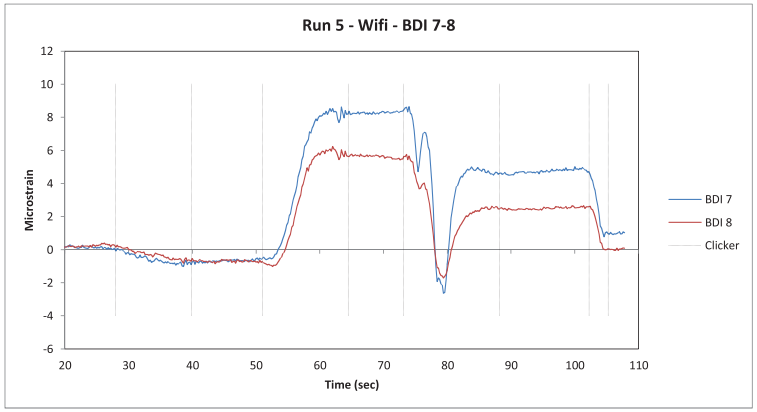
Run 5 - Wifi - BDI 7-8
Microstrain
Time (sec)
BDI 7
BDI 8
Clicker

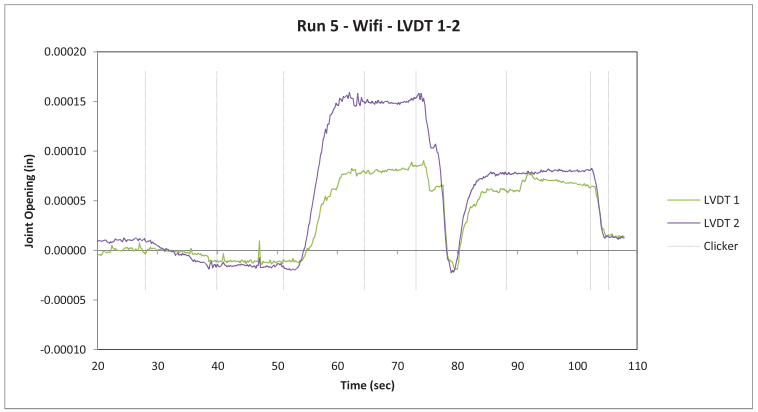
Run 5 - Wifi - LVDT 1-2
Joint Opening (in)
Time (sec)
LVDT 1
LVDT 2
Clicker

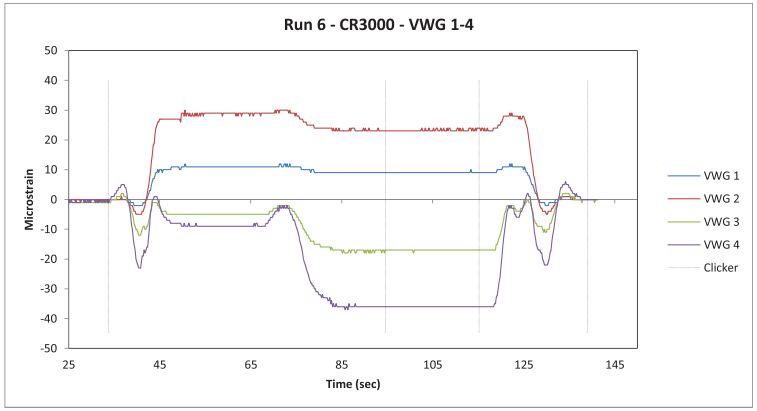
Run 6 - CR3000 - VWG 1-4
Microstrain
Time (sec)
VWG 1
VWG 2
VWG 3
VWG 4
Clicker

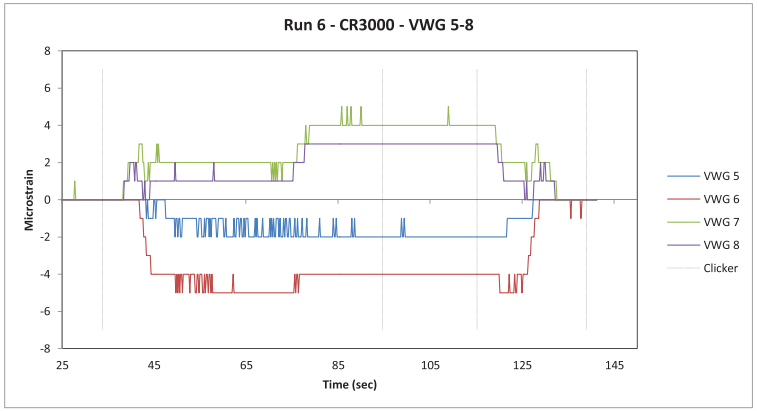
Run 6 - CR3000 - VWG 5-8
Microstrain
Time (sec)
VWG 5
VWG 6
VWG 7
VWG 8
Clicker

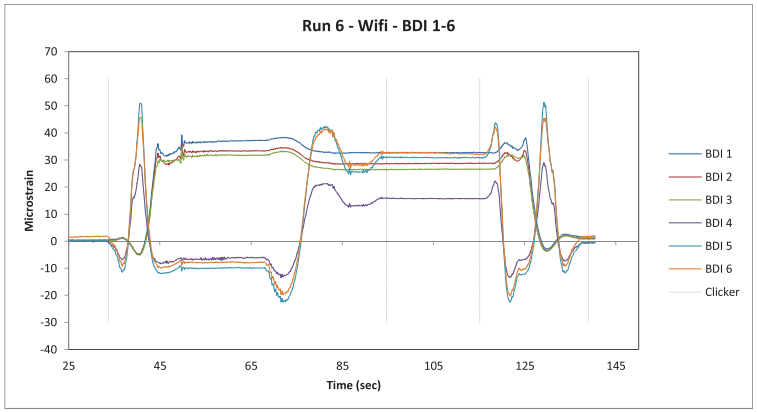
Run 6 - Wifi - BDI 1-6
Microstrain
Time (sec)
BDI 1
BDI 2
BDI 3
BDI 4
BDI 5
BDI 6
Clicker

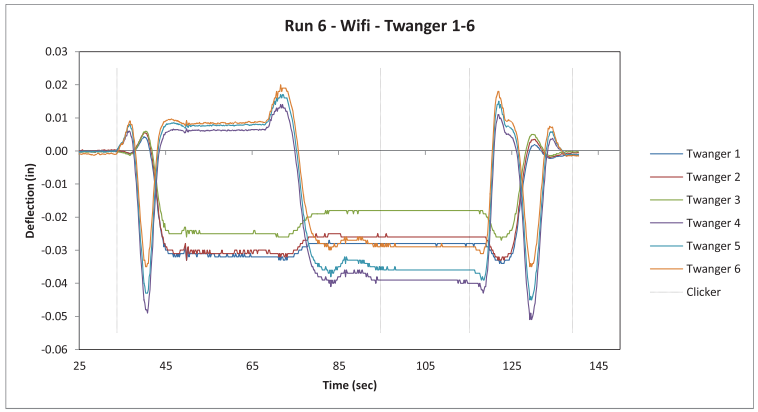
Run 6 - Wifi - Twanger 1-6
Deflection (in)
Time (sec)
Twanger 1
Twanger 2
Twanger 3
Twanger 4
Twanger 5
Twanger 6
Clicker

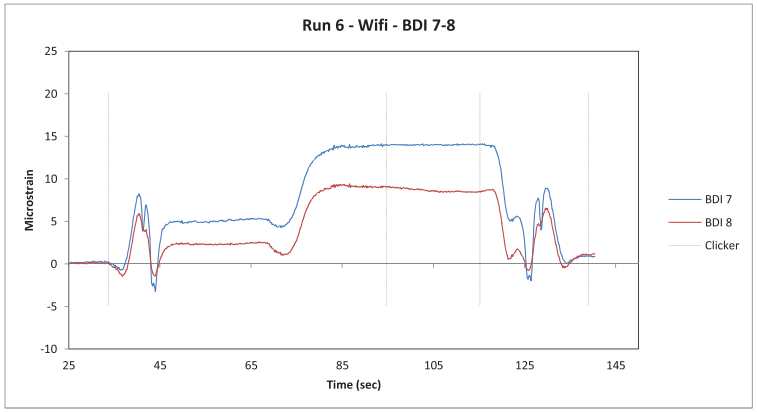
Run 6 - Wifi - BDI 7-8
Microstrain
Time (sec)
BDI 7
BDI 8
Clicker


Run 6 - Wifi - LVDT 1-2
Joint Opening (in)
Time (sec)
LVDT 1
LVDT 2
Clicker

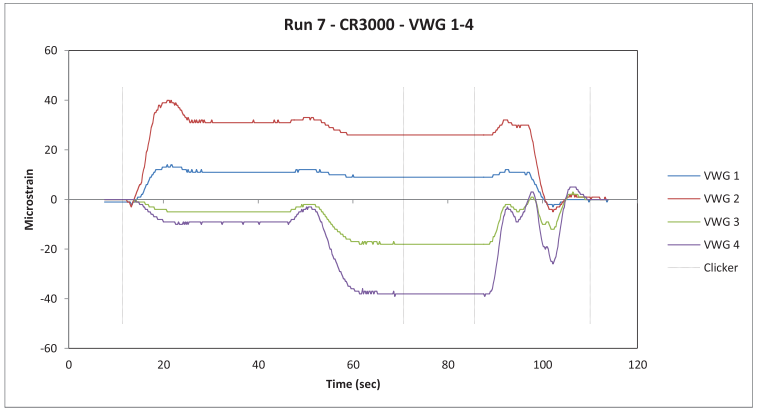
Run 7 - CR3000 - VWG 1-4
Microstrain
Time (sec)
VWG 1
VWG 2
VWG 3
VWG 4
Clicker

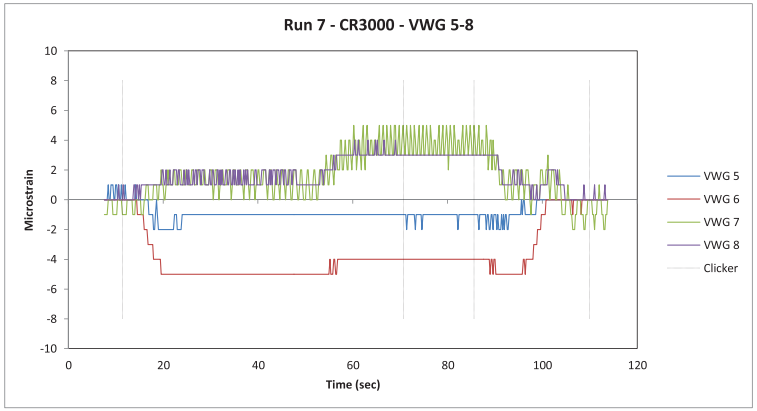
Run 7 - CR3000 - VWG 5-8
Microstrain
Time (sec)
VWG 5
VWG 6
VWG 7
VWG 8
Clicker

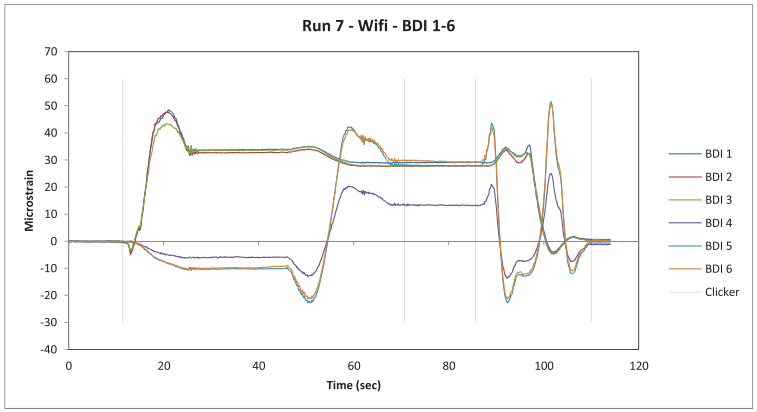
Run 7 - Wifi - BDI 1-6
Microstrain
Time (sec)
BDI 1
BDI 2
BDI 3
BDI 4
BDI 5
BDI 6
Clicker

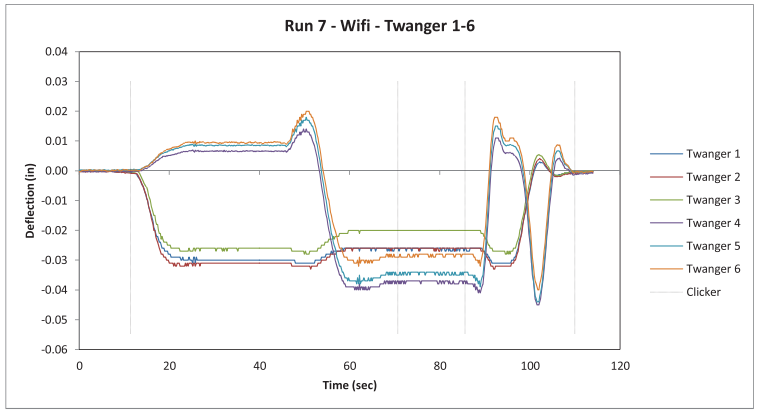
Run 7 - Wifi - Twanger 1-6
Deflection (in)
Time (sec)
Twanger 1
Twanger 2
Twanger 3
Twanger 4
Twanger 5
Twanger 6
Clicker

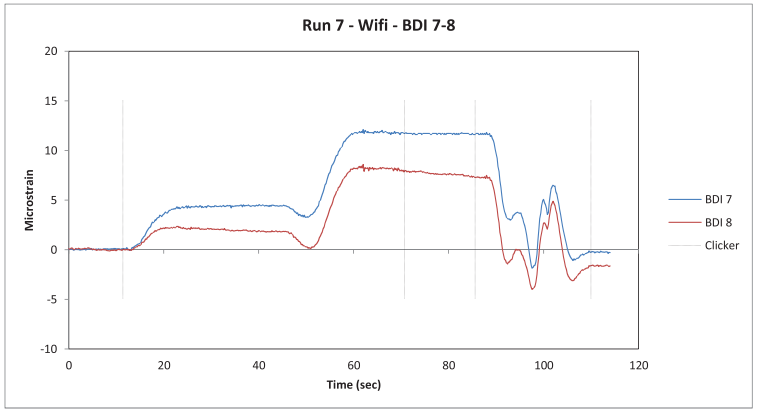
Run 7 - Wifi - BDI 7-8
Microstrain
Time (sec)
BDI 7
BDI 8
Clicker

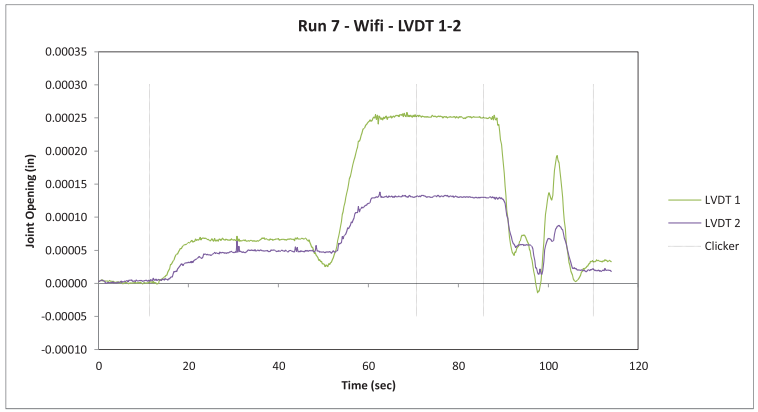
Run 7 - Wifi - LVDT 1-2
Joint Opening (in)
Time (sec)
LVDT 1
LVDT 2
Clicker

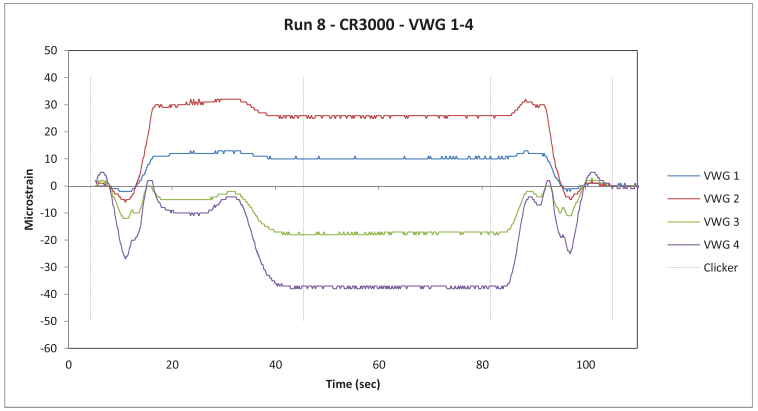
Run 8 - CR3000 - VWG 1-4
Microstrain
Time (sec)
VWG 1
VWG 2
VWG 3
VWG 4
Clicker

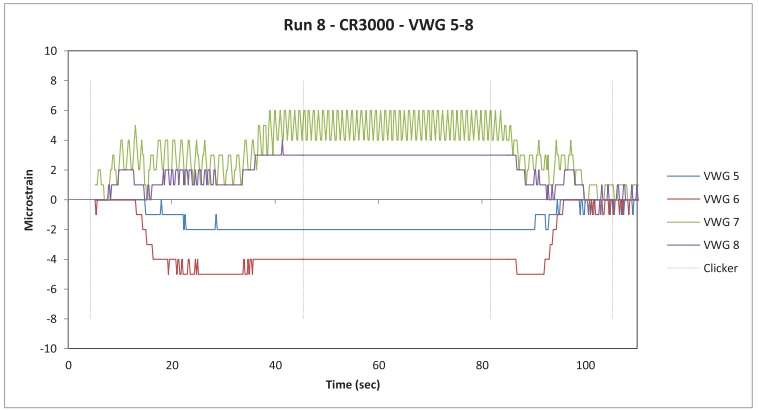
Run 8 - CR3000 - VWG 5-8
Microstrain
Time (sec)
VWG 5
VWG 6
VWG 7
VWG 8
Clicker

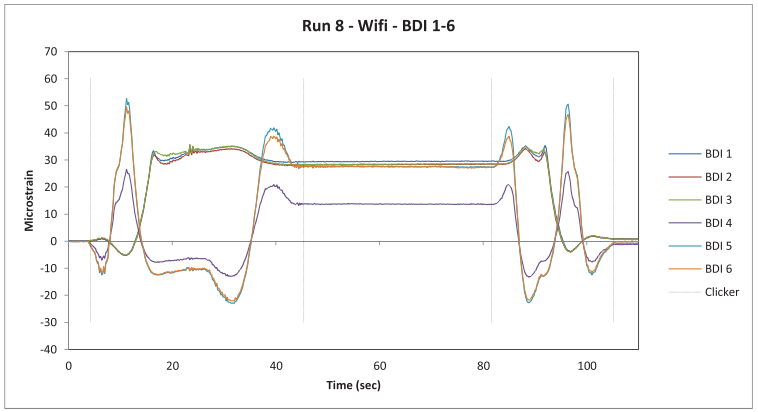
Run 8 - Wifi - BDI 1-6
Microstrain
Time (sec)
BDI 1
BDI 2
BDI 3
BDI 4
BDI 5
BDI 6
Clicker

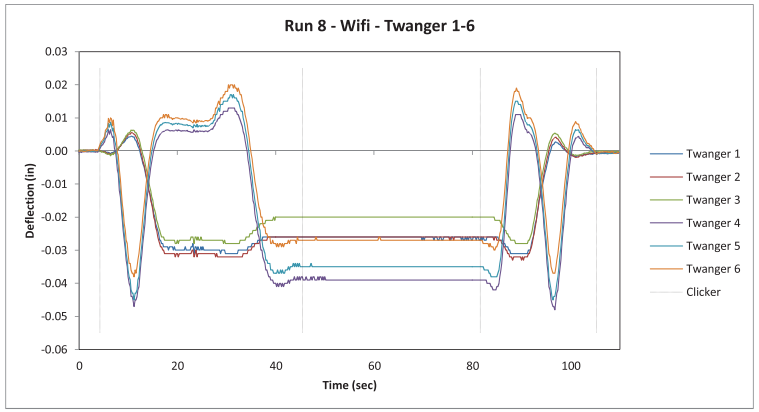
Run 8 - Wifi - Twanger 1-6
Deflection (in)
Time (sec)
Twanger 1
Twanger 2
Twanger 3
Twanger 4
Twanger 5
Twanger 6
Clicker

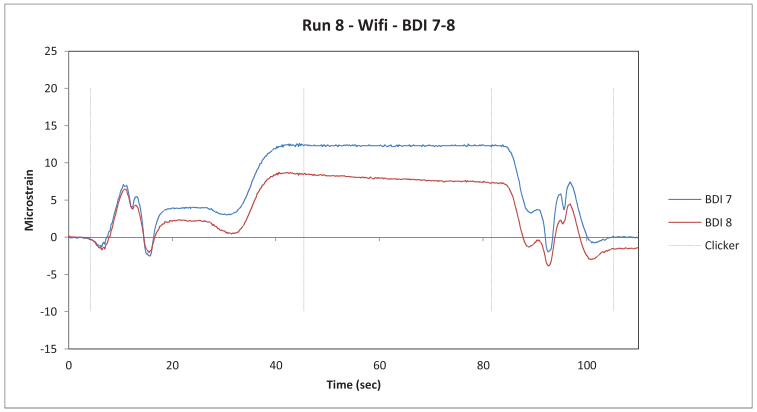
Run 8 - Wifi - BDI 7-8
Microstrain
Time (sec)
BDI 7
BDI 8
Clicker

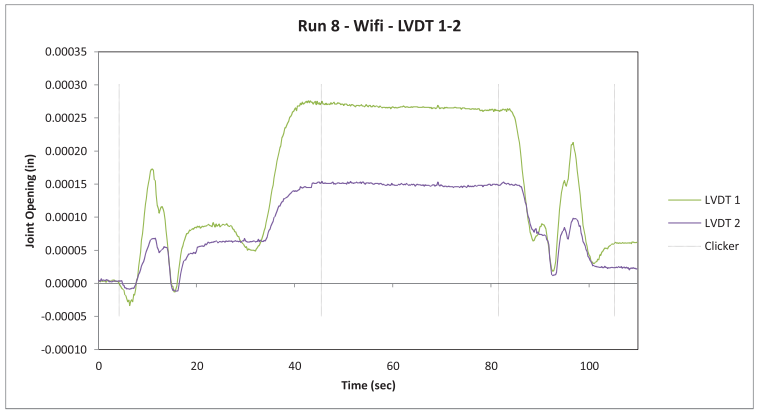
Run 8 - Wifi - LVDT 1-2
Joint Opening (in)
Time (sec)
LVDT 1
LVDT 2
Clicker

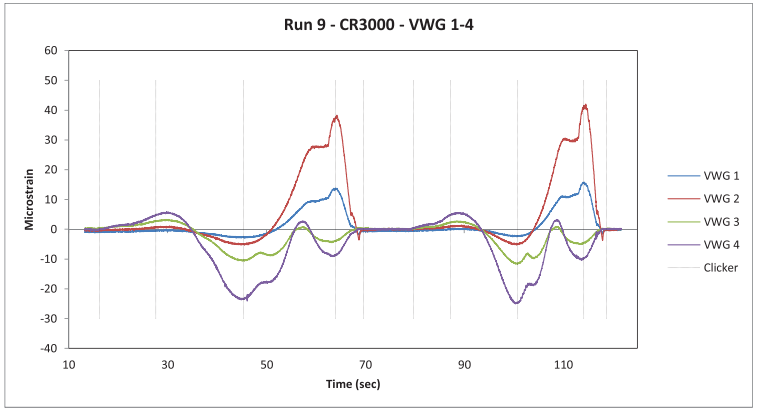
Run 9 - CR3000 - VWG 1-4
Microstrain
Time (sec)
VWG 1
VWG 2
VWG 3
VWG 4
Clicker

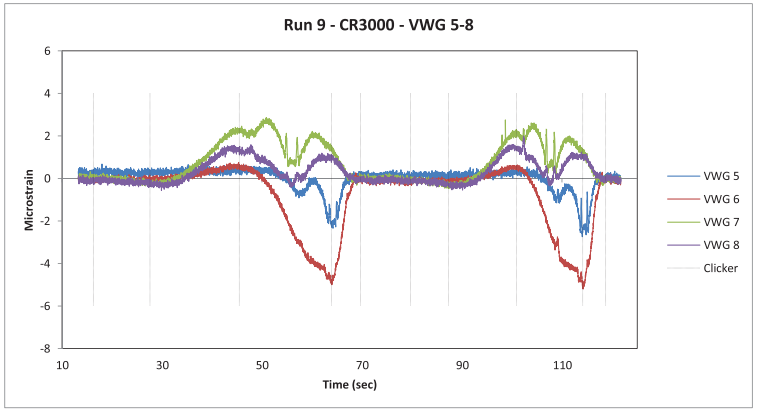
Run 9 - CR3000 - VWG 5-8
Microstrain
Time (sec)
VWG 5
VWG 6
VWG 7
VWG 8
Clicker

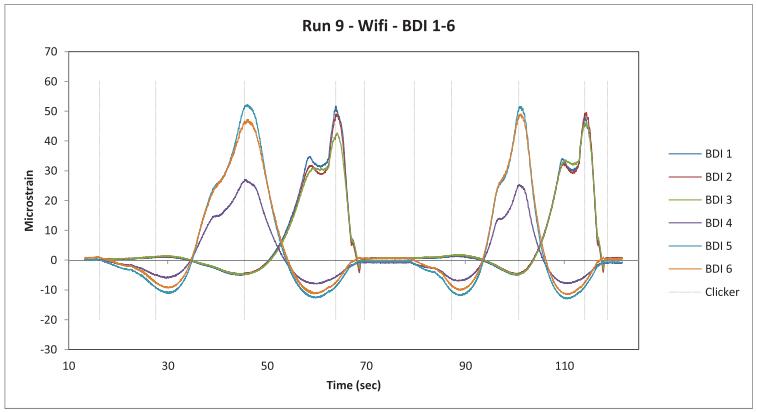
Run 9 - Wifi - BDI 1-6
Microstrain
Time (sec)
BDI 1
BDI 2
BDI 3
BDI 4
BDI 5
BDI 6
Clicker

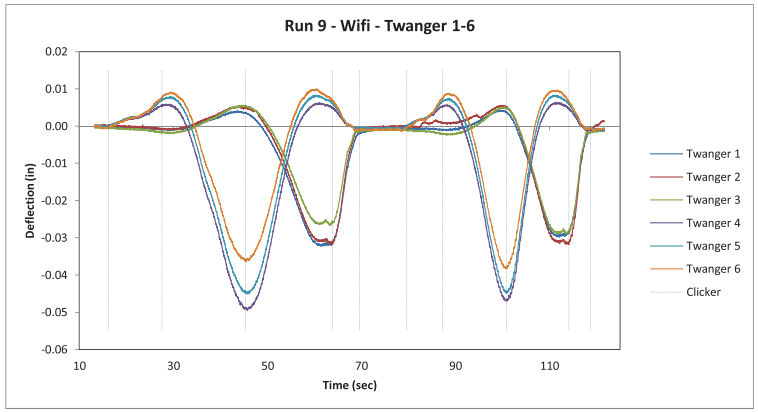
Run 9 - Wifi - Twanger 1-6
Deflection (in)
Time (sec)
Twanger 1
Twanger 2
Twanger 3
Twanger 4
Twanger 5
Twanger 6
Clicker

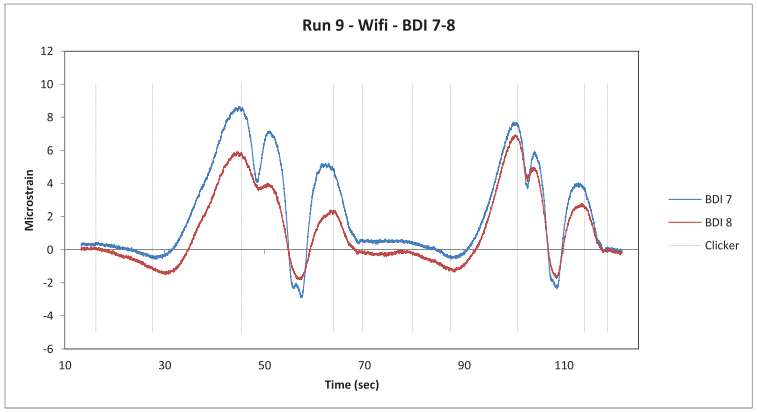
Run 9 - Wifi - BDI 7-8
Microstrain
Time (sec)
BDI 7
BDI 8
Clicker

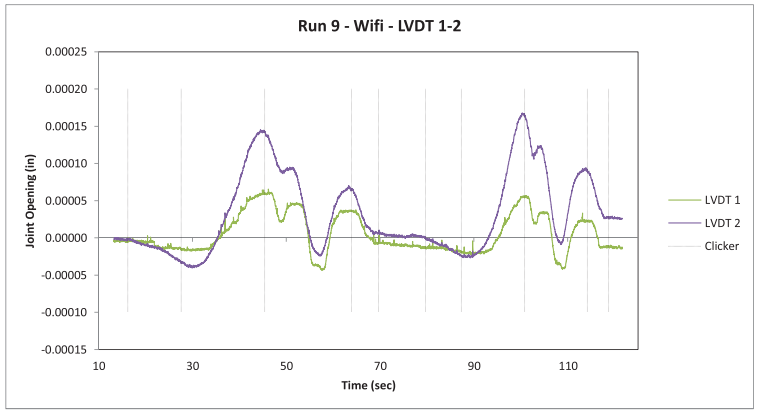
Run 9 - Wifi - LVDT 1-2
Joint Opening (in)
Time (sec)
LVDT 1
LVDT 2
Clicker

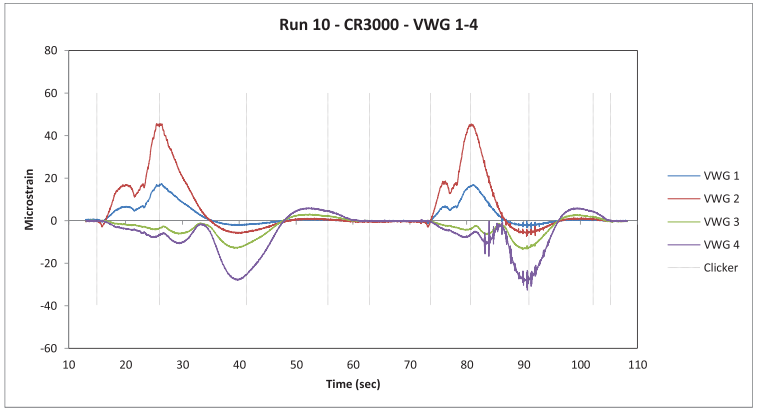
Run 10 - CR3000 - VWG 1-4
Microstrain
Time (sec)
VWG 1
VWG 2
VWG 3
VWG 4
Clicker

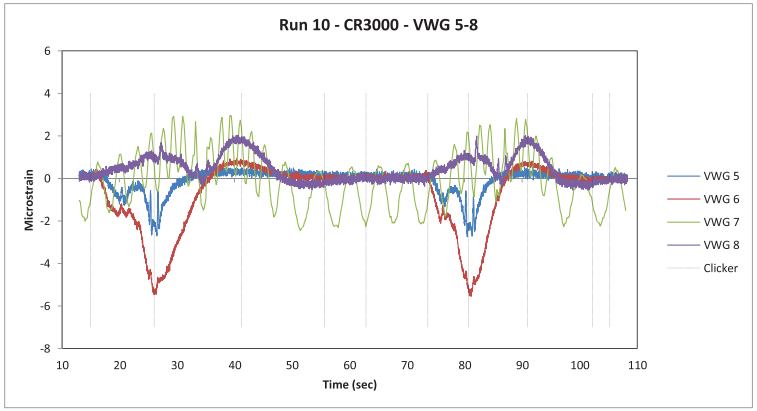
Run 10 - CR3000 - VWG 5-8
Microstrain
Time (sec)
VWG 5
VWG 6
VWG 7
VWG 8
Clicker

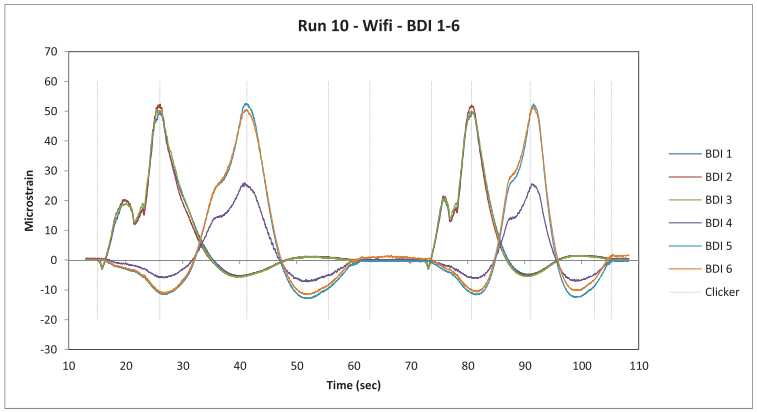
Run 10 - Wifi - BDI 1-6
Microstrain
Time (sec)
BDI 1
BDI 2
BDI 3
BDI 4
BDI 5
BDI 6
Clicker

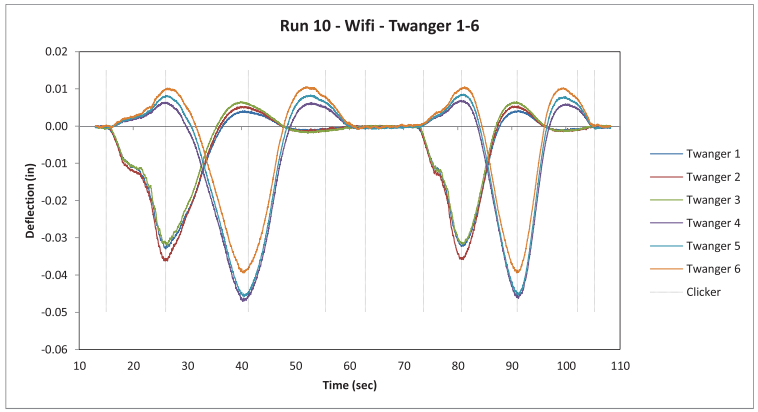
Run 10 - Wifi - Twanger 1-6
Deflection (in)
Time (sec)
Twanger 1
Twanger 2
Twanger 3
Twanger 4
Twanger 5
Twanger 6
Clicker

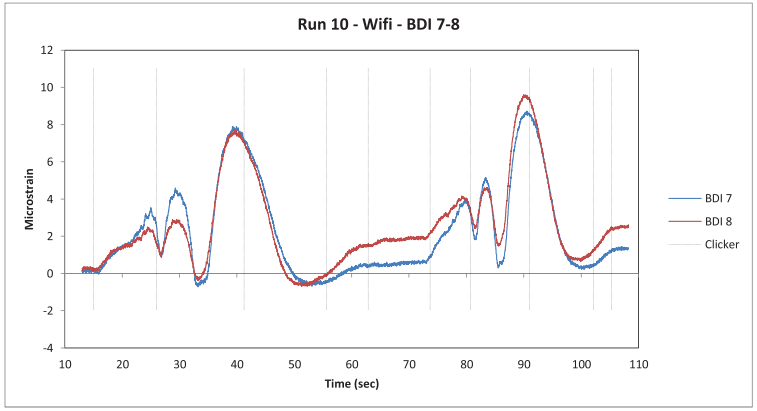
Run 10 - Wifi - BDI 7-8
Microstrain
Time (sec)
BDI 7
BDI 8
Clicker

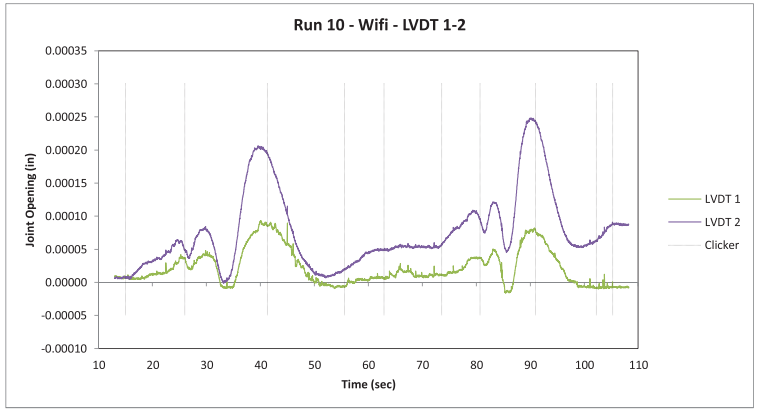
Run 10 - Wifi - LVDT 1-2
Joint Opening (in)
Time (sec)
LVDT 1
LVDT 2
Clicker

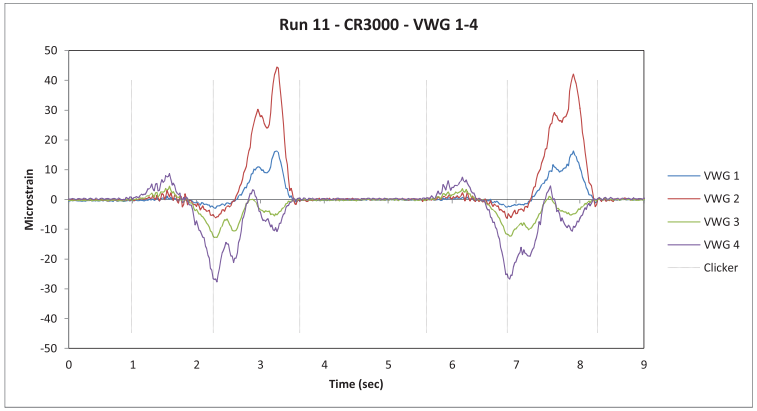
Run 11 - CR3000 - VWG 1-4
Microstrain
Time (sec)
VWG 1
VWG 2
VWG 3
VWG 4
Clicker

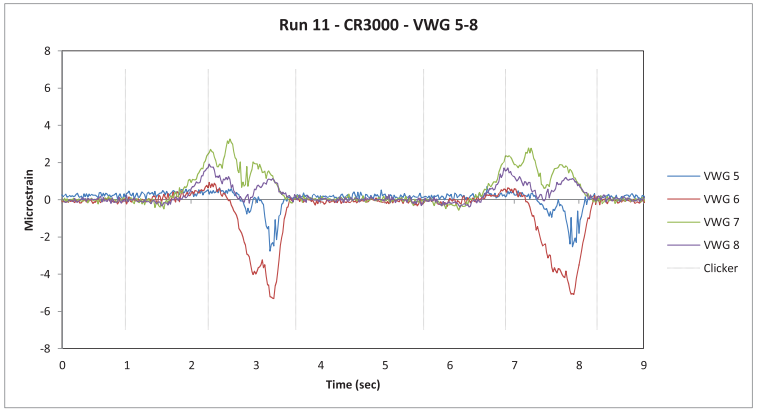
Run 11 - CR3000 - VWG 5-8
Microstrain
Time (sec)
VWG 5
VWG 6
VWG 7
VWG 8
Clicker

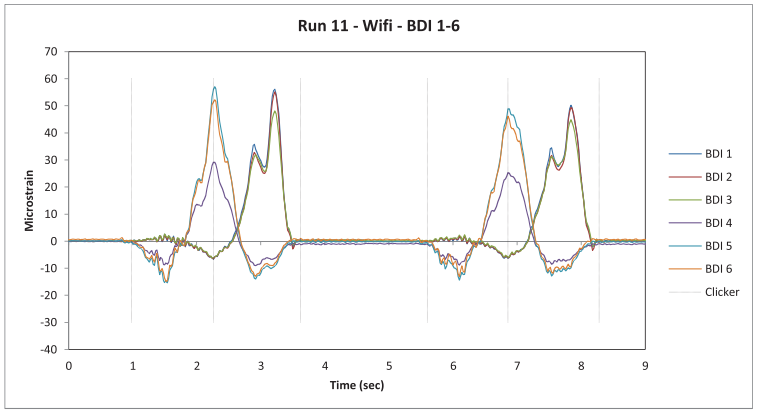
Run 11 - Wifi - BDI 1-6
Microstrain
Time (sec)
BDI 1
BDI 2
BDI 3
BDI 4
BDI 5
BDI 6
Clicker

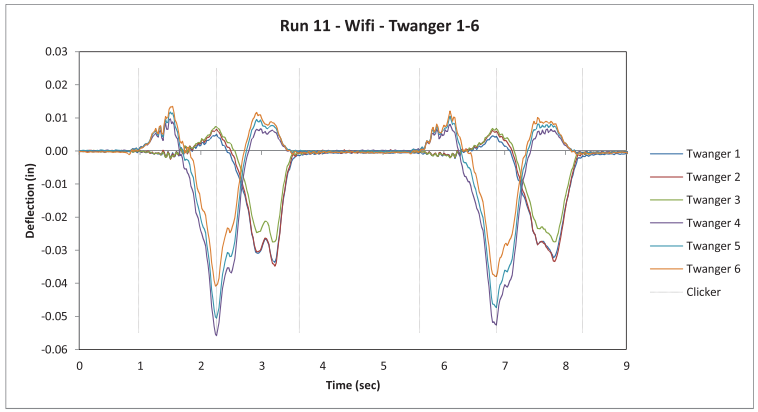
Run 11 - Wifi - Twanger 1-6
Deflection (in)
Time (sec)
Twanger 1
Twanger 2
Twanger 3
Twanger 4
Twanger 5
Twanger 6
Clicker

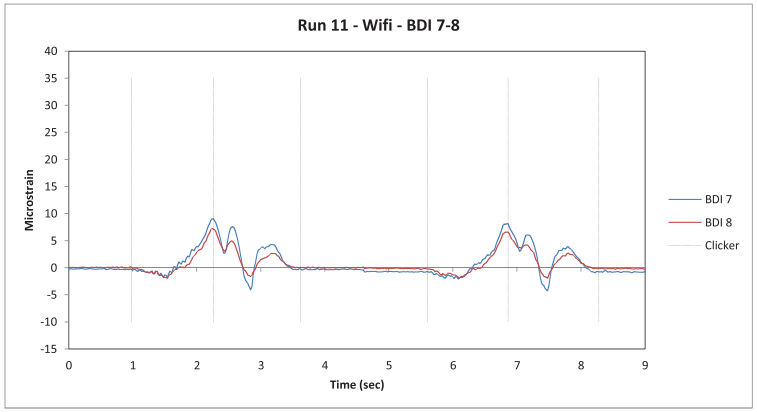
Run 11 - Wifi - BDI 7-8
Microstrain
Time (sec)
BDI 7
BDI 8
Clicker

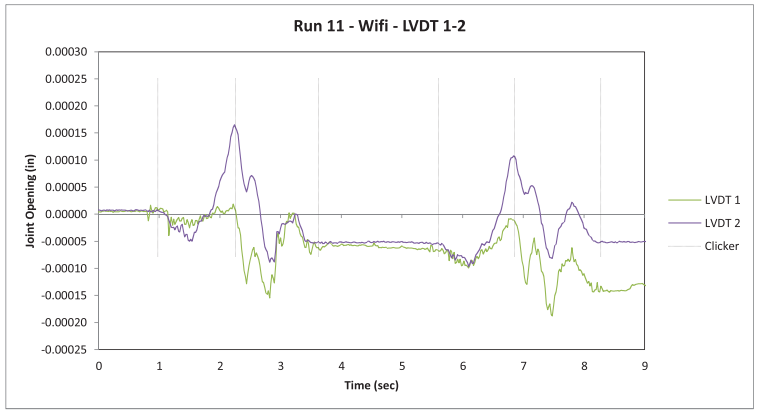
Run 11 - Wifi - LVDT 1-2
Joint Opening (in)
Time (sec)
LVDT 1
LVDT 2
Clicker

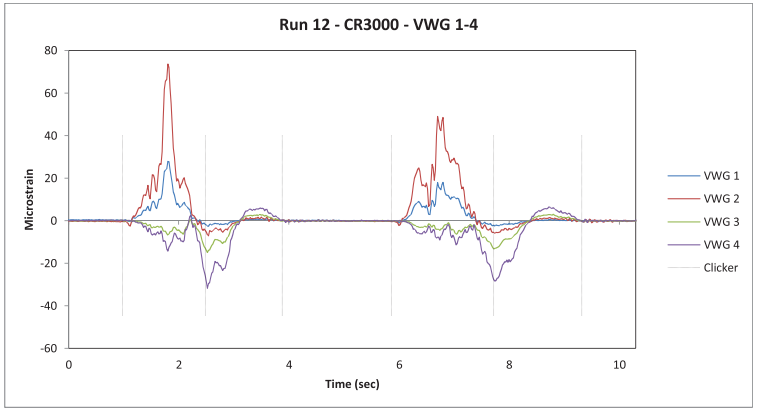
Run 12 - CR3000 - VWG 1-4
Microstrain
Time (sec)
VWG 1
VWG 2
VWG 3
VWG 4
Clicker

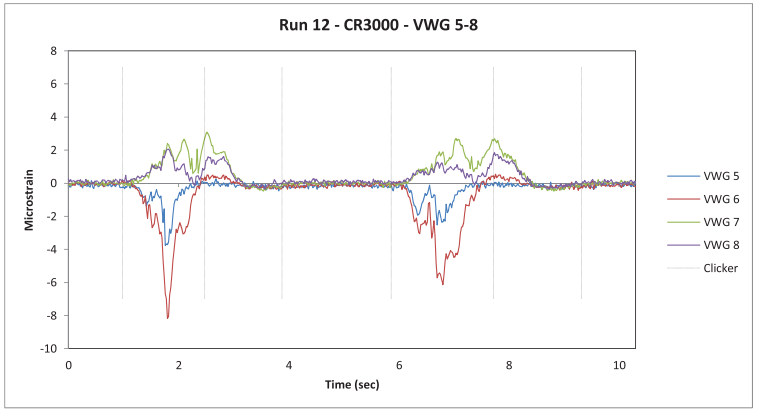
Run 12 - CR3000 - VWG 5-8
Microstrain
Time (sec)
VWG 5
VWG 6
VWG 7
VWG 8
Clicker

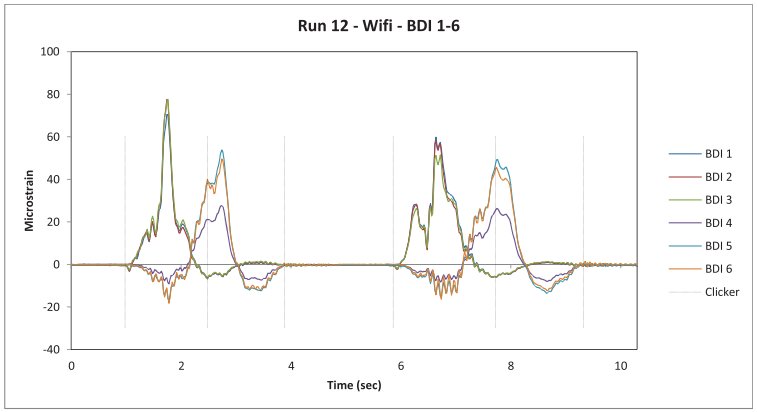
Run 12 - Wifi - BDI 1-6
Microstrain
Time (sec)
BDI 1
BDI 2
BDI 3
BDI 4
BDI 5
BDI 6
Clicker

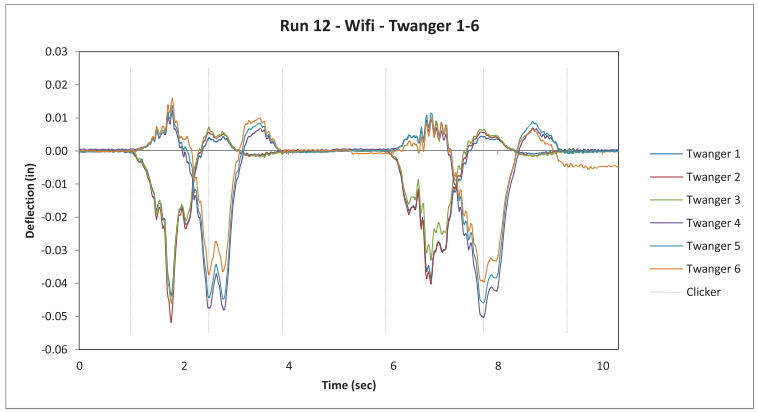
Run 12 - Wifi - Twanger 1-6
Deflection (in)
Time (sec)
Twanger 1
Twanger 2
Twanger 3
Twanger 4
Twanger 5
Twanger 6
Clicker

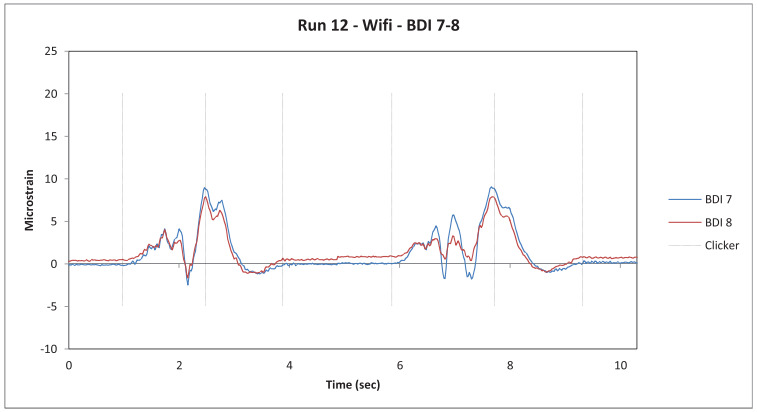
Run 12 - Wifi - BDI 7-8
Microstrain
Time (sec)
BDI 7
BDI 8
Clicker

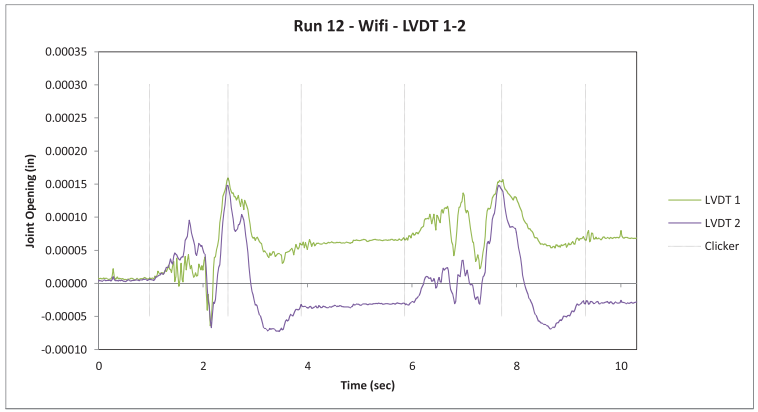
Run 12 - Wifi - LVDT 1-2
Joint Opening (in)
Time (sec)
LVDT 1
LVDT 2
Clicker